PICOSECOND AMPLIFICATION AND ABSORPTION IN THE XeCl LASER

by

Grace Montgomery Reksten, B.Sc., A.R.C.S.

A Thesis submitted for the Degree of Doctor of Philosophy in the University of London and for the Diploma of Imperial College

Department of Physics
Imperial College of Science and Technology
University of London

October, 1981

Til Far

Og

Til Familien

ABSTRACT

Picosecond pulses generated in a flashlamp pumped Rhodamine 6G dye laser were frequency doubled and used to probe the gain and loss in an electron beam and a u.v. preionized discharge pumped XeCl laser.

The small signal gain on the 308nm laser transition of the electron beam pumped XeCl laser was measured to be $\sim 0.28\ cm^{-1}$. Collisional destruction of the weakly bound XeCl ground state was investigated, and the lifetime was found to be $\sim 19\ (\pm 7)$ns at a total pressure of 5 Bar. The dissociation rate due to xenon was estimated by varying the xenon partial pressure, yielding a value of $6{\cdot}3(\pm 1.1) \times 10^{-12} cm^3 s^{-1}$ for k_{Xe}. The presence of unidentified stable species absorbing at the laser wavelength was verified.

The second harmonic wavelength of the mode-locked dye laser was tuned to overlap different vibrational transitions in the discharge pumped XeCl laser in order to investigate the use of XeCl as a tunable amplifying medium. The peak small signal gain on the main laser transition was found to be $\sim 0.078\ cm^{-1}$. Substantial gain was observed on other transitions, but no gain was found for transitions originating from high lying vibrational levels, indicating rapid vibrational relaxation.

By amplifying the u.v. dye laser pulses to saturation levels a rough estimate for the saturation energy density in XeCl, $E_s \sim 480\ (\pm 170)\mu J\ cm^{-2}$, was obtained. Stable species absorbing at the laser wavelength were also observed to be present in the discharge laser.

Mode-locking of the XeCl discharge laser was achieved by two different methods. Injection mode-locking yielded peak single pulse

powers of ∿ 200MW. Pulse durations as short as ∿ 7ps were measured with a Photochron II streak camera. Active mode-locking with an intracavity Pockel's cell loss modulator driven by a GaAs semiconductor switching device, generated longer pulses (∿ 360ps), but proved to be a more versatile method in that no wavelength matching between the dye laser and the XeCl laser was required.

Finally, computer simulations were carried out to model the injection mode-locking and active mode-locking experiments.

ACKNOWLEDGEMENTS

I would first of all like to thank Professor Dan Bradley F.R.S. for his guidance and support throughout this work. I would also like to thank Dr. John Vucusic for his advice and constant encouragement when I first came to the group and worked with flashlamp pumped dye lasers. I also wish to thank Dr. Henry Hutchinson for many useful discussions regarding the excimer work.

I am very grateful to Dr. Bill Sleat, Dr. Wilson Sibbett, Dr. Ken Gratten and particularly Dr. Roy Taylor for generally being very helpful. I am indebted to Mr. Morris Pimm for having the patience to teach me the use of drills and lathes and to Mr. Roy Morrison and the optics workshop for their assistance. Thanks also go to the main workshop for helping with the manufacture of laser equipment. I am very grateful to Mr. Nick Jackson and Miss Louise Symmonds for producing the photographs in this thesis and in the publications. I am also grateful to Miss Janie Coghill for typing this thesis so neatly and for arranging the layout.

Last, but not least, I would like to thank my colleagues and co-workers; Dr. Phil Levy and Dr. Thomas Varghese (who built the discharge laser) for making the experiments with the electron beam pumped and discharge pumped XeCl lasers a happier memory. I will be luckyin the future to find such interesting and entertaining colleagues to work with. In particular, my gratitude goes to my friend and colleague Dr. Walter Margulis whose friendship and support during difficult times made all the difference, and from whom I have learned more physics through interesting discussions than I could from any

textbook. Most of all I thank him for being such a good friend and for all the fun.

The most important acknowledgement goes to my late father, to my mother and my brothers and sisters. Their encouragement and their enthusiasm for this very different subject that I chose was a constant driving force and has made every minute spent in the dark laboratory late at night worth while!

CONTENTS

GENERAL INTRODUCTION

Since excimer lasers were introduced in 1971, the rare-gas halide laser has emerged as the most efficient of this group. Progress in the development of discharge and electron beam pumping has made possible the construction of large systems yielding output energies ranging from millijoules to several hundred joules. High power pulses in the ultraviolet spectral region are useful for many purposes. Generation of controlled thermonuclear fusion, laser isotope separation and remote sensing of the upper atomosphere are examples of research areas where rare-gas halide lasers are employed. Another particularly important application is pumping of dye lasers. Improved excitation schemes and the knowledge gained about the kinetic pathways leading to excimer formation have been important in the development of high power excimer lasers in the blue-green spectral region for uses such as communications with submarines. Ultraviolet laser pulses of picosecond duration are useful in nonlinear optics and also in photochemistry. In excite-and-probe experiments chemical reactions and relaxation processes that take place on extremely fast time-scales can then be resolved.

The subject of this thesis is to investigate the feasibility of employing a rare-gas halide laser as an amplifier or source of picosecond pulses. Frequency doubled ultrashort pulses generated in a mode-locked flashlamp pumped dye laser were used in these investigations for several reasons:

Firstly, the train of frequency doubled pulses probes and time-resolves amplification and absorption processes in the rare-gas halide

medium for the purpose of assessing the magnitude and temporal evolution of gain and loss in electron beam and discharge pumped systems. Secondly, the dye laser pulses are amplified to high peak powers in the rare-gas halide medium, with the excimer laser in a single pass configuration or arranged as a regenerative amplifier. Finally, the output from the dye laser is used to drive an intracavity loss modulator in an active mode-locking arrangement whereby the rare-gas halide laser itself becomes the source of subnanosecond pulses.

The emission wavelengths of the rare-gas halide excimers range from $\sim$ 160nm to $\sim$ 350nm. The laser transition in XeCl coincides with the second harmonic wavelength of the Rhodamine 6G dye laser. The combination of these lasers was therefore chosen for the experiments described in this dissertation.

The mode-locked flashlamp pumped Rhodamine 6G dye laser is well known to be a versatile convenient source of picosecond pulses. Pulses of duration < 10ps with high peak intensities that are advantageous for second harmonic generation can readily be generated. For the purpose of studying transient processes in the XeCl laser, the mode-locked Rhodamine 6G dye laser provides trains of near delta-function shaped probe pulses of low beam divergence. Since the pulse train lasts for hundreds of nanoseconds it is possible to time resolve processes that take place both during and after pumping.

The probe experiments described in Chapters 3 and 4 are concerned with investigating absorption from the bound XeCl ground state in order to estimate the rate of vibrational relaxation and the rate of collisional dissociation. Knowledge of these rates is important, since "bottlenecking" in the ground state limits efficiency, particularly for long gain duration systems.

The presence of transient and stable absorbing species in the gas mixture also reduces efficiency, especially in discharge lasers where the gain medium is generally long. Large absorption factors are then possible. The probe studies in Chapters 3 and 4 are therefore also conducted in order to gain more information about the magnitude and temporal evolution of the absorption coefficients.

In Chapter 4, the probe pulses from the mode-locked dye laser are used to study the gain characteristics of the u.v. preionized discharge pumped XeCl laser. The purpose of this is to investigate the amount of energy that can be extracted in a picosecond pulse,since saturation effects necessarily pose an upper limit on the maximum energy available from the XeCl amplifier.

The XeCl molecule has a weakly bound ground state and the emission bandwidth is thus narrower than in the bound-free excimers such as KrF. Discrete emission bands arise due to the vibrational energy level structure of the excited and ground state manifold. By tuning the dye laser probe pulses to wavelengths corresponding to different vibrational transitions and measuring the corresponding amplification factors, the tunability of XeCl as an amplifying medium is assessed.

Furthermore, if the input pulse is of ultrashort duration, it is important to know if the XeCl medium is homogeniously broadened on the time-scale of the pulse duration. In Chapter 4, the XeCl laser is used as a regenerative amplifier in an injection mode-locking experiment and the bandwidth available to the picosecond pulse is investigated. An estimate of the rate of vibrational relaxation is made, thus indicating whether or not the vibrational levels are cross-coupled on a picosecond time-scale.

The final section of the thesis deals with mode-locking of the discharge pumped XeCl laser. The most generally quoted reason for why rare-gas halide lasers are difficult to mode-lock, is that the duration of gain in the electron beam and avalanche discharge lasers is too short for sufficient pulse compression to take place. In Chapters 5 and 7 two distinct methods by which this problem is circumvented are described, and in Chapters 6 and 8 theoretical models for the mode-locking experiments are presented. The resulting computer simulations illustrating the evolution of the mode-locked pulses are useful in understanding the mode-locking process and in investigating the effect of the number of roundtrips made on the duration of the pulses. It is then possible to establish whether long gain duration electron beam sustained discharge pumping is advantageous for mode-locking of excimer lasers.

In order to directly measure the duration of the ultrashort dye laser pulses and the pulses generated in the XeCl mode-locking experiments, an electron-optical streak camera is employed.

Thus, in summary, the work described in this thesis applies the techniques for ultrashort pulse generation and detection and combines this area of research with the more novel field of high power excimer lasers.

CHAPTER 1

RARE-GAS HALIDE LASERS

1.1 Introduction

The term excimer is used to describe molecules that are bound only in the excited state. When excimer molecules radiate, they dissociate or are only weakly bound for a short time. In 1960 Houtermans suggested that "for these spectra the maser condition is automatically satisfied" [1]. He was referring to the fact that if such molecules could be created, population inversion would necessarily be achieved since the ground state is not bound and therefore not populated. Excimer molecules appeared promising as candidates for efficient lasers emitting in the vacuum ultraviolet or ultraviolet spectral region.

Since the first excimer laser was demonstrated in 1971 [2], this promise has become reality. High energy laser systems have been developed (350J in electron beam pumped KrF [3]) and scaling to even higher powers for applications in laser fusion are planned. Excimer lasers have become the most efficient short wavelength lasers and are therefore useful for many applications such as nonlinear optics [4, 5], lidar techniques [6], laser annealing [7] and isotope separation [8].

Laser action from an excimer was first reported by Basov et al. in 1971 [2]. Lasing was achieved in liquid xenon which was pumped by a high intensity relativistic electron beam. The suggestion to use rare-gas halide excimers for laser emission was first made by Velazco and

Setser [9] after Golde and Thrush had published results of emission studies from ArO and ArCl [10]. Shortly after lasing was reported in XeBr [11], KrF [12], and XeF [13, 14]. This was followed by an intensive study of the rare-gas halides by many researchers. Because the rare-gas halides have a relatively flat ground state potential energy curve compared to other excimers, and consequently narrower bandwidth and higher stimulated emission cross section, they were found to be more efficient than rare-gas excimers and rare-gas oxides. The rare-gas halide lasers are presently the most highly developed excimer lasers. Table 1.1 lists the rare-gas halides that have shown laser action or fluorescence to date [15, 16].

	He	Ne	Ar	Kr	Xe
F	-	F	L	L	L
Cl	-	-	F	L	L
Br	-	-	P?	F	L
I	-	-	-	P?	F

L = Lasing
F = Fluorescence
P = Predissociate
- = Ionic state not lowest excited state

Table 1.1. Rare-gas halide molecules that lase and fluoresce.

1.2 Molecular binding of rare-gas halides

Atoms in a diatomic molecule can be bound by ionic or covalent bonds. Ionic binding is Coulombic in nature and can be described on a classical basis. Covalent binding can only be accurately described by quantum mechanics. In this case the electrons share an orbital that is distributed over the two atoms. If the overlap of the charge

clouds is large, this will be a repulsive state and if the overlap is small, the repulsion is less and may lead to a weakly bound Van der Vaals state. The ground states of the individual rare-gas (Rg) and halogen (X) atoms and ions are all described by ^1S and ^2P terms: $Rg(^1S)$, $X(^2P)$, $Rg^+(^2P)$ and $X^-(^1S)$. Molecular states correlating to these individual atomic and ionic states will therefore always be labelled Σ and π.

1.3 The excited state

The strongly bound excited state of the rare-gas halides (RgX*) is ionic and correlates to a $Rg^+(^2P)$ and a $X^-(^1S)$ ion at infinite internuclear distance. It is a charge transfer state where an electron from an excited rare gas atom "hops" over to the high electron affinity halogen atom. The molecule is then held together by Coulomb forces.

Excited state rare-gas atoms show a strong similarity to the nearest alkali metals in the periodic table. Fig. 1.1 shows the energy level diagram for krypton and its alkali neighbour rubidium [17]. The energy levels of the former are almost identical to those of the latter. The reason for this is that since the

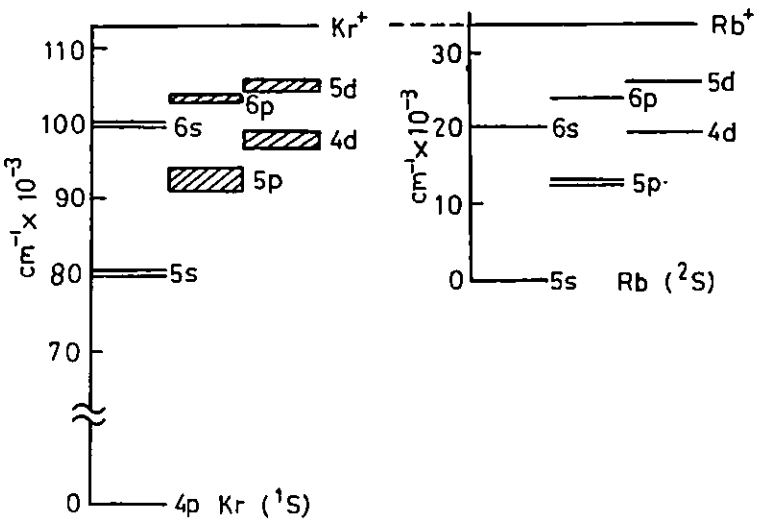

Fig. 1.1. Energy levels of Rb and Kr [17]

energy taken to excite the Kr atom is large, the electron will be in a high orbit and will experience a core of net unit charge as experienced by the S electron in the alkali elements. This similarity has been extremely useful in predicting potential energy curves for rare-gas halide excimers. Since the ionization potential of excited rare-gas atoms is also approximately the same as its alkali "neighbour", the binding energy of rare-gas halide molecules will be similar to ground state alkali halides. The calculation of the equilibrium internuclear separation and vibrational spacing of the bound ionic state in the RgX* molecule is based on this analogy.

By approximating the binding energy of the rare-gas halide ionic state to be equal to the nearest alkali halide, the energy E* of the state can be found. Fig. 1.2 shows the electronic energy level diagram for a typical RgX* molecule.

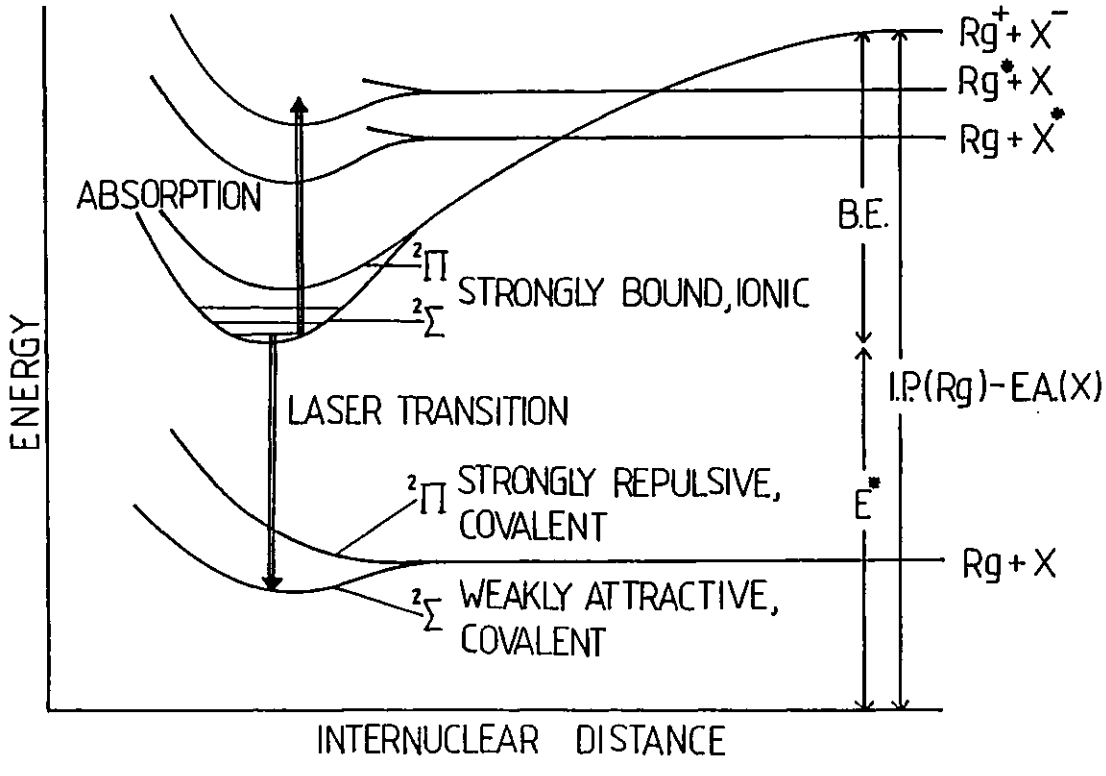

Fig. 1.2. Potential energy curves for a rare-gas halide molecule

The energy of the ionic state at infinite internuclear separation corresponds to the ionization energy of the rare-gas atom minus the electron affinity of the halogen atom.

Hence the energy of the first excited state is approximately

$$E^* = IP(Rg) - E.A.(X) - B.E.\ (\text{alkali halide}) \qquad (1.1)$$

The covalent excited states correlate to excited state rare-gas atoms plus ground state halogen atoms, or to excited state halogen atoms and ground state rare-gas atoms, as shown in Fig. 1.2. The ionic state is normally substantially lower in energy than these covalent states except in certain molecules like the neon halides and possibly some helium halides. In the case of ArBr the covalent potential curves cross the ionic curve at internuclear distances close to the equilibrium internuclear distance and the molecule predissociates. This explains why no laser action has been obtained in ArBr. Predissociation reduces the efficiency in some molecules that have shown laser action such as ArCl, KrCl and XeBr.

The covalent and ionic states of the xenon halides have been calculated by Hay and Dunning [18] and later by other workers who confirmed that the $^2\Sigma$ ionic state lies below the $^2\pi$ ionic state for these molecules. Later however, Kolts et al. [19] found that this was not the case for XeF where the $^2\pi$ state lies lower. XeF has in fact yielded high energy laser output (6J) on the $^2\pi$-$^2\pi$ transition [20]. In molecules where the halogen atom has a high atomic number, spin-orbit effects become important. The $^2\pi$ level then splits into $^2\pi_{\frac{1}{2}}$ and $^2\pi_{3/2}$ states. This effect in the XeCl molecule is illustrated in Fig. 1.3 on page 9.

Labelling of the different states in the rare-gas halides is

conventionally taken as follows:

Ground state: $X(^2\Sigma)$, $A(^2\pi_{1/2,\ 3/2})$

Excited state: $B(^2\Sigma)$, $C(^2\pi_{3/2})$, $D(^2\pi_{1/2})$

The energy ordering of the different levels above the ground state follows the alphabetic labelling. (Except for the C state in XeF which lies lower than the B state).

1.4 The ground state

The rare-gas halide ground state is generally a covalent repulsive state. Bound ground states are found in the XeCl and XeF molecules, hence these molecules are strictly speaking not excimers. The binding energy is low and the well depth is only $\sim 255\,cm^{-1}$ for XeCl [21] and $\sim 1200\,cm^{-1}$ [22] for XeF. The binding energy increases in the sequence XeI, XeBr, XeCl, XeF due to the greater electronegativity of the lighter halides [17]. The $^2\Sigma$ state has lower energy than the $^2\pi$ state since for the $^2\pi$ level, the single occupied halogen orbital is directed towards the closed shell of the rare-gas atom. The potential curve for the $^2\Sigma$ state is nearly flat since the overlap of the electron clouds is smaller than that of the $^2\pi$ state and the exchange repulsion is less. Furthermore, the $^2\Sigma$ state is a mixture of a charge transfer state and a covalent state and can therefore be bound [15]. The $^2\pi$ state is always repulsive.

1.5 Spectroscopy - calculation of σ_s

For laser applications, an important parameter to know is the

stimulated emission cross section σ_s. The small signal gain, α, in the laser will be proportional to the stimulated emission cross section and the population inversion density, ΔN, by the relation

$$\alpha\ (cm^{-1}) = \sigma_s \Delta N \quad . \qquad (1.2)$$

σ_s is proportional to the square of the wavelength of the laser (λ), to the Einstein coefficient for spontaneous emission (A_{nm}) and to the lineshape of the laser transition ($g(\nu_{nm})$)

$$\sigma_s = \frac{\lambda^2}{8\pi} A_{nm}\ g(\nu_{nm}) \qquad (1.3)$$

where n represents the upper laser level and m the lower.

The Einstein A-coefficient can be expressed as

$$A_{nm} = \frac{64\pi^4\ c^3}{3h\lambda_{nm}^3} \left| \underline{R}_{nm} \right|^2 \qquad (1.4)$$

where $\underline{R}_{nm}$ is the transition moment for the two states n and m, and the other symbols have their usual meaning. The transition probability, A_{nm}, is related to the lifetime of the state by the relation

$$\tau = \frac{1}{A_{nm}} \qquad (1.5)$$

This expression does however assume that the transition from n to m is the only transition possible from the state n. If this is not the case the expression $\tau = \frac{1}{A_{nm}}$ should be replaced by $\tau = \frac{1}{\sum_m A_{nm}}$ (i.e. by the sum of the A-coefficients of all the transitions from n to m). In molecules with a dissociative ground state the variation of A_{nm} with frequency is usually small and $A_{nm} \sim \frac{1}{\tau}$ is assumed to be a constant. The expression for the stimulated emission cross section then becomes

$$\sigma_s = \frac{\lambda^2}{8\pi\tau}\ g(\nu_{nm}) \qquad (1.6)$$

If a further assumption is made that the shape of the band is gaussian near the peak of emission, the expression becomes

$$\sigma_s = \frac{1}{4\pi c}\left(\frac{1n2}{\pi}\right)^{\frac{1}{2}} \frac{1}{\tau} \frac{\lambda^4}{\Delta\lambda} \qquad (1.7)$$

The small signal gain ($= \sigma_s \Delta N$) will therefore depend on the fourth power of the wavelength, on the inverse of the spontaneous lifetime and bandwidth of the emission spectrum. Because the ground state potential curves are relatively flat for rare-gas halide molecules, and consequently the bandwidth is narrow, these lasers have proven to be more efficient than other excimer lasers due to the higher stimulated emission cross section. An expression for the small signal gain on vibrational transitions for the molecules that have a bound ground state can be found in Chapter 4. In this case A_{nm} depends strongly on the transition moment. Table 1.2 lists the stimulated emission cross section for some rare-gas halides [23, 24].

RgX*	XeF	XeCl	KrF	XeBr	XeI	ArF
σ_s	5.3	4.5	2.5	2.2	1.4	2.9
10^{-16} cm^2	3.4		1.9	1.5		2.0
	[23]	[23]	[23]	[23,24]	[15]	[23]

Table 1.2. Stimulated emission cross sections

1.6 Emission bands

The allowed optical transitions between the excited ionic states and the ground states are B → X, D → X and C → A. Fig. 1.3 shows the electronic states of XeCl (with spin-orbit splitting) and the allowed

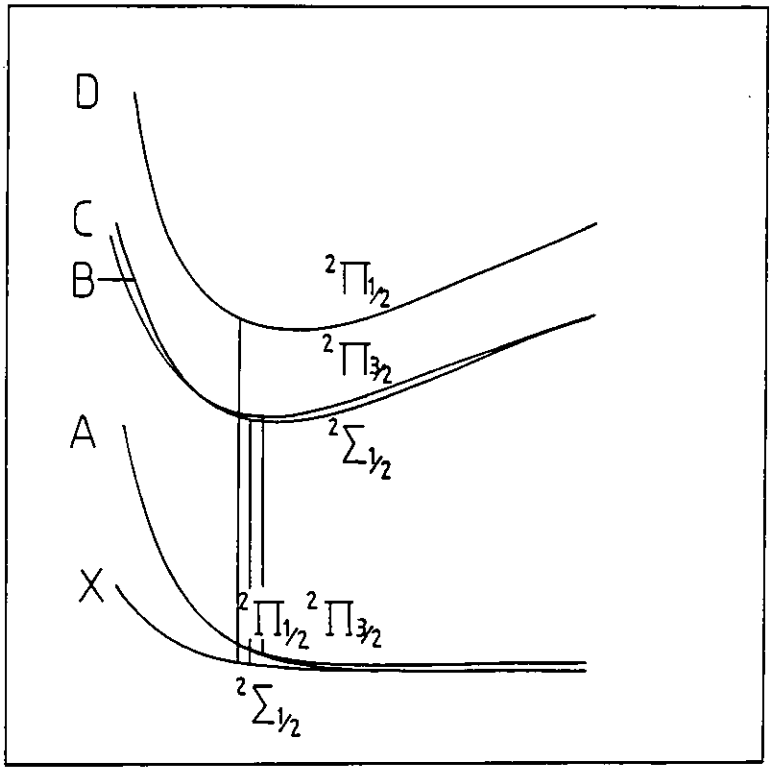

Fig. 1.3

Spin-orbit splitting of the energy levels in XeCl and allowed optical transitions

transitions between them. Since the vibrational spacing in the ionic level is quite large, the spectrum will generally show vibrational structure. At high pressures the structure is less pronounced since the higher vibrational levels are quenched by collisions and the population distribution is relaxed to lower levels. The emission spectrum from XeF is shown in Fig. 1.4 on page 12 . XeF has the most distinct vibrational characteristics since the ground state is relatively tightly bound.

The strongest band in the rare-gas halide emission spectrum is the B - X band. All the bands from charge transfer states correspond to transitions where the valence electron jumps from the negative halogen ion to the rare-gas atom. The transition probability is proportional to the overlap of the electron wave functions and this overlap is largest for the initial and final $p\sigma$ orbitals of the $^2\Sigma \rightarrow {}^2\Sigma$ state (B - X).

Emission from the higher lying D state ($^2\pi_{\frac{1}{2}}$) to the X state is possible because of the mixing of the D state with the B state [15]. The D-X emission is blue-shifted since the D state lies higher than the B state by an amount equal to the spin-orbit splitting. Table 1.3 lists the wavelengths for B-X as well as other transitions in the most important diatomic and triatomic rare-gas halides. The intensity

RgX*	λ(B-X) [15] (nm)	λ(D-X) [15,64] (nm)	λ(C-A) [18,64] (nm)
XeI	253	203	263(292)
XeBr	282	221	302
XeCl	308	235	330(320-360)
XeF	351	210	450
KrI	185		
KrBr	206		
KrCl	222	199	
KrF	249	220	275
ArBr	161		
ArCl	175		
ArF	193	185	203
NeF	108 (114[64])	113	117
	Rg_2X^*	λ [15]	
	Kr_2F	400	
	Ar_2F	290	
	Ar_2Cl	450	
	Kr_2Cl	235	
	Xe_2Cl	450,518 [36]	
	Kr_2Br	325	

Table 1.3

Emission wavelengths in rare-gas halides

of the D-X emission is low, possibly because this level is quenched by collisions [25] and also because the transition moment is less for the $^2\pi \rightarrow {}^2\Sigma$ transition. As expected the spin-orbit splitting is greater for molecules with high atomic numbers.

If the temperature of the gas mixture is increased, bands due to higher lying vibrational levels will appear and the B - X emission will be extended to cover a greater wavelength region. Laser action has been demonstrated on higher vibrational transitions in the case of XeF [26] by elevating the temperature. The output energy for XeF was in fact substantially improved under these conditions, indicating that energy was being fed to the B state from the lower lying C state which then acted as an energy reservoir. This is possible since the C state is longer lived.

$^2\pi \rightarrow {}^2\pi$ transitions are much weaker than $\pi \rightarrow \Sigma$ and $\Sigma \rightarrow \Sigma$. The bandwidth of these transitions is broad due to the strongly repulsive nature of the lower level. Calculations have indicated that the dipole matrix element for transitions to the A state are almost an order of magnitude smaller than those for the B - X transitions [27, 28]. Laser action may still be possible, but the gain will be substantially lower than on the B - X transition. Consequently the cavity losses at the C-A wavelength must be small and the population in the C state large. The latter is not easily achieved if the higher lying C level is quenched at high pressures. Furthermore, losses due to absorption bands of other transient species overlapping the visible bands of the C - A transitions inhibits lasing . In 1979 laser action due to the bound-free XeF C - A transition was first reported by Bishcel et al. [29] and shortly after by Basov et al. [30]. The feasibility of tuning the laser emission in a 100nm wide spectral range was indicated

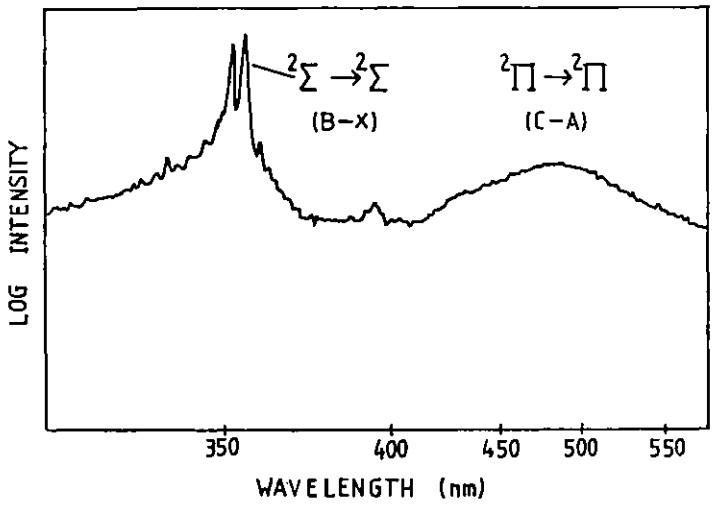

Fig. 1.4. Spectrum for B → X and C → A in XeF* showing vibrational structure [31]

by Basov et al. Table 1.3 lists the wavelength of the C-A transition in some rare-gas halides. Fig. 1.4 shows the B-X and C-A emission spectrum of XeF*.

1.7 Tuning

For spectroscopy applications (such as remote sensing) tuning and narrowing of the laser linewidth is required. Although continuous tuning throughout the fluorescence spectrum is not possible due to the vibrational band structure, limited tunability has been demonstrated with success in several rare-gas halide lasers. Wavelength tuning has been achieved by the use of intracavity prisms [32] and also by replacing the total reflector in the cavity with a grating (at a grazing angle of incidence) and a rotating tuning mirror [33]. Tuning may also be achieved by using intracavity Fabry-Perot etalons. The output energy is then, however, severely reduced as the filter elements reduce the feedback into the cavity and increase the time for lasing to build up. Since the gain duration is normally short in excimer lasers, the light cannot make many passes through the filters and the bandwidth of the transmitted maxima remains relatively broad. Goldhar, Rapoport and Murray have operated an oscillator-amplifier system where they obtained linewidths $\sim$ 10 mÅ from both KrF

and XeCl [34]. In this case three Fabry-Perot etalons were placed in the oscillator. The low power output was then amplified in the KrF amplifier which frequency locked to the weak injected signal. More recently, Fourier transform limited pulses of 0.3 mÅ bandwidth were obtained from an ArF laser by amplifying the narrow linewidth third harmonic output from a C.W. dye laser [35].

Elevation of the laser mixture temperature may extend the tuning range to higher lying vibrational levels as has been shown with XeF [26]. For a laser tuned to a particular vibrational transition, efficient extraction of energy depends on whether population can be transferred from other vibrational levels on a time-scale short compared to the gain duration. The energy stored in the excited state as a whole can then be extracted in a narrow linewidth and the laser is homogeneously broadened. The dye laser is an example of a system that is homogeneously broadened and the energy stored in the upper laser level can be channeled into very narrow linewidths. The XeF laser is thought not to be homogeneously broadened on a time-scale short enough for efficient energy extraction in a narrow linewidth [34]. The case of XeCl will be discussed further in Chapter 5.

1.8 Triatomic rare-gas halides

Considerable interest has been shown lately in triatomic rare-gas halides (Table 1.3 lists the emission wavelengths of some species). These molecules have been recognized as feasible laser candidates for the visible region of the spectrum. The molecules have strongly bound ionic upper states that radiate to repulsive ground states. The emission is therefore broadband and the lower state removal fast,

yielding a tunable laser output. However, since the bandwidth is broad and the upper state lifetime long, the stimulated emission cross section is low. Also, like in the case of C - A emission, laser action is inhibited by broadband transient absorbers in the laser mixture. Laser action in a triatomic rare-gas halide (Xe_2Cl) was first reported by Tang et al. [36] and later by Tittel et al. [37]. The laser bandwidth in both cases was about 30nm and the stimulated emission cross section found by Tang et al.was $\sigma_s \sim 8 \times 10^{-18} cm^2$ confirming the expected low value for the latter. Fig. 1.5 shows the fluorescence and laser spectrum of XeCl and Xe_2Cl. Since the formation of XeCl* is a precursor in the formation of Xe_2Cl, operation of the Xe_2Cl laser requires an optical cavity that is lossy at the XeCl* wavelength.

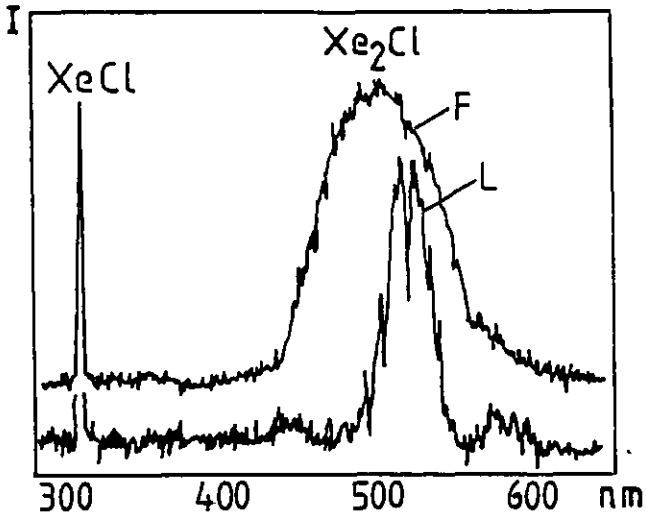

Fig. 1.5

Fluorescence and laser spectrum of XeCl and Xe_2Cl [37]. The redshift of the laser spectrum is thought to be due to the dependence of the stimulated emission cross section on wavelength and also to selective absorption in the blue region of the spectrum.

1.9 Radiative lifetimes

Since the radiative lifetimes of the upper level in rare-gas halide molecules are short ($\sim$ 10ns), they are difficult to determine exactly. In order to avoid quenching of the excited state by collisions,

the measurements have to be made under low pressure conditions. Since the short lived excimer is then formed by a relatively slow process, it is difficult to create enough excited states from which to make the fluorescence lifetime measurements. KrF* and XeF* can be formed by dissociative exitation of KrF_2 and XeF_2, and measurements of radiative lifetimes in these molecules have been made and agree well with the calculated values [38, 39, 40]. Table 1.4 lists the calculated and measured lifetimes of the C-A and B-X transitions as well as the lifetimes of some of the triatomic species. [15]

RgX*	τ(B-X) [15] (ns)	τ(C-A) (ns)	$\tau(Rg_2X)$ [15] (ns)
XeI	12	110 [18]	
XeBr	12, 17.5	120 [18]	
XeCl	11	120 [18]	
XeF	12, 18.8, 16.5, 13.5, 8, 15	98 [41], 113 [42], 93 [43]	
KrF	6.7, 9, 6.8	75 [28]	313, 181
ArF	4.2		128, 185
NeF	2.6		

Table 1.4. Lifetimes in rare gas halides

1.10 Formation kinetics

The kinetic processes leading to the formation of rare-gas halide molecules are extremely complex and not yet fully understood. Since KrF has been the most efficient rare-gas halide laser so far, extensive studies have been made of the kinetics in this system [15, 44]. Only a limited general outline will be given here.

The kinetics of the rare-gas halides are made increasingly complex since the gas mixture consists of three different initial molecular and atomic species and all the resulting products in the plasma. These are:

light rare-gas atoms (buffer gas; $\gtrsim$ 90% of the total mixture), the heavier rare-gas atoms that form the rare-gas halide ($\lesssim$ 10%) and the halogen donor ($\lesssim$ 1%). The halogen donor can be a dimer or a complex molecule. In general the branching ratios for forming rare-gas halides from complex molecules are smaller than from dimers [15]. In certain cases the complex molecule as a halogen donor is preferable, since some of the halogen dimers are extremely corrosive (e.g. F_2) or have absorption bands at the laser wavelength (e.g. Cl_2 at the XeCl wavelengths). Optimum concentration ratios are found by considering formation and quenching processes and by experiment.

Electron excitation by relativistic electron beams or by discharges leads to rapid formation of rare-gas ions or excited state rare-gas atoms:

$$Rg + e_p \rightarrow Rg^+ + e_p + e_s \qquad (1.8)$$

$$Rg + e_p \rightarrow Rg^* + e_p \qquad (1.9)$$

where e_p and e_s represent primary and secondary electrons.
The primary electrons in the e-beam or discharge are mostly absorbed by the lighter rare gas atoms, M, since their number density is very high:

$$M + e_p \rightarrow M^+ + e_p + e_s \qquad (1.10)$$

$$M + e_p \rightarrow M^* + e_p \qquad (1.11)$$

Further excitation of the heavier rare-gas atoms, Rg, can then proceed via the reactions

$$M^+ + Rg \rightarrow Rg^+ + M \qquad (1.12)$$

$$M^* + Rg \rightarrow Rg^* + M \qquad (1.13)$$

The electrons also form negative halogen ions by dissociative attachment to the halogen donor:

$$X_2 + e_p \rightarrow X^- + X \qquad (1.14)$$

$$X_2 + e_s \rightarrow X^- + X \qquad (1.15)$$

Attachment to the halogen atom is particularly important in discharge pumped systems, since electron attachment controls the number of free electrons and thus the plasma impedance. By this electron loss process, the plasma is prevented from collapsing before laser action can take place.

The rare-gas halide molecule is then formed via the following main channels:

Ion recombination: $Rg^+ + X^- (+M) \rightarrow RgX^* (+M)$ (1.16)

$Rg_2^+ + X^- (+M) \rightarrow RgX^* + Rg(+M)$ (1.17)

Direct (harpooning): $Rg^* + X \rightarrow RgX^*$ (1.18)

Displacement: $Rg + MX^* \rightarrow RgX^* + M$ (1.19)

Ion recombination is the main formation channel proceeding with almost unit branching ratio. This is the most important formation process in electron beam pumped lasers. Two-body reactions reach their maximum rate at pressures around one atmosphere. The effective two-body recombination rate depends on the mean free path of the ions. At higher pressures this is reduced due to the high number density of third body particles. Three-body ion-ion recombination reactions are thought to have very high branching ratios, based on the high efficiencies observed from rare-gas halide lasers [15].

The second formation channel is sometimes referred to as the metastable channel, or "harpooning". The latter term is used since it describes a reaction where an electron "hops" from the excited rare-gas atom to the halogen atom - the electron is then thought of as a "harpoon" that forms the excited rare-gas halide species. This is analogous to reactions forming alkali halides where the description originated. The reaction can take place at relatively large internuclear

distances since the ionic potential curve representing the bound rare-gas halide crosses the covalent curves at large internuclear separations. Harpooning branching ratios are frequently equal to unity [45]. This is the main formation channel in discharge pumped systems.

Displacement reactions are only of importance where the light rare-gas form a compound with the halogen. This is the case for KrF in argon. The reaction

$$ArF^* + Kr \rightarrow KrF^* + Ar \qquad (1.20)$$

is an example of this and occurs with a rate constant $\sim 10^{-9}$ $cm^3 s^{-1}$ [46].

A great number of other reactions take place in rare-gas halide mixtures leading to a variety of atomic, ionic and molecular species. One process that should be mentioned, since it represents quenching of the RgX* molecule, is the formation of Rg_2X^* triatomic molecules. The creation of these molecules are also important since they are interesting as laser candidates (Section 1.8).

Table 1.5 lists some of the main kinetic reactions in discharge pumped XeCl together with the corresponding rate constants [16].

1.11 Quenching

Quenching of rare-gas halide molecules is rapid and can under certain conditions take place at every collision. The most important process is quenching of the excited state RgX* molecule by the halogen donor. Quenching by the rare-gas molecules becomes increasingly important at high pressures, yielding triatomic species or other products.

	Reaction	Rate Constant
Electron pumping and quenching processes:	$e + Xe = Xe^* + e$	5.0×10^{-9} cm^3s^{-1}
	$e + Xe = Xe^+ + 2e$	5.0×10^{-11} "
	$e + Xe^* = Xe^+ + 2e$	5.0×10^{-7} "
	$e + Xe^* = Xe^{**} + e$	6.4×10^{-7} "
	$e + Ne = Ne^* + e$	2.8×10^{-12} "
	$e + Ne = Ne^+ + 2e$	1.4×10^{-19} "
	$e + Ne^* = Ne^+ + 2e$	2.8×10^{-8} "
	$e + Ne^* = Ne^{**} + e$	6.6×10^{-7} "
	$e + HCl_{v'=0} = HCl_{v'=1} + e$	2.0×10^{-8} "
	$e + HCl_{v'=1} = Cl^- + H$	5.0×10^{-9} "
	$e + HCl_{v'=0} = Cl^- + H$	5.0×10^{-11} "
Metastable and ion formation via buffer gas:	$Ne^* + Xe = Xe^* + Ne$	6.2×10^{-12} "
	$Ne^+ + Xe = Xe^+ + Ne$	3.0×10^{-11} "
Excimer formation:	$Xe^* + HCl = XeCl^* + H$	5.6×10^{-10} "
	$Xe^+ + Cl^- = XeCl^*$	2.0×10^{-6} "
	$Xe^{**} + HCl = XeCl^* + H$	8.1×10^{-10} "
Radiative:	$XeCl^* \rightarrow Xe + Cl + h\nu$	$\tau = 11ns$
$XeCl^* B(^2\Sigma_{\frac{1}{2}})$ quenching processes:	$XeCl^* + HCl \rightarrow$ products	5.0×10^{-18} cm^3s^{-1}
	$XeCl^* + Xe \rightarrow$ "	4.6×10^{-19} "
	$XeCl^* + Ne \rightarrow$ "	1.0×10^{-20} "
	$XeCl^* + e \rightarrow$ "	
$XeCl\ X(^2\Sigma_{\frac{1}{2}})$ quenching:	$XeCl + HCl \rightarrow$ products	$2.2 \pm .5 \times 10^{-11}$ cm^3s^{-1}
	$XeCl + Xe \rightarrow$ "	$5.6 \pm .8 \times 10^{-12}$ "
	$XeCl + Ne \rightarrow$ "	$1.0 \pm .15 \times 10^{-13}$ "
	$XeCl + e \rightarrow$ "	

Table 1.5

Kinetic reactions in discharge pumped XeCl

In a rare-gas halide laser these processes compete with emission and absorption of radiation:

$$RgX^* \rightarrow h\nu + Rg + X \qquad (1.21)$$

$$h\nu + RgX^* \rightarrow 2h\nu + Rg + X \qquad (1.22)$$

$$h\nu + RgX^* \rightarrow Rg^* + X \qquad (1.23)$$

(1.21) and (1.22) represent spontaneous and stimulated emission and (1.23) represents reabsorption.

The first two are of course desired, whereas the third is one of the many absorption losses that occur in these lasers. A further treatment of the absorption loss processes will be given in Chapter 3.

1.12 Electron beam pumping

Stimulated emission must compete with the rapid quenching processes mentioned above, and the rare-gas halide laser must therefore be vigourously pumped. The excited states also have very short life-times which renders it difficult to sustain a population inversion. The lack of an excitation source of sufficient power meant that although excimer molecules were predicted as laser sources in 1960, it was not until the relativistic electron beam was used that laser action was first reported [2]. The main excitation methods for excimer lasers are electron beam pumping and discharge pumping. Optical pumping is difficult due to the lack of a source of sufficiently short wave-length. Optical pumping of XeF was demonstrated by Mandl and Ewing [47]. A xenon flashlamp pumped Xe (145nm resonance line) which reacted with NF_3 to form XeF*.

E-beam pumping has provided the greatest laser output powers so far [3]. In most e-beam pulse generators, the voltage pulse is provided by a Marx generator. Several capacitors are charged in parallel and discharged into the load in series. This is achieved by triggering a succession of spark gaps with jitters of only a few nanoseconds. By this method the relatively low D.C. ($\lesssim$ 100KV) voltages on the capacitors are added yielding a very high voltage pulse ($\sim$ 1 MV) at the load.

The Marx bank is connected to a cold cathode electron gun. The diode can be coaxial or transverse and the electrons enter the discharge region through a 25-50μm thick foil (aluminium, titanium or stainless steel). A vacuum is maintained ($\sim 10^{-3} - 10^{-5}$ Torr) between the cathode and the anode. Fig.1.6 shows a transverse and a coaxial diode. The coaxial diode has been found to yield the most uniform pumping, in this case 70-80% of the e-beam energy can be uniformly deposited into the gas [48].

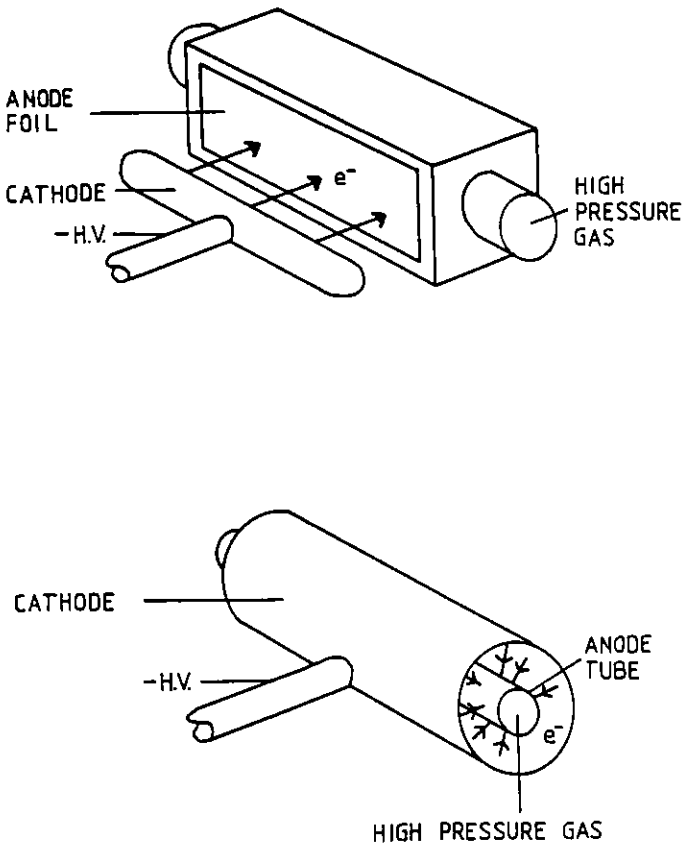

Fig. 1.6. Transverse and co-axial diodes

Current densities as high as 1KA cm^{-2} [17] at the anode can be reached in e-beam systems. As such densities the magnetic field created by the electron beam represents a limit to efficient energy deposition into the gas mixture because of self-pinching.

The magnetic field generated by the electron beam itself focuses the electrons causing non-uniform pumping. Bradley et al. have developed a coaxial diode which utilises a radial current return geometry that changes the magnetic field characteristics favourably yielding more uniform pumping [49] (see Chapter 3).

A Marx bank generator is often used in conjunction with a Blumlein pulse forming network. If the impedance of the load is matched to the PFN, there is no voltage loss and the pulse shape at the load is almost square with a very fast risetime. Fig. 1.7 illustrates a Blumlein PFN.

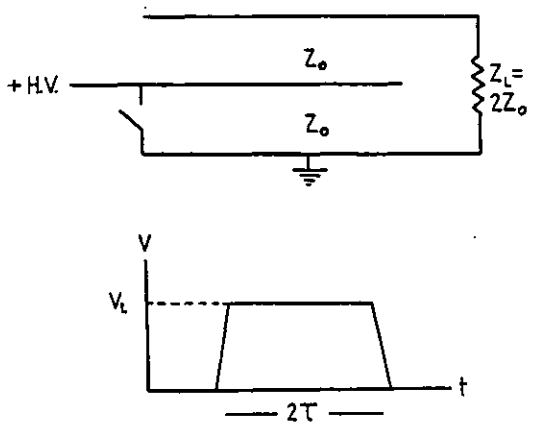

Fig. 1.7. Folded Blumlein P.F.N.

E-beam pump pulse durations range from a few nanoseconds to a few microseconds.

1.13 Avalanche discharge pumping

Avalanche discharge systems are cheaper and more compact than e-beam pumped lasers, but yield lower output energies. The discharge systems offer the greatest potential for high average power, since the repetition rate can be much larger (KHz) than for e-beam systems and since production of rare-gas halide molecules through the metastable channel can be very efficient.

Initial problems with discharge systems were concerned with plasma instabilities. Also, since the excited state rare-gas halide lifetime

is short, low inductance circuits were needed to obtain fast enough current risetimes for efficient pumping. The latter was solved by mounting capacitors very close to the discharge as illustrated in Fig. 1.8. The problem of plasma instability in avalanche discharges was not solved until Burnham and Djeu [50] and Andrews et al. [51] constructed a u.v. preionized discharge system.

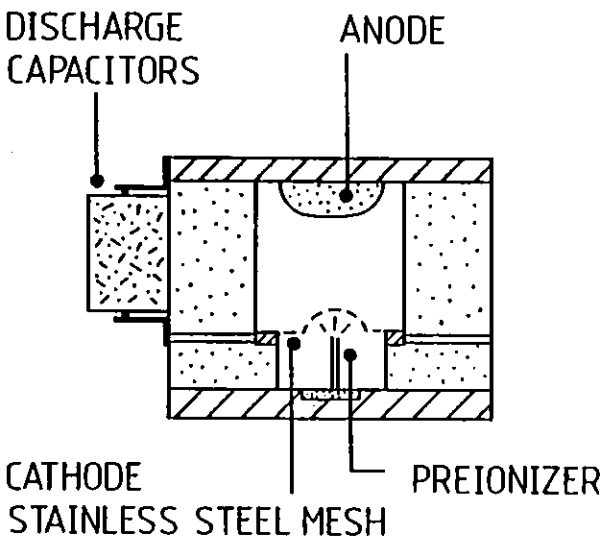

Fig.1.8. U.v. preionized discharge

The discharge power is proportional to the square of the electric field. High electric field gradients increase the electron drift velocity which causes an exponential increase in the number of electrons in the avalanche due to ionization. This causes the discharge to collapse into an arc after a very short time. U.v. preionizing was initially obtained by using flashlamps. More commonly a corona discharge chamber is used in conjunction with the main chamber. The u.v. photons produce a uniform initial electron density, through photoionization, that creates a homogeneous plasma and prevents the strong fields of a single avalanche from dominating the discharge and the formation of a streamer arc. Nevertheless, u.v. preionized discharges are generally only stable for a few tens of nanoseconds. An x-ray preionized system with a very homogeneous discharge was recently reported by Lin and Levatter. The laser pulse duration was $\sim$ 200ns indicating that x-rays generate a very stable plasma [52].

The discharge voltage is provided by low inductance L-C circuits or PFN circuits. Discharge lasers are typically operated at voltages of about 20-100 kV. Current densities reach a few hundred Amperes per square centimeter.

1.14 Electron beam sustained discharge pumping

Electron beam sustained discharges have been used successfully with CO_2 lasers, and an extension to rare-gas halide lasers provided an attractive alternative to e-beam and avalanche discharge pumped lasers. Mangano and Jacob showed that it was possible to produce stable e-beam controlled discharges for a KrF laser [53]. In this case the e-beam provides the stabilising electrons.

Dissociative attachment of electrons to the halogen atom plays an important role in controlling the plasma. Electrons attach to the halogen atoms, thus reducing the total number of electrons and delaying the collapse of the plasma impedance. At the same time, negative halogen ions are formed, being the main precursor to rare-gas halide molecules.

In a stable discharge the electron loss rate (predominately by association with the halogen) should be more than twice the ionization rate [53]. This may be realised in e-beam sustainer systems, and pulse durations $\sim$ 1μs have been demonstrated [54]. The largest output pulse energy obtained for an e-beam sustained discharge system is $\sim$ 50J in a KrF laser [3]. The e-beam voltage was in this case $\sim$ 400kV at a few Amperes per square centimeters current density. The discharge current density was $\sim$ 15A cm^{-2}.

1.15 Amplifier operation; efficiency of e-beam and discharge systems

Since part of the work described in this thesis is concerned with the use of XeCl lasers as amplifiers, a brief outline of the efficiency of different rare-gas halide systems follows. To date, electron beam pumped amplifiers appear to be more feasible for scaling to large volumes, since more energy can be deposited from a relativistic e-beam than from a discharge. In this way high energies can be extracted without a great increase in laser length. Although lengths of several meters are in principle possible, yielding energy outputs of kilojoules, photoabsorption processes may reduce the extraction efficiency drastically. Photoabsorption constants up to a few percent per centimeter have been reported [55, 56, 57].

The highest efficiency reported for an e-beam pumped system is about the same as for a discharge system: of the order of 1% overall. The highest output energy obtained from an e-beam pumped laser is however two orders of magnitude greater than the highest output energy from a u.v. preionized discharge laser:

E-beam pumped (KrF): E_{MAX} = 350J [3]

E-beam sustained discharge (KrF) E_{MAX} = 50J [3]

U.v. preionized discharge (XeCl) E_{MAX} = 5J [59]

The intrinsic efficiency of a laser is defined:

$$\eta_I = \frac{\text{laser output energy}}{\text{pump energy deposited in laser mix}} \qquad (1.24)$$

The pumping efficiency (the efficiency to produce precursors) is

$$\eta_p = \frac{E}{W} \qquad (1.25)$$

where E = the most efficient (lowest energy) precursor

and W = the average energy required to form an ion (or an

excited rare gas atom).

The quantum efficiency is defined as

$$\eta_Q = \frac{h\nu}{E} \qquad (1.26)$$

where $h\nu$ is the energy of a laser photon.

Thus,

$$\eta_I = \eta_P \cdot \eta_Q \qquad (1.27)$$

For KrF in argon [15]:

$$\eta_I(MAX) = 25\% \qquad \text{(e-beam)}$$

$$\eta_I(MAX) \geq 40\% \qquad \text{(discharge)}$$

Maximum intrinsic efficiency corresponds to a situation of minimum kinetic losses and the highest possible extraction of laser energy. It is because the kinetic losses (e.g. losses by inelastic electron collisions in the plasma) are lower in the discharge pumped gas mixture, that the high intrinsic efficiency is in principle possible with these systems. Despite this, the highest reported intrinsic efficiency (15%) is obtained from an e-beam pumped KrF laser [54]. The poorer intrinsic efficiencies obtained to date from discharge lasers are due primarily to low energy extraction efficiency [15]. (Because of transient absorbers formed in the discharge plasma). For the highest reported output energy from an e-beam sustained discharge KrF laser, the extraction efficiency was only 10%. It seems therefore that until energy extraction from long discharge chambers can be increased, the e-beam pumped rare-gas halide laser will remain the amplifier yielding the highest energy output.

1.16 Applications

Large rare-gas halide amplifiers are needed if ultraviolet lasers are to be used for fusion applications. Analysis of plasma interactions in deuterium-tritium fusion targets indicate that optimum wavelengths for improved plasma compression are in the short wavelength spectral region [60, 61]. Rare-gas halide lasers are being developed for this purpose as an alternative to multiplying the frequency of solid state lasers to obtain the shorter wavelengths (e.g. at Lawrence Livermore Laboratory). Considerable effort has therefore been directed towards maximising the energy extraction from rare-gas halide lasers, notably KrF since this has given the best results so far.

XeCl as a lasing medium has also received considerable attention. XeCl lasers are used to amplify narrow linewidth pulses from a XeCl oscillator, or from a frequency doubled dye laser, for the purpose of remote sensing of OH in the upper atmosphere. This system may be used in space on board a NASA space shuttle [62].

Other possible applications of large scale rare-gas halide lasers include communications with submarines using visible transitions such as the C-A transition in XeF at λ = 460nm [63], which is near the optical transmission window in sea water. Although several other laser systems operate at these wavelengths, the use of excimer lasers is preferred since these are more powerful and can be used with greater ease under field conditions [20].

Future prospects in the laser field itself could be the use of u.v. laser pulses of high power to generate coherent x-rays by multi-photon processes.

1.17 Conclusion

Since the rare-gas halide laser was introduced in 1975, research in this field has been extensive. The kinetic pathways leading to formation of the excimer molecules are now fairly well understood. The knowledge gained has led to improved efficiency and increased energy extraction from these lasers. Spectroscopic studies have revealed additional laser candidates with the discovery of triatomic species.

The wavelength range of some rare-gas halide lasers has been extended by the method of elevating the temperature of the active medium. Lasing from more than one electronic level has also been observed, further increasing the wavelength range to the visible spectral region.

Pumping is achieved using electron beams or electric discharges as excitation sources. The former offers the highest pump power density, while the latter is superior in pulse repetition frequency. Large scale systems are therefore likely to be e-beam pumped, while lower energy systems for applications requiring high repetition rates are likely to be discharge pumped.

The development of electron beam sustained discharge lasers has rendered it possible to operate systems with long gain duration. The work on generation of short pulses described in this thesis is particularly relevant to lasers with long gain duration. The extension of the methods described here to e-beam sustained discharge systems should be straightforward.

CHAPTER 1 - References

1 F.G. Houtermans, Helv. Phys. Acta 33, 933 (1960)

2 N.G. Basov, V.A. Danilychev and Y.M Popov, Soviet J. Quantum Electron. 1, 18 (1971)

3 R. Hunter: 7th Winter Colloquium on High Power Visible Lasers, Park City, Utah (1977) and Reference 15

4 W.K. Bishel, J. Bokor, D.J. Kligler and C.K. Rhodes, IEEE J. Quant. Electron., QE-15, 380 (1979)

5 J. Reintjes, Optics Letters, 5, 342 (1980)

6 Osamo Uchino and Mitsuo Maeda, Appl. Phys. Lett., 33, 807 (1978)

7 Giora Yaron and La Verne D. Hess, Appl. Phys. Lett. 36, 220 (1980)

8 H.L. Chen, Lawrence Livermore Laboratory, Private Communication

9 J.E. Velazco and D.W. Setser, J. Chemical Phys., 62, 1990 (1975)

10 M.F. Golde and B.A. Thrush, Chem. Phys. Lett., 29, 486 (1974)

11 S.K. Searles and G.A. Hart, Appl. Phys. Lett., 27, 243 (1975)

12 J.J. Ewing and C.A. Brau, Appl. Phys. Lett, 27, 350 (1975)

13 E.R. Ault, R.S. Bradford Jr. and M.L. Bhaumik, Appl. Phys. Lett., 27, 413 (1975)

14 C.A. Brau and J.J. Ewing, Appl. Phys. Lett, 27,435 (1975)

15 Excimer Lasers, Ed. C.K. Rhodes, Topics in Applied Physics, Vol.30, Chapter 2 and Chapter 4, Springer Verlag (1979)

16 T. Varghese, PhD Thesis, University of London (1981)

17 M.J. Shaw, Prog. Quant. Electron., 6, 3 (1979)

18 P.J. Hay and T.H. Dunning Jr., J. Chem. Phys, 69, 2209 (1978)

19 H.J. Kolts and D.W. Setser, J. Phys. Chem., 82, 1766 (1978)

20 Laser Focus, 28, April (1981)

21 J. Tellinghuisen, J.M. Hoffman, G.C. Tisone and A.K. Hays, J. Chem. Phys. 64, 2484 (1976)

22 J. Tellinghuisen, J.M. Hoffman, G.C. Tisone and A.L. Hays, J. Chem. Phys., 64, 4796 (1976)

23 M. Rokni, J.A. Mangano, J.H. Jacob and J.C. Hsia, IEEE J. Quant. Electron., QE-14, 464 (1978)

24 J. Tellinghuisen, A.K. Hays, J.M. Hoffman and G.C. Tisone, J. Chem. Phys. 65, 4473 (1976)

25 C.A. Brau and J.J. Ewing, J. Chem. Phys., 63, 4640 (1975)

26 J.C. Hsia, J.A. Mangano, J.H. Jacob and M. Rokni, Appl. Phys. Lett., 34, 208 (1979)

27 J.R. Murray and H.T. Powell, Appl. Phys. Lett., 29, 252 (1976)

28 T.H. Dunning and P.J. Hay, Appl. Phys. Lett., 28, 649 (1976)

29 W.K. Bischel, H.H. Nakano, D.J. Eckstrom, R.M. Hill, D.L. Huestis and D.C. Lorents, Appl. Phys. Lett., 34, 565 (1979)

30 N.G. Basov, V.S. Zuev, A.V. Kanaev, L.D. Mikheev and D.B.Stavrovskii, Soviet J. Quant. Electron., 9, 629 (1979)

31 M. Rokni, J.H. Jacob, J.C. Hsia and D.W. Trainor, Appl. Phys. Lett., 35, 729 (1979)

32 T.R. Loree, K.B. Butterfield and D.L. Barker, Appl. Phys. Lett., 32, 171 (1978)

33 James B. Laudenslager, Thomas J. Pacala and I. Stuart McDermid, Paper presented at C.L.E.O. (1981)

34 Julius Goldhar, W.R. Rapoport and J.R. Murray, IEEE J. Quant. Electron., QE-16, 235 (1980)

35 H. Egger, T. Srinivasan, K. Hohla, H. Scheingraber, C.R. Vidal, H. Pummer and C.K. Rhodes, Appl. Phys. Lett., 39, 37 (1981)

36 K.Y. Tang, D.C. Lorents and D.L. Huestis, Appl. Phys. Lett, 36, 347 (1980)

37 F.K. Titel, W.L. Wilson and R.E. Stickel, Appl. Phys. Lett., 36, 405 (1980)

38 J.G. Eden and S.K. Searles, Appl. Phys. Lett., 30, 287 (1977)

39 R. Burnham and N.W. Harris, J. Chem. Phys., 66, 2742 (1977)

40 R. Burnham and S.K. Searles, J. Chem. Phys., 67, 5967 (1977)

41 E.D. Poliakoff, S.H. Southworth, M.G. White, G. Thornton, R.A. Rosenberg and D.A. Shirley, J. Chem. Phys., 72, 1786 (1980)

42 D.C. Lorents, D.L. Huestis, M.V. McCusker, H.H. Nakano and R.M. Hill, J. Chem. Phys., 68, 4657 (1978)

43 R.W. Waynant and J.G. Eden, IEEE J. Quant. Electron., QE-15, 61 (1979)

44 A.E. Greene and C.A. Brau, IEEE. J. Quant. Electron., QE-14, 951 (1978)

45 J.E. Velazco, J.H. Kolts and D.W. Setser, J. Chem. Phys., 65, 3468 (1976)

46 M. Rokni, J.H. Jacob, J.A. Mangano and R. Brochu, Appl. Phys. Lett. 31, 79 (1977)

47 A. Mandl andJ.J. Ewing, Rev. Sci. Instr., 48, 1434 (1977)

48 J.J. Ramirez and K.R. Prestwick, J. Appl. Phys., 50, 4988 (1979)

49 C.D.P. Levy, PhD Thesis, University of London (1980)

50 R. Burnham and N. Djeu, Appl. Phys. Lett., 29, 707 (1976)

51 A.J. Andrews, A.J. Kearsley, C.E. Webb and S.C. Haydon, Opt. Comm., 14, 1 (1975)

52 Jeffrey L. Levatter, Karin L. Robertson and Shao-Chi Lin, Appl. Phys. Lett., 39, 297 (1981)

53 J.A. Mangano and J.H. Jacob, Appl. Phys. Lett., 27, 495 (1975)

54 L.F. Champagne, J.G. Eden, N.W. Harris, N. Djeu and S.K. Searles, Appl. Phys. Lett, 30, 160 (1977)

55 Malcolm C. Gower, Andrew J. Kearsley and Colin E. Webb, IEEE. J. Quant. Electron.,QE-16, 231 (1980)

56 Ehud Zamir, David L. Huestis, Howard H. Nakano, Robert M. Hill and Donald C. Lorents, IEEE J. Quant. Electron., QE-15, 281 (1979)

57 Chapter 3, this thesis

58 M.L. Blaumik, R.S. Bradford Jr. and E.R. Ault, Appl. Phys. Lett, 28, 23 (1976)

59 R.S. Taylor, S. Watnabe, A.J. Alcock, K.E. Leopold and P.B. Carkum, C.L.E.O. (1981)

60 W.T. Toner, Rutherford Laboratory Report, RL-81-040, 402 (1981)

61 R.O. Goodwin, W.F. Hagen, J.F. Holzrichter, W.W. Simmons and J.B. Trenholme, Laser Focus, 58, May (1981)

62 Jet Propulsion Laboratory (N.A.S.A.), Private communication (1981)

63 S.R.I. International, Private communciation (1981)

64 Thom. H. Dunning and P. Jeffrey Hay, J. Chem. Phys., 69, 134 (1978)

CHAPTER 2

THE PROBE LASER

2.1 Introduction

Tunable dye lasers have been shown to be superior to conventional light sources in the study of absorption and emission spectra in different elements [1, 2, 3] since the dye laser offers a high power collimated and narrow linewidth probe beam. Trains of picosecond pulses provide an excellent source to time resolve fast transient phenomena such as absorption and relaxation processes [4, 5]. This is the type of application relevant to this thesis.

When the dye laser was reported in 1966 [6], it was the first laser that could be tuned over a wide continuous wavelength range. Since then it has proved to be an attractive laser source in more than this respect. The active medium is cheap and versatile and can be used in the solid, liquid or gaseous phase. The liquid phase of operation is the most widely used and provides a laser medium of high optical quality, since heating problems can be avoided by the use of simple cooling systems where the dye flows through a heat exchanger.

Pulsed dye lasers can be flashlamp pumped or pumped with other pulsed lasers. C.W. operation has been made possible by pumping the dye with C.W. lasers (e.g. Argon-ion or Krypton-ion lasers). A wide range of pulsed and C.W. systems are commercially available. Pulsed dye lasers are available in a continuous wavelength range extending from the ultraviolet to the near infrared.

The dye laser is capable of channeling high energy into a very

narrow spectral width. By inserting several wavelength selecting elements in the cavity, single-mode operation is possible [7]. High spectral power can then be attained by injection frequency locking of the narrow line output from an oscillator in a chain of amplifiers [8, 9, 10].

Because dye lasers have large spectral bandwidths, pulses of subpicosecond duration can be generated. A C.W. ring laser recently produced pulses of < 0.1 ps duration in a passive mode-locking arrangement where the two pulses travelling in opposite direction in the ring cavity were made to collide in the saturable absorber dye jet [11].

In this chapter a description of the flashlamp pumped dye laser is given. The process of tuning and second harmonic generation are briefly reviewed. A theoretical outline of passive mode-locking followed by a description of the electron-optical streak camera measurement technique is also included, since this forms a reference for the later chapters on generation and measurement of mode-locked pulses from the XeCl laser.

2.2 The flashlamp pumped dye laser

The photo-physics and spectroscopy of organic dye lasers have been extensively reviewed and will not be dealt with here [12]. The most important feature of the dye molecule that should be mentioned, is the characteristic broad absorption band in the u.v. and visible spectral region and the equally broad fluorescence band that is generated when some dyes are dissolved in solution. Because the absorption band in organic dyes is broad, the same type of flashlamps can be used to pump different dyes. (Since the output from the flashlamp will overlap

at least part of the absorption spectrum). The tuning range of the laser can therefore be extended to cover the whole spectrum from the ultraviolet to the infrared by changing the dye in the laser. Rhodamine 6G ($\lambda \sim$ 570nm - 620 nm) is the most efficient of the organic dyes. When frequency doubled, the Rhodamine 6G laser can be tuned to overlap most of the vibrational transitions in XeCl. This dye was therefore used in the experiments described in this thesis.

Because of the near continuum of vibrational and rotational levels that are populated in the dye molecule, the emission band is very broad and gives rise to the desired tunability. The lifetime of the upper electronic level is typically only a few nanoseconds which means that the dye laser is not capable of storing energy as in giant pulse systems. Very high powers can however be generated if another (or several) flash-lamp pumped dye laser is used as an amplifier [13].

The flashlamp pumped dye laser head consists of a dye flowing in a quartz cuvette surrounded by flashlamps and a reflector. The latter serves to concentrate the diffuse light emitted by the flashlamp onto the dye cell. Several configurations are in use, the aim being efficient and uniform pumping of the dye. Elliptical reflectors imaging the light from the linear flashlamp placed at one focus of the ellipse onto the dye cell at the other focus is a popular design [14]. Other alternatives are several flashlamps placed symmetrically around the dye cell in a close coupling arrangement, coaxial flashlamps [15], or a helical flashlamp surrounding the dye cuvette. Fig.2.1 illustrates a laser head of elliptical reflector geometry (double ellipse).

Ethanol is frequently used as a dye solvent. The only disadvantage with alcohol is its relatively poor thermal properties. If the active medium must

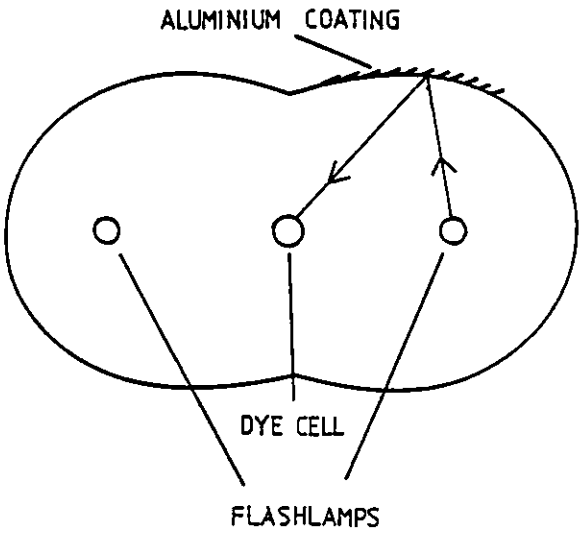

Fig. 2.1. Elliptical geometry reflector

be of very good optical quality, water is used instead.
The dye cell is cooled by flowing the dye through a cooling reservoir and in some cases the dye cell itself is surrounded by a cooling liquid (ethanol, water) in another quartz cell. (This also serves to improve focusing of the pump light onto the dye solution). Cooling of the dye is important due to the heat given off to the solvent by non-radiative de-excitation of the dye molecule [16]. Thermal inhomogenieties result in poor beam quality which is particularly undesirable in probe experiments where the beam profile should be uniform and reproducible .

Several different types of flashlamps are available commercially. The simplest of these is the xenon lamp, but for very high pump powers ablative wall lamps are often used [17]. The flashlamps are operated in conjunction with high voltage capacitors and a spark gap (or thyratron valve). If circuit inductance is minimized, risetimes as short as a few hundred nanoseconds can be attained. Depending on the powersupply, repetition rates of up to 100Hz are possible. With high repetition rates the flashlamps must be cooled by circulating water in a quartz envelope surrounding the lamp. The lifetime of commercial xenon flashlamps can be over a million shots. The lifetime of the Rhodamine 6G dye in solution is, however, limited to less than this (depending on the active volume and on the wavelength of the pump) since the molecules dissociate when irradiated by u.v. light. Thus the dye solution has to be changed after a suitable period of time.

Flashlamp pumped dye lasers are the cheapest tunable laser sources available. Because the output from the flaslamps partly overlaps the absorption spectrum of most dyes, this type of laser also represents the most versatile system. Output powers range from microjoules to several joules, and pulse durations from picoseconds to microseconds, depending on the mode of operation. In particular, these lasers are suitable for the type of probe measurements performed in this work, where the probe laser had to be incorporated in existing laboratory configurations. Since the mode-locked dye laser is relatively small and convenient to operate, this posed no problem. Mode-locking techniques for flashlamp pumped dye lasers are well established, and the laser provides reproducible output pulses under most operating conditions.

2.3 The twin lamp mode-locked Rhodamine 6G laser

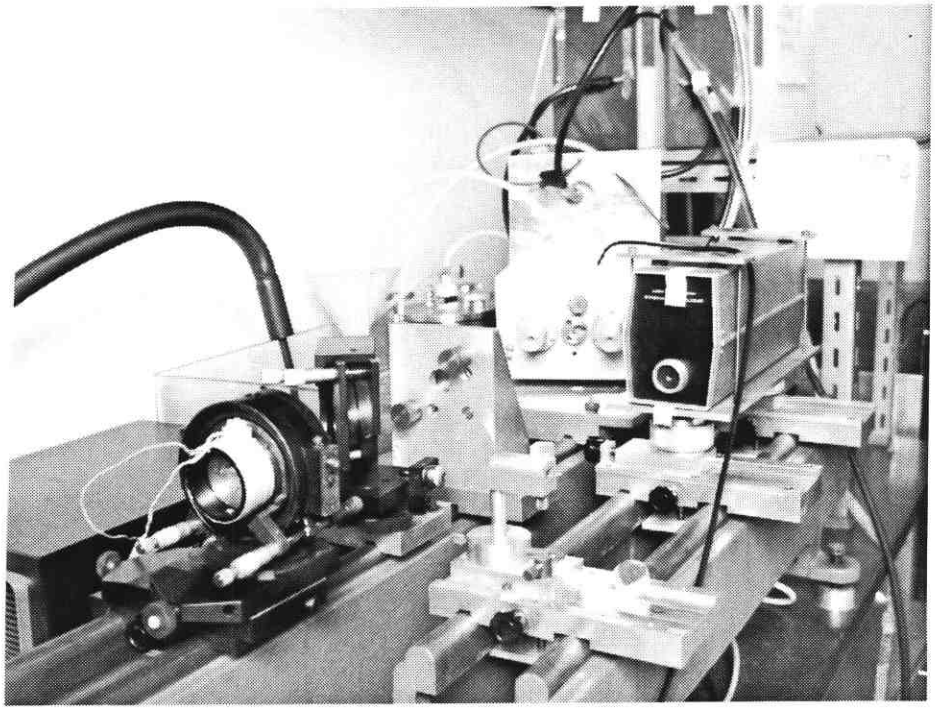

Fig. 2.2. The flashlamp pumped dye laser.

Fig. 2.2 shows the flashlamp pumped dye laser used throughout this work with the frequency doubling crystal situated in a temperature controlled oven in front of the laser head. The laser utilized a double elliptical reflector geometry as shown in Fig. 2.1. The two linear xenon flashlamps (English Electric, GAA12) were placed at the extreme ellipse foci and the 17cm long quartz dye cell

(∿ 4mm i/d, ∿ 8mm o/d) at the shared focus of the double ellipse. The quartz windows were Brewster angled. No cooling was needed for the flashlamps, since the laser was a single shot system and the lamps thus had time to cool between shots (∿ 1-2 minutes). The Rhodamine 6G dye was dissolved in distilled water (1.5×10^{-4} M/L) with 5% Ammonyx-LO (N, N Dimethyldodecylamine-N-oxide) and circulated through a cooling bath. (The Ammonyx-LO was added in order to prevent dimerisation of the Rh 6G molecules which inhibits lasing). The beam divergence of the laser had previously been measured to be ∿ 3-5 milliradians.

The resonator was completed by a ∿ 50% reflectivety dielectric coated output coupler and a ∿ 100% reflectivity back mirror. The mode-locking dye cell was contacted onto the latter in a ∿ 2mm thick cuvette (wedged to prevent the formation of a sub-cavity). The saturable absorber used was DODCI (3,3 diethyloxadicarbo- cyanine iodine) in an ethanolic solution. The concentration was ∿ 10^{-4} M/L and the mode-locking dye was not flowed since the laser did not operate at a repetition rate. Fig. 2.3a illustrates the resonator.

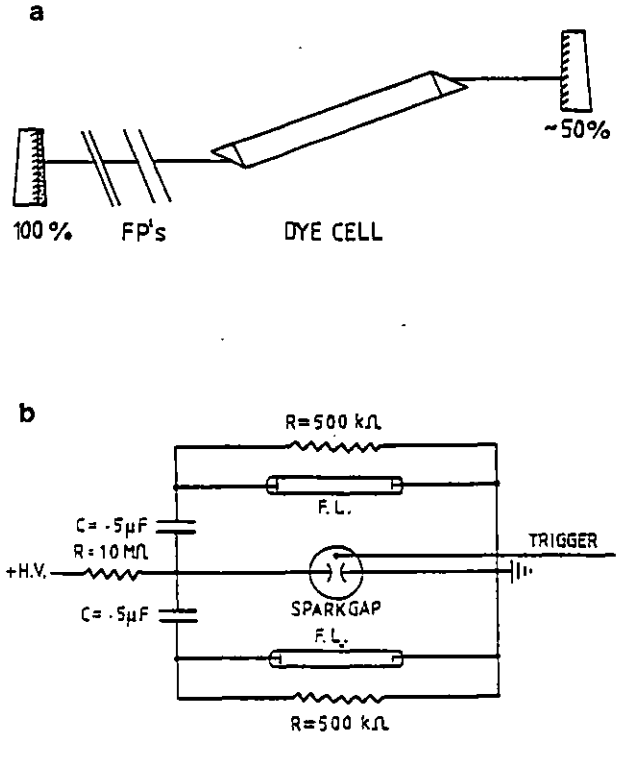

The electrical energy dissipated in each flashlamp was ∿ 100J, stored in 0.5μF capacitors (Hivatronic 30kV) that were connected in series with the two flashlamps. A spark gap (type EGG 32B) triggered the lamps. Fig. 2.3b shows the electrical circuit.

Fig. 2.3
The dye laser resonator and electrical circuit

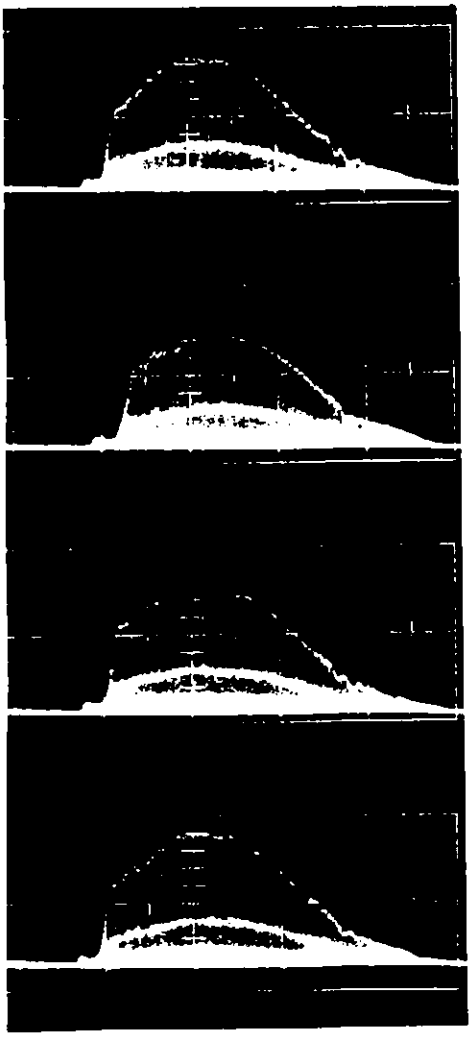

Fig. 2.4. Oscillogram of dye laser pulse trains (500ns/div).

The energy output of the non mode-locked laser reached ∿ 100mJ in a 1.5μs pulse at 25kV charging voltage. The energy of the mode-locked output was ∿ 10mJ at the same charging voltage. An estimate of the energy per mode-locked pulse indicated a peak energy ∿ 20μJ/pulse. Reducing the saturable absorber dye concentration did not change the energy content in the pulses significantly, but did lead to longer pulse trains and ultimately to double pulsing. The mode-locked output was very reproducible as seen in Fig. 2.4 where four consecutive pulse trains are shown on a 500 ns/div timescale (Tektronix 519 oscilloscope).

2.4 Tuning

Tuning of the mode-locked dye laser was achieved by employing one or two intracavity Fabry-Perot etalons. The Fabry-Perot elements were slightly tilted to avoid the formation of subcavities. The free spectral range (F.S.R.) of the Fabry-Perot is the wavelength difference between successive transmitted maxima and is defined as

$$\text{F.S.R.} = \lambda^2/2d\cos\theta \qquad (2.1)$$

where λ = peak wavelength

d = etalon spacing

θ = beam angle of incidence

When two Fabry-Perots are used, the etalon spacing must be chosen such that the free spectral range of one etalon is greater than the bandwidth of the other in order to ensure that only one narrow bandwidth maxima is transmitted through the two etalons. In our case the etalon spacings were 5μm and 50μm respectively.

The bandwidth of the transmitted maxima depends on the finesse of the etalon. This is defined as

$$\text{finesse} = \text{F.S.R.}/\Delta\lambda = \frac{\pi\sqrt{R}}{1-R} \qquad (2.2)$$

where R is the reflectivity of the etalon plates. The latter was 65% and the finesse of our etalons was thus ∿ 7.

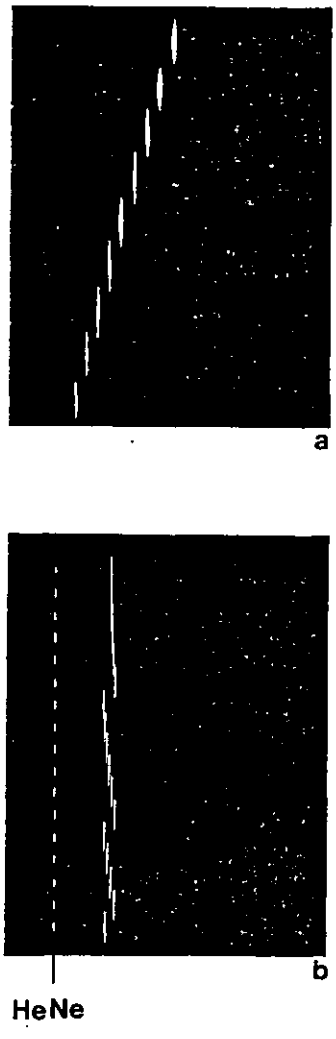

With one 5μm Fabry-Perot in the cavity the linewidth of the mode-locked laser output was ∿ 20Å, with both etalons the bandwidth reduced to ∿ 5Å. Fig. 2.5a shows the spectrum of the mode-locked laser which was tuned from ∿ 627nm to ∿ 598nm by adjusting the angle of the single 5μm Fabry-Perot. Fig. 2.5b shows the mode-locked laser output spectrum with two etalons in the cavity. In this case the angle of the second 50μm etalon was adjusted sufficiently to move three successive maxima (i.e. 3 F.S.R.) through the bandpass of the first etalon. The spectra were recorded on a .5m Hilger and Watts grating spectrograph and photographed on Polaroid 107 film.

Fig. 2.5. Dye laser spectra

2.5 Second harmonic generation

The limited number of dyes and pumping sources available means that the tuning range of dye lasers does not extend further into the ultraviolet spectral region than ∿ 340nm. It is, however, possible to convert the output from standard or mode-locked dye lasers by frequency conversion in nonlinear crystals. The second harmonic frequency can be generated in birefringent crystals (such as ADP; ammonium dihydrogen phosphate or KDP; potassium dihydrogen phosphate).

A near continuous range of ultraviolet wavelengths from ∿ 240nm to 340nm is available by frequency doubling of different dye lasers [18]. This renders the dye laser very attractive for the study of excimer lasers, and second harmonic generation is therefore an important process in this type of dye laser application.

When a uniaxial anisotropic crystal is subjected to an intense varying electric field, the atoms in the medium become polarized. The nonlinear induced polarization can be expressed as

$$P = \varepsilon_o (\chi_1 E + \chi_2 E^2 + \chi_3 E^3 + ...) \qquad (2.3)$$

where χ_1, χ_2, χ_3 are the nonlinear susceptibileties and E is the electric field. It is the second term that is responsible for second harmonic generation. If the applied optical field is of the form $E = E_o \sin \omega t$ the second term in 2.3 becomes

$$P^{2\omega} = \varepsilon_o \chi_2 E_o^2 \sin^2 \omega t = \tfrac{1}{2}[\varepsilon_o \chi_2 E_o^2 (1-\cos 2\omega t)] \qquad (2.4)$$

In isotropic crystals, all even terms of E vanish, hence second harmonic generation is only possible in anisotropic media. In general $\underline{P}$ and $\underline{E}$ are not parallel. In the uniaxial anisotropic crystal, such as ADP and KDP, this means that the dielectric constant in the z-direction

is different to the dielectric constant in the x and y-direction: $\varepsilon_x = \varepsilon_y \neq \varepsilon_z$. The crystal is then birefringent and for an optical wave propagating in the crystal two directions of polarization satisfy Maxwell's equations. The two allowed directions of polarization have different refractive indices, the ordinary (n_o) and extraordinary (n_e) refractive index.

Because of the two refractive indices it is possible to find a direction of propagation such that $n_o^{1\omega} = n_e^{2\omega}$. The fundamental frequency wave will for this direction of propagation stay in phase with the second harmonic wave it generates. This allowes the superposition of the second harmonic wave at the exit of the crystal by constructive interference. The phase matching condition $n_o^{1\omega} = n_e^{2\omega}$ can be satisfied by choosing the correct angular direction of the light wave propagating through the crystal (angle-tuned) and/or by accurate control of the crystal temperature (since the refractive index varies with temperature) (temperature-tuned). The expression for the second harmonic power per unit area as a function of propagation distance z is

$$I^{2\omega} = \frac{(2\omega)^2(\tfrac{1}{2}\chi_2)^2(I^{1\omega})^2}{2(n^{1\omega})^2 n^{2\omega} c^3 \varepsilon_o} \left[\frac{\sin(\omega/c|n^{1\omega}-n^{2\omega}|z)}{\omega/c|n^{1\omega}-n^{2\omega}|}\right]^2 \qquad (2.5)$$

Clearly, the second harmonic power is maximised when the phase matching condition $n^{1\omega} = n^{2\omega}$ is satisfied. Since perfect phase matching is only possible for single frequencies, the conversion efficiency will be lower for lasers with broad bandwidths. The conversion efficiency for mode-locked pulses should therefore be reduced since the bandwidth is generally broadened. The second harmonic intensity does, however, depend on the square of the intensity of the fundamental wave. The latter will be higher for ultrashort pulses than for long duration pulses, thus making up for the loss of efficiency due to the large bandwidth.

The output from the mode-locked Rhodamine 6G laser described in the previous section was frequency doubled in a 2.5cm long angle-tuned ADP crystal. The crystal was cut at $\sim 60^{\circ}$ relative to the optic axis. The correct phase matching angle could be found by varying the angle of the crystal face to the input beam. It was important to keep the crystal at a constant temperature in order to avoid variations in refractive index (and hence in wavelength of the probe laser). ADP is hygroscopic and the constant temperature of the oven mount was therefore kept high ($33\pm.5^{\circ}$C) to prevent water vapour from forming on the crystal surface. Fig. 2.6 shows the possible crystal angles for a mode-locked input beam tuned to 616nm by a single 5μm Fabry-Perot etalon. (Bandwidth ~ 20Å). The bandwidth of the second harmonic signal generated was only ~ 3Å, illustrating lack of phase-matching for the remainder of the input spectrum.

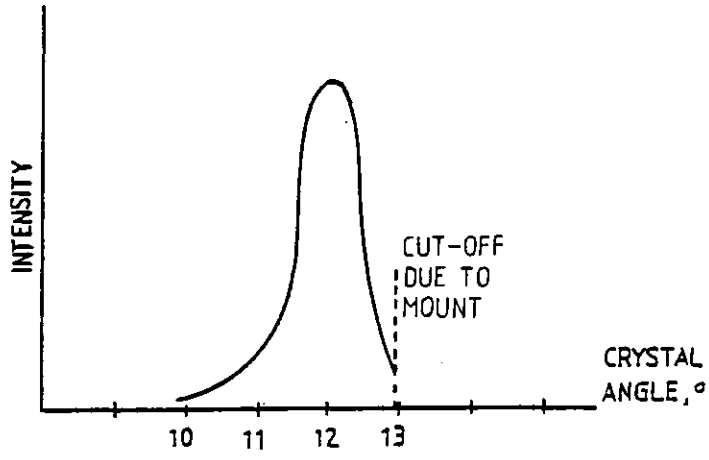

Fig. 2.6. Second harmonic signal varying with crystal angle.

The conversion efficiency could not readily be estimated by comparing the energy of the fundamental and second harmonic output since the u.v. pulse train was not intense enough to register with a calorimeter. From single pulse energy measurements performed at a later stage, we estimated the conversion efficiency to be $\sim$ 5-10%. With two etalons in the dye laser, the bandwidth of the input beam was ~ 5Å and the bandwidth of the second harmonic signal ~ 1Å. The conversion efficiency

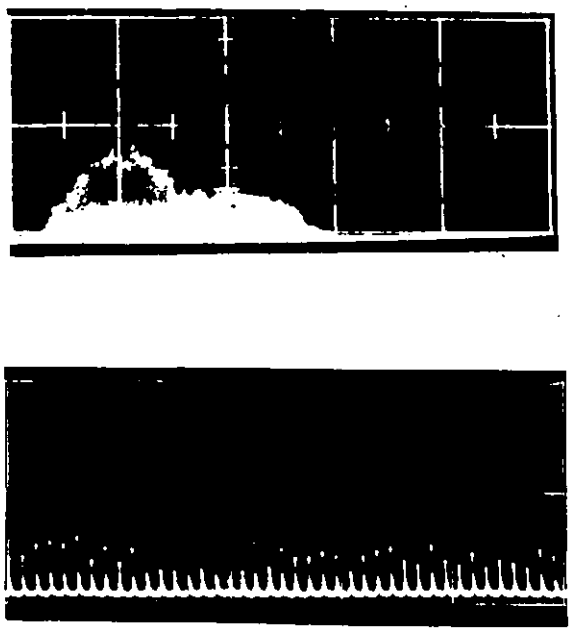

Fig. 2.7.Second harmonic pulse trains

was then slightly higher. Fig. 2.7 shows oscillograms of the second harmonic pulse train on a 200ns/div, 50 ns/div and 10ns/div time-scale (Tektronix 519 oscilloscope). The profile of the pulse train is less smooth than the fundamental train due to the dependence of the second harmonic intensity on the square of the fundamental power. (See Equation 2.5).

The second harmonic of the Rhodamine 6G wavelengths from $\sim$ 600-620nm overlap the fluorescence and lasing spectrum of the XeCl excimer laser. Hence by adjusting the Fabry-Perot etalons in the dye laser cavity as well as the angle of the ADP crystal, the system could be tuned to provide a u.v. pulse train overlapping any desired transition in XeCl. The mode-locked pulses could then serve as probe pulses for absorption or gain studies by splitting the pulse train in two and comparing the amplitude of a pulse having probed the XeCl laser with the pulse directly incident on the detector. The mode-locked pulse provides a "delta function" probe that superposes on any slowly varying background noise signal in the detector. Any variation in amplitude due to absorption or amplification could easily be measured by measuring the height of the pulse on the oscilloscope trace. Since a new probe pulse is provided every $\sim$ 5ns from the dye laser pulse train, almost continous time resolution is

possible if several shots are taken. (Necessary due to the jitter in the arrival of the pulses relative to the gain in the XeCl laser). This method of probing was found superior to using a non mode-locked probe beam. This is particularly the case when the dye laser is used in conjunction with excimer lasers since the latter generate noise signals that are difficult to isolate and are indistinguishable from non mode-locked probe pulses on the oscilloscope trace.

2.6 Mode-locking theory

Perfect mode locking corresponds to a case where all the longitudinal modes in the laser are locked in phase at a certain position in the laser cavity. The output then consists of a series of pulses separated by the cavity roundtrip time. If the gain or loss of a laser is modulated at this frequency, a mode-locked output can be generated. (Active mode-locking). Gain modulation is frequently used as a method of mode-locking CW dye lasers. The laser is then pumped by a mode-locked gas laser with a pulse separation equal to the roundtrip time of the dye laser cavity, thus modulating the gain of the dye laser at the roundtrip frequency. Since no gain is available between the pump pulses, the dye laser output is also a mode-locked pulse train. Loss modulation by inserting an intracavity acousto-optic or electro-optic modulator driven at the roundtrip frequency is another widely used method of active mode-locking. Most C.W. gas lasers employ acousto-optic loss modulators [19].

The pulses generated by active mode-locking are generally not as short as those obtained in passively mode-locked systems [20]. Passive mode-locking is however, only possible if a saturable absorber can be

found that has an absorption spectrum which overlaps the emission spectrum of the particular laser. For u.v. and i.r. lasers such dyes are not generally available. Other criteria must also be satisfied: preferably the recovery time of the absorber (i.e. the "gate-opening time")must be short. If this is not so, other pulse shortening mechanisms must be present in order to obtain ultrashort pulses. The absorption cross section should also be of the right magnitude; if this is low very high intensities are required to bleach the dye and saturation is less likely to take place.

Passive mode-locking has been used successfully in mode-locking of giant pulse lasers (Neodymium and Ruby lasers) and dye lasers such as the Rhodamine 6G laser. The bandwidth-pulse duration product of the latter imply that, theoretically, pulses of a few femtoseconds duration should be possible. To date the shortest pulses reported are < 0.1ps in duration [11].

When passive mode-locking is considered in the time domain, the standing wave modes existing in the cavity are replaced by groups of photons travelling in the resonator. This method of investigating the temporal profile of the pulses directly, is less complicated than describing the pulse shortening process in the frequency domain where a knowledge of the phase of the modes is required.. In the time domain the cavity flux is thought of as initially consisting of random fluorescence fluctuations of typical duration as short as the inverse of the bandwidth of the laser. The noise"spikes"are absorbed by the saturable absorber until the intensities are sufficiently high, due to amplification in the active medium, to saturate the mode-locking dye which is normally contacted to the 100% reflector. If the recovery time of the dye is fast, the dye will not stay bleached for a long

enough period to transmit other intense noise fluctuations and only a few short duration spikes are fed back into the active medium.

With each roundtrip in the laser a part of the leading edge of the "pulse" or group of "spikes" is absorbed by the mode-locking dye, thus sharpening the leading edge. Several such groups of intense "spikes" can develop and travel up and down the amplifier; the laser output will then consist of several interleaved pulse trains and the laser is "multiple pulsing". If the laser is kept near threshold, however, New et al. have shown in a theoretical simulation that the parameters can be chosen such that only one intense noise spike will develop and the output consist of a single train of ultrashort pulses [21, 22].

New and other workers have also shown that in dye lasers the process of gain saturation is as important as saturable absorption in the formation of ultrashort pulses [23, 24]. Since the recovery time of saturable absorbers used in conjunction with dye lasers is much longer than the pulse durations obtained, the short pulses could not have developed without an additional pulse shortening mechanism also taking place. It can be shown by rate equation approximation that if the recovery time of the active medium is of the order of the cavity roundtrip time and much greater than the recovery time of the saturable absorber ($T_a \sim T_{cav} >> T_b$), a pulse formed in the cavity will have its trailing edge sharpened by gain saturation. The reason for this is simply that if the small signal gain in the laser is high and the pulse intense, the leading edge will saturate the gain, and the trailing edge will not be amplified. Sharpening of the whole pulse is, however, only likely to occur if the amplified leading edge is restrained from "running away". This is achieved by sharpening of the leading edge by

saturable absorption. Thus if the pulse width is to be reduced, there must be a net loss at the leading and trailing edge of the pulse, whereas there is a net roundtrip gain at the peak. The peak is favoured if the absorber has saturated before the amplifier. Thus another requirement for net pulse shortening is that the absorber cross section be at least twice as large as the cross section for amplification ($\sigma_b/\sigma_a > 2$ for a collimated beam) [23, 24].

The requirements for pulse shortening are well satisfied for Rhodamine 6G dye lasers employing DODCI (3,3-diethyloxadicarbo-cyanine iodine) or DQOCI (1,3'-diethyl4,2'-Quinolyloxacarbocyanine iodine) as saturable absorbers. It has not yet been possible, however, to mode-lock many other dye lasers successfully due to the lack of suitable saturable absorbers. Extensive research is, however, being conducted in the field of laser dyes and several new candidates become available every year. Active mode-locking techniques can be used with pulsed and C.W. dye lasers, but the pulse durations obtained are not as short as with the systems employing saturable absorbers [25, 20].

2.7 Measurement of ultrashort pulse durations

The three most widely used methods of measuring the duration of ultrashort pulses are:

1) two photon fluorescence;
2) second harmonic generation;
3) electron-optical streak camera.

These methods have been extensively reviewed in the literature and only the streak camera will be discussed here since this is relevant to the work presented in this thesis [26, 27].

The only direct method of measuring the duration of picosecond pulses is employing an electron-optical streak camera. In this system photons incident on the streak camera photocathode are converted into electrons that are accelerated towards the anode of the camera. By applying a voltage ramp on deflection plates situated behind the anode (which is made with an aperture through which the electrons pass), the electrons are swept across a phosphor screen at the back of the streak camera tube. The temporal information in the optical pulse is thus converted into spatial information which can readily be measured. This can be achieved by intensifying the image at the phosphor with an image intensifier unit and recording the intensified image on film. Fig.2.8 shows a schematic diagram of the streak camera arrangement.

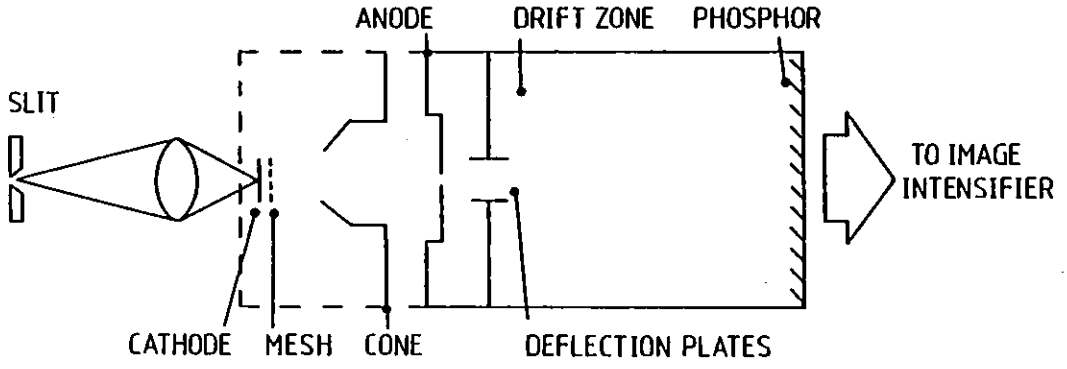

PHOTOCHRON II STREAK TUBE

Fig. 2.8. Schematic of the electron-optical streak camera

The streak camera resolution was initially limited to $\sim$ 20ps by the photo-electron transit time spread in the streak tube [28], given by

$$\Delta\tau_D = m\Delta V/eE \qquad (2.6)$$

where e, m = electron charge, mass

ΔV = half-width of initial electron velocity distribution.

In order to reduce the transit time spread, E must clearly be maximised. (The electrons then "forget" their initial velocities). When a camera

with a fine mesh extraction electrode at a high potential near the cathode was developed by Bradley [29], pulses as short as 5ps could be resolved. Presently streak cameras with ∿ 1ps resolution are commercially available.

The recorded pulse half-width can to an approximation be expressed as

$$\Delta\tau_R = ((\Delta\tau_s)^2 + (\Delta\tau_D)^2 + (\Delta\tau_p)^2)^{\frac{1}{2}} \qquad (2.7)$$

where $\Delta\tau_s = 1/v \cdot n$ is the time resolution limit due to the finite spatial resolution (n) of the image tube at a particular writing speed (v), $\Delta\tau_D$ is the transit spread resolution (Equation 2.6) and $\Delta\tau_p$ is the real pulse duration.

2.8 Temporal measurement using a Photochron II streak camera

The u.v. sensitive Photochron II streak camera with an S20 photocathode was used to determine the duration of the frequency doubled pulses from the passively mode-locked flashlamp pumped Rhodamine 6G dye laser described earlier. The laser was tuned to 308nm (the main XeCl laser transition) by a single 5μm Fabry-Perot etalon.

Assuming a dynamic spatial resolution of 10 lp/mm, and a transit time spread of ∿ 2ps, the resolution of the streak camera in this mode of operation should be ∿ 3ps. A four stage image intensifier (E.M.I. type T2001, 9914) was used in conjunction with the streak tube, thus intensifying the image ∿ 10^6 times. Fig. 5.9 shows a photograph of the streak camera and the image intensifier.

An avalanche transistor krytron circuit provided the voltage ramp (∿ 5kV) for the deflection plates. An optic fibre coupled part

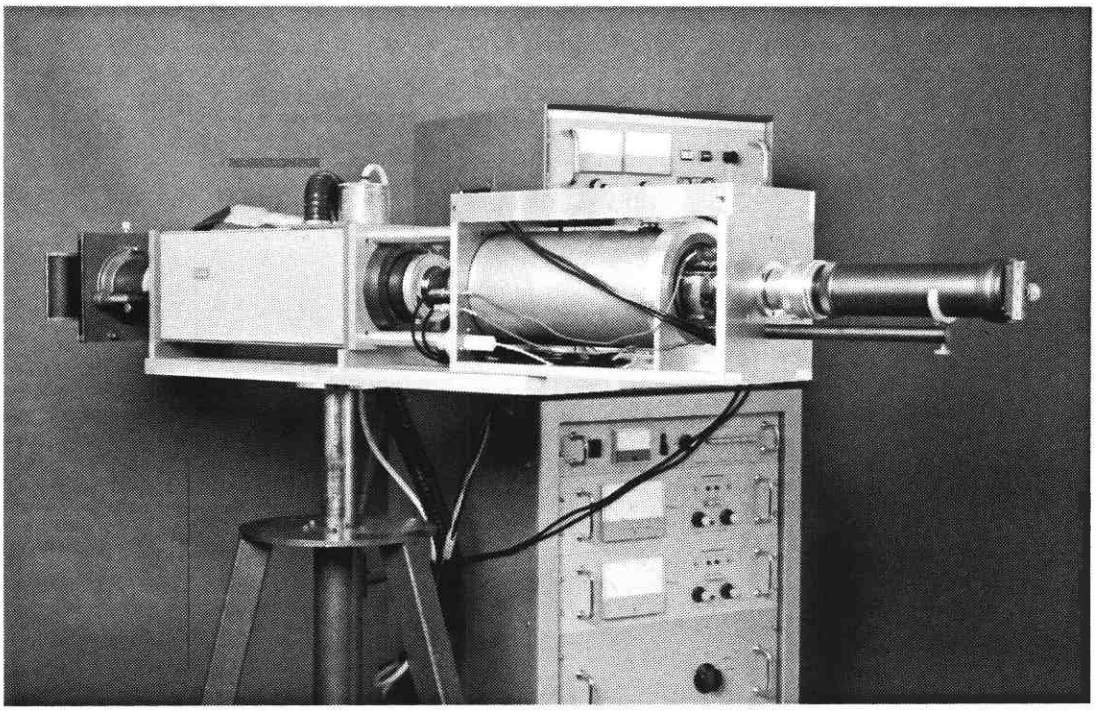

Fig. 2.9. The electron-optical streak camera and EMI image intensifier

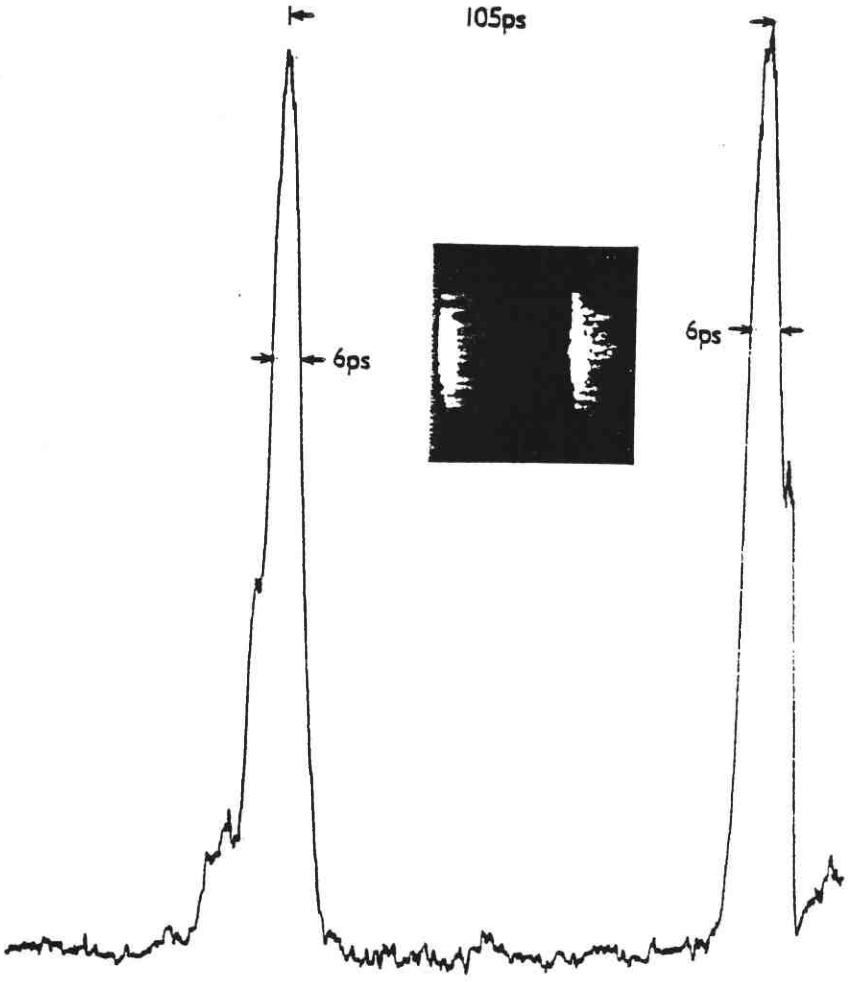

Fig. 2.10. Streaks and microdensitometer trace of dye laser pulses

of the dye laser flashlamp output into a trigger delay generator which triggered the krytron. The delay was chosen so that the ramp would sweep as the pulses in the middle of the dye laser train were incident on the streak camera slit (∿ 80μm wide). The second harmonic pulses were then focused onto the photocathode by the streak camera lenses.

The pulses were recorded on Kodak HP5 film and scanned using a Joyce-Loebl microdensitometer. The F.W.H.M. was determined by recording a neutral-density step-wedge on the same film as the streaks, and scanning this to find the appropriate half-intensity point. The shortest pulses were ∿ 6ps in duration and were not bandwidth limited. (The bandwidth limit for pulses of ∿ 3Å bandwidth is ∿ 0.5ps). The streak photograph together with a microdensitometer trace is shown in Fig.2.10.

2.9 Conclusion

A flashlamp pumped Rhodamine 6G dye laser was mode-locked using DODCI as a saturable absorber. The output was frequency doubled in ADP, thus generating a train of picosecond u.v. pulses. The laser was tuned by one or two Fabry-Perot etalons giving rise to a mode-locked second harmonic output of respectively ∿ 3Å and ∿ 1Å spectral width.

The output from the laser was very reproducible and the laser could readily be tuned to overlap vibrational transitions in the XeCl laser in order to time resolve absorption and amplification features of this laser. Since the second harmonic power depends on the square of the fundamental power, frequency doubling was more efficient with the mode-locked laser. The bandwidth of the u.v. mode-locked pulse train with two Fabry-Perot etalons in the dye laser was wide enough

to cover rotational structure of the XeCl vibrational bands, but narrow enough to distinguish between the bands. The relatively wide bandwidth generated with a mode-locked laser was therefore desired.

The mode-locked pulses were chosen as probe signals for the excimer laser experiments rather than the unmode-locked output from the dye laser, since the amplitude of the delta function shaped pulses is relatively simple to measure and since the very short duration probe pulses could be distinguished from any background noise signal in the detector and therefore represented a measurement free of distortion. The energy density in each pulse was considerably less than the saturation energy density quoted for XeCl and absorption and amplification measurements would therefore be in the linear regime.

Finally, the flashlamp pumped dye laser was simple to operate and could readily be assembled near the electron beam pumped XeCl laser or the discharge pumped XeCl laser that were to be studied.

CHAPTER 2 - References

1 E. Zamir, D. Huestis, H.H. Nakano, R.M. Hill and D.C. Lorents, IEEE J. Quant. Electron.,QE-15, 281 (1979)

2 T.W. Hansch, D.R. Lyons, A.L. Shawlow, A. Siegel, Z-Y. Wang and G-Y Yan, Submitted to Opt. Comm.

3 V. Sethu Raman, G.J. Small and E.S. Young, Rev. Sci. Instrum., 11, 1436 (1977)

4 I.V. Tomov, R. Fedosejevs, M.C. Richardson, W.J. Sarjeant, A.J. Alcock and K.E. Leopold, Appl. Phys. Lett., 31, 747 (1977)

5 Adam P. Bruckner, Appl. Opt., 17, 3177 (1978)

6 F.P. Schafer, W. Schmidt, J. Volze, Appl. Phys. Lett., 9, 306 (1966)

7 S. Blit, U. Ganiel and D. Treves, Appl. Phys. 12, 69 (1977)

8 M. Maeda, O. Uchino, T. Okada and Y. Miyazoe, Jap. Journ. Appl. Phys. 14, 1975 (1975)

9 M.M. Salour, Opt. Comm., 22, 202 (1977)

10 V. Ganiel, A. Hardy and D. Treves, IEEE J. Quant. Electron, QE-12,704(1976)

11 R.L. Fork, B.I. Greene and C.V. Shank, Appl. Phys. Lett., 38, 671 (1981)

12 Dye Lasers, Ed. F.P. Shäfer, Topics in Applied Physics, Vol. 1, Spring Verlag (1973)

13 R.S. Adrian, E.G. Arthurs, D.J. Bradley, A.G. Roddie and J.R. Taylor, Opt. Commun., 12, 140 (1974)

14 J.Y. Allain, Appl. Opt. 18, 287 (1979)

15 J. Bunkenburg, Rew. Sci. Instr., 43, 1611 (1972)

16 Kenneth Lee Matheson and James M. Thorne, Appl. Phys. Lett., 35, 314 (1979)

17 Roy Taylor, PhD Thesis, University of London (1974)

18 A. Hirth, K. Vollrath and J.Y. Allain, Opt. Commun., 20, 347 (1977)

19 L.L. Steinmetz, J.H. Richardson and B.W. Wallin, Apl. Phys. Lett., 33, 163 (1978)

20 J.P. Ryan, L.S. Goldberg and D.J. Bradley, Opt. Commun., 27, 127 (1978)

21 G.H.C. New and D.H. Rea, J. Appl. Phys., 47, 3107 (1976)

22 G.H.C. New, K.E. Orkney and M.J.W. Nock, Opt. and Quant. Electronics, 8, 425 (1976)

23 G.H.C. New, Opt. Commun., 6, 188 (1972)

24 G.H.C. New, IEEE J. Quant. Electron. QE-10, 115 (1974)

25 W. Margulis, W. Sibbett and J.R. Taylor, Opt. Commun., 35, 135 (1980)

26 D.J. Bradley, Opto-electronics, 6, 25 (1974)

27 Ultrashort Light Pulses, Ed. L. Shapiro, Topics in Applied Physics, Vol. 18, Springer Verlag (1977)

28 D.J. Bradley and G.H.C. New, Proc. IEEE, 313 (1974)

29 D.J. Bradley, U.K. Provisional Patent Spec. 31 167/70 (1970)
U.S. Patent 3761 614 (1973)

CHAPTER 3

PICOSECOND AMPLIFICATION AND ABSORPTION IN THE ELECTRON BEAM PUMPED XeCl LASER

3.1 Introduction

In order to scale rare-gas halide lasers to large volumes for applications such as nuclear fusion, electron beam pumping and efficient energy extraction is needed. Several important rare-gas halide molecules; XeF, XeCl and possibly XeBr [1], have bound ground states. A population inversion does therefore not automatically exist when the upper level is populated as is the case for molecules that have repulsive ground states (e.g. KrF). To maintain laser oscillation and to avoid absorption of the laser flux from the ground state to the excited state, population must be rapidly removed from the ground state. This is particularly important for lasers with long gain duration where "bottlenecking" in the ground state can pose a serious limit on efficiency.

Removal of population from the lower laser levels occurs by vibrational redistribution and by subsequent collision-induced dissociation, or by direct collisional dissociation. Fulgum et al. found that vibrational levels in the XeF ground state manifold dissociated with the same rate [2]. They concluded that a quasi-equilibrium is rapidly established within the vibrational manifold due to collisions with atoms or molecules. Thus the whole XeF(X) state decays at a single rate as molecules are dissociated from high lying vibrational levels via collisions with the background gases:

$$XeF\ (X) + M \xrightarrow{k_{dis}} Xe + F + M \qquad (3.1)$$

In this work, the temporal evolution of the ground state population and of the small signal gain in the e-beam pumped XeCl laser was investigated by measuring absorption and amplification coefficients attributed to different vibrational transitions. The probe measurements were made using the frequency doubled mode-locked dye laser described in the previous chapter.

The rate of collisional dissociation due to xenon was also estimated, by varying the xenon concentration while keeping the pressure of the other constituent gases (HCl and Ne) constant.

3.2 The XeCl ground state

The potential energy curves for the XeCl molecule are illustrated in Fig. 3.1. From an analysis of the XeCl emission spectrum Tellinghuisen et al. determined the XeCl (X) dissociation energy to be $\sim 255 cm^{-1}$ [4]. Twelve vibrational levels lie within this well and the energy spacing between the first and second

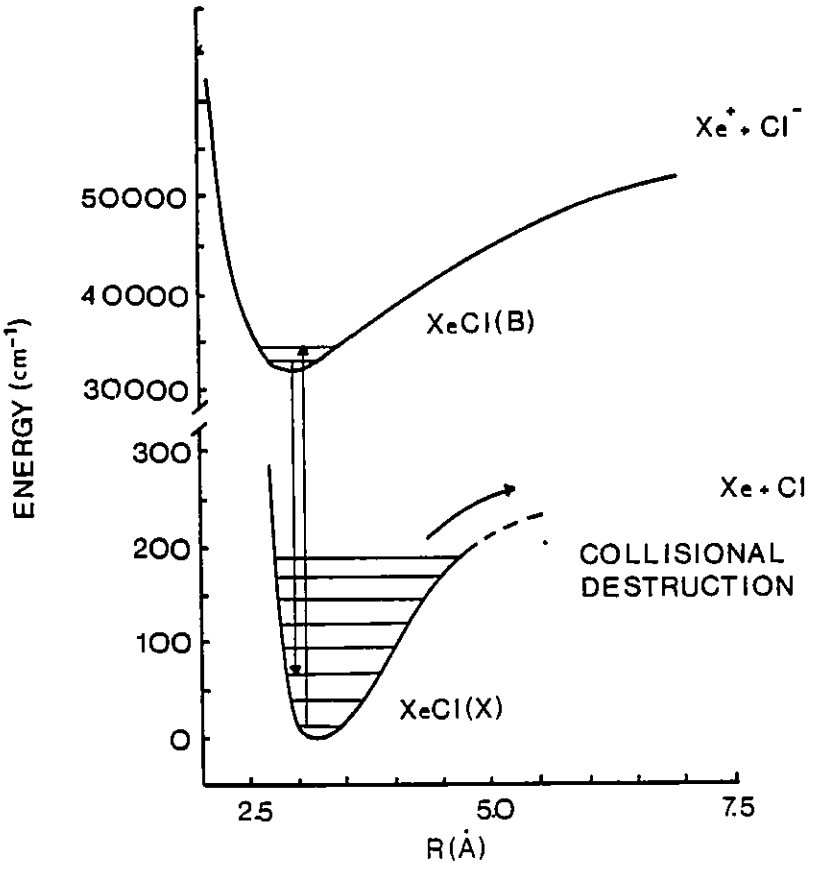

Fig. 3.1. Potential energy diagram for XeCl [3] showing amplification and absorption.
(Note different scale for upper and lower curve)

vibrational levels is $\sim 27 cm^{-1}$. At thermal equilibrium the relative populations in the ground state levels follow the Bolzmann distribution:

$$N_n = N_o e^{h(\nu_n - \nu_o)/kT} \qquad (3.2)$$

where n denotes the nth vibrational level and o denotes the lowest vibrational level. The other symbols have their usual meaning.

A schematic of the thermalized population distribution is shown in Fig.3.2.

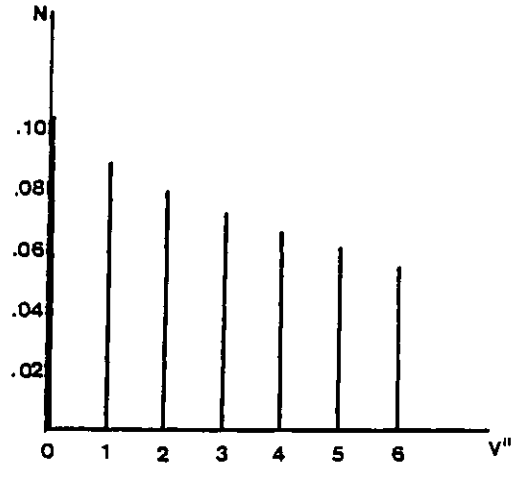

Fig. 3.2
Bolzmann population distribution in the XeCl-X-state (T=360°K)

Tellinghuisen calculated that the rise in gas kinetic temperature due to the e-beam pumping was $\sim 60^{\circ}K$, hence the true temperature in the laser may be substantially higher than $300^{\circ}K$[5]. The population distribution is therefore calculated for a temperature of $360^{\circ}K$.

3.3 Rate equation analysis

In the rate equation analysis of the XeCl ground state the vibrational levels are represented by two levels; $N_1(t)$ and $N_2(t)$. $N_1(t)$ denotes the population in the lower laser levels ($\nu'' = 1, 2$) and $N_2(t)$ denotes the population in the other vibrational levels. If the population in the upper laser level (B state; $\nu' = 0$) is $N_3(t)$, the rate equations are

$$\frac{dN_1}{dt} = N_3(t)\,(\omega_i + \omega_{31}) + N_2(t)\omega_{21} - N_1(t)(\omega_{12} + \omega_i + \omega_D) \qquad (3.3)$$

and

$$\frac{dN_2}{dt} = N_3(t)\omega_{32} - N_2(t)(\omega_{21} + \omega_D) + N_1(t)\omega_{12} \qquad (3.4)$$

where ω_{12}, ω_{21} is the average rate of vibrational relaxation in and out of levels 1 and 2, ω_i is the rate of stimulated (or induced) emission and absorption, ω_{31}, $_{32}$ is the rate of spontaneous emission and ω_D is the rate of collisional dissociation. The latter is assumed to be constant for each vibrational level. This is true for a potential well which is shallow such as the XeCl ground state and is confirmed by the experiment described later in this chapter. Fig. 3.3 illustrates the two level model of the XeCl ground state.

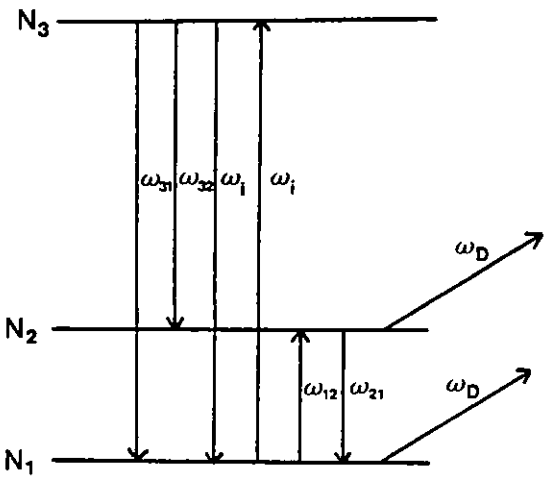

Fig. 3.3. Two level model of the XeCl ground state

If the assumption is made that after a time $t = t_o$ spontaneous and stimulated emission (and absorption) has ceased, then for $t > t_o$ the rate equations reduce to

$$\frac{dN_1(t)}{dt} = N_2(t)\omega_{21} - N_1(t)\ (\omega_{12} + \omega_D) \qquad (3.5)$$

$$\frac{dN_2(t)}{dt} = N_1(t)\omega_{12} - N_2(t)\ (\omega_{21} + \omega_D) \qquad (3.6)$$

The coupled, linear differential equations have exact solutions of the form:

$$N_{1,\ 2} = A_{1,2}\ e^{\lambda_1 t} + B_{1,\ 2}\ e^{\lambda_2 t} \qquad (3.7)$$

λ_1 and λ_2 can be found by differentiating 3.5 and 3.6 and the constants $A_{1,2}$ and $B_{1,2}$ can be found assuming the boundary conditions: $N_1(0) = N$ and $N_2(0) = 0$.

The Bolzmann factor for the population distribution is $f = \frac{N_2}{N_1}$ and by the principle of detailed balance : $N_1\omega_{12} = N_2\omega_{21}$. The solution then becomes:

$$N_1 = \frac{N}{1+f} \left(f\, e^{-\omega_D t} + e^{-(\omega_{12} + \omega_{21} + \omega_D)t}\right) \tag{3.8}$$

$$N_2 = \frac{N}{1+f} \left(e^{-\omega_D t} - e^{-(\omega_{12} + \omega_{21} + \omega_D)t}\right) \tag{3.9}$$

If the rate of vibrational relaxation ω_{12}, ω_{21} is fast compared to the rate of dissociation: ω_{12}, $\omega_{21} >> \omega_D$ and if $t > \omega_{12}^{-1}$, ω_{21}^{-1} equation 3.8 and 3.9 reduce to:

$$N_1 = \frac{Nf}{1+f}\, e^{-\omega_D t} \tag{3.10}$$

$$N_2 = \frac{N}{1+f}\, e^{-\omega_D t} \tag{3.11}$$

Expression 3.10 and 3.11 imply that at a time $t > \omega_{12,21}^{-1}$ the thermalized population in the ground state decays at a rate ω_D independant of vibrational number. The rate of collisional dissociation depends on the collision rate of all the molecules that contribute to the destruction of the ground state. The total rate of dissociation is then in our case

$$\omega_D = \omega_{Xe} + \omega_{HCl} + \omega_{Ne} \tag{3.12}$$

In this chapter t_o, the time when stimulated and spontaneous emission have ceased, is estimated. The lifetime of several vibrational levels is then determined by measuring absorption from the different levels in the ground state at times $t > t_o$. The rate of dissociation can then be determined and the above assumptions investigated. The dissociation rate due to xenon is also estimated by varying the partial pressure of xenon and using the relation

$$\omega_{Xe} = k_{Xe}[Xe] \tag{3.13}$$

where [Xe] is the number density of xenon (cm^{-3}) and k_{Xe} is the rate constant ($cm^3\ s^{-1}$).

3.4 Experimental

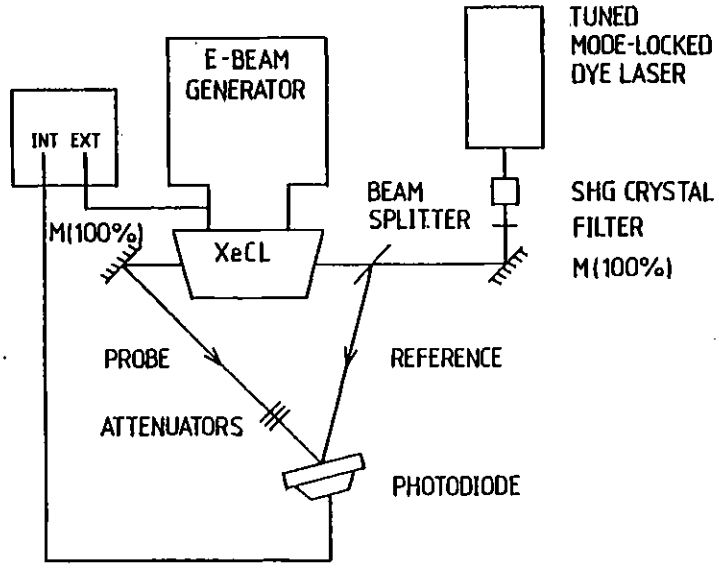

Fig. 3.4. Schematic of experimental arrangement

Fig.3.4 shows a schematic of the experimental arrangement.

The flashlamp pumped Rhodamine 6G probe laser is described in the previous chapter. The duration of the mode-locked pulses was typically ∿ 5-10ps and the separation between the pulses in the .5μs long pulse train ∿ 6.2ns. The energy in the fundamental wavelength output was a few millijoules. The energy density in a single frequency doubled picosecond pulse was measured to be ∿ 1μJ cm^{-2} (Chapter 4, Section 4.5). The energy density in the probe pulses was therefore considerably lower than the saturation energy density for XeCl (700μJ cm^{-2} [6]) which ensured that the measurements were in the linear regime. The probe laser was tuned to the appropriate XeCl transitions by two intracavity Fabry-Perot interferometers. (Plate separations 50 and 5μm). This gave rise to a fundamental wavelength output of ∿ 5Å spectral width. When the output was frequency doubled in ADP, the bandwidth reduced to ∿ 1Å. This bandwidth was large enough to distinguish between individual bands. However, since the bands

overlap to a certain extent, some inaccuracy in the results is expected (see Chapter 4, Section 4.8). Care was taken to probe transitions that did not overlap exactly with other strong bands, using the table of Franck-Condon factors given in Ref. 4. The dye laser spectrum was monitored by a Hilger and Watts 0.5m Czerny-Turner spectrograph. (Resolution $\sim$ 1Å). The spectrum was recorded on Polaroid 665 (positive-negative) film and scanned on a microdensitometer (Joyce Loebl Autodensidater). A standard mercury lamp was used to calibrate the wavelength. The accuracy of the tuning was $\sim \pm$ 0.5Å.

The e-beam generator used was a Pulserad 110 model. The charging voltage was 1MV, generated by a 10 stage Marx bank. The voltage output from the co-axial pulse-forming line was 500kV, which was switched onto the co-axial laser diode. The diode utilized a radial return geometry pioneered by Bradley et al.[7]. In this design a conducting sheet is connected to the cylindrical stainless steel anode through a slot in the cathode, and the return current flows radially out from the diode. This reduces the magnitude of the magnetic field and changes the direction of the current so that electrons do not pinch towards the centre of the anode, resulting in more uniform pumping [8]. The current at the anode was $\sim$ 35kA ($\sim$ 900A cm^{-2}). The XeCl cell was 15cm long and the quartz windows were antireflection coated with MgF_2 and tilted to prevent the laser from reaching threshold during the probing experiments. The gas mixture used was typically 0.2% HCl + 3% Xe + Ne at 5 Bar total pressure. With a resonator comprising an aluminium and MgF_2 coated reflector (R $\sim$ 85%) and the quartz window as the output coupler, a maximum laser output energy of $\sim$ 1.35J (F.W.H.M. $\sim$ 20ns) was obtained.

Synchronization between the dye laser and the e-beam pumped XeCl laser was not critical since the train of probe pulses lasted

several hundred nanoseconds and the e-beam pump pulse only ∿ 30ns. Synchronization was achieved by triggering the e-beam from a T.R.W. delay pulse-generator (model 46A) which was in turn triggered by the flash-lamp output from the dye laser. (By monitoring the flashlamp output with an optic fibre that illuminated a photodiode (ITL S20)). The T.R.W. delay generator delivered a 250V trigger pulse with a risetime of ∿ 20ns to the Pulserad. (The risetime of the flashlamp signal was too slow and too low in amplitude to trigger the Pulserad 110 directly). A suitable delay was chosen so that the e-beam would fire as the first probe pulses from the dye laser passed through the XeCl cell.

3.5 The measurement procedure

The measurements of the small signal gain and absorption coefficients were made using the following method: The frequency doubled dye laser pulse trainwas split in two by a quartz beamsplitter; one part directed towards a photodiode (ITL S20) and the other part making a single or double pass through the XeCl cell before being directed towards the same photodiode. The photodiode thus detected two interleaved pulse trains and the amplitude ratio of the pulses gave the gain or loss in the cell. Each pulse in the train probed the absorption at a different point in time, and the evolution of the absorption processes could thus be investigated. The ratio between probe and reference pulses was normalised to a calibration ratio, taken when the e-beam was not fired, to account for all other losses (e.g. absorption by optical elements). Fig.3.5 shows an oscillogram of the interleaved trains of probe and reference pulses when the e-beam is fired (top) and when the e-beam is off (bottom). The time-scale is 20ns/div. The top trace also shows the amplified spontaneous

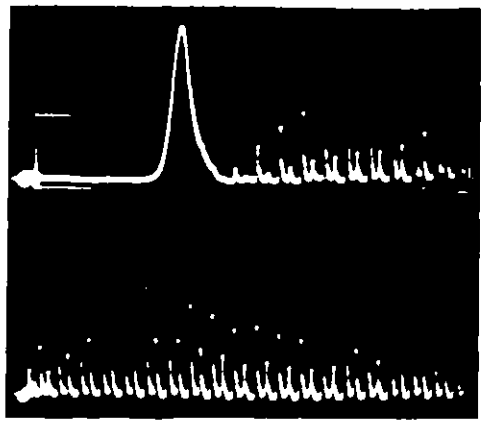

Fig. 3.5

Oscillogram of the interleaved trains of probe and reference pulses when the e-beam is fired (top) and when the e-beam is off (bottom) (20 ns/div)

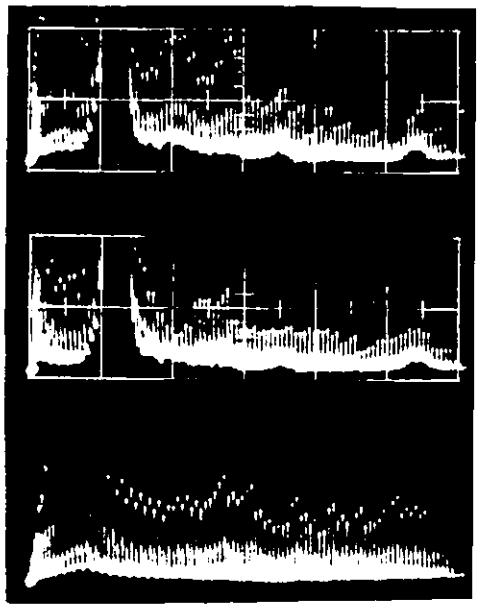

Fig. 3.6

Oscillogram of interleaved probe and reference pulse trains. Top two: e-beam on, bottom: e-beam off. (50ns/div)

emission which is detected together with the probe pulses. The ratio of probe and reference pulses in the lower trace serves as the calibration ratio for the top trace. The ratio is ∿ 1:2 on the calibration trace and is much smaller when the e-beam is fired indicating absorption. Fig. 3.6 shows the probe and reference pulse trains further into the after-glow on a 50ns/div time-scale. The bottom trace is the corresponding calibration trace.

As can be seen from these oscillograms, the a.s.e. signal was significant due to the high gain in the XeCl laser. Therefore, when the probe pulses were double passed through the XeCl cell, a quartz flat was used as the back reflector rather than an aluminium coated mirror since the greater feedback from the latter would cause the laser to reach threshold. An aperture was for the same reason placed in front of the quartz flat exposing an area equivalent to the area of the probe beam. In order to reduce the a.s.e. incident on the photodiode a spatial filter was placed in the path of the probe beam in front of the detector. Fig 3.7 shows a photograph of

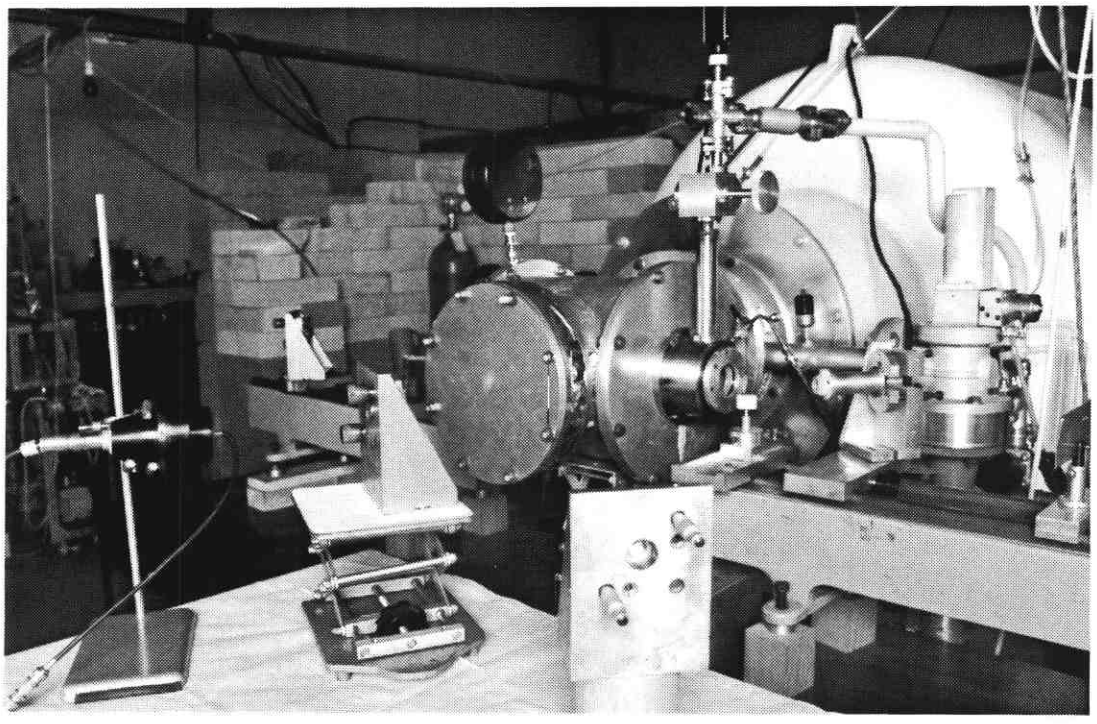

Fig. 3.7. The electron beam pumped XeCl laser

the e-beam pumped XeCl laser and the optical components for a double pass probe experiment. (Double pass probing was necessary to increase the accuracy of the measurements for transitions with low transition probability).

The calibration ratio (e-beam not fired) can be expressed as:

$$C = \frac{A_p}{A_r} \tag{3.14}$$

where $A_{p,r}$ is the amplitude of the probe and reference pulse on the oscilloscope. This amplitude is directly proportional to the energy in the pulse, (see Chapter 4, Section 4.5). In a gain medium of length L and small signal gain (or absorption) g_o, the ratio of the probe and reference amplitudes gives the amplification factor G_E according to the relation:

$$G_E = \frac{A_p/A_r}{C} = e^{g_o L} \tag{3.15}$$

(This assumes that there are no saturation effects).

Hence,

$$g_o = \ln\{\frac{A_p/A_r}{C}\} L^{-1} \qquad (3.16)$$

gives the gain or loss coefficient. Calibration traces of the probe and reference beam were recorded before each absorption or gain measurement. Since any reduction of intensity of the probe beam, such as part of the beam spilling outside the photodetector, would be interpreted as absorption, care was taken to ensure that the whole beam was incident on the photodiode at all times. A lens was therefore placed in the probe beam after this had passed through the XeCl cell.

3.6 Small signal gain

The temporal evolution and magnitude of the small signal gain on the 0-2 laser transition was investigated with the dye laser tuned to the 308nm laser wavelength. When the picosecond probe pulses traversed the XeCl laser while the e-beam was fired, the probe pulses were amplified due to the gain in the medium. The amplified probe pulses were attenuated by a known factor by calibrated optical filters. The amplitude of the pulses could then be compared to the reference pulse amplitudes and to the calibration ratio, and the small signal gain seen by each pulse could be calculated. A profile of the temporal evolution of the gain was then obtained since the dye laser probe pulses sampled the gain every 6.2ns (the separation between pulses in the train).

The attenuation factor of the glass filters was measured by comparing the calibration ratio (e-beam off) between the probe and reference signal with and without the filters in the probe beam. The attenuation factor could then be found directly by dividing one calibration

ratio by the other. This method was found more accurate than using the available spectrophotometer (Beckman Ratio Recording Spectrophotometer).

The linearity of the ITL S20 photodiode was also investigated. The calibration ratio between the probe and reference beam was found with optical filters of known transmission in front of the photodiode. These were then removed and calibrated electrical attenuators were used instead (in conjunction with the Tektronix 519 oscilloscope). The two interleaved pulse trains were then intense enough to saturate the photodiode. This caused the calibration ratio to change. The photodiode response was found to be linear for signals $\lesssim$ 50V from the photodiode. Care was taken in all the experiments to attenuate the beams incident on the photodiode, in order to keep the voltage signal generated significantly lower than 50V.

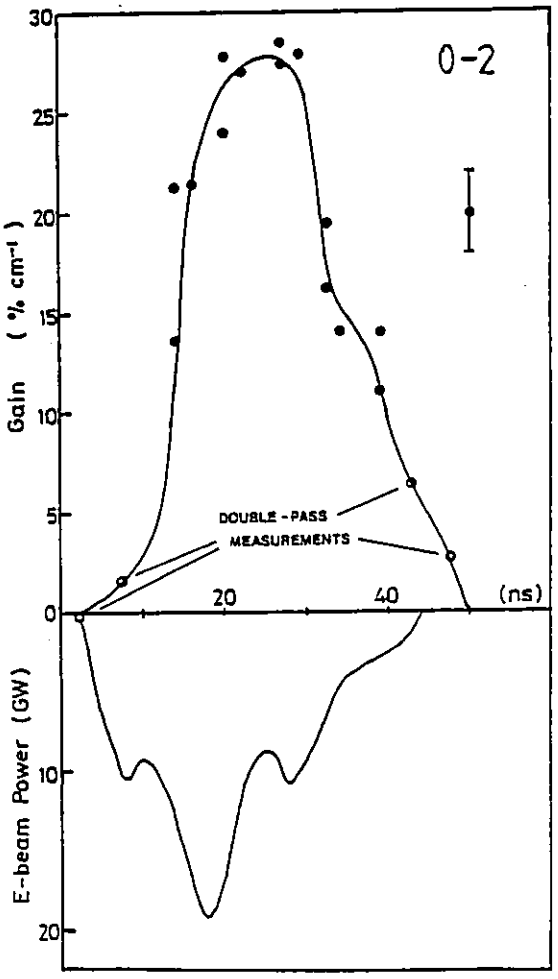

Fig. 3.8
Small signal gain and e-beam power

Having determined that the pulse amplitude measured on the oscilloscope was linearly proportional to the photon density, the small signal gain could be calculated. Fig. 3.8 shows the temporal evolution of the small signal gain, as well as the e-beam pump power, for the main 0-2 laser transition. The peak of the gain occurs $\sim$ 5-10ns after the peak of the pump pulse. The peak small

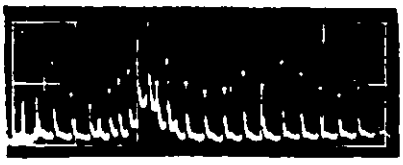

Fig. 3.9
Oscillogram of amplified probe pulses and reference pulses.

signal gain was $\sim 0.28 cm^{-1}$, corresponding to a single pass amplification factor of 67. The gas mixture for this experiment was 0.2% HCl + 6% Xe + Ne at 5 Bar total pressure. The oscilloscope trace of the amplified pulses is shown in Fig. 3.9. Initial gain was also observed on the oscilloscope traces containing the absorption measurements for the 1-0 transition. In this case no attenuating filters were placed in the probe beam in order to detect the probe signal, and the peak of the amplified pulses was too intense ("off scale") to measure. The peak small signal gain was therefore not estimated for this transition.

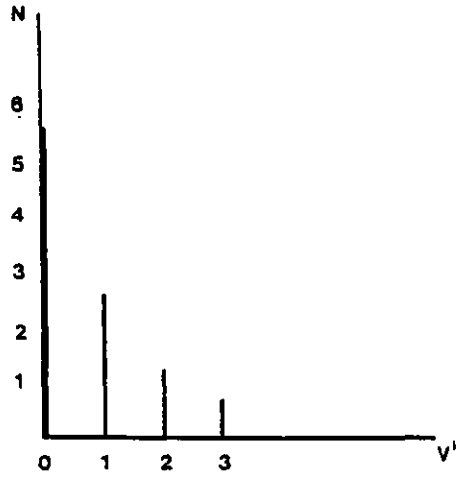

Fig. 3.10
Relative population distribution in the XeCl-B-state ($T = 360^{o}K$).

No initial gain was observed on transitions from $v'=2$. Transitions from higher vibrational levels in the upper state were not probed. The fact that gain was observed only from $v'=0$ and 1, but not from $v'=2$ indicates that the population in the upper manifold has thermalized rapidly. Fig. 3.10 shows the relative population in the upper state vibrational manifold at thermal equilibrium. The population in the $v'=2$ level is low, confirming that for a vibrationally relaxed B-state the gain on transitions from higher vibrational levels would not be significant.

3.7 The ground state lifetime

In order to measure decay of absorption from the XeCl ground state due to depletion of population in the different vibrational levels, it was important to ensure that the ground state population was no longer increasing, due to fluorescence, at the time after the e-beam pump pulse when the probe measurements were being made (i.e. determine t_o to find when equations 3.5 and 3.6 are valid). This can be estimated by measuring the fluorescence decay time of the different transitions probed. The fluorescence from the XeCl cell was recorded using a 1m Hilger and Watts Czerny-Turner spectrograph. The spectrograph was used as a monochromator and a fast ITL S20 photodiode was placed at the exit slit. The spectrograph grating was set to monitor fluorescence from the following transitions: $\nu' - \nu''$ = 0-0, 0-1, 0-2, 1-5 (chosen because of their high Franck-Condon factors [4]). Fluorescence from other transitions than the laser transitions was, however, too weak to detect. Fig. 3.11 shows the fluorescence time profile of the 0-2 transition. The fluorescence decay time was found to be $\sim$ 26ns. Thus absorption measurements should be performed later than 26ns after the peak of the e-beam pump pulse.

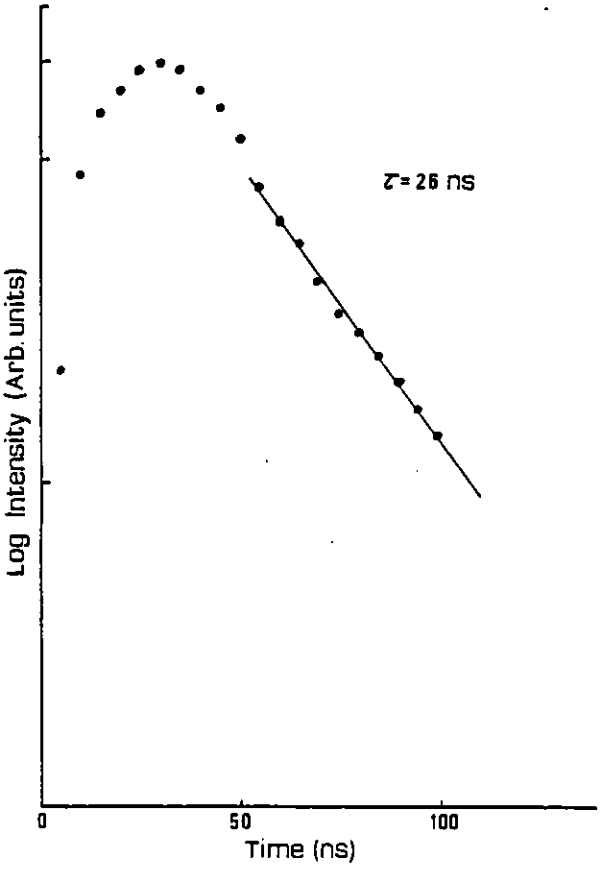

Fig. 3.11
Fluorescence profile for the 0-2 XeCl transition

The absorption from several $\nu' - \nu''$ transitions

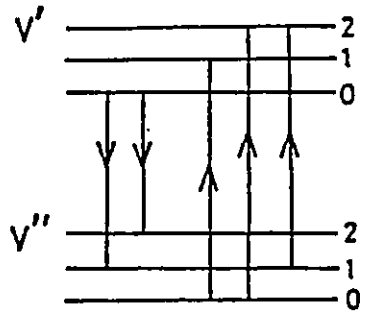

v'-v''	λ(Å)
0-1	3079.6
0-2	3082.1
1-0	3058.7
2-0	3040.8
2-1	3043.3

Fig. 3.12. Vibrational transitions probed

was probed. Fig. 3.12 illustrates these and lists the wavelengths. The photodiode monitoring the probe and reference pulses was used in conjunction with a Tektronix 519 oscilloscope which was triggered by a signal from the current monitor outlet on the Pulserad. Thus the oscilloscope trace containing the two interleaved probe and reference pulse trains started ∿ 10ns before the e-beam pump pulse. The time of probing relative to the pump pulse could therefore be determined with an accuracy of a few nanoseconds. As can be seen in Fig. 3.6, the initial data are obscured by the a.s.e. signal emitted by the laser when the e-beam was fired. Since the measurements of absorption were made in the afterglow period when the ground state population was decaying away - this gap in data did not present a problem.

The ratio of probe and reference pulses in each oscillogram was measured in the time period of ∿ 100-200ns after the start of the pump pulse. Several shots were taken for each transition probed and the results averaged in 5 or 10ns time slots. Thus a time profile of the absorption in the afterglow was obtained. For each transition the absorption decayed rapidly after the e-beam pumping and the fluorescence had ceased. The decay curve was fitted to an exponential of the form

$$A = A_o \, e^{-t/\tau} \qquad (3.17)$$

where A is the absorption coefficient, A_o is the maximum absorption coefficient

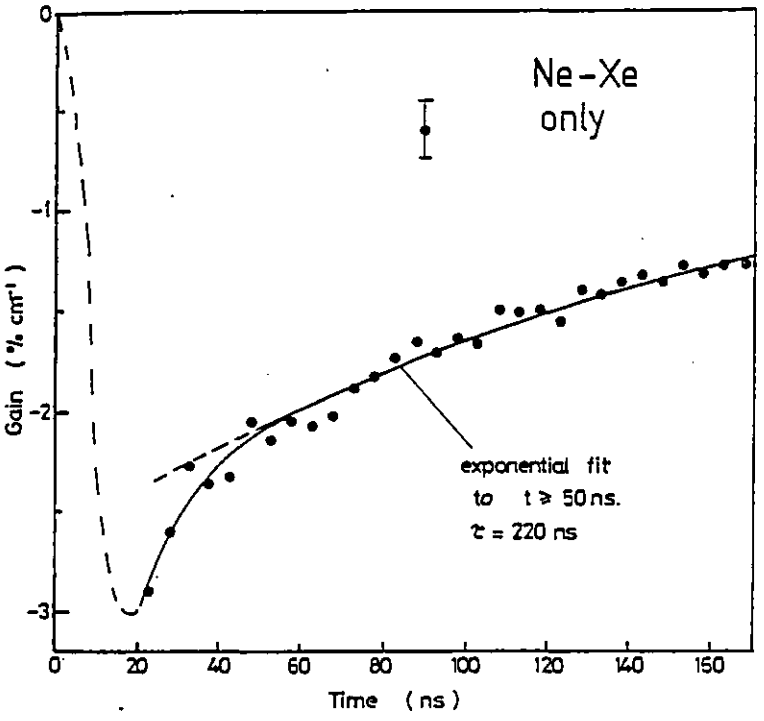

Fig. 3.13
Absorption coefficient plotted against time for a mixture of Xe and Ne

and τ is the decay time constant.

The fast decaying absorption was attributed to absorption from the XeCl ground state, since the absorption decreased when the probe laser was tuned off the bands. Also no fast decaying absorption was found when a mixture of Xe and Ne only was probed. Fig. 3.13 shows a plot of the absorption found with HCl removed from the gas mixture. This absorption decayed with a time constant of several hundred nanoseconds.

Figs. 3.14 and 3.15 show the time profile of afterglow absorption and also the log-linear plot of the fast decaying component for the 2-1 and 2-2 transitions. The 2-2 transition has a very low Frank-Condon factor (.007 compared to .240 for the 0-2 transition) and the amplitude of absorption is reduced as expected. The error bars represent the standard deviation in each time slot. Table 3.1 lists the lifetimes found for each vibrational level probed. The mean lifetime was estimated to be $\sim$19($\pm$7)ns. The results thus indicate that within the experimental accuracy, the levels decay with the same rate (ω_D^{-1}) confirming that removal of population from the ground state by collisional dissociation is followed by a rapid redistribution due to vibrational relaxation. The levels can then be said to be in a quasi-equilibrium, and the theoretical assumption outlined in

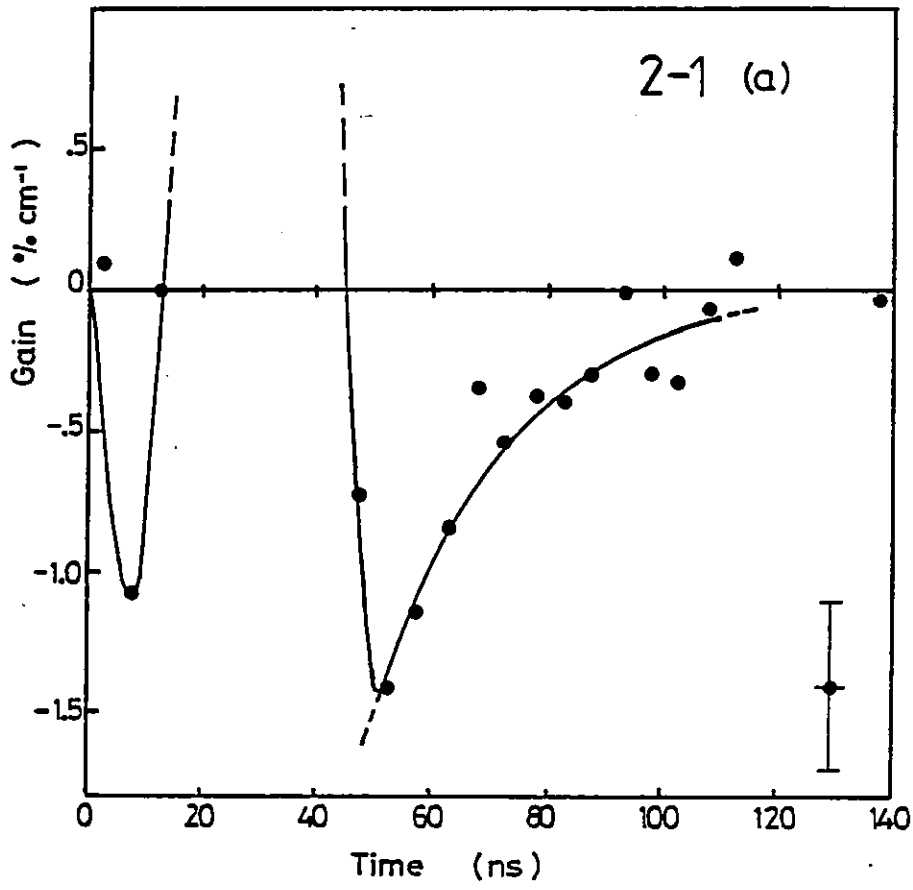

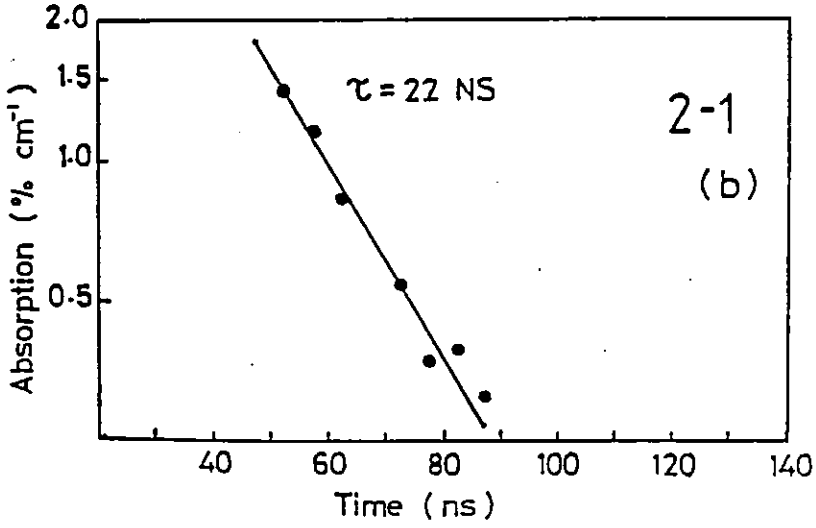

Fig. 3.14. Temporal profile of the absorption coefficient for the 2-1 transition

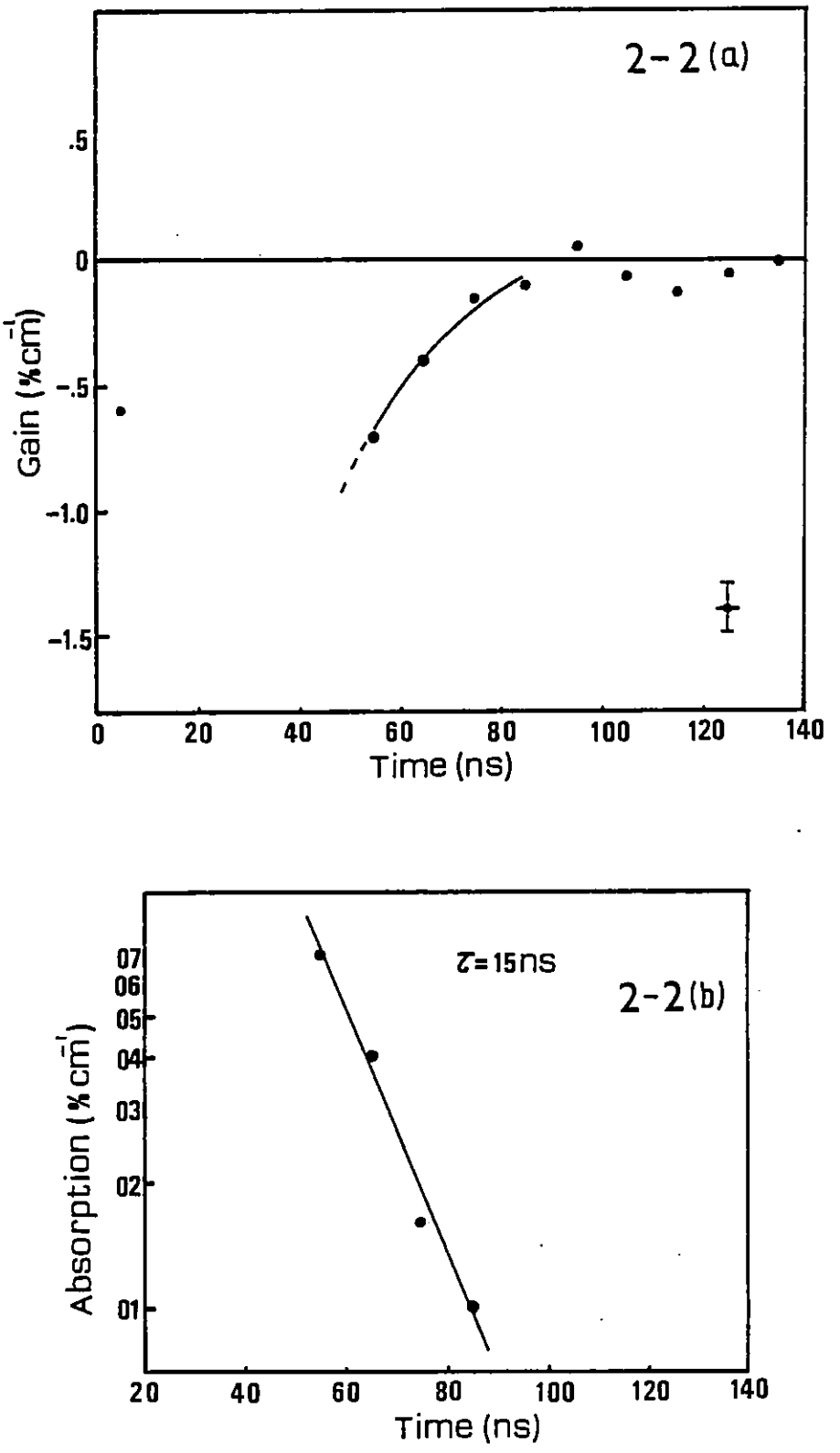

Fig. 3.15. Temporal profile of the absorption coefficient for the 2-2 transition

Transition ($\nu'-\nu''$)	Decay Time (ns)	Gain
0 - 2	21 ± 9	Yes
2 - 1	22 ± 6	No
2 - 2	15 ± 6	No
2 - 0	{ 25 ± 7 11 ± 7	No
1 - 0	-	Yes
Mean = 19 ± 7 ns		

Table 3.1. XeCl vibrational transitions with lifetimes

Section 3.3 are satisfied.

The relatively large scatter in the data are due to inaccuracy in measuring the pulse amplitude. Variations as large as 50% in the absorption coefficient are possible by a measuring error of only 0.2mm in the amplitude of the pulse on the oscilloscope trace. Inaccuracy in determining the baseline of the oscilloscope trace due to noise also contributes to the uncertainty.

3.8 Transient absorbers

Another severe limitation in the accuracy of the results should be stressed; namely the presence of background transient absorbers. This has also been noted by other workers [9]. For some transitions a second absorption peak could be observed $\sim$ 100ns after the pump pulse. The amplitude of this second peak increased with increased

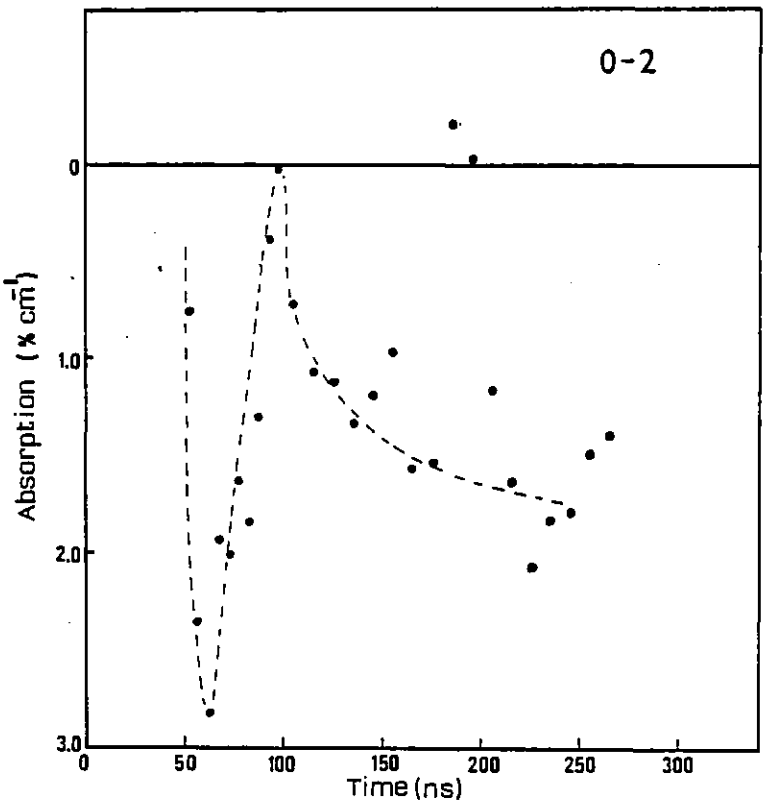

Fig 3.16. Temporal evolution of the absorption coefficient for the 0-2 transition

Xe partial pressure. Fig.3.16 shows the temporal profile of the absorption coefficient for the 0-2 laser transition. In this case the time-scale on the oscillogram is 100ns/div and the absorption data were plotted ∿ 300ns into the afterglow. Rokni et al. found that in a mixture of Ne/Xe/F_2 absorption increased with increased Xe pressure due to formation of Xe_2^+ and highly excited Xe [10]. The theoretical absorption spectrum for Xe_2^+ does however show that the absorption cross section at the XeCl laser wavelength should be significantly lower than at the XeF laser wavelength [11]. Furthermore, at the time when the second absorption peak occurs (∿ 100ns after the pump pulse) the number density of Xe_2^+ and Xe* is expected to be lower than immediately after the pump pulse which indicates that the transient absorber is some other species. Photoionization of metastable rare-gas atoms is thought to be unimportant since the cross sections at the XeCl wavelengths around 300nm are small [12]. The absorption could, however, be due to excited state absorption from Xe_2Cl^* which is formed in the afterglow of e-beam excitation [13, 14]. Since many metastable atoms and molecules are present in the gas mixture, the unidentified absorption could be the superposition of contributions from several species which renders further identification difficult.

3.9. Long lived absorbers

By measuring calibration ratios between probe and reference beams after consecutive e-beam shots were fired, the presence of long lived, stable absorbing species could be determined. If no such long term absorbers were created, the calibration ratio should remain constant before and after consecutive e-beam shots since all external conditions were unchanged. Fig. 3.18 shows the decrease in calibration ratio A_p/A_r with the number of e-beam shots. After ∿ 10 e-beam shots had been fired, the probe amplitude was reduced by ∿ 30%. The measurements were made with a fresh gas mix of 0.3% HCl + 2% Xe + Ne at 5 Bar total pressure. The calibration ratio seemed to stabilize after ∿ 10 shots. Gower et al. found in discharge excited rare-gas fluoride lasers that the dominant stable molecular species absorbing at the laser wavelength was due to air impurity in the gases [15]. For XeCl, however, they found no appreciable long term absorption. Tang et al. found evidence of an absorber with a time constant of several microseconds [13]. This accumulated with successive shots and necessitated replacement of the gas mixture after each shot. Further investigations in order to identify the stable absorber in our experiment were not pursued, since this was outside the scope of the experiment.

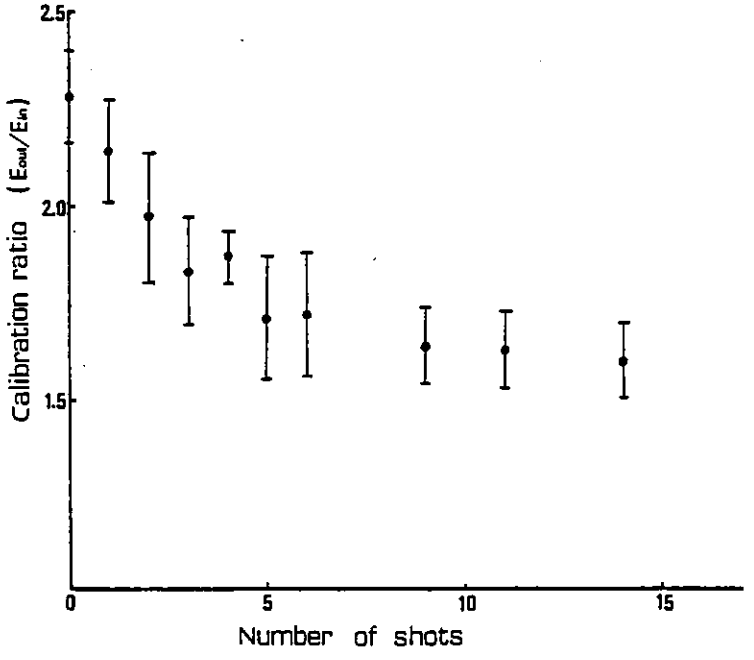

Fig. 3.17. Calibration ratio against the number of e-beam shots

3.10 The ground state dissociation rate due to xenon

Since the ground state decays with approximately the same rate for each vibrational level, data from the 0-2 and 2-0 absorption curves were used to determine the rate constant due to Xe. The partial pressure of Xe was varied while the number density of HCl and Ne was kept constant at 5 Bar total pressure. The percentages of Xe used were: 1%, 2%, 3%, 6% and 10% of the total pressure. The collisional dissociation rate for xenon can be expressed as

$$k_{xe} = \tau^{-1} [Xe]^{-1} \qquad (3.18)$$

where τ is the ground state lifetime found for a particular number density of Xe and $[Xe]$ is the concentration of xenon (cm^{-3}). Fig.3.19 shows the inverse of the ground state lifetimes for the 0-2 and 2-0 transitions plotted against the number density of Xe. The rate constant found by least squares analysis was $k_{xe} = 6.3\ (\pm\ 1.1) \times 10^{-12} cm^3 s^{-1}$.

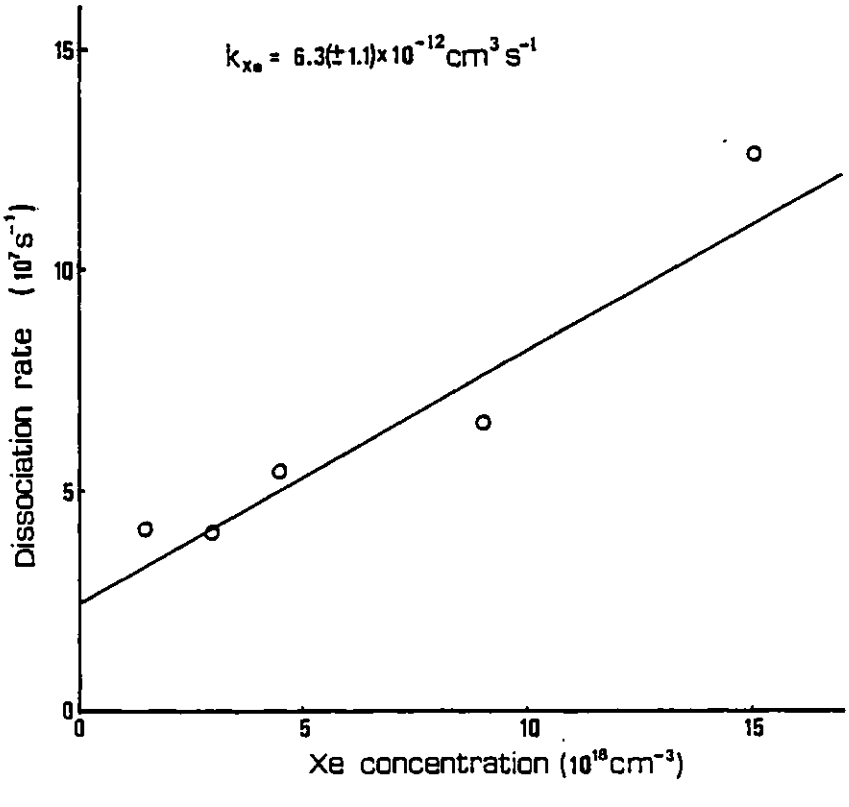

Fig. 3.18. Inverse of XeCl-X-state lifetime against Xe partial pressure

This is in reasonable agreement with the collisional dissociation rate reported by Waynant et al. ($5.6 \pm .8 \times 10^{-12} cm^3 s^{-1}$) who performed a similar experiment [3].

3.11 Conclusion

The lifetimes measured for different vibrational XeCl ground state levels, have been found to be independent of vibrational number, in good agreement with the theoretical prediction that assumes vibrational redistribution to be fast compared to the rate of dissociation. Further evidence that the population in the ground state rapidly redistributes to other vibrational levels was also indicated since the absorption from lower laser levels ($v'' = 2, 1$) was not found to be significantly higher than from other vibrational levels. Hence, the removal of population by vibrational relaxation must be fast, since population would otherwise have accumulated in the lower laser levels. Thermalization in the excited state vibrational manifold is also thought to occur at a fast rate since no gain was observed from higher lying vibrational transitions.

The presence of unidentified transient absorbers and also of stable absorbing species was verified. The identification of these was not within the scope of this experiment. Further information about the nature of these species should, however, become available by performing similar absorption studies while varying the gas constituents and partial pressures. Knowledge of the absorption processes is important if efficient energy extraction is to be achieved.

The rate constant for quenching of the XeCl-X-state by xenon was found to be $\sim 6.3 (\pm 1.1) \times 10^{-12} cm^3 s^{-1}$. When compared to the rate

constants reported by other workers, this shows that quenching of the ground state by Xe is less rapid than quenching by the halogen donor HCl.

CHAPTER 3 - References

1 S.L. Shostak and R.L. Strong, Chem. Phys. Lett., 63, 370 (1979)

2 S.F. Fulghum, M.S. Feld and A. Javan, Appl. Phys. Lett., 35, 247 (1979)

3 R.W. Waynant and J.G. Eden, Appl. Phys. Lett., 36, 262 (1980)

4 J. Tellinghuisen, J.M. Hoffman, G.C. Tisone and A.K. Hays, J. Chem. Phys. 64, 2484 (1976)

5 Joel Tellinghuisen,J. Chemical Phys., 65, 4473 (1976)

6 M. Rokni, R.A. Mangano, J.H. Jacob and J.C. Hsia, IEEE J. Quantum Electron., QE-14, 464 (1978)

7 M.M.R. Hutchinson and D.J. Bradley, U.K. Patent Application No. 16769/78.

8 C.D.P. Levy, PhD Thesis, University of London, p.25 (1980)

9 E. Zamir, D.L. Huestis, H. Nakano, R.M. Hill and D.C. Lorents, IEEE J. Quantum Electron., QE-15, 281 (1979)

10 M. Rokni, J.H. Jacob and J.A. Mangano, Appl. Phys. Lett., 32, 622 (1978)

11 W.R. Wadt, D.C. Cartwright and J.S. Cohen, Appl. Phys. Lett., 31. 672 (1977)

12 K.J. McCann and M.R. Flannery, Appl. Phys. Lett., 31, 599 (1977)

13 K.Y. Tang, D.C. Lorents and D.L. Huestis, Appl. Phys. Lett., 36, 347 (1980)

14 F.K. Tittel, W.L. Wilson and R.E. Stickel, Appl. Phys. Lett., 36, 405 (1980)

15 M.C. Gower, A.J. Kearsley and C.E. Webb, IEEE J. Quantum Electron, QE-16, 231 (1980)

CHAPTER 4

PICOSECOND AMPLIFICATION AND ABSORPTION IN THE DISCHARGE PUMPED XeCl LASER

4.1 Introduction

Subnanosecond pulses in the u.v. spectral region can be generated by amplifying short duration, frequency doubled pulses from a dye laser in a rare-gas halide laser of the same wavelength. The latter can be scaled to produce high powers. Amplification of third harmonic Nd:glass laser pulses of ∿ 200ps duration in XeF demonstrated peak energies of ∿ 1mJ in a single pulse [1]. The output from a high power mode-locked Rhodamine 6G dye laser was frequency doubled and amplified in a XeCl laser yielding peak powers of 700MW [2]. In a third experiment pulses from a XeCl oscillator were amplified in a XeCl amplifier after having passed through a Pockel's cell pulse slicer [3]. The peak power obtained was ∿ 10MW.

This chapter describes amplification of second harmonic dye laser pulses that were tuned to different transitions in a discharge pumped XeCl laser. Measurements of the small signal gain coefficient, g_o, was obtained in each case. In a double pass experiment, where the dye laser wavelength overlapped the main laser transition (0-2), the saturation energy density E_s was estimated. The aim of these experiments was to investigate the use of the discharge pumped XeCl laser as a high power, tunable amplifier and to find the energy densities at which the amplifier would saturate, thus setting an upper limit to the maximum energy that could be extracted.

Absorption studies were also conducted in order to determine the lifetime of the XeCl ground state. A comparison could then be made

with the results obtained with the e-beam pumped XeCl laser as described in the previous chapter. However, because laser action in avalanche discharge lasers can terminate due to the onset of arcs, particular care had to be taken to ensure that the absorption was due to the XeCl groud state and not to scattering.

4.2 Pulse propagation in amplifiers

The amplification of pulses of duration longer than the excited state lifetime or storage time of the medium is determined by the available energy of the medium during the pulse. However, for pulses whose duration is shorter than the storage time, the instantaneous inversion determines the available energy. Hence, in such a case, the amplifier can be considered a two level system. If a two level model is used, the assumption that the vibrational relaxation in the upper and lower manifold takes place on a time scale longer than the duration of the pulse must be made.

In the two level model described by Frantz and Nodvik [4] a further assumption is that the linewidth of the transition is neglected. The pulse propagating through the medium is also assumed to have a square intensity profile and the total population in the two levels is assumed constant. Thus;

$$\tau_{sp} >> \tau, \quad \frac{1}{\omega_{vib}} >> \tau, \quad N_1(t) + N_2(t) = \text{const.} \tag{4.1}$$

and

$$n_o(t) = \begin{cases} n_o & , 0 \leq t \leq \tau \\ 0 & , \text{otherwise} \end{cases} \tag{4.2}$$

where τ_{sp} = spontaneous lifetime

τ = duration of the pulse travelling in the amplifier

ω_{vib} = rate of vibrational relaxation

$N_1(t)$ = number density of molecules in the ground state

$N_2(t)$ = number density of molecules in the excited state

$n_o(t)$ = $n(o, t)$ is the input photon density

$n(x, t)$ = photon density of the pulse travelling in the amplifier.

The photon transport equation describing the pulse passing through the amplifier has the form:

$$\frac{\partial}{\partial t} n(x, t) + c \frac{\partial}{\partial x} n(x, t) = \sigma c n(x, t) \Delta N \qquad (4.3)$$

where σ = stimulated emission cross section

$\Delta N = N_2(t) - N_1(t)$ = population inversion (taken to be uniform throughout the medium).

The assumption is also made that all the stimulating photons cause an increase in population of the ground state only:

$$\frac{\partial}{\partial t} N_1(t) = \sigma c n(x, t) \Delta N \qquad (4.4)$$

and that all the stimulated photons are due only to the upper state:

$$\frac{\partial}{\partial t} N_2(t) = - \sigma c n(x, t) \Delta N . \qquad (4.5)$$

By transformation of variables to new co-ordinates x/c and t- x/c, the frame of reference is stationary with respect to the pulse. The set of equations 4.3, 4.4 and 4.5 can then be solved to give an expression for the photon density in the pulse at a distance x in the amplifier in terms of the number density of photons ($n = n_o c\tau$ in cm^{-2}) in the pulse at the entrance of the amplifier:

$$n(x, t) = \frac{n_o}{1-\{1-\exp(-\sigma \Delta N x)\}\exp(-2\sigma n(t-x/c)/\tau)} \quad \text{for} \quad 0 \leq t-x/c \leq \tau \qquad (4.6)$$

$$= 0, \text{ otherwise}$$

For the end of the pulse, where $t - x/c = \tau$, we see that if

$$2\sigma\eta << \exp(-\sigma\Delta N x) \tag{4.7}$$

the energy gain $n(x, t)/n_o$ reduces to the exponential law:

$$\frac{n(x, t)}{n_o} = \exp(\sigma\Delta N x) \tag{4.8}$$

Thus, if the photon density in the pulse travelling in the amplifying medium is low, the exponential gain law is valid throughout the pulse and the finite pulse width can be ignored. (It should be noted that if the inequality 4.7 does not hold, the exponential law is still recovered if the pulse is of infinitesimal width). In all other cases where the inequality 4.7 is not satisfied, the energy gain defined as

$$G_E = \frac{-\int_{-\infty}^{\infty} n_L(t)\, dt}{\int_{-\infty}^{\infty} n_o(t)\, dt} = \frac{E_o}{E_i} \tag{4.9}$$

will increase less than exponentially. Thus the tail end of the pulse will see a population inversion which has been altered by the leading edge. The energy gain in terms of input and output energy density (E_i and E_o) and saturation energy density ($E_s = \frac{h\nu}{2\sigma}$, defined as the energy at which the small signal gain is reduced by a factor of $\frac{1}{2}$ [51]) is

$$E_o = E_s \ln\{1 + \exp\sigma\Delta N L(\exp E_i/E_s - 1)\} \tag{4.10}$$

where

$\sigma\Delta N = g_o$ is the small signal gain.

and L = the length of the active medium

If we assume a small signal gain of $\sim 0.07 cm^{-1}$ for the discharge XeCl laser the inequality 4.7 is

$$\frac{2\sigma\eta}{\exp(-g_o L)} \sim 0.3 \text{ for } E_i \sim 1\ \mu J\ cm^{-2}$$

(typical energy density of a frequency doubled dye laser pulse)

For the second pass through the amplifier η will be much larger since the pulse was amplified in the first pass and $\frac{2\sigma\eta}{\exp(-g_o L)} \sim 3$.

We therefore conclude that for double pass amplification, assuming a small signal gain $g_o \sim 0.07 cm^{-1}$, some saturation of the medium will be expected.

For single pass amplification, the gain can however, to an approximation, be calculated according to the exponential law

$$E_o = E_i \exp(g_o L) \qquad (4.11)$$

4.3 Experimental

The mode-locked flashlamp-pumped Rhodamine 6G dye laser described earlier was used for the amplification and absorption experiments. The two Fabry-Perot etalons (with plate separations 5μm and 50 μm) in the cavity provided tuned second harmonic probe pulses with a bandwidth of $\sim 1 Å$. This was broad enough to cover rotational structure and narrow enough to select vibrational bands in the XeCl laser. The duration of the pulses was typically 5-10ps and the u.v. dye laser pulse train lasted $\sim$ 0.5-1.0μs.

The XeCl amplifier [6]was a transverse u.v. preionized discharge produced between two shaped electrodes separated by 2.3cm. The active region was $\sim$ 79cm long. The anode was a sand blasted aluminium rod. (Aluminium chloride which is formed when aluminium electrodes are used, dissociates in the discharge and produces aluminium which absorbs at the main laser wavelength (308 nm). Therefore , the laser performance was, at a later stage, found to improve with the use of a nickel plated electrode). The cathode was a stainless steel mesh, and the preionizing discharge occured between the mesh and stainless steel pins situated

beneath the mesh. The discharge capacitor consisted of 15 "Sprague" capacitors in parallel, arranged as close to the electrodes as possible in order to minimize inductance. The storage capacitor was a 0.17μF "Hivatronic" capacitor. Fig. 4.1 shows a schematic of the discharge chamber and electrical circuit, and Fig. 4.2 shows a photograph of the discharge laser with a voltage monitor connected across the "Sprague" capacitors.

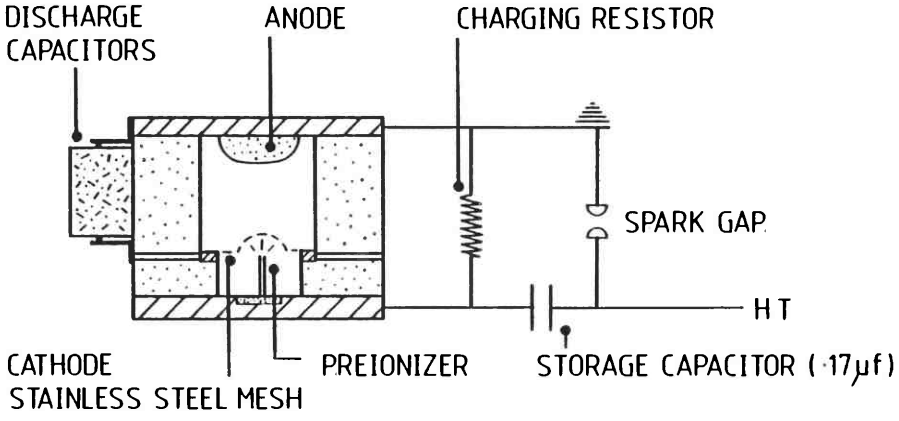

Fig. 4.1. Electrical circuit for the XeCl discharge laser.

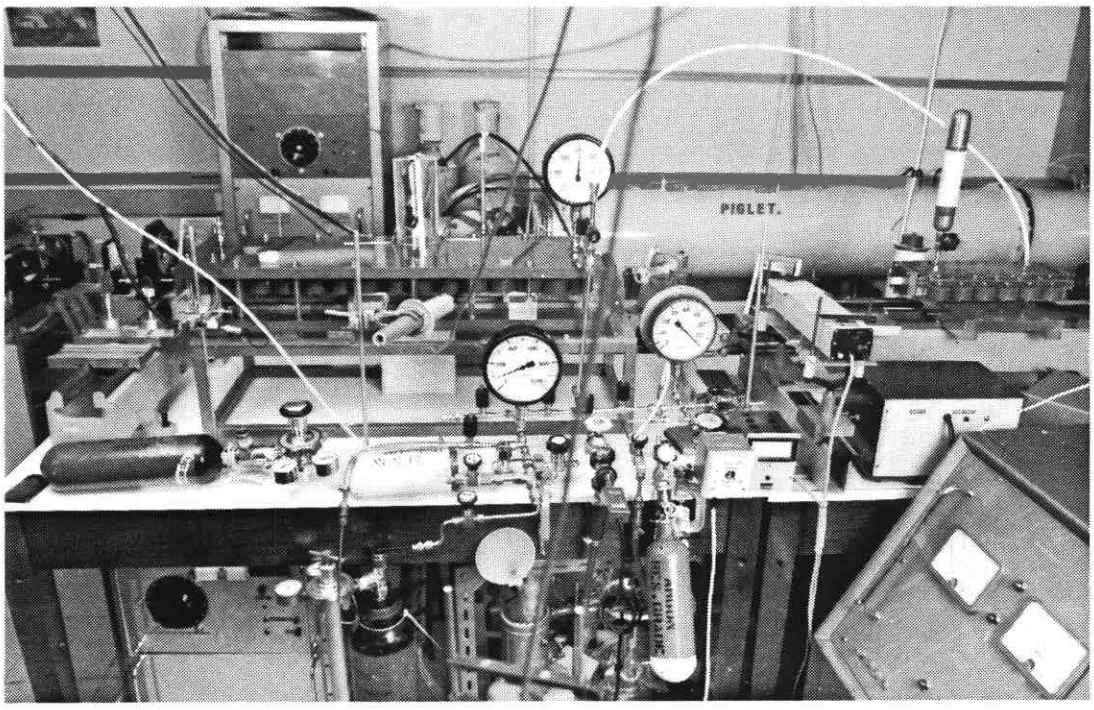

Fig. 4.2. The XeCl discharge laser

The gas mixture was typically 0.3% HCl + 4.5% Xe + Ne at 2000 Torr total pressure. The maximum output energy obtained in the lasing mode was ∿ 70mJ (F.W.H.M. ∿ 25ns) at 30kV charging voltage. The resonator was in this case a flat dielectric mirror (R ∿ 100%) and a quartz flat (R ∿ 8%) output coupler. Since the aim of this experiment was to investigate XeCl as an amplifying medium, it was desirable to prevent self-oscillations. The windows of the laser were therefore antireflection coated and tilted to prevent feedback. Because of the large gain in the amplifier, amplified spontaneous emission (a.s.e.) was difficult to suppress and appeared as a background signal in oscilloscope traces when attenuating filters were not used in conjunction with the photodiode.

Synchronization between the two lasers was not critical, since the duration of the dye laser pulse train was much longer than the gain duration in the XeCl amplifier. Synchronization was achieved with an arrangement similar to that used in the previous experiment with the e-beam laser. The output from the dye laser flashlamps triggered a T.R.W (Model 46A) delay pulse generator by the use of an optic fibre and a photodiode. After a suitable delay a fast risetime signal of ∿ 500V was delivered to the thyratron of the discharge laser through a transformer which was connected between the trigger delay generator and the thyratron. The ratio of turns was 1:2, hence the amplitude of the signal triggering the thyratron was ∿ 1kV. In this way the earth was kept floating at the secondary, thus protecting the T.R.W.generator from noise spikes. The synchronization was checked regularly during the experiments by monitoring the dye laser and XeCl output on the same photodiode (ITL S20). Perfectly synchronized, the oscilloscope trace showed the ∿ 10 ns duration amplified spontaneous emission pulse superposed in the centre of the 500ns dye laser pulse train.

4.4 The measurement procedure

As described in Chapter 3, Section 3.5, measurements of amplification and absorption coefficients were made by dividing the pulse train from the dye laser into a reference beam, which was directed straight to the photodiode (ITL S20), and a probe beam which passed through the XeCl amplifier and onto the same photodiode. (Used in conjunction with a Tektronix 519 oscilloscope). By comparing the amplitude ratio between the two interleaved pulse trains with the calibration ratio taken with no discharge pumping, the amount of gain or absorption in the amplifier could be determined (from 4.11) according to the expression

$$g_o = \ln \left(\frac{A_p/A_r}{C} \right) L^{-1} \qquad (4.12)$$

where g_o = small signal gain or loss

A_p = amplitude of the probe pulse

A_r = amplitude of the reference pulse

$C = A_p/A_r$ with no discharge pumping

L = length of the amplifier

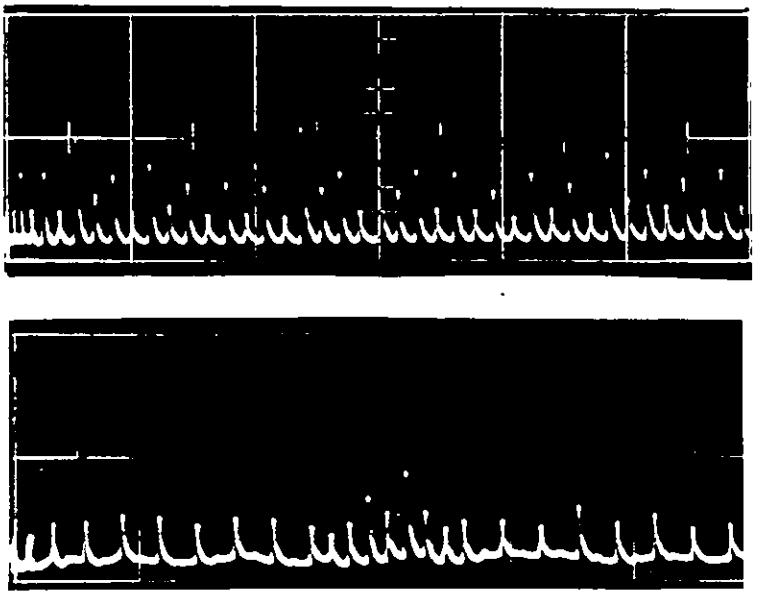

Fig. 4.3. Oscillogram of calibration and amplification pulse trains(20ns/div) Optical attenuation on lower: 256X

Fig.4.3 shows oscillograms of the reference and probe pulse trains when the discharge laser was not fired (top) and with the discharge on (bottom). The constant ratio between the reference and probe pulses in the top trace is the

calibration ratio used to determine the amplification coefficient from the lower trace. Only five of the pulses in the probe train are visible in the bottom trace, since due to the high intensity of these amplified pulses, the output probe beam was attenuated by calibrated glass filters. The amplitude of the amplified pulses was determined by multiplying the pulse height on the oscilloscope trace by the attenuation factor and the gain could then be calculated from 4.12.

4.5 Single pulse energy measurements

In order to determine whether relations 4.11 and 4.12 were valid for single pass gain measurements, an estimate of the energy density in the frequency doubled dye laser pulses was necessary. Since the pulse duration ($\lesssim$ 10ps) is much less than the photodiode and oscilloscope response time ($\sim$ 0.7ns), the oscilloscope trace represents the integrated signal from the photodiode. Hence, the area under the oscilloscope trace is proportional to the total charge due to the pulse which is in turn proportional to the energy in the pulse. Fig. 4.4 illustrates the oscilloscope trace of a picosecond pulse on a fast time-scale. Since

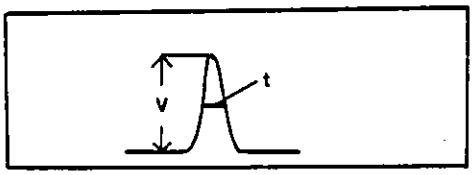

Fig. 4.4
Oscilloscope trace of picosecond pulse(schematic)

$$Q = \int i \, dt = \frac{V.t}{R} ,$$

the charge due to the pulse is found by measuring the amplitude, V, and duration, t (F.W.H.M.), of the pulse on the oscilloscope trace. If the quantum efficiency of the photodiode, η, is known, an approximate value for the energy of the pulse is given by

$$E_p = \frac{V.t.h\nu}{R.\eta.e} \qquad (4.13)$$

where the symbols have their usual meaning.

The quantum efficiency of the ITL S20 photodiode used was estimated using 4.13 for known values of E_p. Laser pulses from the XeCl amplifier (self-lasing) were used and E_p could then be measured with a Quantronix Model 504 calorimeter. The value of η was $\sim 4.7 \times 10^{-3}$. (The photodiode had a diffuser in front of the photocathode, which explains the relatively low quantum efficiency).

By placing Polaroid film(Polaroid 665) at the amplifier entrance and exposing the film to the second harmonic pulse train (attenuated) the beam area could be estimated. The beam area was $\sim 0.5 cm^2$ and the energy density in a single u.v. picosecond pulse was typically $\sim 1 \mu J\ cm^{-2}$ (from 4.12). The inequality 4.7 was thus satisfied and single pass gain measurements were made using the exponential law 4.12.

4.6 Measurement of small signal gain coefficients at the XeCl laser wavelength

In the gain measurements, the amplified probe pulses were attenuated by glass microscope slides. The transmission of a single slide at the XeCl wavelengths was found to be $\sim$ 25%. The transmission factor was measured using the method described in Chapter 3, Section 3.6. The photodiode used was the same as the one described in Chapter 3 and was thus found to be linear for the light intensities in this experiment.

The experimental arrangement is shown in Fig. 4.5. The dye laser was tuned to overlap the 0-2 laser transition at 308.2nm. The temporal evolution of the small signal gain was investigated for the gas mixtures

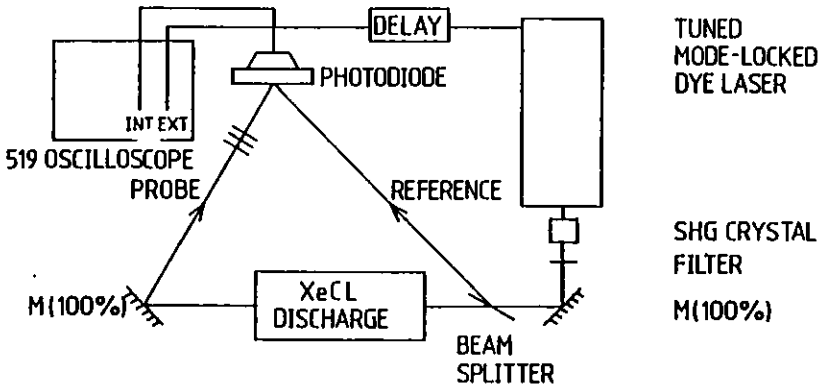

Fig. 4.5

Experimental arrangement for single pass gain measurements

6 Torr HCl + 90 Torr Xe + Ne = 1500 Torr and 2000 Torr. The charging voltage was 30kV. Fig.4.6 shows the temporal profile obtained. The peak gain found for the higher total pressure of 2000 was $\sim 0.078 cm^{-1}$. At the lower pressure of 1500 Torr, the peak small signal gain reached $\sim 0.06 cm^{-1}$. The former corresponds to a single pass amplification $G_E \sim 474$ and the latter to $G_E \sim 114$.

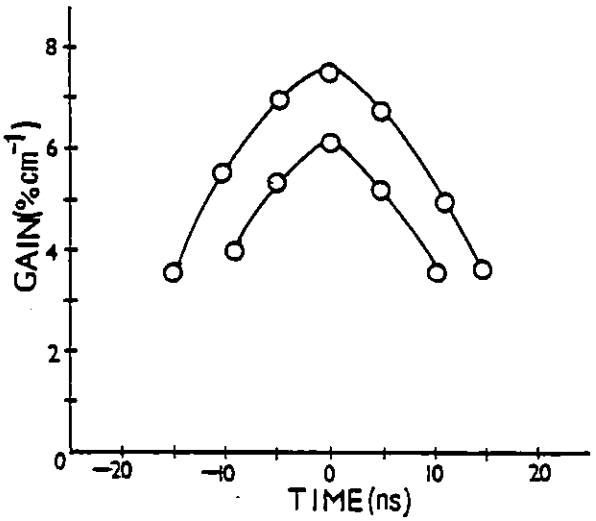

Fig. 4.6

Temporal profile of small signal gain for λ = 308nm at a total pressure of 2000 Torr (top) and 1500 Torr (bottom curve)

The high gain obtained at increased buffer gas pressure could be due to better energy deposition in the gas since the breakdown voltage is greater at higher pressures. The pumping is therefore increased. More excited states should also be formed at greater Ne concentrations, since the rate of Xe metastable and ion formation via the buffer gas is relatively high. (See Chapter 1, Table 1.5). Thus the gain measurements described in the next section were performed at 2000 Torr total pressure.

4.7 The XeCl laser as a pulse amplifier

The dye laser was tuned to overlap the following vibrational transitions in XeCl: 0-2, 0-0, 1-6, 1-2 and 3-0. These were chosen because of their high Franck-Condon factors (except for 1-2). The gain measurements were made using the method described in Section 4.4 and the dye laser wavelength was measured before and after each experiment, using a Hilger and Watts 0.5m Czerny-Turner spectrograph. The spectrum was recorded on Polaroid 665 positive-negative film together with the spectrum from a mercury calibration lamp. The wavelength was then determined by scanning the spectrum on a Joyce-Loebl microdensitometer.

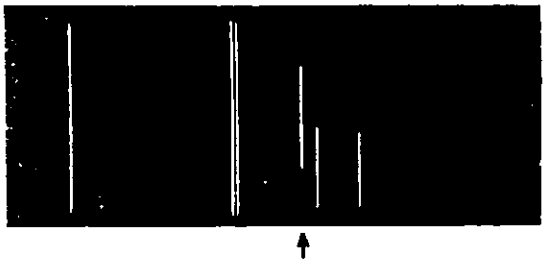

Fig. 4.7
Spectrum of second harmonic output and mercury lines

Fig. 4.7 shows the spectrum of the second harmonic output from the mode-locked dye laser. Table 4.1 lists the peak small signal gain and amplification factors and wavelengths. The temporal evolution of the gain on these transitions was similar to that in Fig. 4.6 and Fig. 4.9.

TRANSITION v' → v"	WAVELENGTH λ(n.m.)	FRANCK-CONDON FACTOR	PEAK SMALL SIGNAL GAIN (g_o) % cm^{-1}	MAX AMPLIFICATION $\exp(g_o L)$
0 — 2	308.21	0.240	7.8	480
0 — 0	307.70	0.104	4.8	45
1 — 6	307.30	0.136	3.8	20
1 — 2	306.37	0.011	1.6	4
3 — 0	302.32	0.089	0	1

Table 4.1. Results from the single pass gain experiment (The Franck-Condon factors are taken from Reference 7).

The lack of gain on the 3-0 transition (which has a high Franck-Condon factor) indicates that the population in the XeCl-B-state vibrational manifold has thermalized very fast causing a rapid reduction of population in the $v' = 3$ level. Fig.3.8 in Chapter 3 shows that the equilibrium population in $v' = 3$ is only $\sim$ 5% of the total population. Rapid vibrational relaxation was also indicated in the experiment with the e-beam pumped XeCl laser, since no gain was observed from transitions originating from the $v' = 2$ level. Thus one may conclude that if the tuning range of the XeCl amplifier is to be extended to cover the whole spectral region from 302nm to 309nm, the amplifier must be operated at an elevated temperature. This has been tried with XeF [8] and laser emission was obtained from the $v' = 1$ transition at elevated temperatures.

4.8 Discussion

The small signal gain at a transition ν_{nm}, where n denotes a vibrational level in the excited state (v') and m denotes a vibrational level in the ground state (v''), is proportional to the population inversion between the two levels, the lineshape function and the Einstein A-coefficient (probability of spontaneous emission). (See Chapter 1, Expressions 1.1 and 1.2). The Einstein A-coefficient is

$$A_{nm} = \frac{64\,\pi^4\,c^3}{3h\,\lambda_{nm}^3}\,|\underline{R}_{nm}|^2 = \frac{1}{\tau_{nm}} \qquad (4.14)$$

where $\underline{R}_{nm}$ is the transition moment, τ_{nm} is the spontaneous lifetime and the other symbols have their usual meaning.

The transition moment $\underline{R}_{nm}$ can be expressed as

$$|\underline{R}|^2 = \underline{R}_e^2\,|\int \psi_n \psi_m \, dr|^2 \qquad (4.15)$$

$\underline{R}_e$ is the electronic transition moment and depends, to some extent, on the internuclear distance. ψ_n and ψ_m are the vibrational eigenfunctions and depend on internuclear distance, r, only. The Einstein B-coefficient (probability of stimulated emission and absorption) is related to the Einstein A-coefficient by

$$B_{nm} = \frac{\lambda_{nm}^3}{8\pi h} A_{nm} \tag{4.16}$$

Thus if we combine 4.14, 4.15 and 4.16 we find that the probability of stimulated emission is proportional to the square of the electronic transition moment and to the square of the integral over the product of the vibrational eigenfunctions of the two states involved. The latter is the "overlap integral", and the square of the overlap integral is the Franck-Condon factor. The intensity of a particular transition therefore depends on the Franck-Condon factor and on the electronic transition moment

$$I_{nm} \propto F_{nm} \cdot \underline{R}_e \tag{4.17}$$

where $\left|\int \psi_n \psi_m \, dr\right|^2 = F_{nm}$, the Franck-Condon factor.

The Franck-Condon factors are normalized since

$$\sum_n \left(\int \psi_n \psi_m \, dr\right)^2 = \sum_m \left(\int \psi_n \psi_m \, dr\right)^2 = 1 \quad [9] \tag{4.18}$$

If we combine the small signal gain

$$g_o = \frac{\lambda^2}{8\pi\tau_{nm}} \Delta N \, g(\nu) \tag{4.19}$$

with 4.14 and 4.15 a new expression for the small signal gain is obtained:

$$g_o = \frac{8\pi^3 c^3}{3h\lambda_{nm}} \Delta N \, \underline{R}_e^2 \left|\int \psi_n \psi_m \, dr\right|^2 g(\nu) \tag{4.20}$$

hence $g_o \alpha \frac{1}{\lambda_{nm}} \Delta N \underline{Re}^2 F_{nm} g(\nu)$ (4.21)

If the electronic transition moment is assumed to be constant (valid for transitions with small change in the internuclear distance) the gain on two different transitions ($\nu' - \nu''$) and ($\nu' - \nu''$)* can be compared using the relation

$$\frac{g_o^*}{g_o} = \frac{\lambda \Delta N^* F^* g(\nu)^*}{\lambda^* \Delta N F g(\nu)} \quad (4.22)$$

Since the total fluorescence bandwidth of XeCl is not expected to be homogeneously broadened on a time-scale of a few picoseconds (the duration of the probe pulse), the lineshape function is that of the single band $g(\nu_{nm})$. $g(\nu)$ for different vibrational transitions between the same two electronic levels of a molecule is expected to be relatively constant and the assumption that $g(\nu)^* \sim g(\nu)$ can therefore be made [10]. 4.22 then reduces to

$$\frac{g_o^*}{g_o} = \frac{\lambda \Delta N^* F^*}{\lambda^* \Delta N F} \quad (4.23)$$

The relative population inversion between two ($\nu' - \nu''$) transitions is then

$$\frac{\Delta N^*}{\Delta N} = \frac{g_o^*}{g_o} \frac{\lambda^*}{\lambda} \frac{F}{F^*} \quad (4.24)$$

In the experiment g_o was measured for transitions originating on the same ν' vibrational level and terminating on different ν'' vibrational levels (1-6 and 1-2 plus 0-2 and 0-0). g_o was also found for transitions originating from different ν' levels, terminating on the same ν'' levels (0-2 and 1-2). For a population distribution that is thermalized, the population in higher lying vibrational levels should be smaller than the population in lower levels. The ratios

$\frac{\Delta N_{02}}{\Delta N_{00}}$, $\frac{\Delta N_{02}}{\Delta N_{12}}$ and $\frac{\Delta N_{16}}{\Delta N_{12}}$ should thus all be greater than unity.

Inserting the values from Table 4.1 in 4.24 gives $\frac{\Delta N_{02}}{\Delta N_{00}} \sim 0.70$, $\frac{\Delta N_{02}}{\Delta N_{12}} \sim 0.22$ and $\frac{\Delta N_{16}}{\Delta N_{12}} \sim 0.19$

Contrary to expectations, the ratios are all less than unity. Since the small signal gain g_o is proportional to the log of the amplification factor (4.12), a large change in amplification factor only results in a small change in g_o. (For a 50% change in E_o/E_i, the change in g_o is only 6%). Hence inaccuracy in the amplification coefficient is not responsible for causing the low value of $\frac{\Delta N^*}{\Delta N}$.

It is, however, conceivable that the bands that were probed could have overlapped other bands due to the close vibrational spacing in the ground state. Further investigation of the violet degraded XeCl bands shows that, depending on the population distribution in the rotational levels, emission lines in the 0-1 progression with high rotational numbers can overlap the 0-0 band . Since the Franck-Condon factor for this transition is very high (0-1 is a laser transition), the gain g_o measured for the 0-0 transition could be due partly to the 0-1 band.

The same argument also applies to other transitions. Furthermore, since the tuning accuracy in the experiment was limited to $\pm$ .5Å, the probe could have been centered slightly off the peak of the band. The accuracy of the measurements was thus not sufficient to draw any conclusions about the relative population distribution in the vibrational levels. Better results could be obtained by employing a probe laser of narrower linewidth.

4.9 Gain saturation; estimation of E_s

For pulses that have double passed the XeCl amplifier, the relation 4.7 is no longer valid. The amplification factor G_E can not be found by the exponential law, since the gain experienced by the tail end of the pulse is modified by the leading edge of the pulse. The energy density of the amplified pulse E_o can be expressed in terms of the energy density of the incident pulse E_i and the saturation energy density $E_s = \frac{h\nu}{2\sigma}$ by

$$E_o = E_s \ln \left[1 + \exp g_o L(\exp E_i/E_s - 1)\right] \qquad (4.25)$$

By measuring E_o, E_i and g_o for a particular transition the saturation energy density can be calculated. Thus an estimate for the stimulated emission cross section is obtained:

$$\sigma_s = \frac{h\nu}{2E_s} \qquad (4.26)$$

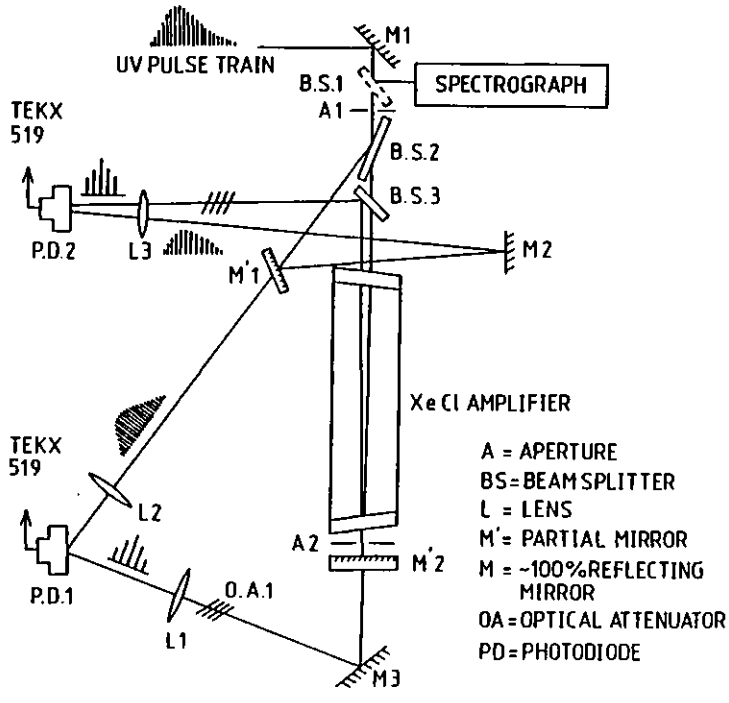

Fig. 4.8
Experimental arrangement for the gain saturation experiment

An experiment was set up to simultaneously measure the single pass gain, g_o, the input pulse energy density, E_i, and the output pulse energy density, E_o (after a double pass), for the 0-2 transition. The experimental arrangement is shown in Fig. 4.8. PD1 (ITL S20) was set up to monitor

the interleaved probe and reference pulse trains for the single pass gain measurements. The single pass probe beam was in this case transmitted to the photodiode through the ∿ 95% reflectivity back reflector. The remainder of the probe beam was reflected back down the XeCl amplifier for a second pass. The energy of the probe pulse at this point was taken as E_i in 4.25. Care was taken to tilt the back reflector slightly to prevent the beam from overlapping the single pass path. This also ensured that the amplifier was not sufficiently well aligned to reach threshold. The beamsplitter BS_3 and mirrors M_1 and M_2 were arranged to direct the reference and probe beam for the double pass measurements, needed to find E_o in 4.25, to the second photodiode PD2 (ITL S20). Both photodiodes were connected to a Tektronix 519 oscilloscope. The two oscilloscopes were triggered simultaneously by the TRW delay pulse generator that triggered the discharge thyratron. By measuring the amplification factor G_E of the single pass pulses the small signal gain g_o could be found and also the input energy E_i. The energy density of the probe pulse at the amplifier entrance was estimated by correlating the amplitude of the reference pulses at PD1 with pulse energies measured earlier with PD2 placed at the amplifier entrance (i.e. by cross-correlating the photodiodes). The pulse area was measured by the method described in Section 4.5. The energy of the output pulse was found by multiplying the incident pulse energy by the amplification factor found in the double pass measurements ($\frac{A_p/A_r}{C}$). The aperture A_2 was inserted to limit the feedback from the 95% reflector in order to prevent self-lasing of the XeCl amplifier.

The gas mixture consisted of 6 Torr HCl + 90 Torr Xe + Ne = 1600 Torr, hence the peak small signal gain was lower than the value obtained for the 0-2 transition at 2000 Torr pressure.

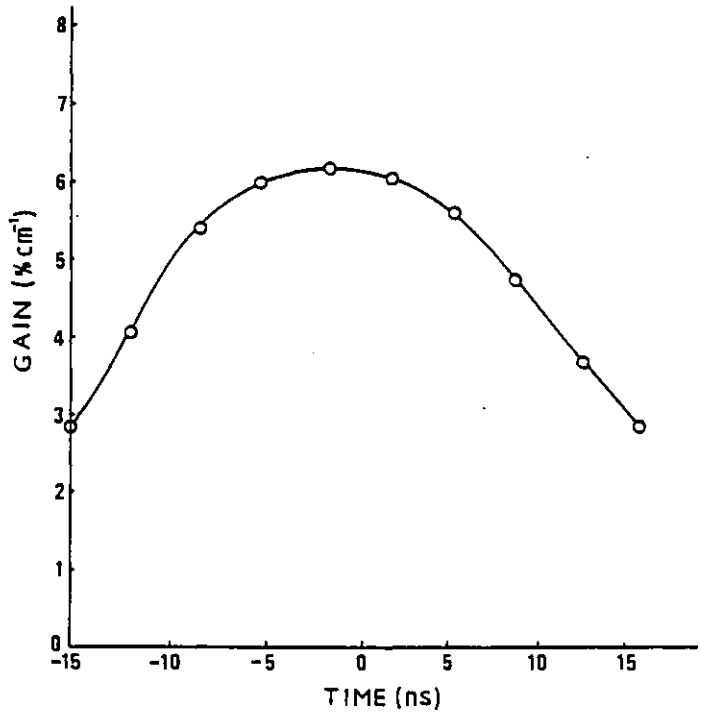

Fig.4.9. Temporal profile for the small signal gain (0-2 transition)

Fig. 4.9 shows the temporal profile of the small signal gain obtained for one of the probe experiments performed. Since the double pass probe pulse reached the centre of the amplifier ∿ 3ns later than the single pass pulse that measured the gain, the g_o value used for each value of E_i and E_o was interpolated from the small signal gain curve. Thus, by knowing E_i and g_o for a particular value found for E_o, the saturation energy density could be calculated from 4.25.

The equation can not be solved analytically. A computer was used and the value for E_s was found by iteration.

The value obtained was $E_s = 484\ (\pm 178)\mu J\ cm^{-2}$. There are several reasons for the large scatter in the results. Firstly the Frantz-Nodvik relation (4.25) assumes that the total population in the two levels is constant (pumping is ignored). Since pumping of the discharge laser is rapid and the gain changes appreciably during a pass through the amplifier, this assumption is not necessarily valid. Also the values used for E_i and E_o ($\mu J\ cm^{-2}$) were only approximate due to the inaccuracy in determining the pulse area from the polaroid burn.

By inspection of the Frantz-Nodvik expression (4.25) we find that the function

$$F(E_s) = E_o - E_s \ln (1 + \exp g_o L(\exp E_i/E_s - 1) \quad (4.27)$$

only has a root if

$$E_o < E_i \exp(g_o L) \quad (4.28)$$

which means that for very small values of E_i there will be no saturation. Fig. 4.10 illustrates how sensitive the function 4.27 is to changes in the values of Ei (and hence that these measurements should be very accurate to obtain an accurate value for E_s). The different curves are the functions $F(E_s)$ plotted for the values $E_o = 80 \mu J cm^{-2}$ and $g_o = 0.055\ cm^{-1}$ by varying Ei from 1.0 to 2.1$\mu J\ cm^{-2}$

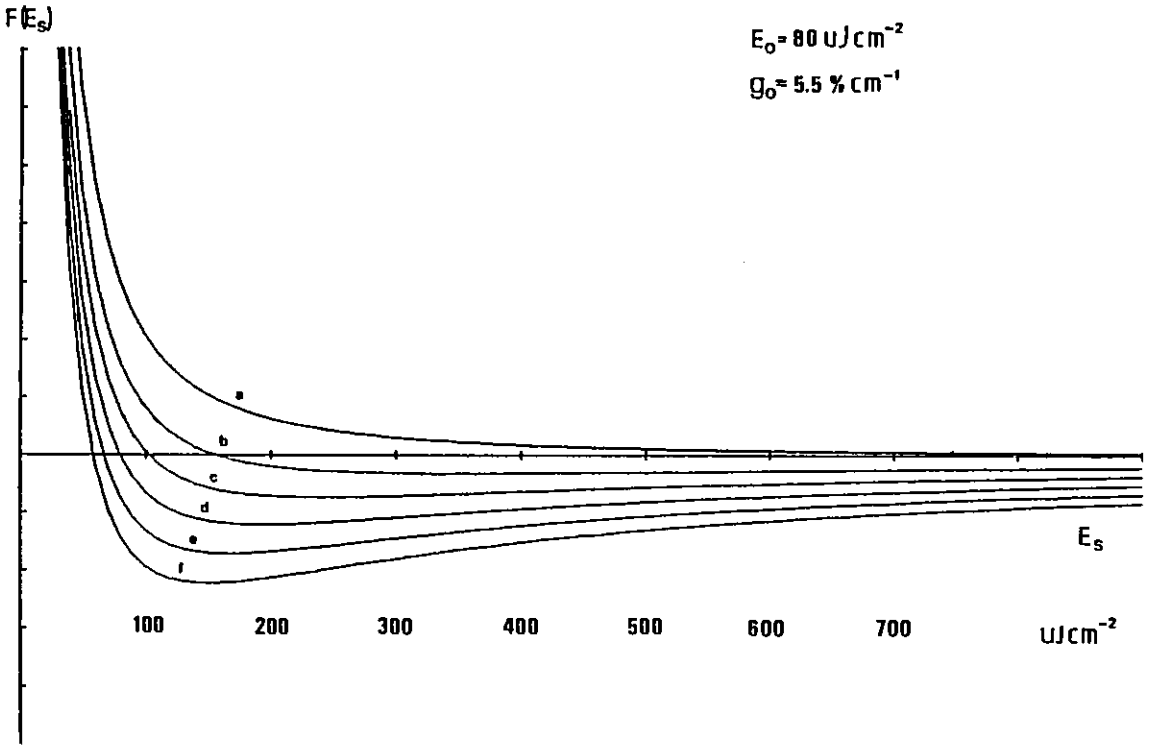

Fig. 4.10. $E_o - E_s \ln(1 + \exp g_o L(\exp E_i/E_s - 1))$

a: $E_i = 1.0\ \mu J\ cm^{-2}$

b: $E_i = 1.3\ \mu J\ cm^{-2}$

c: $E_i = 1.5\ \mu J\ cm^{-2}$

d: $E_i = 1.7\ \mu J\ cm^{-2}$

e: $E_i = 1.9\ \mu J\ cm^{-2}$

f: $E_i = 2.1\ \mu J\ cm^{-2}$

in steps of 0.2μJ cm^{-2}. The intersection of the curve with the horizontal axis gives the root E_s of the function. Note that for E_i = 1μJ cm^{-2}, the inequality 4.28 is not satisfied, and the input pulse energy is too low for the medium to saturate with a small signal gain $g_o \sim 0.055\ cm^{-1}$. For higher input energies, the medium does show saturation, but the value obtained for E_s varies tremendously with input energies since the saturation is still not very strong. (In our experiment E_i was calculated from the single pass data and was taken as the energy of the pulse when reflected back into the cavity for the second pass. Typically E_i was $\sim$ 15-20μJcm^{-2}).

From the single pass and double pass measurements made, a plot of E_o against E_i indicates that the pulses in our experiment only experienced minimal saturation effects. This is shown in Fig. 4.11 where some of the data are plotted together with the theoretical curve for E_s = 480μJ cm^{-2}.

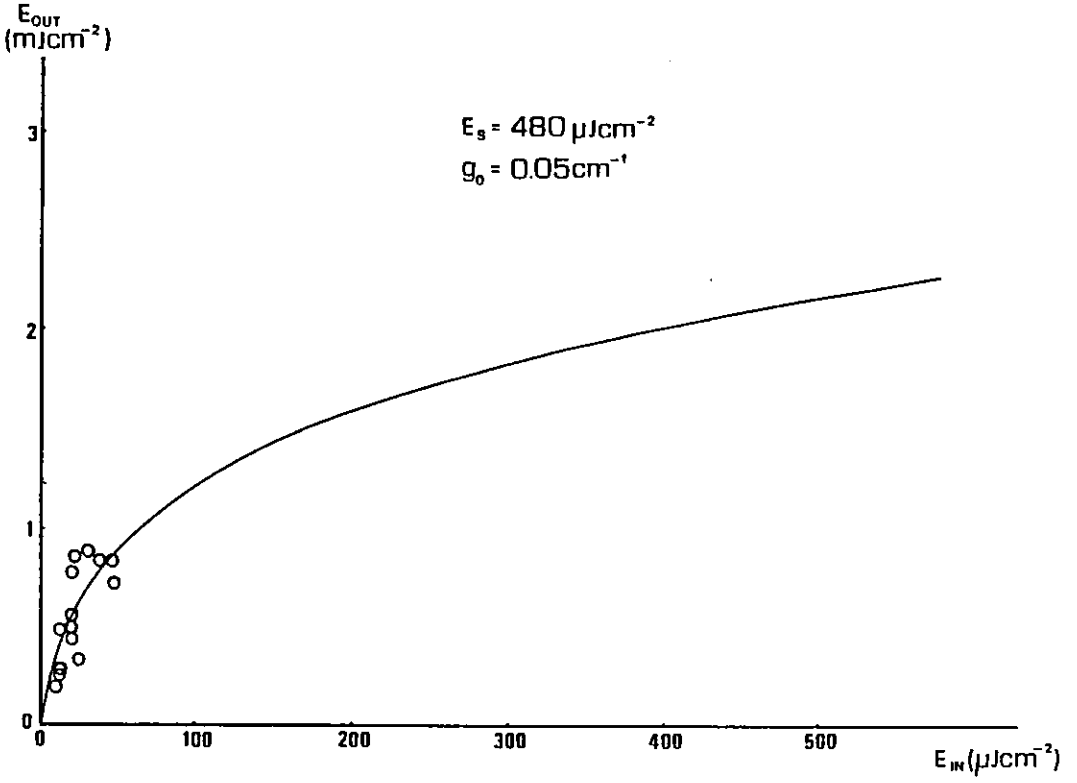

Fig. 4.11. Output energy against input energy for E_s = 480μJ cm^2 and $g = 0.055 cm^{-1}$. Experimental data are also shown.

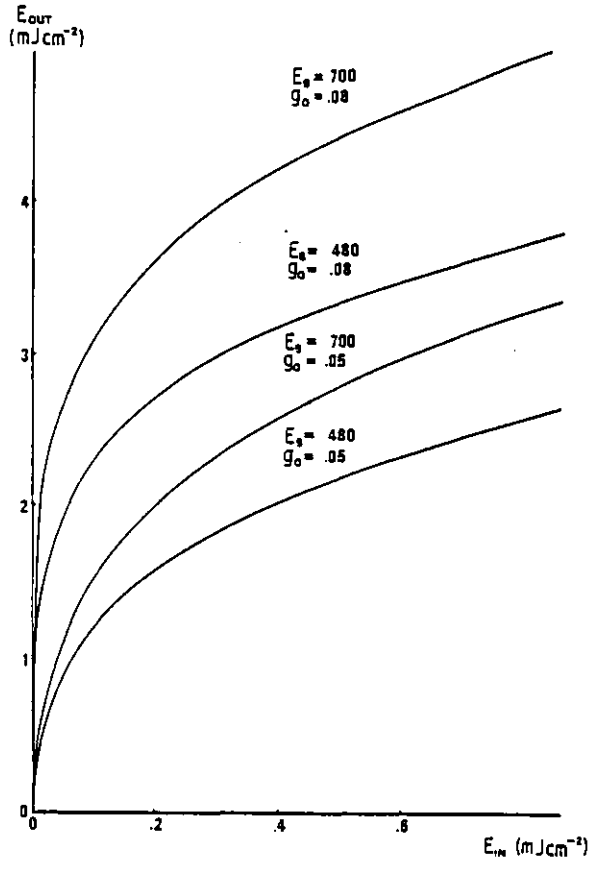

Fig. 4.12. Output energy against input energy

Nevertheless, the value of 484μJcm^{-2} agrees within the experimental accuracy with the reported value of 700μJ cm^{-2}. [11]. The stimulated emission cross section corresponding to our value of E_s would be $\sigma_s = 6.6 \times 10^{-16}$cm^2 which is higher than the quoted value for XeCl(4.5×10^{-16} cm^2).

Fig. 4.12 shows E_o plotted against E_i for a small signal gain of 0.05cm^{-1} and 0.08cm^{-1}. Assuming the experimental and reported values for E_s, the plots indicate that the energy extraction from the amplifier is limited due to saturation effects. The maximum energy that can be extracted in a single pulse from a discharge laser of this type is thus a few millijoules.

4.10 Absorption studies

In order to measure the dissociation time of the XeCl ground state in the discharge laser (as described in Chapter 3 with the e-beam laser), absorption measurements were made with the dye laser tuned to different vibrational transitions in XeCl. Absorption in different gas mixtures was also investigated. It was expected that arcing in the afterglow period could interfere with the absorption measurements. Since the number density in the excited and ground state in the discharge laser

is much lower than in the e-beam laser, we also expected smaller absorption coefficients than those found for the e-beam laser.

The probe measurements were made using the same experimental arrangement as for single pass gain (Fig. 4.5). The ratio between probe and reference beams, compared to the calibration ratio taken with the amplifier off, gave the absorption coefficient. The photodiode (ITL S20) monitoring the interleaved pulse trains was used in conjunction with a Tektronix 519 oscilloscope. The oscilloscope was triggered externally with a signal from the TRW delay generator that triggered the discharge laser. The presence of amplified spontaneous emission ($\sim$ 10ns in duration) at the start of the oscilloscope traces gave a calibration for the probe time relative to the pump pulse. In the figures shown, t = 0 corresponds approximately to the peak of the pump pulse. A computer program was written to analyse the absorption data. The computer averaged the data in timeslots of 5 or 10ns and calculated the standard deviation in each slot. The number of data in each slot was typically $\sim$ 15. A time period up to $\sim$ 220ns into the afterglow was investigated.

Table 4.2 lists the wavelength of the probe pulses, the corresponding XeCl transition, the gas mixture used and the absorption decay time found in the experiment. The absorption reached a peak $\sim$ 50-60ns after the pump pulse and decayed away relatively rapidly. The computer fitted the absorption data to an exponential decay and calculated the resulting time constant (lifetime). The time constant was greater than that found for the e-beam laser which was, however, expected since the pressure in the discharge laser was much lower. Figs. 4.13, 4.14, 4.15, 4.16 and 4.17 show the computer plots for the absorption profiles corresponding to the transition listed in Table 4.2 and the corresponding

log-linear plots yielding the lifetimes. The computer program is listed in Appendix 1.

λ probe (nm) (Transition)	Gas Mixture (Torr)	Decay constant τ (ns)	Maximum absorption coefficient % cm^{-1}
308.2 (0-2)	6HCl + 90Xe + Ne = 1500	54	0.31
308.2 (0-2)	6HCl + 80Xe + He/Ne= 1500	86	0.22
616.0	6HCl + 60Xe + Ne = 2000	31	0.56
306.4 (1-2)	6HCl + 90Xe + Ne = 2000	57	0.58
308.2 (0-2)	Ne = 2000	65	1.00

Table 4.2. The absorption measurements

Investigation of these results indicated that we could not attribute the absorption to the XeCl ground state. The temporal evolution of the transient absorption found with pure Ne in the amplifier was very similar to the absorption found at the same wavelength with all the gases in the laser, except for the initial gain. Furthermore , the absorption of visible pulses also had a similar time profile, although the rate of decay was faster. The absorption coefficient was much higher with pure Ne in the vessel. Identification of the absorbing species was not pursued further, since the similarity of the results for different wavelengths indicated that arcs may, as expected, have been the cause of the transient reduction in probe pulse intensity.

By measuring the calibration ratio between probe and reference

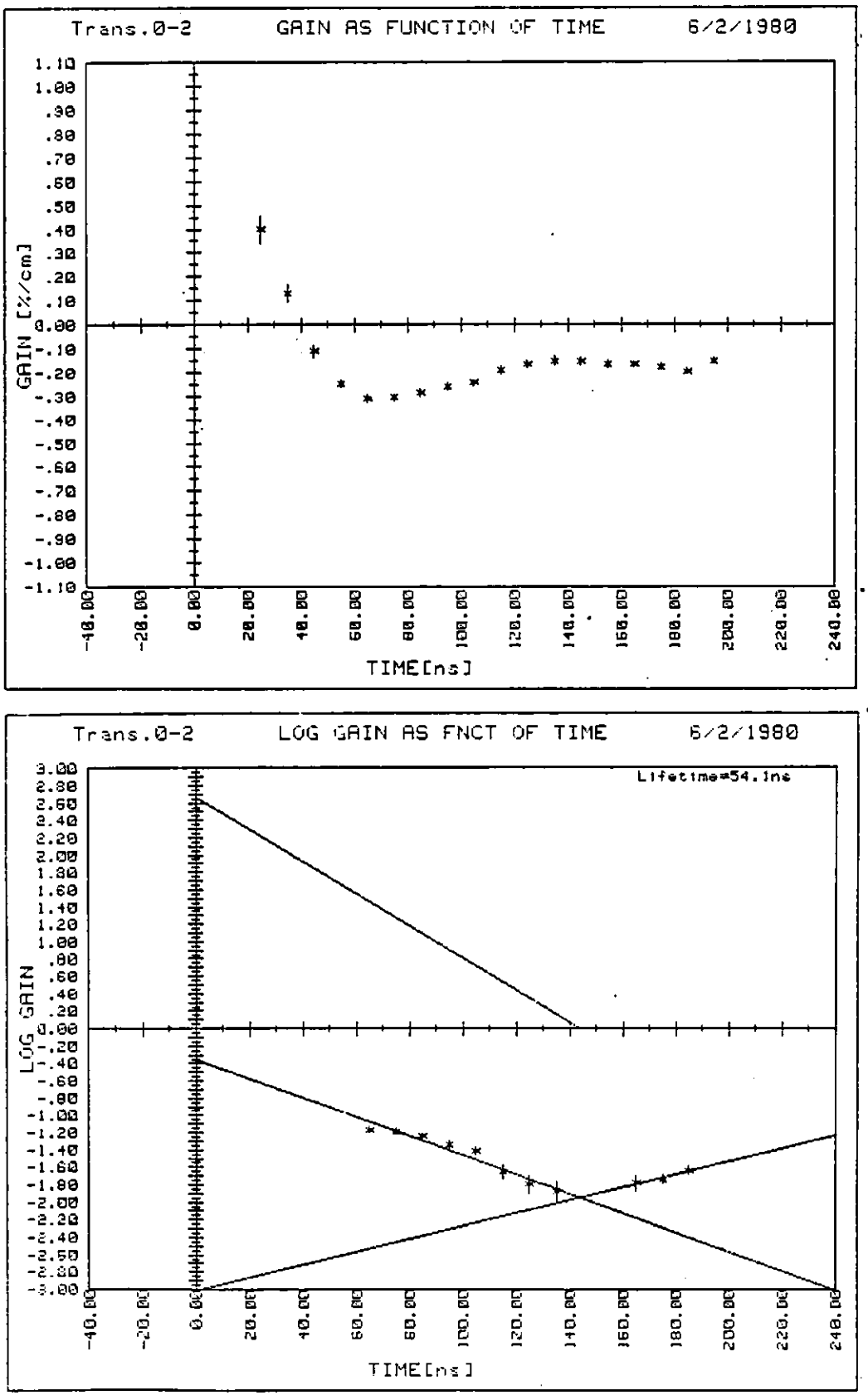

Fig. 4.13. Temporal profile of the absorption coefficient at λ = 308nm (0-2). Buffer gas = Ne, total pressure = 1500 Torr

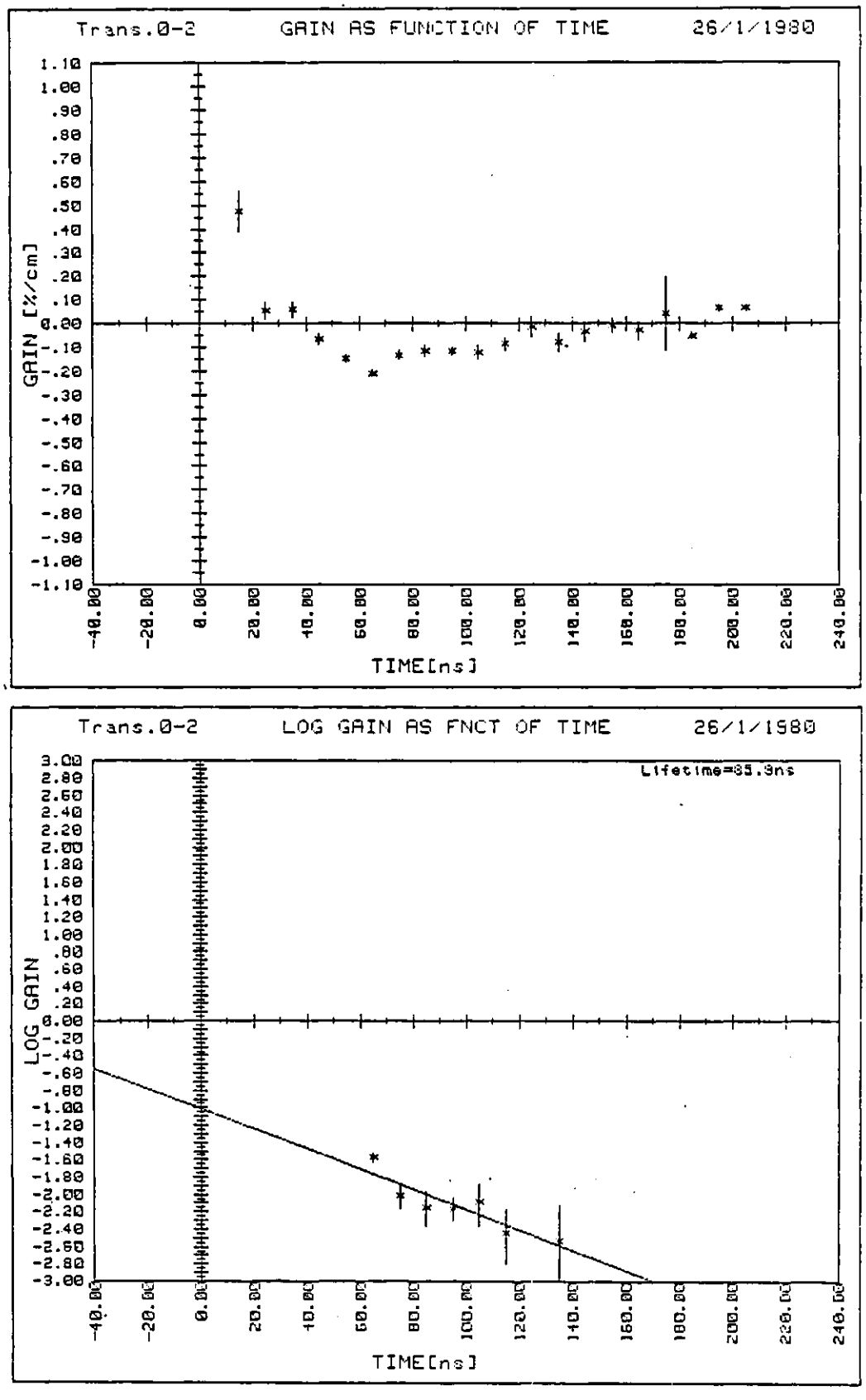

Fig. 4.14. Temporal profile of the absorption coefficient at λ = 308nm (0-2). Buffer gas = He and Ne, total pressure = 1500 Torr.

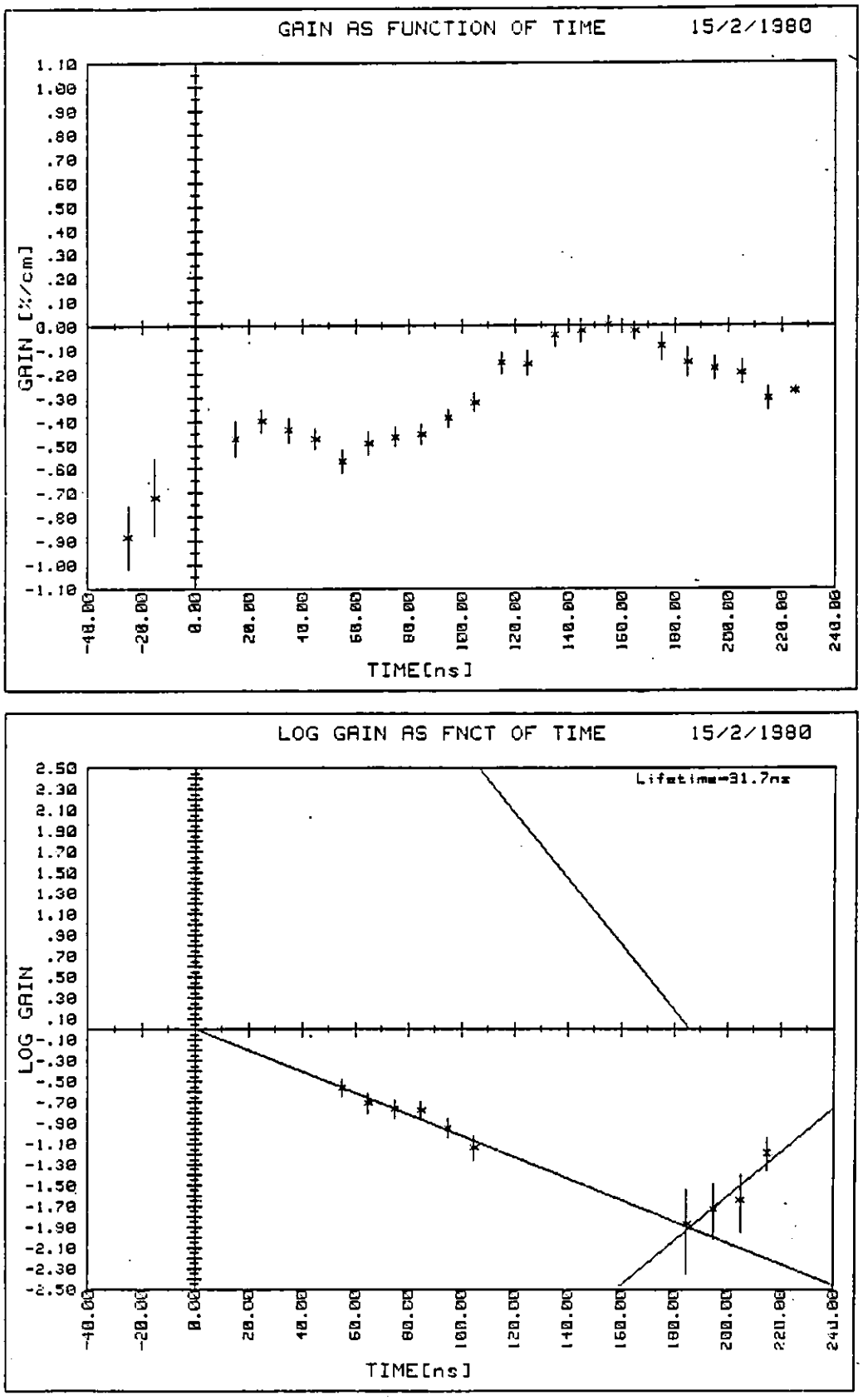

Fig. 4.15. Temporal profile of the absorption coefficent at λ = 616nm. Buffer gas = Ne, total pressure = 2000Torr.

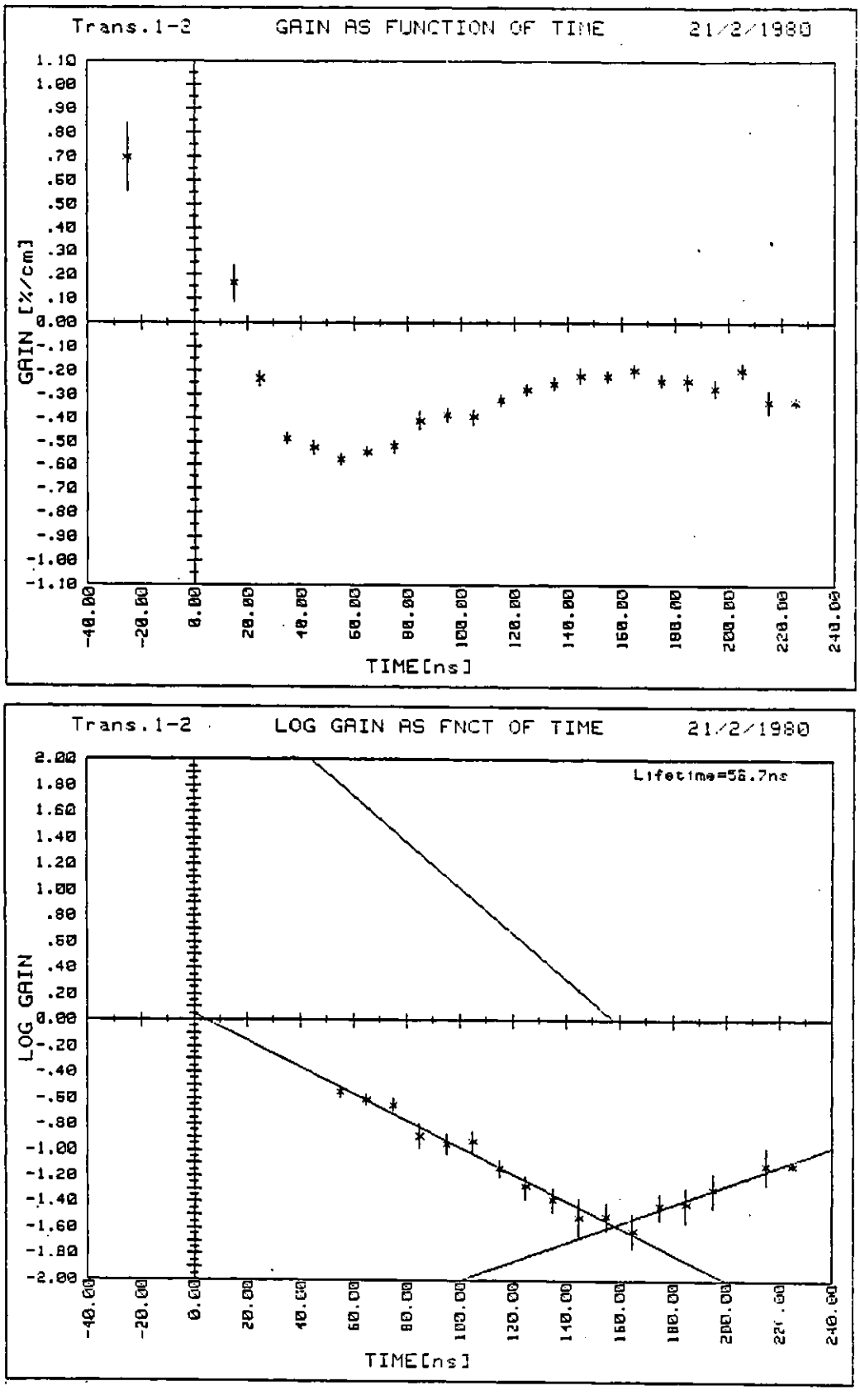

Fig. 4.16. Temporal profile of the absorption coefficient at λ = 306nm (1-2). Buffer gas = Ne, total pressure = 2000 Torr.

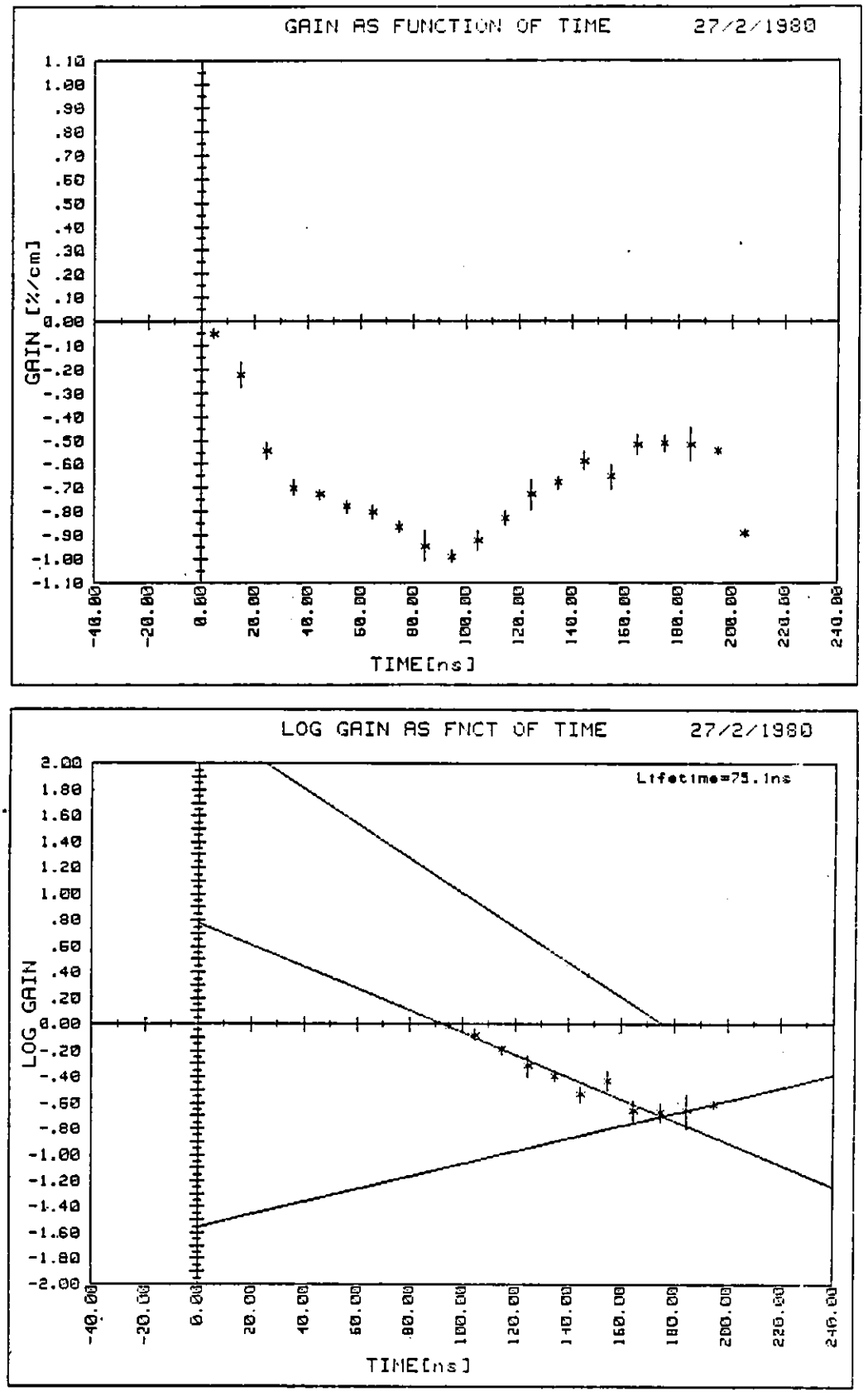

Fig. 4.17. Temporal profile of the absorption coefficient at λ = 308nm. Pure Ne gas at 2000 Torr total pressure

amplitudes after successive shots with the laser, the presence of stable, long term absorbers was verified. Fig. 4.18 shows the reduction of calibration ratio A_p/A_r, with all other parameters fixed. Since the anode electrode was made of aluminium which absorbs at the laser wavelength, this could well have been the absorbing species (as mentioned earlier, aluminium chloride is formed due to reactions with chlorine. Aluminium is then formed by dissociation).

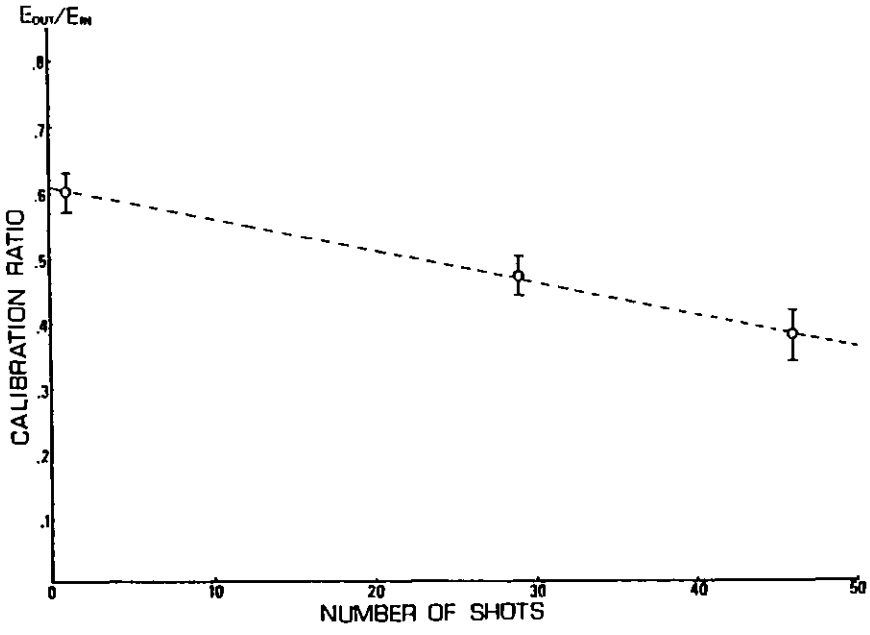

Fig. 4.18. Calibration ratio against number of laser shots

4.11 Conclusion

Since the measurements of absorption coefficients could not be attributed to dissociation of the XeCl ground state the emphasis of the probe experiments with the discharge laser was on the amplification measurements. Appreciable gain was observed on vibrational transitions from lower lying levels in the XeCl-B-state. No gain was, however, observed on the 3-0 vibrational transition which has a relatively high transition probability. This lack of gain was attributed to rapid thermalization in the excited state manifold, since the population

in higher vibrational levels is very low for a thermalized state. Hence, unless the temperature of the amplifier is elevated, significant amplification will only occur for wavelengths that coincide with transition from low lying upper state levels with high Franck-Condon factors.

The XeCl discharge laser was capable of amplifying short duration pulses tuned to the laser transition with energy gains as high as 500 per pass. Double pass amplification factors of $\sim$ 4200 were obtained yielding peak energies of $\sim$ 800μJ in a single pulse. At these energy densities saturation effects were present. Saturation of the XeCl medium poses a limit to the energy that can be extracted from the laser by a single pulse. Using the measured value for the saturation energy density $(\frac{h\nu}{2\sigma})$, the maximum energy extractable was found to be limited to a few millijoules per pulse. The input intensity would have to be very high to deplete all the energy in a single or double pass, however, if the laser were used in a regenerative amplifier configuration, single pulse powers of several hundred megawatts should be feasible. This will be discussed further in the next chapter.

CHAPTER 4 - References

1 I.V. Tomov, R. Fedosejevs, M.C. Richardson, W.J. Sarjeant, A.J. Alcock and K. E. Leopold, Appl. Phys. Lett., 31, 747 (1977)

2 M. Maeda, T. Mizunami, A. Sato, O. Uchino and Y. Miyazoe, Appl. Phys. Lett., 36, 636 (1980)

3 T.J. Pacala and J.B. Laudenslager, Appl. Phys. Lett., 37, 366 (1980)

4 Lee M. Frantz and John S. Nodvik, J. Appl. Phys., 34, 2346 (1963)

5 A. Yariv, Quantum Electronics, Wiley, 168 (1975)

6 T. Varghese, PhD Thesis, Univeristy of London (1981)

7 Joel Tellinghuisen, J. Chem. Phys., 64, 2484 (1976)

8 J.C. Hsia, J.A. Mangano, J.H. Jacob and M. Rokni, Appl. Phys. Lett., 34, 208 (1979)

9 G. Herzberg, Spectra of Diatomic Molecules, D. Van Nostrand Co., 203 (1950)

10 A. Thorne, Spectroscopy Group, Imperial College, private communication (1981)

11 M. Rokni, J.A. Mangano, J.H. Jacob and J.C. Hsia, IEEE J. Quant. Electron., QE-14, 464 (1978)

CHAPTER 5

INJECTION MODE-LOCKING OF THE XeCl LASER

5.1 Introduction

High power, ultrashort pulses in the u.v. spectral region are important for many applications such as nonlinear optics, spectroscopy and photochemistry [1, 2, 3]. Considerable effort has been made to mode-lock rare-gas halide lasers. Active mode-locking of a XeF laser using an acousto-optic modulator produced an output with $\sim$ 70% modulation depth and "individual" pulse durations of $\lesssim$ 2ns [4]. Passive mode-locking of a KrF laser was also only partially successful with modulation depths limited to 85% and pulse durations of $\lesssim$ 2ns [5]. Failure to obtain picosecond pulses arose mainly because of the short duration of gain ($\sim$ 15ns) in these systems. With short gain duration lasers it is not possible to have a sufficient number of roundtrips to produce appreciable pulse narrowing. In order to circumvent this problem, we have employed the method of injection mode-locking to achieve, for the first time, picosecond pulses with a rare-gas halide laser.

In the experiment presented in this chapter, the frequency doubled mode-locked pulse train from the flashlamp pumped dye laser was injected into the discharge pumped XeCl laser described in the previous chapter. The XeCl laser locked temporally to the injected pulses and a mode-locked output pulse train was generated by the excimer laser yielding picosecond pulses with peak powers in excess of 100MW. With a homogeneously broadened linewidth of $\sim$ 1Å, pulses of $\sim$ 1ps in duration can be generated in the XeCl medium. Thus the XeCl laser is capable of yielding pulses of duration at least as short as the injected pulses.

The process of injection mode-locking can be considered the same

as multipass amplification. If the cavities of the "master" and "slave" oscillator are well matched, the "slave" oscillator becomes a regenerative amplifier, provided, of course, that no self-oscillation of the amplifier takes place. If the injected pulses from the "master" oscillator are of sufficient power, the amplifier gain should soon saturate, and the pulse durations from the amplifier could become shorter than the injected pulses (or alternatively longer as will be discussed in the next chapter).

In a medium that is homogeneously broadened over several vibrational levels on a time-scale comparable with the pulse duration, injection frequency locking can also take place. The pulse propagating in the medium can then draw energy from all the bands within the homogeneously broadened bandwidth. In this Chapter injection mode-locking with the input pulses tuned to the XeCl laser wavelength is described. Injection mode-locking on a vibrational transition differing from the main laser transition in XeCl was also attempted and the results are discussed. The vibrational relaxation rate was estimated, hence determining the bandwidth available to the picosecond pulse. This is necessary to know in order to estimate the duration of bandwidth limited pulses. In dye lasers, due to the large bandwidth of the medium, generation of femtosecond pulses is possible and has been demonstrated [6]. If several bands were available to the picosecond pulses in XeCl, subpicosecond pulse generation would be feasible for these lasers also.

5.2 Experimental

The experimental arrangement is shown in Fig.5.1. The mode-locked Rh6G dye laser was the same as described earlier. At $\sim$ 20kV flashlamp charging voltage, the energy density of a single second harmonic pulse

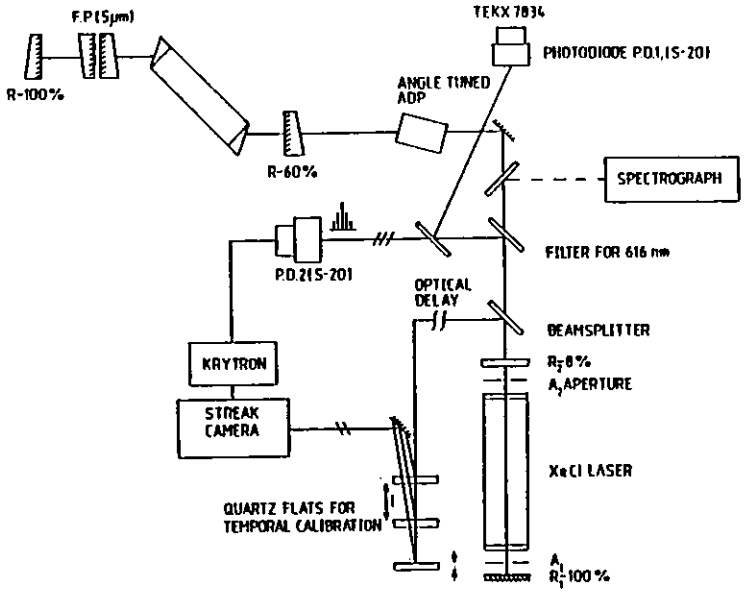

Fig. 5.1. Schematic of the experimental arrangement

was $\sim$ 1μJ cm^{-2}. The separation between pulses in the 0.5-1.0 μs long dye laser pulse train was $\sim$ 8.3 ns which matched the roundtrip time of the XeCl laser. Tuning was achieved with one Fabry-Perot etalon in the cavity. This gave rise to a second harmonic bandwidth of $\sim$ 2.5Å.

The u.v. dye laser pulse train was injected into the XeCl cavity through a quartz flat, R_1, that served as the output coupler for the amplifier. A flat 95-100% reflectivity mirror, R_2, completed the resonator. Two apertures, A_1 and A_2, restricted lasing in the cavity to an area approximately equal to that of the injected beam.

The discharge laser was the same as the one described in Chapter 4, Section 4.3 and was operated under high gain conditions. The quartz windows were antireflection coated and tilted to prevent the formation of a sub-cavity. The gas mixture was typically 6 Torr HCl + 90 Torr Xe + Ne = 2000 Torr. This was found to yield a peak single pass gain $\sim$ 500 as described in Chapter 4. The maximum output energy obtained in the lasing mode (without apertures A_1 and A_2) was $\sim$ 70mJ in a 25-30 ns pulse at 30kV charging voltage. This was the voltage used throughout the experiment.

The dye laser and XeCl laser were synchronized in the same way as described in Chapter 4, Section 4.3. The output from the dye laser flashlamp triggered a TRW delay generator which in turn triggered the

thyratron of the discharge laser. The trigger pulse to the thyratron was suitably delayed so that the discharge laser would fire when the shortest pulses late in the dye laser pulse train were being injected. The synchronization was repeatedly checked during the experiment, by monitoring the unmodulated laser output from the XeCl amplifier and the dye laser output on the same photodiode. Fig. 5.2 shows a photograph of the experimental arrangement.

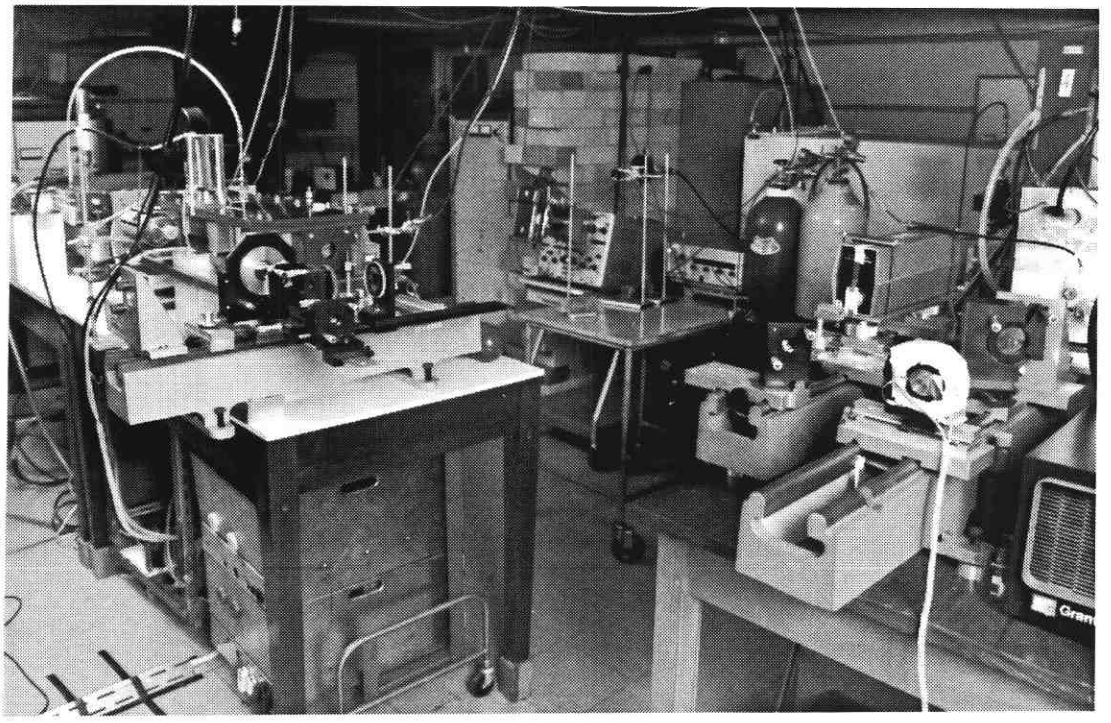

Fig. 5.2. The experimental arrangement

5.3 Injection mode-locking on the XeCl laser transition

The process of injection mode-locking implies that all the gain of the slave laser is swept out by the pulses from the master oscillator, so that the former does not reach threshold. In this way all the available energy in the slave laser will be contained in the short pulses. For complete saturation to occur, the path of the injected beam must fold back on itself when reflected from the back mirror. Otherwise, regions of the amplifier where the gain is not depleted can amplify spontaneous emission so that the slave laser reaches threshold.

Careful adjustments were therefore made so that the injected pulses followed a path exactly along the axis of the XeCl laser. This alignment was found critical for injection locking to take place. If the two lasers were not well aligned with respect to each other, the modulation of the XeCl output was incomplete as seen in Fig.5.3. The oscilloscope trace shows the amplified injected pulses superposed on a strong background lasing component.

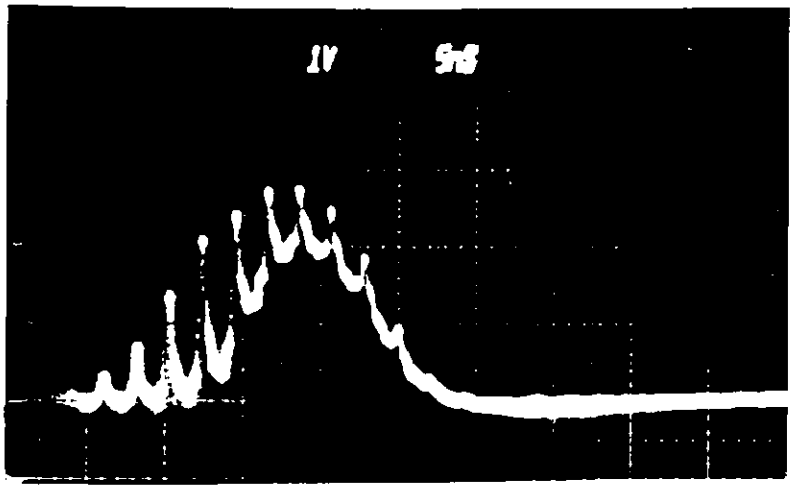

Fig. 5.3. Oscillogram of incomplete injection mode-locking

The length of the dye laser cavity was carefully adjusted to be equal to that of the XeCl cavity or half this length. Cavity matching had to be very accurate for good injection mode-locking to take place. Any temporal mismatch between the pulse propagating in the XeCl laser and the injected dye laser pulses increases with the number of roundtrips. Sub-pulses could therefore be resolved on a fast time-scale on the oscilloscope by looking at the last pulses in the train where the mismatch was greatest. An oscillogram of this is shown in Fig. 5.4. The durations of the late pulses are greater than the oscilloscope and photodiode response time and the two last

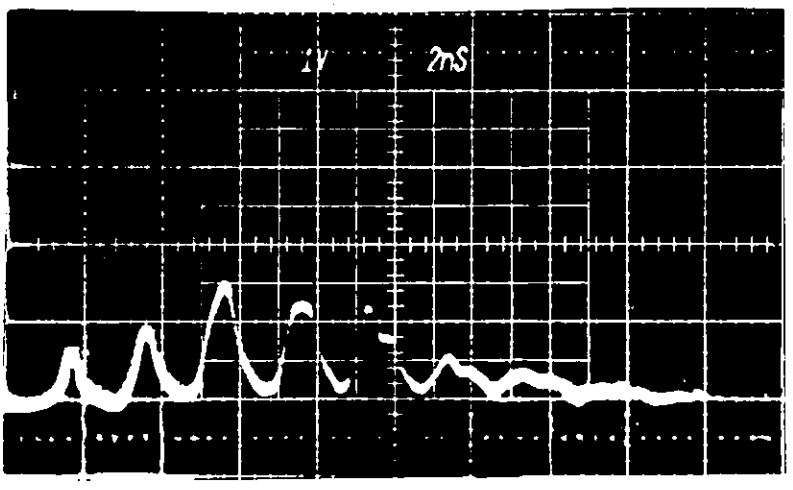

Fig. 5.4. Oscillogram of injection mode-locked output from a mismatched system

pulse envelopes clearly consist of more than one pulse. In most cases it was sufficient to monitor the pulses in this way and subsequently adjust the cavity lengths.

We felt that a small cavity mismatch could be tolerated provided the length of the XeCl cavity was shorter than that of the dye laser. In this case the rapidly growing pulse reflected back into the XeCl amplifier, just before the next injected dye laser pulse, would deplete the gain so that the small trailing dye laser pulse would experience very little gain and hence not be amplified. This, however, depends on how fast the gain recovers. Late in the pulse train where the mismatch is the greatest, the injected pulse might trail so far behind the amplified pulse that the gain has time to recover and this pulse grows.

With the two lasers well aligned and the cavity lengths matched, the XeCl laser was found to lock completely to the injected pulses. The injection mode-locked output was monitored by a fast ITL S20 photodiode used in conjunction with a Tektronix 7834 storage oscilloscope. Several optical attenuators (glass microscope slides) were placed in front of the photodiode to reduce the signal to levels where the response of the photodiode is linear. Fig.5.5 shows the oscilloscope trace of the free-lasing XeCl output and the injection mode-locked output on a 5ns/div time-scale(5.5a and 5.5b). The first mode-locked pulse train corresponds to a situation where the dye laser cavity length is the same as the XeCl laser cavity length. In this case the output consists of four intense pulses and the train lasts $\sim$ 40ns. In the second mode-locked pulse train (5.5c) the dye laser cavity length is still the same as the excimer laser cavity length, but the pumping of the dye laser is increased and the dye laser is therefore double pulsing. Hence the XeCl laser is in effect also

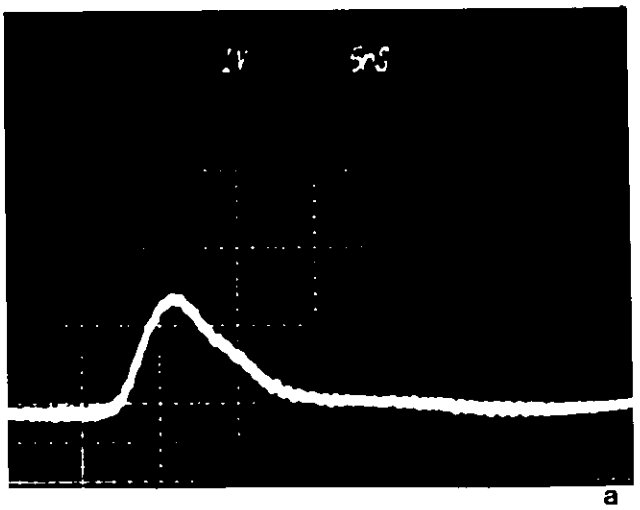

a

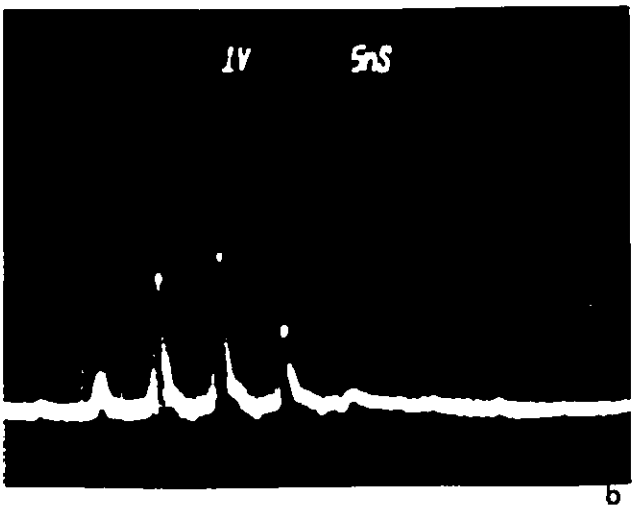

b

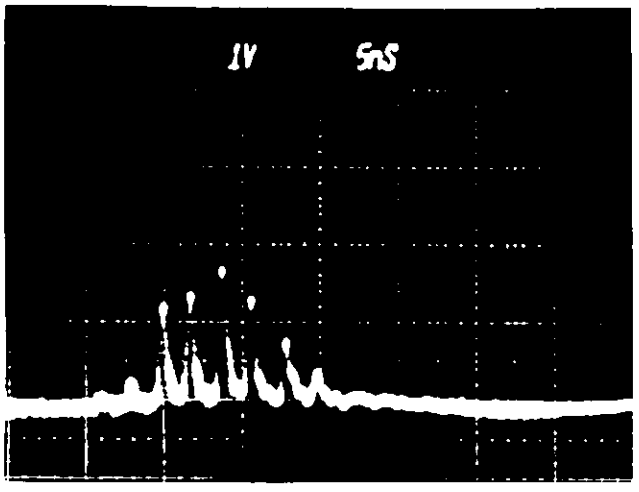

c

Fig. 5.5

Free-running and injection mode-locked output from the XeCl laser. (The free-running output is recorded at a different time from the mode-locked pulses, and the vertical scales are therefore not identical). Optical attenuation: ∿ 1025X

double pulsing and the pulse train consists of more pulses. The latter corresponds to a situation where the dye laser cavity length is half the length of the XeCl laser cavity.

In order to check whether injection mode-locking was really taking place, the XeCl laser output was monitored with the u.v. dye laser pulses alternatively blocked off and injected in consecutive shots. (To check that the XeCl laser was definitely above threshold when the gain was not depleted by the injected pulses). Over a large number of shots (∿ 20), the unmode-locked laser output from the XeCl amplifier typically had a peak amplitude of ∿ 6 $\pm$ 2V on the oscilloscope trace. The injection mode-locked pulses on the same scale had significantly higher amplitude (> 15V peak) and no background was observed between the pulses.

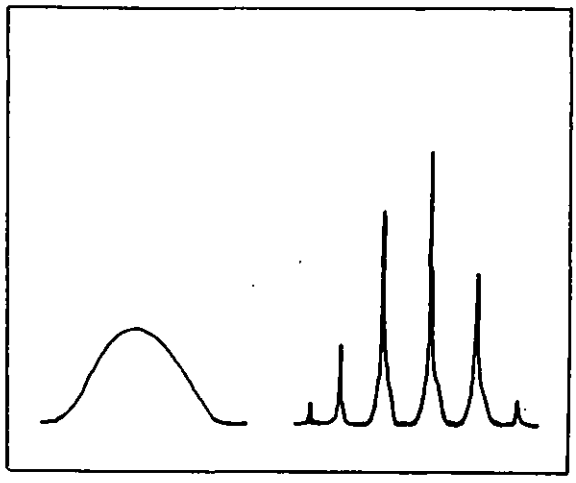

Fig. 5.6
Illustration of typical free-running and mode-locked output oscillograms.

Fig. 5.6 illustrates the oscilloscope traces. Hence we concluded that the laser energy available was being channeled into the ultrashort pulses and that the laser was injection mode-locked.

The injection mode-locked output from the XeCl laser was directed towards the photodiode by a quartz beamsplitter, (∿ 10% of the output intensity). This signal was too low to be detected by the available calorimeter and could not be increased by replacing the quartz beamsplitter by a mirror since this would reduce the energy of the pulses being injected into the XeCl amplifier. However, by measuring the area under the mode-locked pulse on the oscilloscope trace, an estimate could be obtained for the peak pulse energy, (see Chapter 4, Section 4.5). The maximum single pulse energy observed was ∿ 2mJ. Assuming an input pulse energy of ∿ 500nJ, this corresponds to an energy gain of 4000. The value obtained is in reasonable agreement with the maximum energy extractable taking saturation effects into account, as shown in Chapter 4, Fig. 4.11.

For injection mode-locking to take place, the injected pulses must be of sufficient energy to saturate the XeCl laser after a few passes, otherwise self-oscillation can build up and compete with the mode-locked pulse as discussed earlier. The threshold input pulse energy required for good injection mode-locking was estimated by attenuating the input beam sufficiently for background lasing to appear. This was investigated by inserting 1-4 calibrated glass

microslides in the input beam. Each slide transmitted only 25% of the 308nm pulses from the dye laser. With two microslides in the dye laser beam, the oscillogram showed background lasing between the injected pulses. Thus we conclude that for the XeCl laser used in our experiment, an input pulse energy density $\gtrsim .1\mu J/cm^2$ is needed to injection mode-lock the excimer laser. These measurements were averaged over several shots to account for variations in the dye laser input pulse energy.

An injection mode-locked pulse train can also develop from a single injected pulse. In this case no cavity matching would be required. From the single pass amplification data in Chapter 4 (Fig. 4.9) and from corresponding oscilloscope traces of the XeCl laser output we find that the threshold for lasing is reached $\lesssim$ 10ns after the gain starts to build up. Hence for the injected pulse to dominate over self-lasing, it would need to be injected during this 10ns period. Syncronization between the dye laser and the XeCl laser would therefore be critical, and jitter between the two systems should be < 10ns. This was not possible with the trigger arrangement used in our experiment, due to the relatively slow risetime of the dye laser flashlamp output that started the trigger chain.

5.4 Pulse duration measurements

The durations of the frequency doubled dye laser input pulses were measured using a Photochron II streak camera. The duration of the shortest pulses was $\sim$ 6ps. The streak camera used is described in Chapter 2, Section 2.7, and the streak records together with a micro-densitometer trace of the pulses are shown in Fig. 2.10.

The duration of the injection mode-locked pulses was measured using the same Photochron II streak camera. The experimental arrangement is shown in Fig. 5.1. In order to reduce the number of reflecting surfaces in the beam path, a window with one antireflection coated surface was inserted into the XeCl cavity and aligned with the back reflector thus serving as an output coupler.

The intense injection mode-locked pulses were directed towards PD2 and the signal from the first of these was used to trigger a Krytron circuit which provided the voltage ramp for the streak camera deflection plates. Due to the laboratory configuration, the streak camera had to be placed near both the dye laser and the discharge laser. The electrical noise generated when these lasers were fired was considerable. It proved extremely difficult to use the Krytron circuit to provide the ramp, since the Krytron would more often than not trigger from noise signals thus delivering the voltage ramp at the wrong time with respect to the arrival of the pulses at the deflection plates. (In order to avoid these problems, semiconductor switching devices can be used in conjunction with the streak camera [7,8]. This was tried in a preliminary experiment, but was not pursued further due to problems with the GaAs switch employed).

Fig.5.7 shows streaks of the injection mode-locked output with three different streak camera writing speeds. The top streak record shows the whole injection mode-locked pulse train. The separation between the pulses is $\sim$ 4ns and both the dye laser and XeCl laser are therefore double pulsing. No background between the pulses is observed, thus the laser is completely injection mode-locked. The next plate shows a single picosecond pulse reflected from the front and back surfaces of the first delay-line plate. The plate thickness corresponds to a separation of $\sim$ 100ps between the two streaks. The

last streak record (slightly out of focus) shows the same on an expanded time-scale. (Streak writing speed $\sim 5 \times 10^9 cms^{-1}$). A microdensitometer trace corresponding to a streak at the same writing speed (recorded on Kokak HP5 film) is shown in Fig. 5.8. The shortest pulse duration found was $\sim$ 7 ps. Because of severe jitter in the triggering of the streak camera, it was not possible to determine whether the streaks corresponded to pulses early or late in the XeCl pulse train.

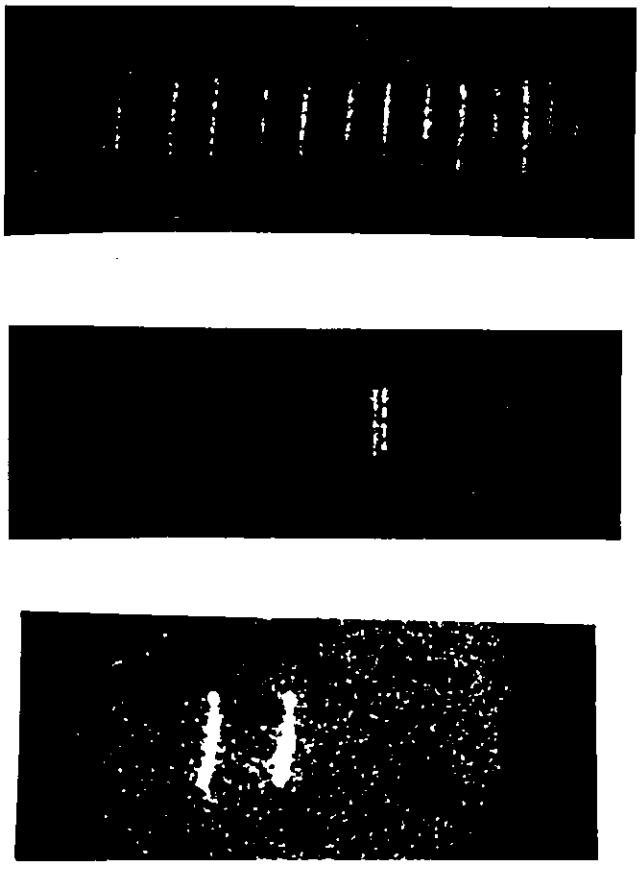

Fig. 5.7. Streaks of injection mode-locked output

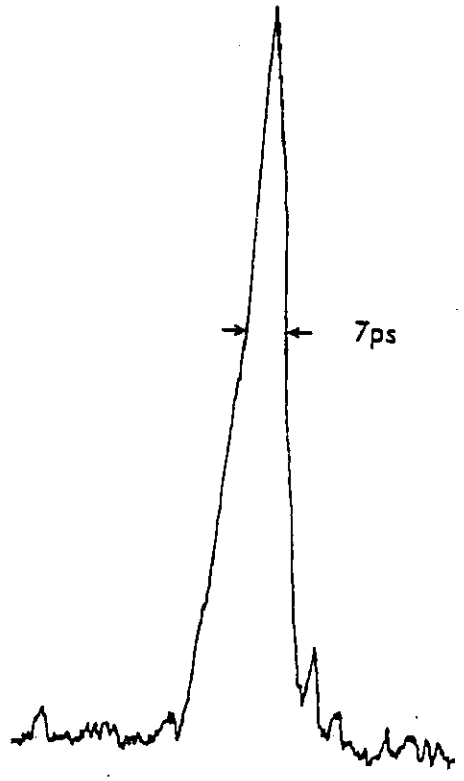

Fig. 5.8. Microdensitometer trace of streak photograph

5.5 Injection mode-locking on the 1-6 transition

The Franck-Condon factor of the 1-6 transition (λ =307.3nm) is the fourth highest in the XeCl manifold, (.136 compared to .240 for the 0-2 laser transition, Ref. 4, Chapter 4). In order to investigate

whether the XeCl laser would lock completely to injected pulses overlapping this transition, the dye laser was tuned to 307.3nm and injected into the XeCl cavity in the same way as previously described. All other conditions were the same as for the 0-2 transition. The XeCl laser did not, in this case, lock completely to the input pulses. A free-running component from the XeCl laser transitions (0-1, 0-2) was always present. The output was similar to that shown in Fig. 5.3, where the amplified pulses are simply superposed on the laser output from the 0-2 and 0-1 transitions.

For the gain on the 0-2 and 0-1 transitions to be depleted, the population in the $v' = 0$ level must relax into the $v' = 1$ level on a time-scale comparable to the pulse duration ($\sim$ 5-10ps). The average time between collisions under the conditions in our experiment is estimated to be $\sim$ 100ps. At this pressure ($\sim$ 2000 Torr) in the XeCl laser, it would therefore not be possible to deplete the population in the laser level quickly enough for injection frequency and mode-locking to take place on transitions originating from higher lying vibrational levels.

Goldhar et al. reported injection frequency locking of a XeF laser on a nanosecond time-scale[9]. A narrow band signal from an etalon tuned XeF laser was used to lock a regenerative amplifier on the main laser transition. They found that the rotational cross-relaxation was fast, but found no coupling between vibrational bands.

5.6 Injection frequency and mode-locking on transitions from the $v' = 0$ level

With only one Fabry-Perot in the dye laser cavity, the bandwidth

of the frequency doubled output was $\sim$ 2.5 Å. Thus when the dye laser was tuned to the 0-2 wavelength, the spectrum of the injection mode-locked output contained a component due to the 0-1 transition. Fig.5.9 shows the spectra from the injection mode-locked pulse train (top) and the dye laser input (bottom) together with the free-running XeCl output spectrum (centre).

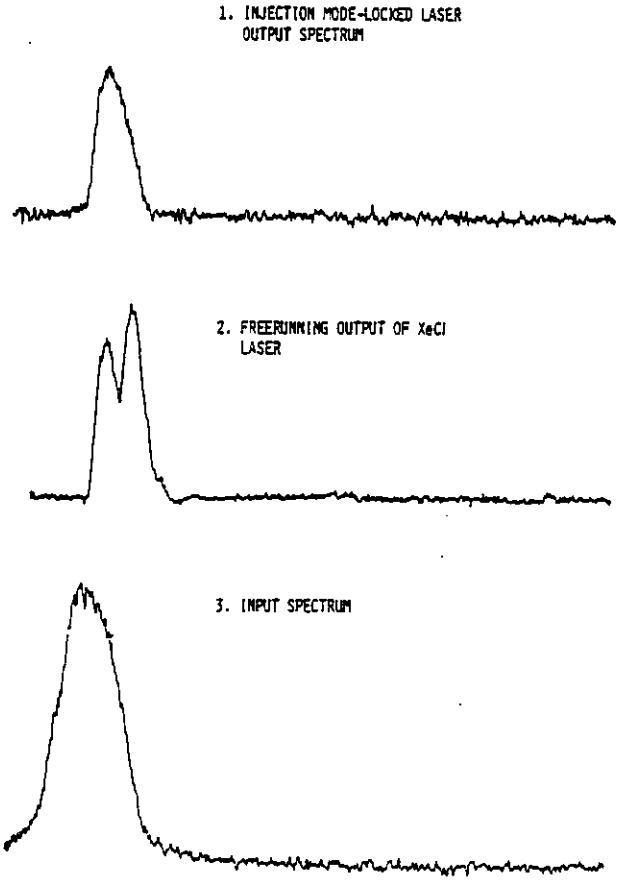

Fig. 5.9. Spectra of mode-locked output, free-running output and input

The dye laser was also tuned to wavelengths that overlapped other XeCl transitions originating from the lowest excited state vibrational level. The transitions probed were: 0-0, 0-1, 0-2, 0-3 and 0-4, and the wavelengths ranged from λ = 307.8nm to λ = 308.7nm. The respective Franck-Condon factors are : .104, .226, .240, .190 and .112. (Lasing in XeCl has only been observed from the 0-1, 0-2 and 0-3 transitions, and with our laser only from the 0-1 and 0-2 transitions).

The injection mode-locked output was monitored using the fast photodiode and the storage oscilloscope and the spectrum of the injection mode-locked output was simultaneously recorded. The dye laser input wavelength was adjusted immediately prior to each measurement. When the dye laser was tuned between the 0-0 and 0-1 transitions, lasing from the 0-2 transition was suppressed. When the dye laser spectrum overlapped the weaker 0-4 transition, lasing from 0-1 and 0-2 was observed and the modulation depth was only $\sim$ 15%. Thus we conclude that if the input pulses are tuned to overlap a strong transition from the $v' = 0$ level then emission from the other laser levels can be suppressed, since the population in the $v' = 0$ level gets depleted by the injected pulses. Fig. 5.10 shows the spectrum of the XeCl pulse train together with the dye laser spectrum with the latter tuned to a wavelength overlapping the 0-4 and 0-3 transitions (λ = 308.6nm).

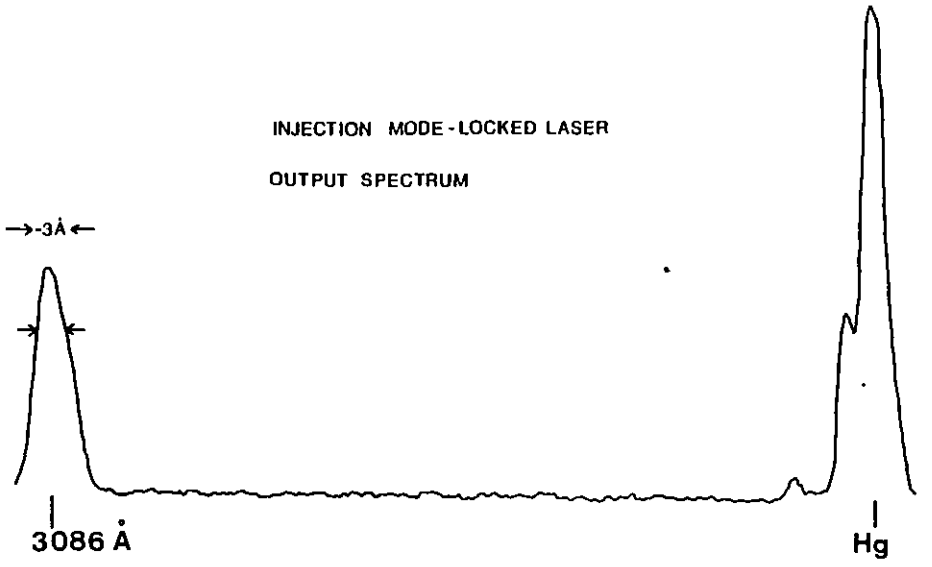

Fig. 5.10. Spectrum of injection mode-locked output with input detuned from main laser transitions

No component from the 0-1 or 0-2 transitions are present. The experiment was however, conducted under low gain conditions. It is conceivable that with higher gain it may not be possible to suppress the free-lasing component from the laser transitions with low power input pulses.

5.7 Gain recovery

The separation between injected pulses in our experiment was either ∿ 4 or ∿ 8ns depending on whether the dye laser was double pulsing or not. In neither case did the XeCl laser reach threshold between the pulses, and no free-running component was emitted when the input wavelength covered the laser transitions. In certain cases, however, when the dye laser double pulsed, the separation between pulses was very small. Injection mode-locking was found to take place even if the input pulses were separated by only 1-2ns. Fig. 5.11 shows the oscilloscope

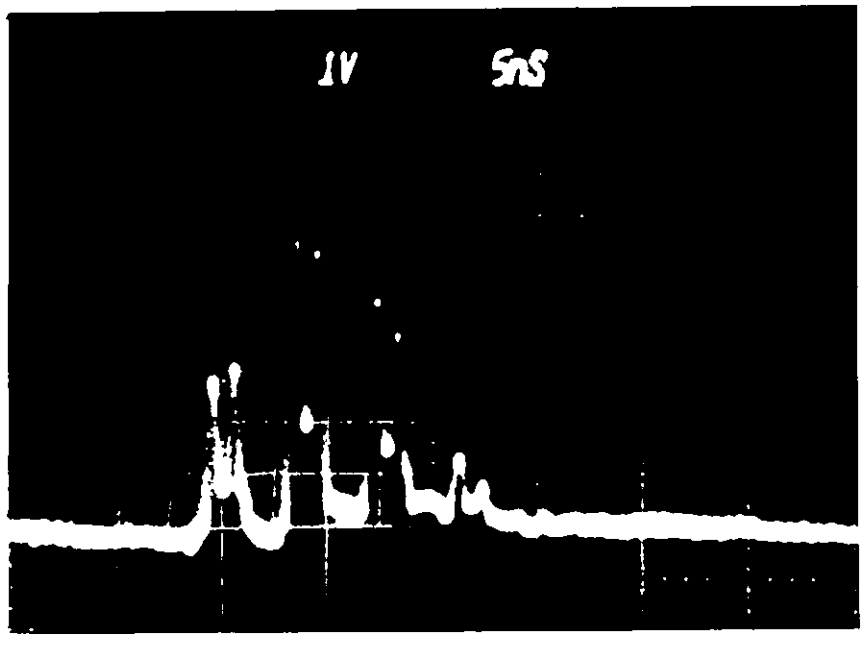

Fig. 5.11. Injection mode-locked output corresponding to input pulses of irregular separation.

trace of the pulse train emitted by the XeCl laser when dye laser pulses of irregular separation was injected. The separation between the pulses is ∿ 2.5ns. Hence, the conclusion to be drawn from this is that the gain must have fully recovered in this time-scale, since the second injected pulse following closely after the first has been amplified to the same intensity.

In fact, the oscilloscope trace shown in Fig. 5.4 illustrates a similar situation. In this case, however, the two closely separated pulses that can be seen under each pulse envelope are due to a cavity mismatch. This indicates that the gain in the laser can recover on a time-scale of less than 1ns. Fig. 5.12 shows an oscilloscope trace of such a double pulse. The oscilloscope response time is too slow to resolve the two pulses, since the pulse separation is only a few hundred picoseconds. Arranging a small cavity mismatch is thus a possible way of determining how fast the gain recovers. Several sub-pulses will trail behind the main pulse if the XeCl cavity roundtrip time is less than the separation between pulses. The more roundtrips, the greater the separation between the first and last of these will be. Hence, if a pulse trails sufficiently far behind the first intense pulse for the gain to have recovered, it will be amplified and can be detected. If a streak camera is used to monitor the output pulses, the gain recovery time can then be estimated.

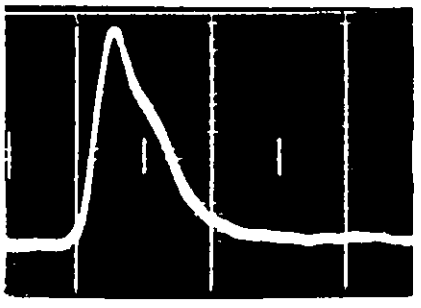

Fig. 5.12
Injection mode-locked pulse. (2ns/div)

On a time-scale of a few hundred picoseconds pumping is not significant. The rapid recovery of gain is therefore an indication that vibrational relaxation in the XeCl-B-state is fast. The average

time between collisions at the pressures used in our experiment is estimated to be ∿ 100ps. Thus it is feasible that vibrational relaxation can take place during a few hundred picoseconds.

5.8 Conclusion

Low power mode-locked dye laser pulses have been frequency doubled and used to injection mode-lock the XeCl discharge laser. A 100% modulated injection mode-locked pulse train lasting 30-40ns was generated yielding peak powers of 200MW and pulses as short as 7ps.

If the number of roundtrips were increased, for instance by the use of e-beam sustained discharge pumping, further pulse shortening could occur because of gain saturation effects, as will be discussed in the next chapter. This, together with saturable absorption in a mode-locking dye is responsible for pulse compression in passively mode-locked dye lasers. If an appropriate dye were available, a hybrid system could be employed with a saturable absorber in the amplifier cavity, also yielding shorter pulses. In order to generate bandwidth limited pulses (∿ 1ps) the use of bandwidth limiting elements in the cavity could be advantageous, although this would be at the expense of output power.

Information about the vibrational relaxation time of the XeCl-B-state was obtained by investigating the gain recovery time in the XeCl laser. Vibrational relaxation was found to take place on a time-scale longer than 5-10ps, based on the result that the XeCl laser did not injection lock to pulses overlapping the 1-6 transition,which indicated that the gain on the 0-1 and 0-2 laser transitions could not be depleted sufficiently fast by relaxing to the $v' = 1$ level. The gain on the

laser transitions was, however, found to recover in less than 1ns. We therefore estimate that vibrational cross relaxation in the upper state manifold takes place on a time- scale of a few hundred picoseconds.

The method of injection mode-locking could be extended to other rare-gas excimer and exiplex lasers; using the third harmonic of the Nd:glass laser to mode-lock the XeF laser, and the fourth harmonic of the Ruby laser to mode-lock the Xe_2 laser.

CHAPTER 5 - References

1 W.K. Bischel, J. Bokor, D.J. Kliger and C.K. Rhodes; IEEE J. Quant. Electron., QE-15, 380 (1979).

2 J. Reintjes, Optics Letters; 5, 342 (1980).

3 J.B. Laudenslager, T.J. Pacala and I.S. McDermid, presented at CLEO (1981).

4 C.P. Christensen, L.W. Braverman, W.H. Steiner and C. Wittig; Appl. Phys. Lett., 29, 424 (1976).

5 T. Efthimiopoulos, J. Banic and B.P. Stoicheff; Can. J. Phys., 57, 1437 (1979).

6 R.L. Fork, B.I. Greene and C.V. Shank; Appl. Phys. Lett., 38, 671 (1981).

7 W. Margulis, W. Sibbett, J.R. Taylor and D.J. Bradley; Opt. Comm., 32, 331 (1980).

8 W. Margulis, PhD Thesis, Imperial College, University of London (1981).

9 J. Goldhar, J. Dickie, L.P.Bradley and L.P. Pleasance, Appl. Phys. Lett., 31, 677 (1977).

CHAPTER 6

INJECTION MODE-LOCKING: A THEORETICAL MODEL

6.1 Introduction

Theoretical models for the evolution of passively mode-locked pulses in quasi-continuous and giant pulse lasers have been extensively reviewed [1, 2, 3]. For quasi-continuous dye lasers, the models have shown that gain saturation and bleaching of the mode-locking dye are equally important in the pulse shortening process. In giant pulse systems saturation of the active medium does not shorten the pulse duration significantly. The recovery time of the saturable absorber is however relatively short compared to individual cavity fluctuations and picosecond pulses can be generated during the limited time-span of the giant pulse event. The saturable absorbers used for dye lasers have longer recovery times and the pulse developing in the cavity must make many passes through the amplifier and absorber before the combined effect reduces the pulse duration to $\lesssim$ 10ps. Passive mode-locking of rare-gas halide lasers has been attempted, but it has to date not been possible to bleach the dyes completely and obtain a 100% modulated output [5, 6].

The single pulse energy estimated for the injection mode-locked pulses in our experiment was sufficient to saturate the gain of the excimer laser. From the streak camera measurements described in the previous chapter it was not possible to investigate the effects of saturation on the pulse evolution, since it was difficult to determine exactly which pulse in the train was being streaked. (And also since the output and corresponding input pulse were not streaked

simultaneously.) In order to determine whether gain saturation, in the absence of a saturable absorber, would actually compress the pulses, a model for the evolution of the pulses in the injection mode-locked XeCl laser was developed. A computer was used to solve the nonlinear differential equation that describes the pulse traversing the XeCl amplifying medium. The output pulse profile after a pass through the amplifier was then determined as a function of the input pulse, the small signal and saturated gain. The pulses injected from the dye laser were superposed on the feedback component of the previous amplified pulse. A small mismatch between the XeCl laser cavity and the dye laser cavity was introduced in the simulation and the effect this had on the injection mode-locking was investigated. Frequency dispersion was neglected in order to make the analysis simpler.

6.2 The computer model

The Frantz-Nodvik model described in Chapter 4 (Section 4.2) was used in the computer simulation [7]. The model assumes that the active medium is a two level quantum system and solves the photon transport function for a pulse travelling through the inverted medium:

$$\frac{\partial}{\partial t} n(x, t) + c \frac{\partial}{\partial x} n(x, t) = \sigma c n(x, t) \Delta N \qquad (6.1)$$

where $n(x, t)$ = number density of photons in the pulse

σ = stimulated emission cross section ($4.5 \times 10^{-16} cm^2$ [8])

$\Delta N = N_2(t) - N_1(t)$ = population inversion

If the assumption that all the stimulated photons cause a reduction of population in the upper level only (N_2) and cause an increase of population

in the lower level (N_1) only, then the additional equations to be solved are:

$$\frac{\partial}{\partial t} N_2(t) = -\sigma c n(x, t)\ \Delta N \tag{6.2}$$

and

$$\frac{\partial}{\partial t} N_1(t) = +\sigma c n(x, t)\ \Delta N \tag{6.3}$$

If $\Delta_o(x) = \Delta N(x, -\infty)$ is the population inversion before the pulse enters the amplifier and $n_o(t)$ is the photon density at the entrance of the amplifier, the general solution of equations 6.1, 6.2 and 6.3 becomes

$$\frac{n(x, t)}{n_o(t - x/c)} = \frac{1}{1 - \{1-\exp(-\sigma\int_o^x \Delta_o(x')dx')\}\ \exp(-2\sigma c\int_{-\infty}^{t-x/c} n_o(t')dt')} \tag{6.4}$$

$$= G(x, t), \text{ the energy gain of the pulse.}$$

The energy gain, i.e. the ratio of the output pulse photon density to the input pulse photon density, can then be evaluated. If the energy density of the input pulse is low, the expression reduces to the exponential law. However, in most cases the leading edge will find exponential gain, while the trailing edge will find reduced gain due to depletion of the population inversion by the leading edge. A change in the shape of the pulse and a shift of the centre of the pulse is therefore expected. The shift of the peak means that the centre of the pulse appears to have a velocity greater than the speed of light. (This does not violate Einstein's theory of relativity, since it is not the velocity of the individual photons that exceeds the speed of light).

The equation for the energy gain G(x, t) can be solved numerically by the computer. In the paper by Frantz and Nodvik the population inversion is assumed constant throughout the gain medium (i.e. pumping is ignored). Since pumping in the discharge laser is rapid

even on a timescale of a few nanoseconds, the population inversion can change substantially during one pass through the amplifier. In our model, pumping was taken into account by varying the small signal gain (g_o) experienced by the pulse according to the temporal profile of the discharge pumping. The small signal gain curve was assumed to be gaussian shaped with a peak value of g_o = 0.075/cm. This was consistent with measurements described in Chapter 4. Fig. 6.1 shows the small signal gain profile used in the simulation.

For a certain distance, x, in the amplifier g_o corresponds to the term: $\sigma\int_0^x \Delta_o(x')\,dx'$ in Equation 6.4. The 80cm long XeCl amplifier was in the computer simulation split into eight 10cm long segments and g_o was considered constant in each segment*. The mode-locked pulse was described by 1600 points, each corresponding to a duration of 50fs. The temporal profile of the pulse at the exit of each 10cm segment was found by solving Equation 6.4 point by point. The depletion of gain by the previous points in the pulse was in this way accounted for. The

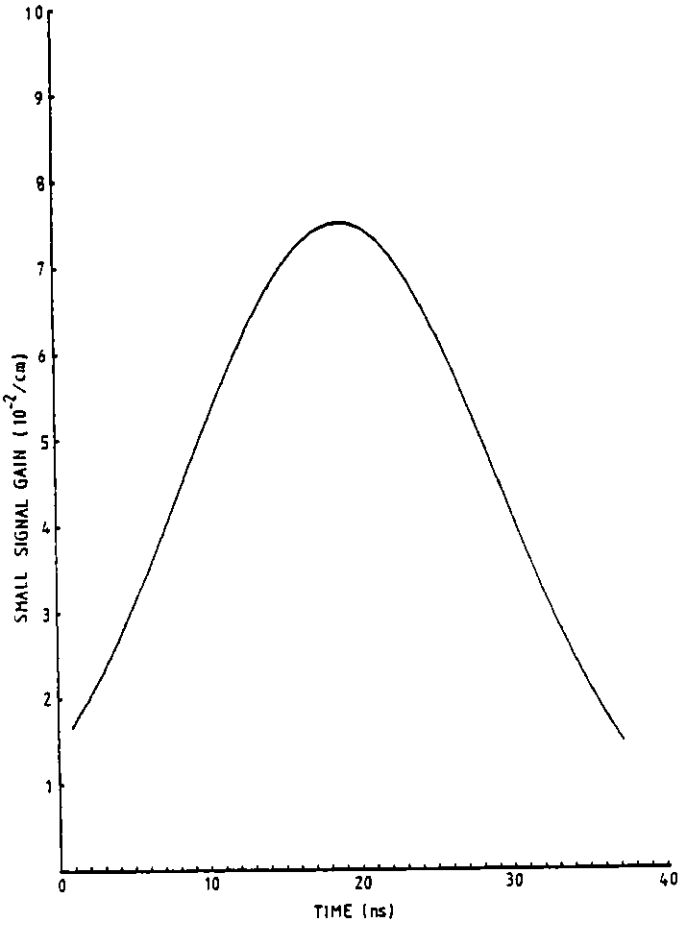

Fig. 6.1
Small signal gain used in the computer simulation (F.W.H.M ∿ 25ns).

*In order to check that the segment size of 10cm was not too large, a few runs were tried with 1cm segments. The results were not significantly different.

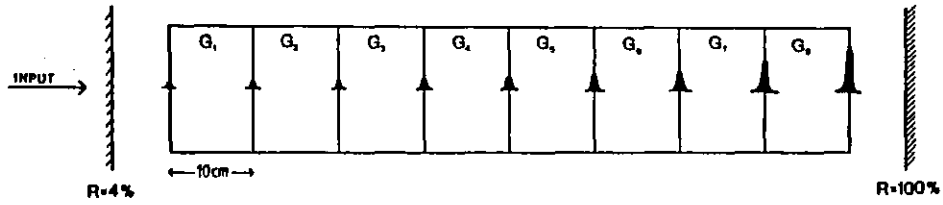

Fig. 6.2
Mode-locked pulse propagating through amplifier segments

photon density incident on a new segment corresponded to the integral of all the points in the pulse. Fig. 6.2 illustrates the propagation of the pulse through the amplifier segments. The computer program is listed in Appendix 1.

In the expression for the energy gain in Chapter 4 (Section 4.2), the pulse shape is assumed to be square.
In the simulation presented here, we have considered three different profiles for the injected input pulses. These were

gaussian: $N_o(t) \alpha \exp(t/2\sigma)^2$

hyperbolic secant: $N_o(t) \alpha \text{sech}^2(t/1.763.\tau_p)$

and lorentzian: $N_o(t) \alpha 1/(t^2 + \tau_p^2)$

where $N_o(t)$ is the photon density and τ_p is the duration of the injected pulses. It was, however, not possible to simulate the injection mode-locking experiment using a lorentzian input pulse shape for reasons that will be discussed later.

6.3 Gain saturation

The output pulse profiles found after consecutive roundtrips in the XeCl amplifier varied considerably with the injected pulse shape. Already at the end of the first roundtrip through the amplifier, the

gain showed saturation. Thus, the amplification of the tail of the pulse was less than the amplification of the leading edge. In the second and third roundtrip the gain was strongly saturated and the tail of the pulse experienced no net gain. This caused the peak of the pulse to shift for all the input pulse shapes. Fig. 6.3(a) and (b) show the evolution of the energy gain (6.4) within the picosecond pulse duration plotted with the corresponding mode-locked pulse (N(x, t)). Fig. 6.3(a) corresponds to the output pulse of the amplifier after the first roundtrip for a gaussian input pulse of 6ps duration. The energy density of the pulse was 1μJ cm^{-2}. The plot shows that the photons in the first 2ps of the pulse have depleted the gain sufficiently for the rest of the pulse to experience reduced amplification. The total energy density in the pulse at the exit of the amplifier was in this case 59μJ cm^{-2} and the duration 5.9ps. In Fig. 6.3(b) the corresponding situation is shown at the exit after the third roundtrip. The small signal gain is now much higher due to pumping, and when the pulse has reached the peak, all the gain has been depleted. The tail then experiences no net gain (G = 1). The total energy density in the pulse was in this case $\sim$ 1.1mJ cm^{-2} and the duration 5.5ps.

6.4 Pulse evolution for gaussian input pulses

The gaussian pulse profile is characterised by a sharp leading and trailing edge compared to hyperbolic secant or lorentzian shapes. Less energy is therefore concentrated in the wings of the pulse and the leading edge does not "run away" as is the case for a lorentzian pulse. Fig. 6.4 shows the pulse evolution for a gaussian shaped injected pulse of 6ps duration. This duration was chosen for the injected

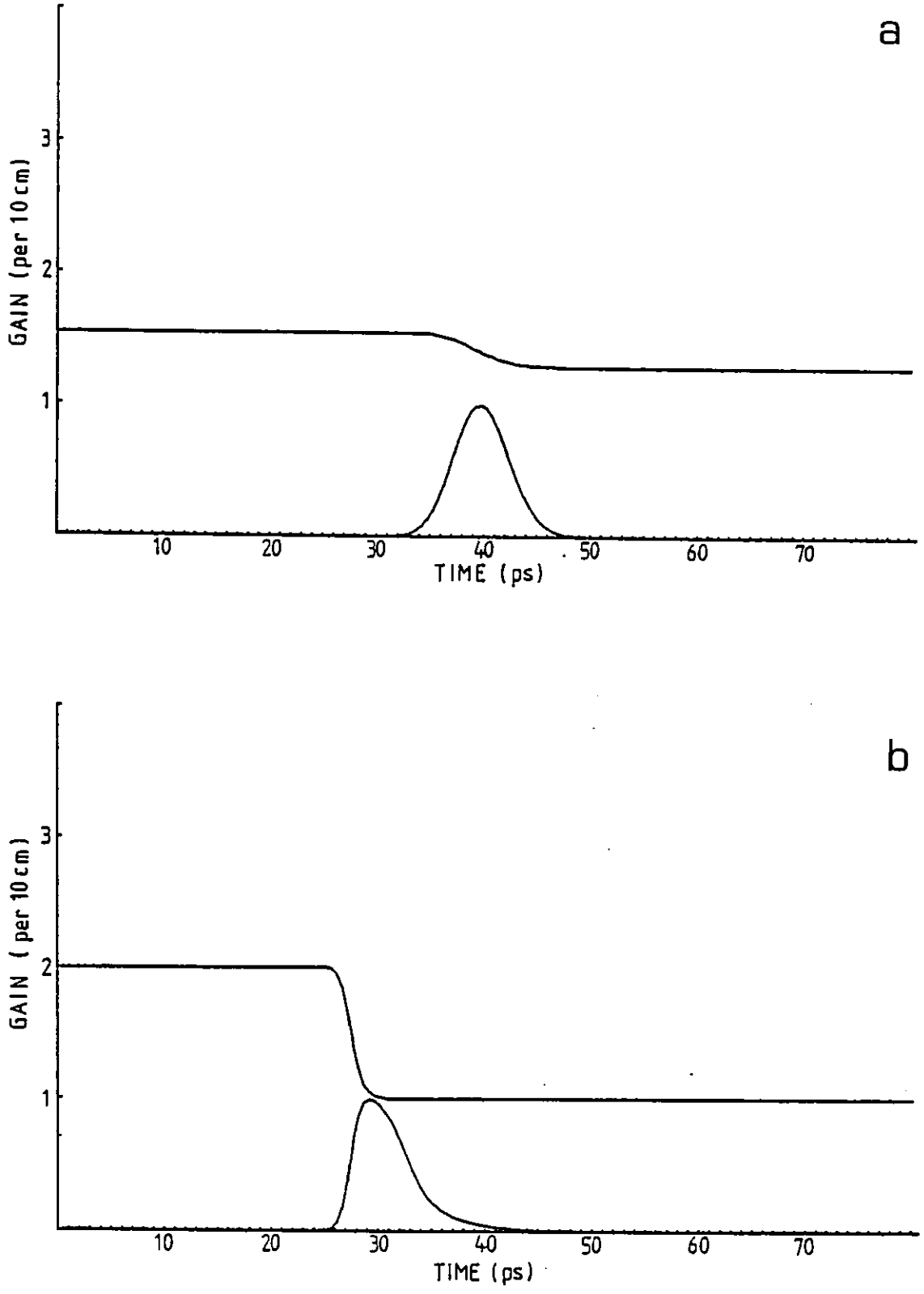

Figs. 6.3(a) and (b)

Plot of the equation for energy gain with the mode-locked pulse for the first (a) and the third (b) roundtrip

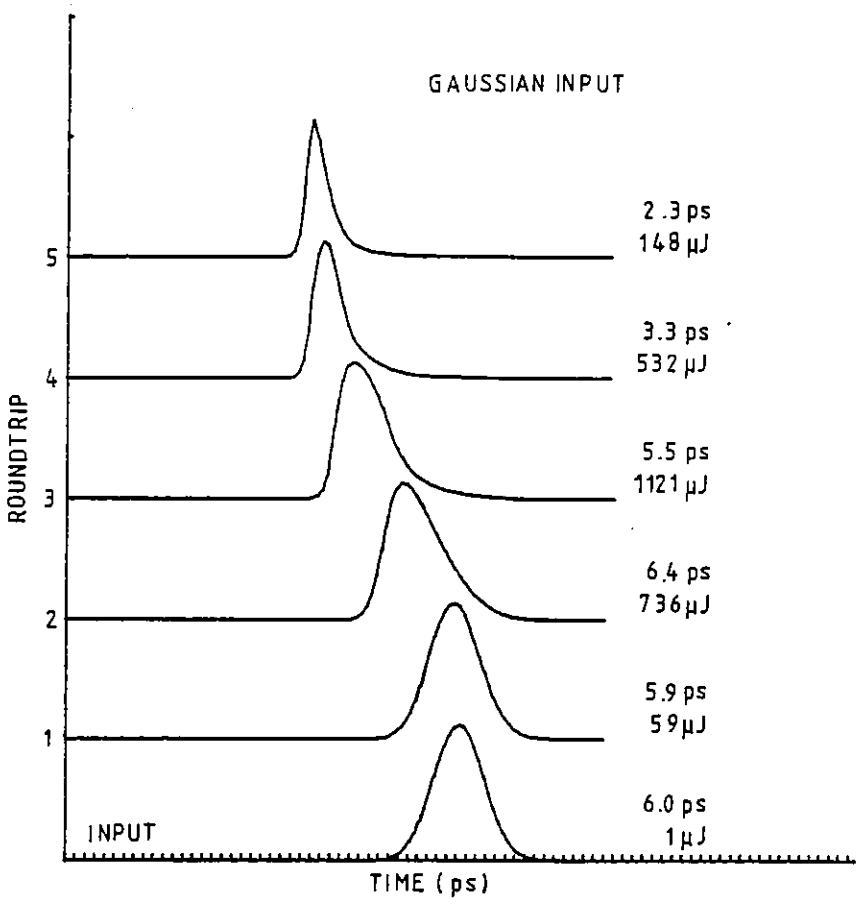

Fig. 6.4
Pulse evolution for gaussian input pulses. No mismatch

pulses in all the computer simulations, since this was the shortest duration found for the dye laser pulses in the measurement described in Chapter 2, Section 2.8. For the same reason the energy density of the input pulses was chosen to be 1 μJ cm^{-2}. The pulse duration and energy density of the pulse after consecutive roundtrips in the XeCl laser are indicated in Fig. 6.4. For every roundtrip 4% (= reflectivity of the output coupler) of the output pulse was fed back into the XeCl amplifier together with the next injected pulse from the dye laser pulse train.

The significant effects of gain saturation appear after the second

roundtrip. The peak of the pulse has then shifted by ∿ 6ps and the pulse duration has increased to ∿ 6.4ps. The pulse shape is no longer gaussian and is asymmetric. This is not surprising, since the peak of the pulse traversing the amplifier experiences less gain than the leading edge due to saturation, causing the trailing edge to fall off slowly. After the fourth and fifth roundtrip the pulse shape is again symmetric, since the tail end "shoulder" disappears due to gain saturation. Thus the plots show that the net effect of gain saturation is to cause the peak of the pulse to shift forward and the leading edge to sharpen. This ultimately results in pulse compression, and after five roundtrips the pulse duration is reduced from 6ps to 2.3ps. The peak of the pulse has then shifted forward by 15ps.

The peak energy density (after the third roundtrip) is ∿ 1.1mJ cm^{-2} which is in good agreement with peak pulse energy obtained in the experiment (1-2mJ). When a temporal mismatch of + 6ps was introduced in the program to account for a difference in the roundtrip time of the dye laser and excimer laser (corresponding to a cavity mismatch of 1.8mm), the injection mode-locking evolved as shown in Fig. 6.5. The excimer laser cavity was in this case taken to be longer than the dye laser cavity. Therefore, the pulse fed back trailed the pulse being injected by an increased amount every roundtrip. This resulted in a double pulse appearing after the second roundtrip. The forward shift of the peak is now enhanced since the gain is depleted by the early injected pulse rather than by the pulse fed back into the cavity by the output coupler. In the third roundtrip the injected pulse competes with the feedback component, since both are very intense. In the fourth and fifth roundtrip the effect of the injected pulse is less important, since the gain is reduced due to pumping and the injected pulse (1μJ cm^{-2}) cannot grow large enough to compete with

the feedback component ($\sim$ 75 $\mu J\ cm^{-2}$).

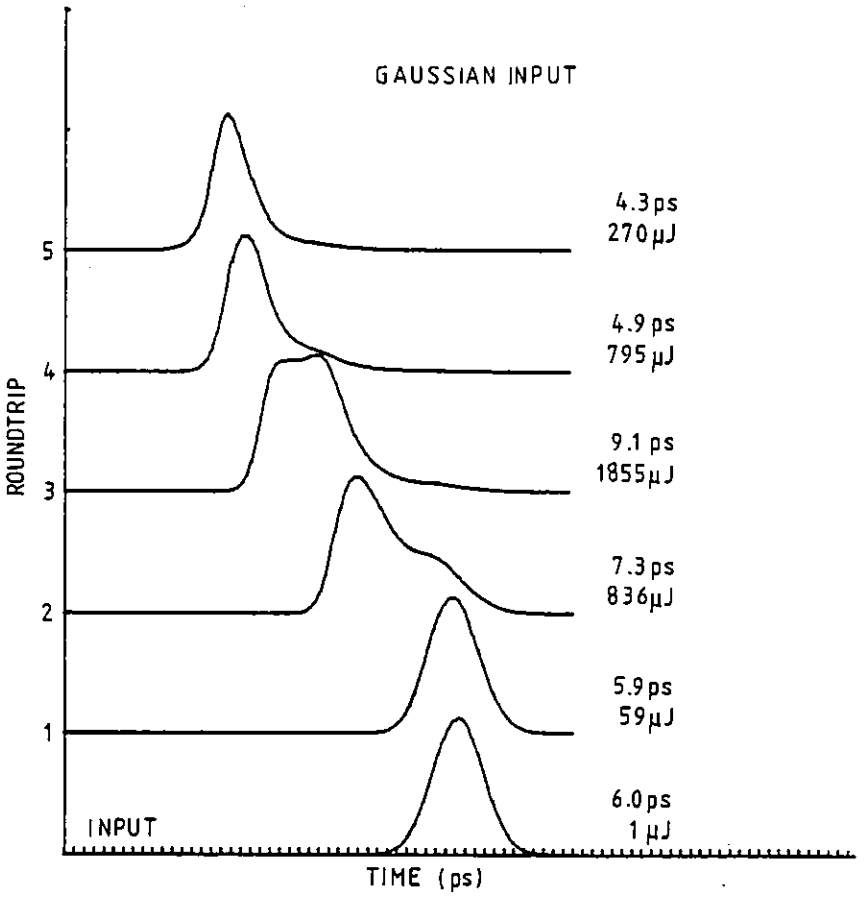

Fig. 6.5. Pulse evolution for gaussian input pulses (+ 6ps mismatch).

Apart from causing structured pulses, the mismatch also results in pulses of longer duration and higher energy density than with the perfectly matched cavities.

Fig. 6.6 shows the pulse evolution with a mismatch of -6ps, corresponding to the XeCl laser cavity being shorter than the dye laser cavity. The effect of the mismatch is now almost undetectable. This is to be expected, since the injected pulse now always trails the pulse that is fed back into the excimer laser by an increasing amount every roundtrip. Due to gain saturation it therefore experiences very little gain and never grows sufficiently to cause a structured intensity profile. The evolution of the pulses is therefore very similar to the perfectly matched case (Fig. 6.4).

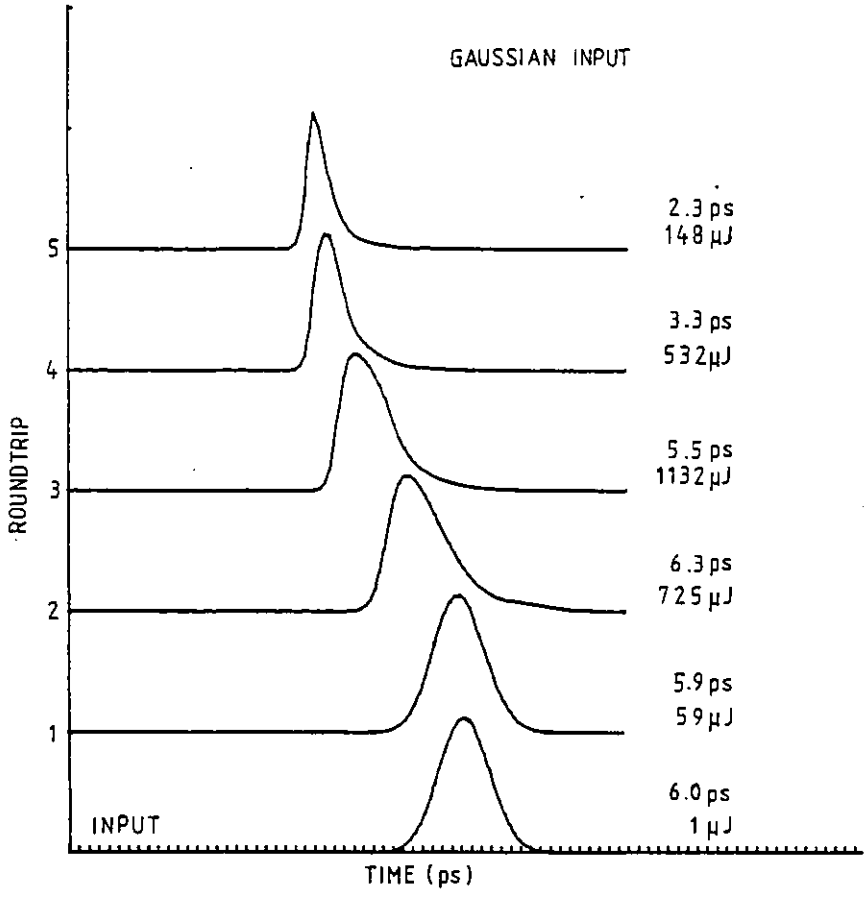

Fig. 6.6
Pulse evolution for gaussian input pulses. (-6ps mismatch).

6.5 Pulse evolution for hyperbolic secant input pulses.

Fig.6.7 shows the evolution of the injection mode-locked pulses for hyperbolic secant input pulses. The plots show a more dramatic shift forward of the peak than for the gaussian input pulses; after five roundtrips the peak has shifted by a total of 34ps. The pulses broaden considerably in the second and third roundtrip. The broadening can be explained by the relatively slowly rising shape of the leading edge. The gain then saturates less rapidly than for a sharper leading edge, causing a larger proportion of the pulse to be

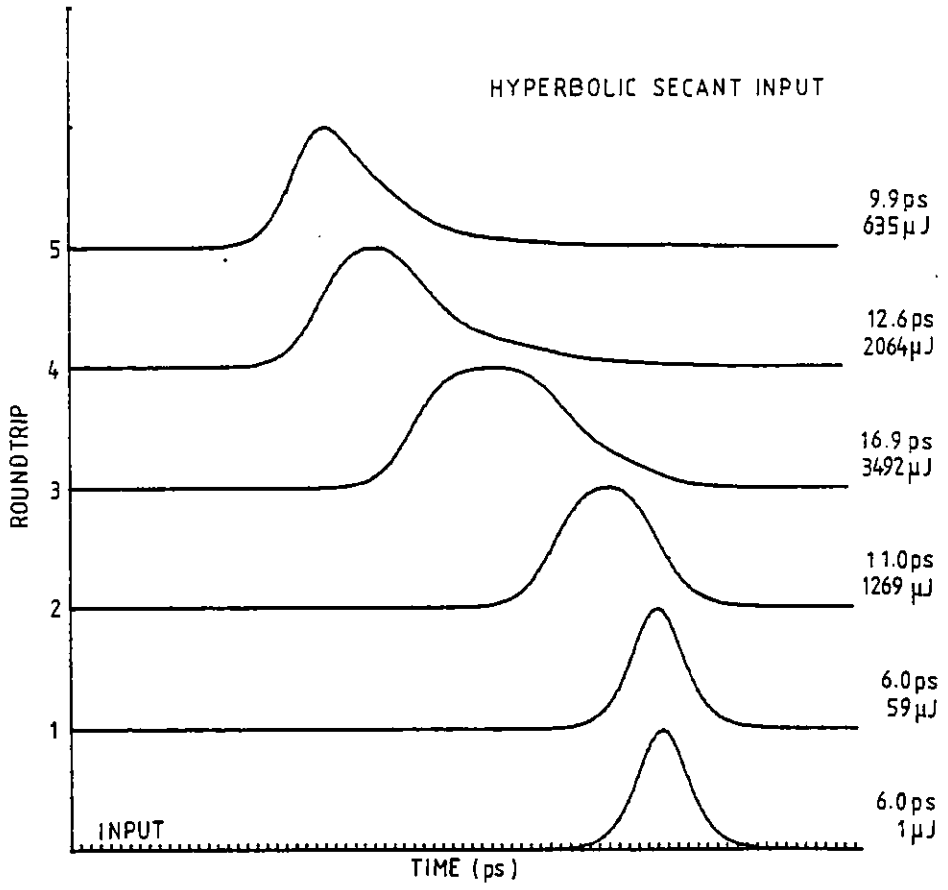

Fig. 6.7

Pulse evolution for hyperbolic secant input pulses. (No mismatch)

amplified and thus increasing the pulse width. After the third roundtrip, the energy in the pulse is high enough to saturate the gain early and the pulse starts to compress.

Fig.6.8(a) and (b) shows the pulse evolution for mismatched excimer and dye laser cavities. Again the temporal mismatch was chosen to be $\pm$ 6ps. Fig. 6.8(a) corresponds to a XeCl laser cavity that is longer than the dye laser cavity. The effect of the mismatch is not significant, apart from shifting the peaks of the pulses forward. The pulse durations are almost the same as for the perfectly matched case, except for the second roundtrip where the pulse has a slight double structure. With the shorter XeCl laser cavity the mismatch has no

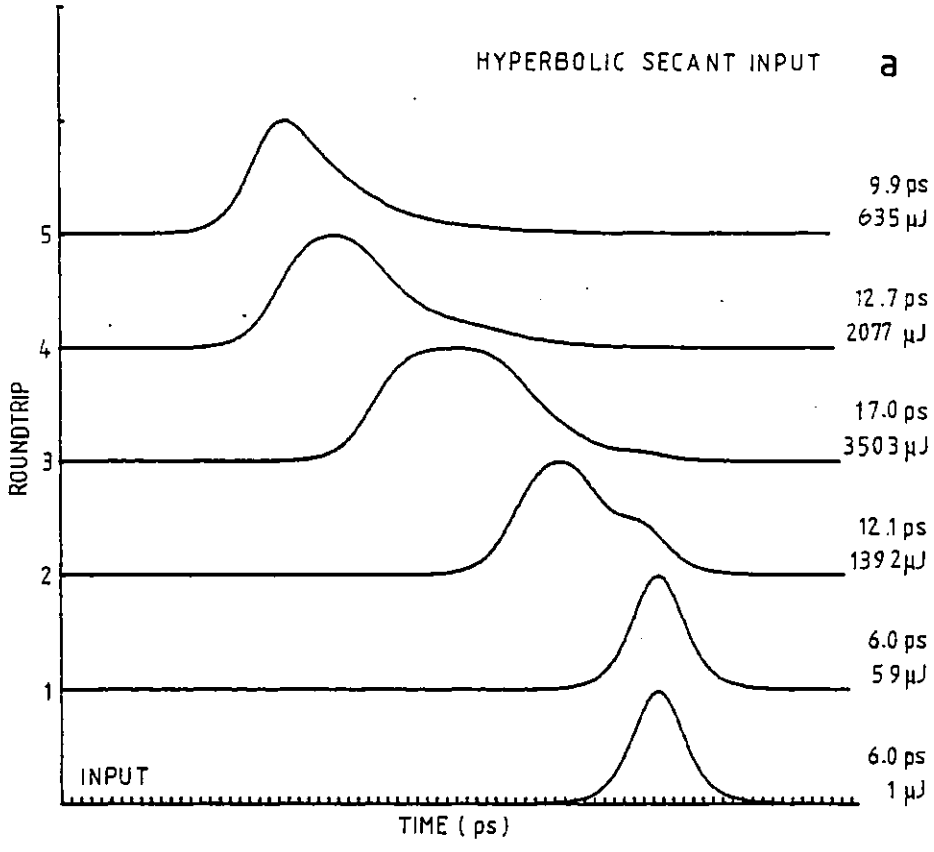

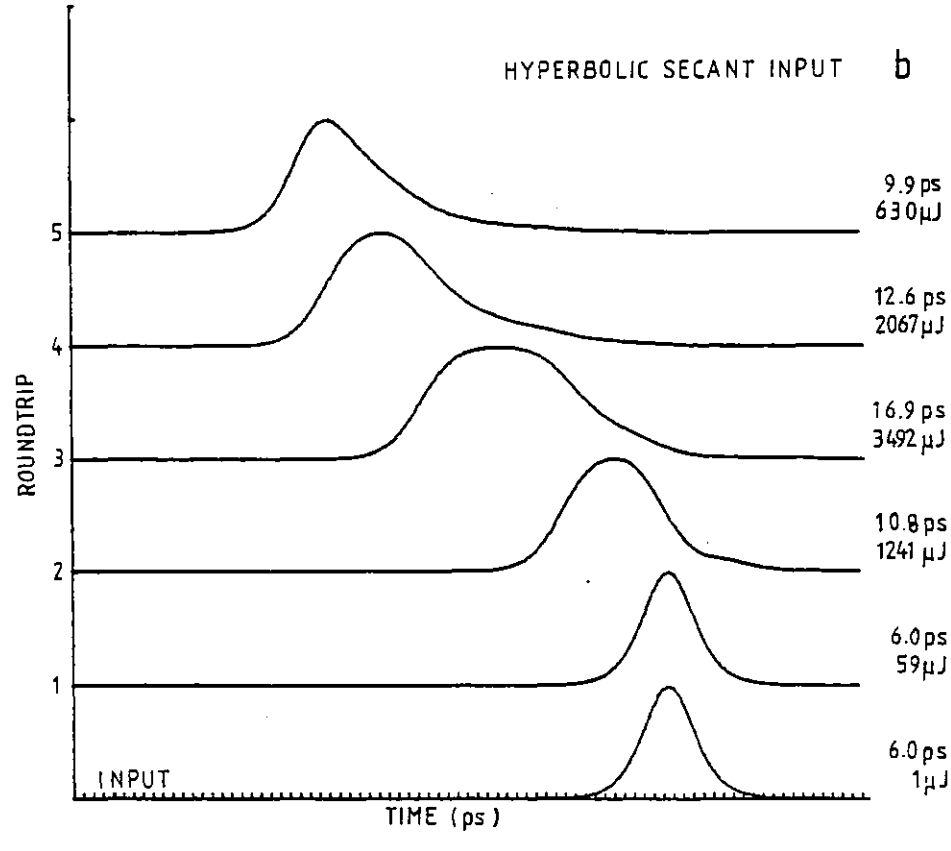

Figs. 6.8 (a) and (b)

Pulse evolution for hyperbolic secant input pulses. (± 6ps mismatch)

effect at all, apart from a weak shoulder appearing on the pulse after the second roundtrip.

6.6 Pulse evolution for lorentzian input pulses

A characteristic of lorentzian pulses is that the "wings" are fairly spread out and contain a significant fraction of the pulse energy. The photon density at the start of the leading edge is therefore not negligible. The result is that the leading edge is strongly amplified after a very short time. This causes the gain to saturate and the trailing edge to sharpen. However, since there is no saturable absorber to deplete the rapidly growing leading edge [9], the net result is that after a few roundtrips the pulse broadens and looses its symmetrical shape. Fig.6.9(a) shows the computer simulation of the evolution of a lorentzian input pulse train. A low small signal gain of $g_o = 0.035 cm^{-1}$ at the peak was assummed for the XeCl laser and the input pulse duration was again taken to be 6ps. The energy density of the input pulses was in this case only 0.2 $\mu J\ cm^{-2}$. For each roundtrip the superposition of a new pulse being injected into the excimer laser from the dye laser was taken into account as in the previous simulations. The plots show how the peak remains centered and the leading edge starts growing.

In Fig. 6.9(b) the pulse evolution assuming a small signal gain of 0.04 cm^{-1} at the peak is shown. Here the leading edge rises even more dramatically, and after five roundtrips (ten passes) it starts competing with the peak of the pulse in intensity. The shape of the pulse is highly asymmetric since the leading edge has "run away" and the trailing edge has been sharpened by gain saturation.

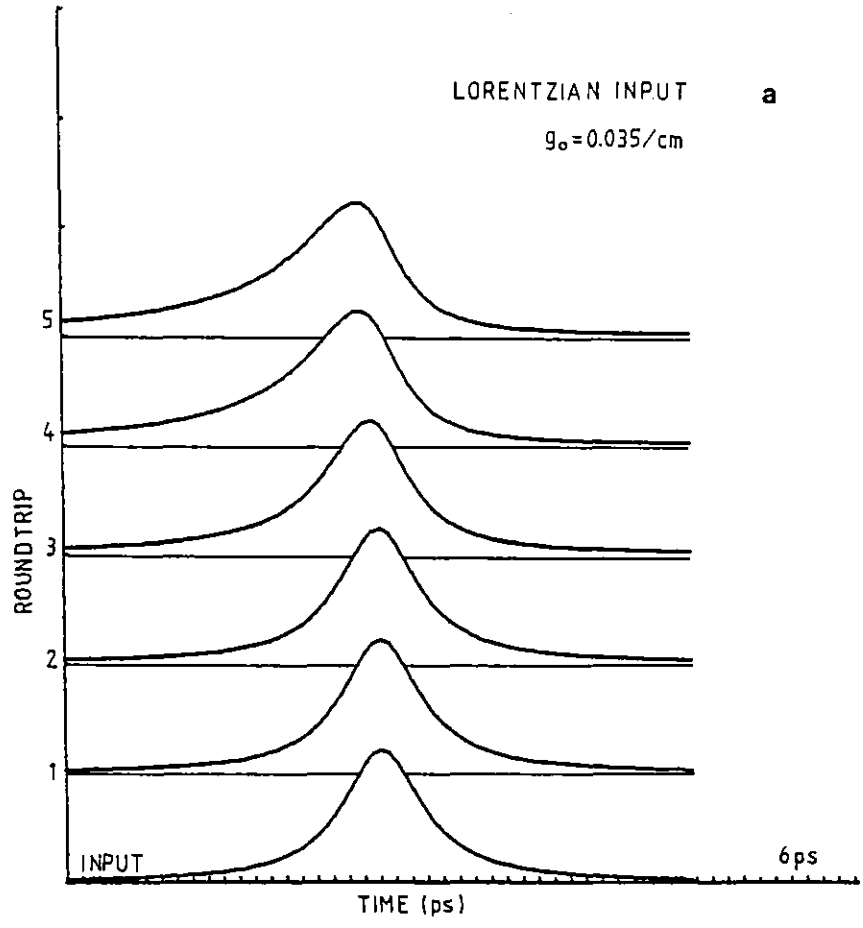

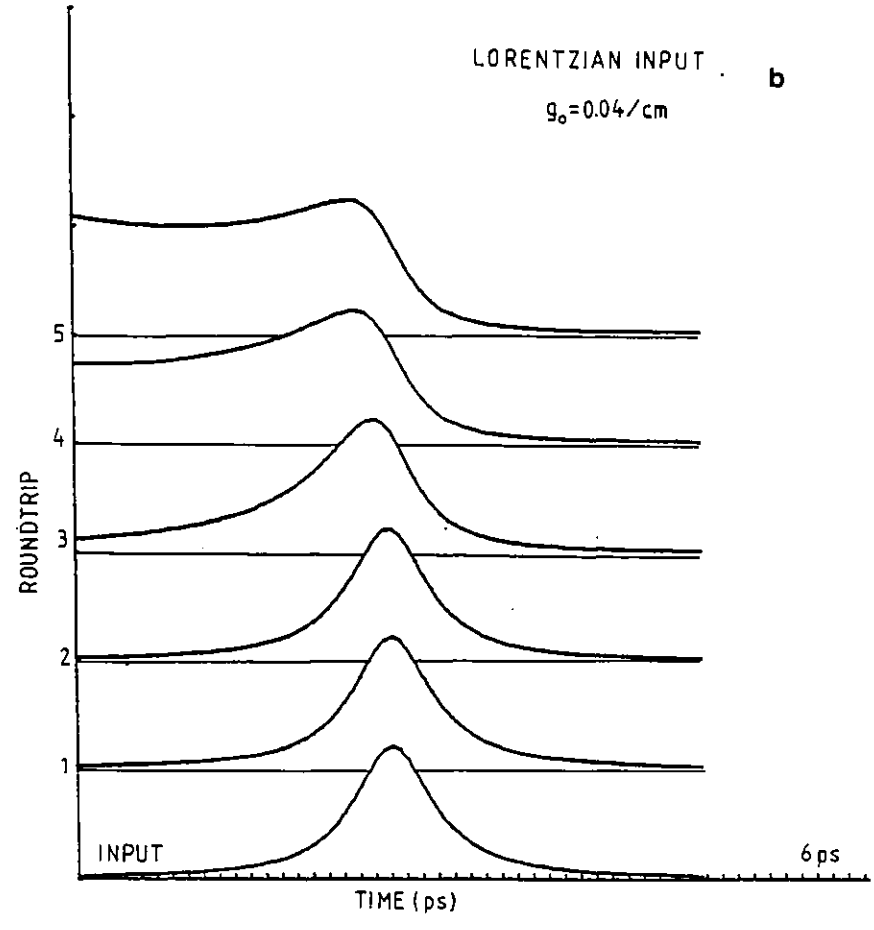

Figs. 6.9(a) and (b)

Pulse evolution for lorentzian shaped input pulses. Energy density of injected pulses: 0.2μJ cm^{-2} (No mismatch)

When higher values for the small signal gain were used in the simulation, the leading edge grew so rapidly that after very few passes all the energy was concentrated in the first half picosecond of the leading edge. The peak had therefore shifted to the first points in the array of 1600 that described the pulse . This was clearly not a realistic situation and was due to the limits of the theoretical model. The input pulse in the simulation did not have a sharp"cut-off"at t = 0, thus the very initial value for the photon density grows too high and causes depletion of all the gain before the actual pulse arrives.

6.7 Conclusion

For the small signal gain values characteristic of rare-gas halide lasers, the effects of gain saturation become evident after very few roundtrips in the laser. This means that in an injection mode-locking experiment, gain saturation will most certainly modify the shape and duration of the pulses. Depending on the input pulse shape, broadening or compression might occur.

For gaussian and hyperbolic secant input pulses the peak invariably shifts forward. A mismatch between the peak of the pulse developing in the excimer cavity and the injected pulses will then be introduced, even if there initially was no mismatch. However, since the injected pulses trail the intense peak of the pulse fed back from the output coupler, the effect of the "mismatch" is negligible since gain saturation will ensure that the injected pulse experiences very little gain.

If a real mismatch is introduced between the excimer laser and

dye laser cavity lengths, the pulse evolution will only be influenced if the former is longer than the latter. Some double pulse structure will then occur, but after a few more roundtrips, the sub-peaks disappear because of gain saturation. A complete analysis should, however, incorporate gain recovery, since if this is rapid, pulses trailing the main pulse may be amplified. This was, however, outside the scope of our study.

In conclusion, the simulations show that gain saturation does not necessarily lead to pulse compression. Knowledge of the input shape is needed, to predict whether the pulses in an injection mode-locking experiment will broaden or compress. Excellent agreement was obtained between the simulation and the experiment in estimating the peak energy density thus confirming the maximum energy density that can be extracted in a single pulse from a XeCl laser of this dimension.

CHAPTER 6 - References

1 G.H.C. New, Phil. Trans. R. Soc. Lond. A-298, 247 (1980)

2 Hermann A. Haus, IEEE J. Quant. Electron., QE-11, 736 (1975)

3 T.K. Lim and B.K. Garside, Opt. Comm.12, 8 (1974)

4 G.H.C. New, Proc. IEEE., 67 380 (1979)

5 T.Efthimiopoulos, J. Banic and B.P.Stoicheff, Can. J. Phys., 57 1437 (1979)

6 C.P. Christensen, L.W. Braverman, W.H. Steier and C. Wittig, Appl. Phys. Lett., 29, 424 (1976)

7 Lee M. Frantz and John S. Nodvik, J. Appl. Phys.,34, 2346 (1963)

8 Excimer Lasers, Chapter 4, Ed. Ch.K. Rhodes, Topics in Applied Physics Vol.30, Springer Verlag (1979)

9 G.H.C. New, Opt. Comm. 6, 188 (1972)

CHAPTER 7

ACTIVE MODE-LOCKING OF THE XeCl LASER

7.1 Introduction

Injection mode-locking was shown in the previous chapters to be a feasible method of generating ultrashort pulses with excimer lasers. The method does, however, depend on matching the wavelength of the master oscillator to the laser transition of the excimer slave oscillator. For some excimer lasers a mode-locked master oscillator that can be frequency doubled to the correct wavelength may not be available. This is particularly the case for short wavelength lasers.

Passive mode-locking depends on spectral matching of the laser medium and the saturable aborber, and is therefore also a less versatile method than active mode-locking.

Active mode-locking by intracavity gain (or strictly speaking loss) modulation in Nd:YAG lasers has been demonstrated by several workers [1, 2]. Gas lasers have also been mode-locked in this way [3, 4]. Active mode-locking of a discharge pumped XeF laser was reported by Christensen et al. [5]. An intracavity acousto-optic device was used to modulate the gain. The modulation depth obtained was, however, limited to $\sim$ 70% and the pulses were relatively long ($\lesssim$ 2ns). The short duration of gain limited the number of roundtrips possible and hence the temporal compression of the pulses.

Recently a new method of active mode-locking was reported [6]. A flashlamp pumped dye laser was used to activate a semiconductor switching device. The picosecond voltage pulses thus generated were applied to an intracavity Pockel's cell that actively modulated a

coumarin dye laser. In this chapter the extension of this technique to rare-gas halide lasers is described. A GaAs switch driven by the flashlamp pumped Rh6G dye laser activated an intracavity Pockel's cell in the discharge pumped XeCl laser, and a 100% modulated train of 5-8 subnanosecond pulses was generated by the excimer laser.

7.2 Experimental

A schematic of the experimental arrangement is shown in Fig. 7.1 The mode-locked Rh6G dye laser was the same as the one used in the previous experiments. Wavelength tuning of the dye laser was achieved by a single intracavity Fabry-Perot interferometer. The laser was tuned to $\lambda \sim 605$nm where the best mode-locking occurs. The output was a pulse train of $\sim$ 1-1.5μs duration. The total energy of the train was $\sim$ 10mJ and the energy in a single pulse approximately 20-30μJ, which is sufficient to efficiently activate the GaAs device. The duration of the ultrashort pulses was $\sim$ 5-10ps. The cavity length of the dye laser was adjusted to be either equal to or half the length of the XeCl cavity. The best results were obtained with the shortest cavity. The dye laser beam

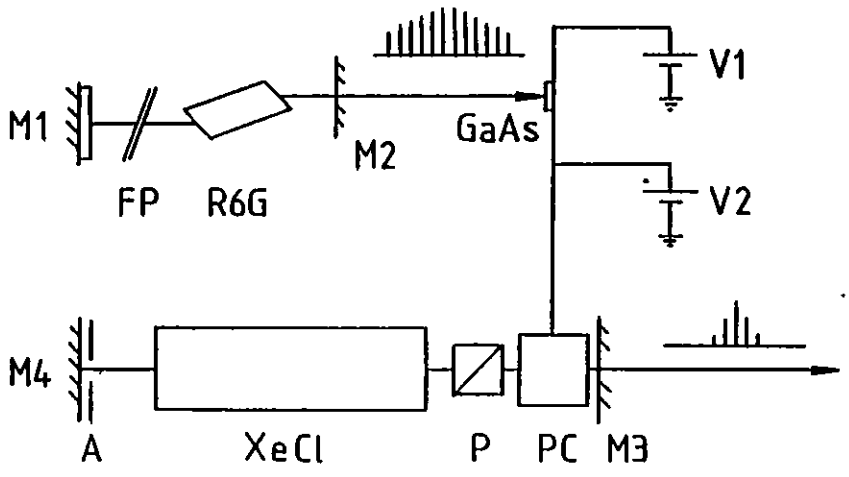

SCHEMATIC OF EXPERIMENTAL ARRANGEMENT FOR ACTIVE MODE-LOCKING

P = POLARISER, PC = POCKELS CELL, A = APERTURE, M1, M2, M3, M4 ARE MIRRORS

Fig. 7.1. Experimental arrangement

area was then larger and more uniform which gave a better illumination of the semiconductor switch.

The discharge XeCl laser was operated just above threshold at ∿ 20 kV charging voltage. The gas mixture used was 12 Torr HCl + 100 Torr Xe + Ne = 1500 Torr. The anode electrode had been changed from aluminium to a nickel plated electrode and the optimum gas mixtures were therefore slightly different to the earlier combinations. The XeCl cavity was defined by mirrors M_4(R∿100%) and M_3(R∿80%) and the roundtrip time was ∿ 8.3ns. A Glan-Thompson polarizer (P) was inserted between the laser medium and the KDP Pockel's cell (PC) which was placed very close to the output coupler M_3. Apertures (A) of ∿ 1cm diameter were inserted at both ends of the cavity to restrict lasing to the area covered by the Pockel's cell.

The two lasers were syncronized as in the earlier experiments by triggering a TRW delay generator with the signal from a photodiode monitoring the flashlamp output from the dye laser. The TRW generator then delivered a trigger signal to the thyratron of the discharge laser after a suitable delay. As before, jitter was not critical since the duration of the dye laser pulse train was much longer than the duration of gain in the excimer laser.

7.3 Gain modulation

The gain modulating arrangement was similar to the one in Ref. 6 and worked as follows:

Initially lasing in the XeCl amplifier is inhibited by the application of a D.C. voltage $V_{\lambda/4}$ to the Pockel's cell. Fluorescence emitted by the amplifier in the direction of the output coupler M_3 is

partly transmitted through the polarizer P which rejects the vertical component of the light. When passing through the KDP crystal the horizontally polarized light becomes circularly polarized due to the D.C. voltage on the crystal. The light then reaches mirror M_3 circularly polarized, is reflected back and after a second pass through the Pockel's cell has its linear polarization restored, but rotated by a total of 90^o. It is then rejected by the polarizer, and since no feedback is allowed into the amplifier, the laser does not reach threshold. When, however, a short duration voltage pulse is added to the D.C. voltage $V_{\lambda/4}$, the polarization of the light is rotated by a total of more than 90^o. A short duration burst of light which is not linearly polarized is then formed. Its horizontal component is not rejected by the polarizer and is fed back into the amplifying medium allowing the amplifier to reach threshold. The arrival of this pulse at the Pockel's cell after a roundtrip in the cavity is syncronized with the application of a subsequent short duration voltage pulse switched by the GaAs device, allowing further amplification and the build-up of a mode-locked pulse train. Synchronization is achieved by adjusting the dye laser pulse separation to correspond to the XeCl cavity roundtrip time or half of this. Fig. 7.2 illustrates the modulation process.

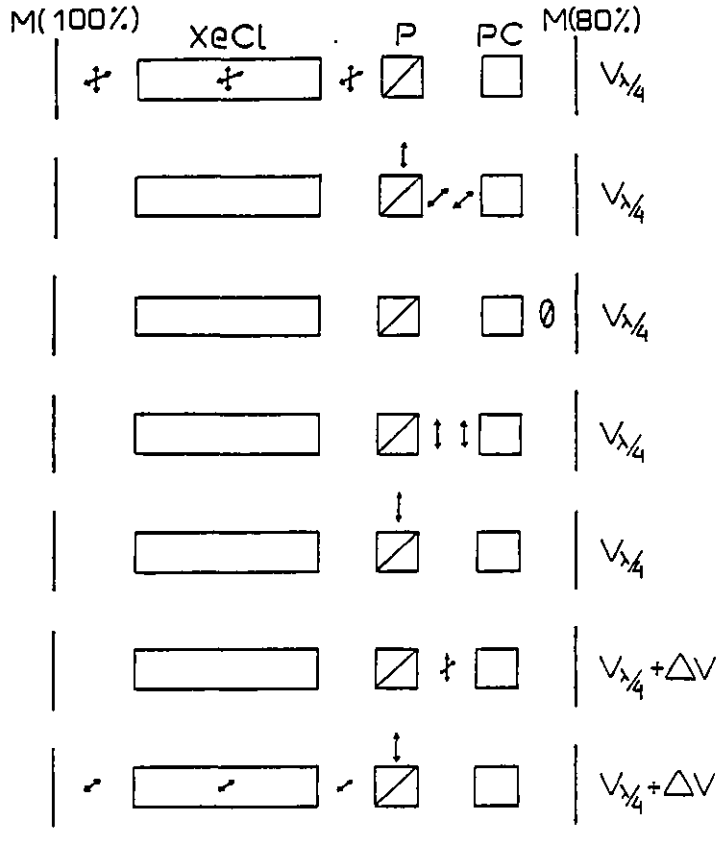

Fig. 7.2. The modulation process
P = Polarizer, PC = Pockel's cell
↕ = vertically polarized light
↗ = horizontally polarized light
0 = circularly polarized light

7.4 The semiconductor switching device

The mode-locked dye laser pulses were used to drive the semiconductor switch so that voltage pulses could be supplied to the Pockel's cell. Picosecond opto-electronic switching was first demonstrated by Auston in 1975 [7]. Since then Si, GaAs and GaP semiconductors, have been shown to be capable of switching kilovolts with picosecond risetimes [8, 9].

The GaAs switch consists of a slab of semi-insulating Cr doped GaAs connected between a D.C. power supply and the load (in our case the Pockel's cell). The electrodes on the switch used in our experiment were silver and were painted on the substrate. Ideally the electrodes should have been evaporated on, however, painting the electrodes was a versatile method and new switches could readily be made in case of electrical breakdown. The gap size was $\sim$ 2mm which meant that the switch could only hold off $\sim$ 800V. Fig.7.3 illustrates the semiconductor switch. Initially the high resistivity ($\rho \sim 1 \times 10^{8} \Omega$cm) of the device prevents voltage from appearing across the load. However, when illuminated by a picosecond laser pulse, photoinduced carriers cause the conductivity of the semiconductor to increase by several orders of magnitude. In this way the voltage is effectively transmitted to the Pockel's cell.

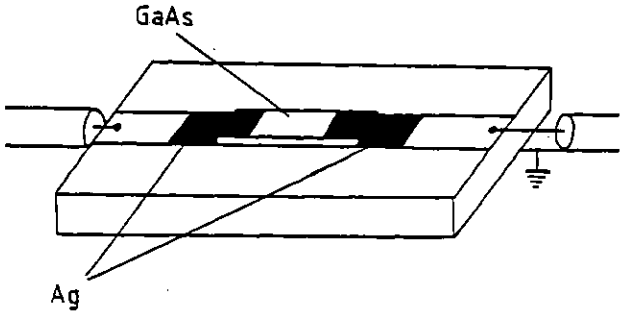

Fig. 7.3. Semiconductor switching device.

Semi-insulating GaAs is ideal for ultrafast switching since the recombination time of optically excited carriers in Cr doped GaAs is

only $\sim$ 100ps [10]. The separation between pulses in the dye laser output train was $\sim$ 4ns during most of the experiment, thus the semiconductor had to "turn off" in a time less than this to be ready for the next pulse. In Si, due to slow recombination times, the repetition rate is too slow for this type of operation, unless a second optical pulse is used to turn the device "off" after the desired amount of time [7]. Another advantage with GaAs is the very high resistivity leading to very low leakage currents and limited thermal problems. The bias voltage does therefore not have to be pulsed as is the case with Si switches. If the electric field across the slab is limited to $\lesssim$ 3kV cm^{-1}, electrons in the conduction band exhibit very high mobilities ($\gtrsim$ 7 x $10^3 cm^2 V^{-1} s^{-1}$). In this case relatively modest optical energies ($\sim$10μJ) illuminating the device is sufficient for efficient switching. (Also by limiting the voltage applied to the switch, electrical breakdown can be avoided). With the photon energy available in the ultrashort laser pulses ($\sim$ 2eV for $\sim$ 600nm wavelength pulses) electrons can be directly excited from the valence to the conduction band (E_{gap} = 1.4eV for GaAs), and single-photon induced conductivity is dominant.

Fig.7.4a is an oscillogram of the train of voltage pulses switched by the GaAs device when illuminated by the mode-locked dye laser pulses. In this case the semiconductor acts as an optical detector. The switch was connected to a Tektronix 7834 oscilloscope through calibrated electrical attenuators. The oscilloscope traces showed that voltage pulses of $\sim$ 200V were switched with a D.C. bias of 700V. When accounting for the fact that the signal seen on the oscilloscope is integrated due to the 0.7ns risetime of the 7A19 amplifier used, the true amplitude of the 200V signal is found to be $\sim$ 350V [11]. For the

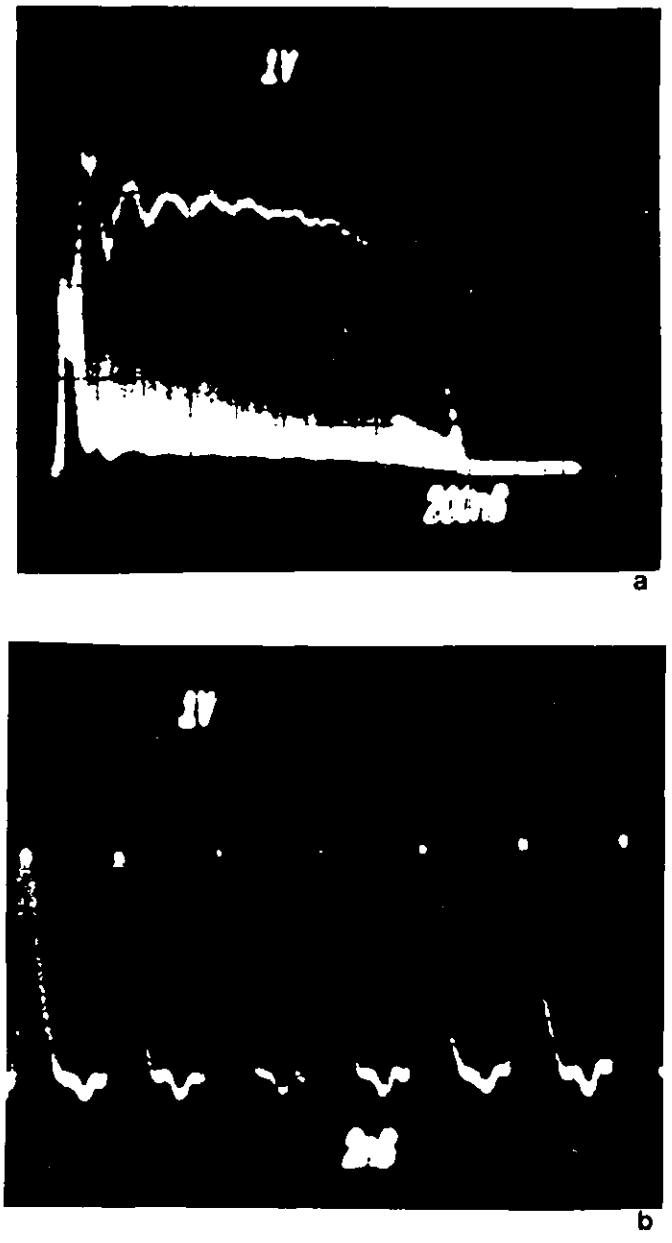

Fig. 7.4 (a) and (b)

Oscillogram of voltage pulses switched by the GaAs device

(a) 200ns/div
(b) 2ns/div

particular configuration used only half the applied D.C. voltage can be switched [10], hence the switching efficiency was ∿ 100%. In Fig. 7.4b the voltage pulses are shown on an expanded time-scale indicating oscilloscope limited rise and fall times.

It should be pointed out that the voltage pulses appearing across the Pockel's cell exhibited ringing and were somewhat integrated and therefore differed considerably from those shown in Fig. 7.4. This was mainly due to impedance mismatch, stray inductance and the finite capacitance (∿ 5pF) of the Pockel's cell. The Pockel's cell (E.O.D. PC 12KD) used in our experiment had a risetime of ∿ 250ps.

7.5 Experiment and results

Initially the Pockel's cell and polarizer had to be aligned

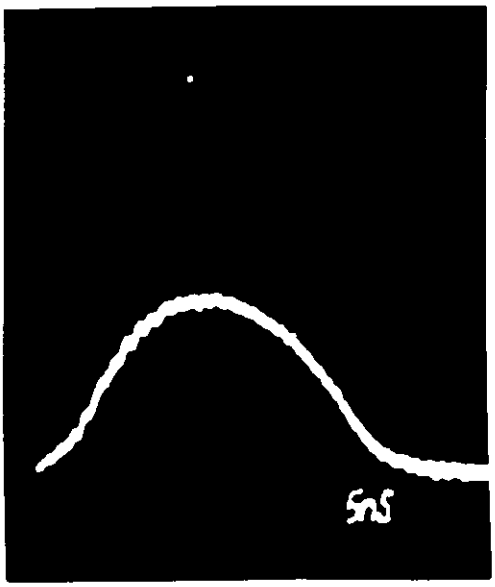

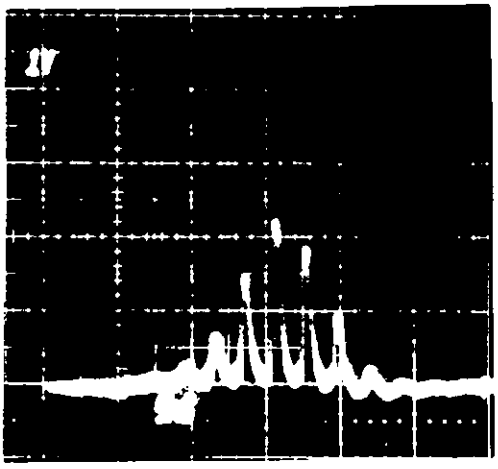

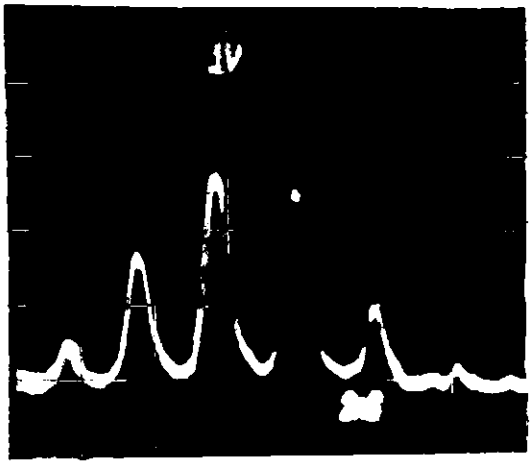

Fig. 7.5(a), (b) and (c)
Unmodulated and mode-locked XeCl laser output.
a, b): 5ns/div
c): 2ns/div

so that the XeCl laser did not reach threshold when a voltage $V_{\lambda/4}$ was applied to the Pockel's cell.

It was very important to properly align the polarizer. Otherwise the modulation of the output was poor, since some feedback would always be present. When this was done the Pockel's cell was positioned using the He-Ne alignment laser situated behind M_4. The position of the Pockel's cell was adjusted so that the reflection coming back from mirror M_3 (having passed through the Pockel's cell twice) disappeared with the D.C. voltage at $\sim$ 1.8kV. The corresponding quarter wave voltage for the u.v. light was $\sim$ 650V. Since the gain in the XeCl laser was high, the optical elements in the cavity were slightly misaligned to prevent the formation of subcavities. When the D.C. voltage $V_{\lambda/4}$ was then applied to the Pockel's cell, the laser consistently did not reach threshold. With no voltage on the Pockel's cell, the unmodulated XeCl laser output was typically as shown in Fig. 7.5(a). The output was monitored by an ITL S20 photodiode in conjunction with the Tektronix 7834

storage oscilloscope.

When pulses of ∿ 350V amplitude from the dye laser activated switch were added to the $V_{\lambda/4}$ D.C. bias on the Pockel's cell, the XeCl laser did reach threshold. A train of 5-8 100% modulated pulses was emitted as seen in Fig. 7.5(b). The train lasted 20-30ns, and the pulses exhibited oscilloscope limited rise and fall times as shown in the expanded time scale of Fig.7.5(c).

The peak pulse energy was not sufficient to detect with the available calorimeter. Since the pulse duration was not necessarily shorter than the response time of the photodiode and oscilloscope, the oscilloscope trace did not correspond to the integrated current and the method of measuring single pulse energies described in Chapter 4, Section 4.5 could not be used. From the amount of optical attenuators needed to see the pulses on the oscilloscope compared with the injection mode-locked pulses, a rough estimate for the energy in the pulses could be obtained. By this method we estimated the energy to be 1-2 orders of magnitude lower than the peak energy in the injection mode-locked case which was 1-2mJ. The electrical energy deposited in the discharge laser was, however, much lower in this experiment since the charging voltage was only ∿ 20kV. A straight comparison is therefore not really valid. Apart from the fact that the laser was just above threshold, the low energy was mainly due to the lossy elements in the laser cavity. The Pockel's cell windows, for instance, were made of glass with a "cut-off" at 300nm. Thus the absorption losses were considerable. Also, if the voltage switched onto the D.C. voltage $V_{\lambda/4}$ had been equal to $V_{\lambda/4}$, the short burst component fed back into the laser would have been more intense, since the burst of light emerging from the Pockel's cell would then have been completely horizontally polarized.

7.6 Streak camera pulse duration measurements

The pulse durations were measured using the Photochron II u.v. streak camera (with an S20 photocathode). The streak camera voltage deflection ramp was generated by a fast Krytron circuit as described in Chapters 2 and 5. The Krytron was in this case activated by part of the signal from the TRW delay trigger generator to the XeCl thyratron. The signal to the ramp was suitably delayed by cable so that the ramp would sweep when the pulses had arrived at the streak camera. The output pulses from the XeCl laser were directed towards the streak camera slit by a single $\sim$ 100% reflectivity mirror. Temporal calibration for the streaks was provided by the known separation between the pulses in the train. Slow sweep speeds were used ($\sim 1.4 \times 10^{8} cms^{-1}$) yielding a temporal resolution of $\sim$ 100ps. In this way streaks from the whole pulse train could be seen on the phosphor screen and any background between the pulses detected. Furthermore, the jitter present due to electrical noise from the lasers was less severe. Again it had proved difficult to isolate the Krytron circuit properly from this noise, as in the injection mode-locking experiment.

The shortest pulse duration detected was $\sim$ 360ps. Fig. 7.6 is a microdensitometer trace of two consecutive pulses showing no background and thus 100% modulation. In this case the roundtrip time of the dye laser cavity was half that of the XeCl cavity yielding output pulses separated by $\sim$ 4ns as seen in Fig. 7.5 (b) and (c). Therefore the excimer laser is double pulsing, and the streaks shown correspond to pulses that have evolved from different initial bursts of light. The recorded width of the pulse shown on the left is $\sim$ 380ps. When deconvolving the 100ps temporal resolution of the camera (assuming a dynamic spatial resolution of $\sim$ 10 lp/mm), this corresponds to a real

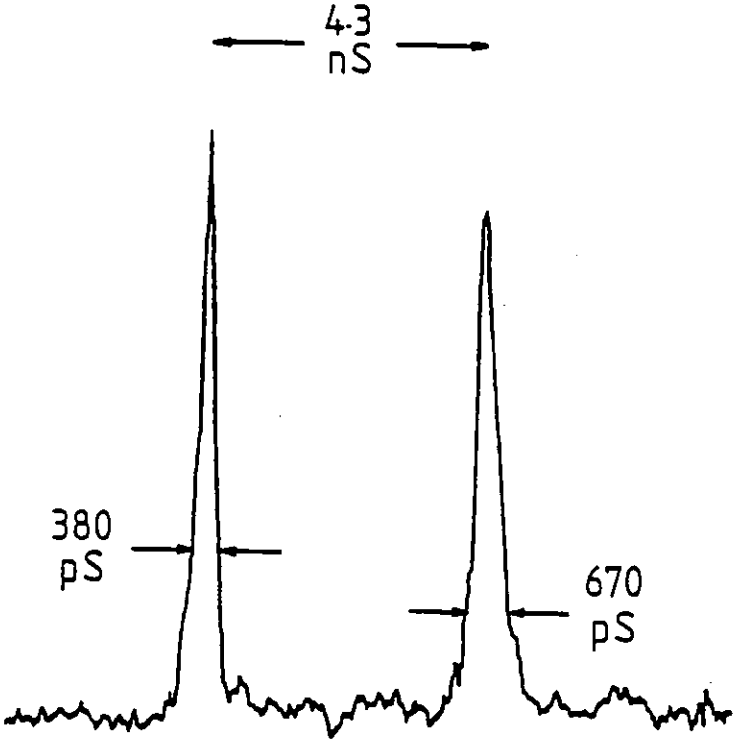

Fig. 7.6

Microdensitometer of streak photograph showing two consequtive output pulses.

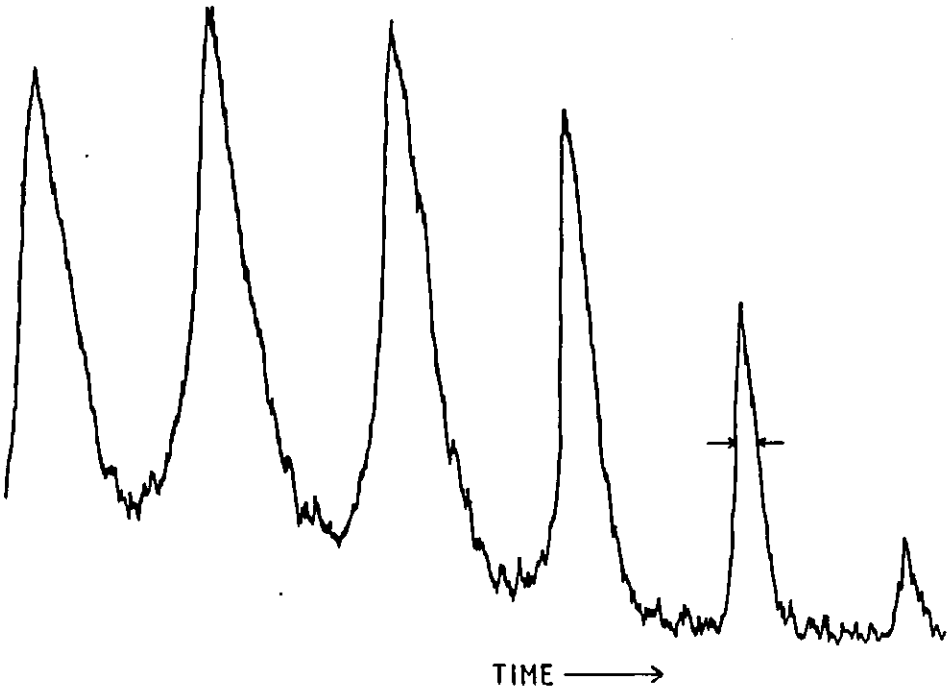

Fig. 7.7

Microdensitometer trace of streak photograph showing XeCl pulse train. The half-intensity point is indicated on the last pulse. (Recorded F.W.H.M. ∿ 500ps)

pulse duration of ∿ 360ps.

A microdensitometer trace showing several pulses in the XeCl pulse train is shown in Fig. 7.7. The durations of these pulses were not determined due to overexposure of the streak photograph. The traces indicate that the leading edge of the pulses is sharper than the trailing edge. This was consistent with the results from the computer simulation described in the next chapter.

7.7 Suggestions for generating shorter pulses

The compression of the pulses depends on the number of passes made through the modulator. Therefore a large number of roundtrips is advantageous. Alternatively, a second Pockel's cell could be placed in the excimer laser cavity since this would be equivalent to doubling the number of passes. The introduction of a second modulator was attempted in our experiment. The additional Pockel's cell together with a Glan-Thompson polarizer was placed near the 100% back reflector. The voltage pulse to both elements was supplied by the same GaAs device and synchronization was achieved by connecting the modulators with a suitable length of cable. The additional cable did, however, introduce reflections and caused the signal seen by the first Pockel's cell to deteriorate. With the added elements in the cavity the losses were extremely high, since the second Pockel's cell also had glass windows. The output from the laser was therefore not very reproducible and the attempt was abandoned.

In the experiment described in Reference 6 where a coumarin dye laser was mode-locked by this method of gain modulation, pulse durations ∿ 30ps were obtained using the same Pockel's cell. In this case gain

saturation of the dye medium could have been important in the pulse compression process. The computer simulations in Chapter 6 showed that gain saturation can lead to shorter pulses also in the XeCl laser. In order to generate the high intensities needed for saturation to occur, it is important to reduce the losses in the cavity by choosing suitable optical elements. If the energy density were sufficient to saturate a dye in a passive mode-locking experiment, a hybrid system could be employed, yielding even shorter pulses.

Finally, the voltage applied to the Pockel's cell should be equivalent to the full quarter wave voltage. The losses as the pulse traverses the polarizer are then minimised and the intensity of the pulse fed back into the active medium is maximised.

7.8 Conclusion

Active mode-locking of the discharge pumped XeCl laser was demonstrated. 100% modulated trains of subnanosecond pulses were generated yielding single pulse durations as short as $\sim$ 360ps.

The experiment demonstrated that voltage pulses generated by a semiconductor switching device provide a loss modulating signal of very fast rise and fall time when applied to an intracavity Pockel's cell modulator. The signal is of shorter duration and of greater modulation depth than the sinusoidal waveforms that are characteristic of acousto-optic loss modulators. Consequently the pulse durations obtained were shorter than those obtained using acousto-optic devices.

Finally, since this method of mode-locking does not depend on

wavelength matching between two lasers, it could easily be extended to other excimer systems.

References - Chapter 7

1 L.M. Osterink and J.D. Foster, J. Appl. Phys., 39, 202 (1968).

2 Dirk J. Kuizenga and A.E. Siegman; IEEE J. Quant. Electron., QE-6, 673 (1970).

3 L.E. Hargrove, R.L. Fork and M.A. Pollack; Appl. Phys. Lett., 5, 4 (1964).

4 D.E. Caddes, L.M. Osterink and Russel Targ; Appl. Phys. Lett., 12, 74 (1968)

5 C.P. Christensen, L.W. Braverman, W.H. Steiner and C. Wittig, Appl. Phys. Lett., 29, 424 (1976)

6 W. Margulis, W. Sibbett and J.R. Taylor, Opt. Commun., 35, 153 (1980).

7 D.H. Auston, Appl. Phys. Lett., 26, 101 (1975)

8 G. Mourou and W. Knox, Appl. Phys. Lett., 35, 492 (1979)

9 W. Margulis and W. Sibbett, Opt. Comm., 37, 224 (1981)

10 Chi H. Lee, Appl. Phys. Lett., 30, 84 (1977)

11 W. Margulis and S. Laval, Submitted for publication to Appl. Phys. Lett. (1981)

CHAPTER 8

ACTIVE MODE-LOCKING: A THEORETICAL MODEL

8.1 Introduction

Active mode-locking with acousto-optic modulators has been successfully demonstrated with several lasers such as Nd:YAG, Nd:Glass and Argon ion systems. The analysis of the mode-locking process has been extensively treated by Kuizenga et al. and by other workers [1, 2]. The steady state duration of a gaussian pulse in a homogeneously broadened laser can be derived analytically and is proportional to the inverse of the modulation frequency and depth and to the inverse of the square root of the number of roundtrips. The primary difficulty in generating short pulses by these methods of active mode-locking in rare-gas halide lasers has been that the mode-locked pulses could not make a sufficient number of passes through the modulator for the pulse width to shorten appreciably.

In our experiment the Pockel's cell modulator rather than an acousto-optic modulator was used. The shape of the modulation signal is in this case determined by the voltage delivered to the Pockel's cell by the semiconductor switch. The voltage signal is a pulse of picosecond duration, and the transmission function of the modulator (which depends strongly on the shape of the voltage signal applied to the Pockel's cell) is thus not sinusoidal as for acousto-optic modulators. The analysis by Kuizenga et al. can therefore not be employed. A full theoretical analysis of the mode-locking process in our experiment would be outside the scope of this work and only a brief investigation is described here.

8.2 The Pockel's cell loss modulator

In a birefringent material such as KDP light has two allowed directions of propagation and is split into an ordinary ray and an extraordinary ray. When an electric field is applied to the KDP Pockel's cell, the phase of the extraordinary ray is retarded. If the voltage applied is equal to $V_{\lambda/2}$ the resultant polarization when the light emerges from the crystal is rotated by 90°. Alternatively, if the light passes twice through the crystal, the corresponding voltage is $V_{\lambda/4}$ as in our experiment.

When a short duration voltage pulse is added to $V_{\lambda/4}$, the polarization of the light that has passed twice through the crystal when the added field was on, will be rotated by more than 90°. A short duration burst of light is then fed back into the active medium and evolves as a mode-locked pulse. The duration of the light pulse will depend strongly on the duration of the voltage pulse applied to the Pockel's cell.

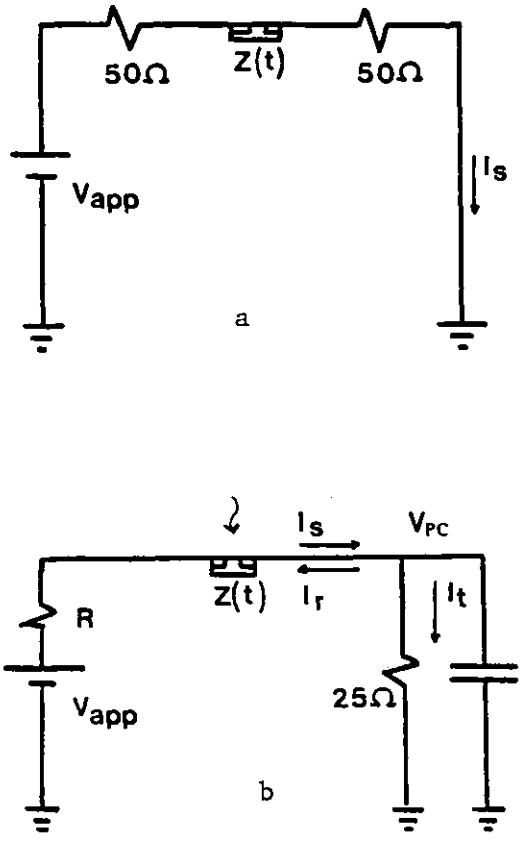

Fig.8.1
Equivalent circuits for the active mode-locking arrangement

The shape and duration of the voltage pulse can be found by considering the equivalent circuits shown in Fig.8.1a and b.

When illuminated by the pulses from the dye laser, the current switched by the GaAs device is

$$I_s(t) = \frac{V_{app}}{100+Z_o e^{t/\tau}} \qquad (8.1)$$

where V_{app} is the D.C. voltage bias across the semiconductor gap and $Z_o e^{t/\tau}$ is the impedance of the conducting switch [3]. The time constant has the value 100ps which is the recombination time of optically excited carriers in Cr doped GaAs. (Reference 10 in Chapter 7).

Since energy and charge are conserved, the expressions:

$$I_s(t)^2 \times 50\Omega = I_T(t) \times V_{PC}(t) + I_R(t)^2 \times 50\Omega \tag{8.2}$$

and

$$I_s(t) = I_R(t) + I_T(t) \tag{8.3}$$

can be solved to find the current transmitted into the junction of the Pockel's cell and the 25Ω load as shown in Fig. 8.1b. (The 25Ω load corresponds to the impedance of the coaxial cables that were connected in parallel from the Pockel's cell to V_2 and to the 50Ω termination used in the experiment).

Therefore,

$$I_T(t) = 2I_s(t) - V_{PC}/50 \tag{8.4}$$

The current charging the Pockel's cell, $I_{PC}(t)$, is then found by subtracting the current charging the cables, represented by the 25Ω impedance, from $I_T(t)$:

$$I_{PC}(t) = (2I_s(t) - V_{PC}(t)/50) - \dot{V}_{PC}(t)/25 \tag{8.5}$$

If the Pockel's cell is considered a perfect capacitor, the current can be related to the voltage by

$$I_{PC}(t) = c\, dV_{PC}(t)/dt \tag{8.6}$$

Using 8.1, the expression yielding the voltage on the Pockel's cell becomes

$$C\frac{dV_{PC}(t)}{dt} = \frac{2 \times V_{app}}{100+Z_o e^{t/\tau}} - \frac{3V_{PC}(t)}{50} \tag{8.7}$$

This equation can be solved numerically thus obtaining the amplitude and the temporal profile of the voltage pulse which is later added to the D.C. bias $V_{\lambda/4}$ on the Pockel's cell.

The intensity of the light emerging from the Pockel's cell modulator, $P_{OUT}(t)$, in terms of the input intensity, $P_{IN}(t)$, is

$$P_{OUT}(t) = P_{IN}(t) \sin^2\left(\frac{\pi V_{PC}(t)}{2 V_{\lambda/4}}\right) \qquad (8.8)$$

The temporal evolution of the voltage pulse $V_{PC}(t)$ therefore determines the intensity profile of the transmitted light pulse. Maximum transmission occurs when $V_{PC}(t) = V_{\lambda/4}$.

8.3 Computer simulation

The intensity profile of the light pulse as the mode-locked pulse train evolves can be simulated by solving Equation 8.7 numerically and using Relation 8.8 for every roundtrip. The temporal evolution of the pulse with successive passes through the modulator can then be investigated. The initial fluorescence intensity experienced by the Pockel's cell modulator was in our model taken to be constant. (Assuming that the detector is not capable of resolving signals varying at optical frequencies). Passive losses were incorporated by introducing a loss factor of 0.1, and the gain per roundtrip was for normalization purposes chosen to be 100.

Fig. 8.2 illustrates the cavity model. The current delivered by the switch was assumed to have negligible risetime and the losses in the cavity are illustrated by the reflectivity of the output coupler. Saturation effects were neglected in order to make the analysis simple.

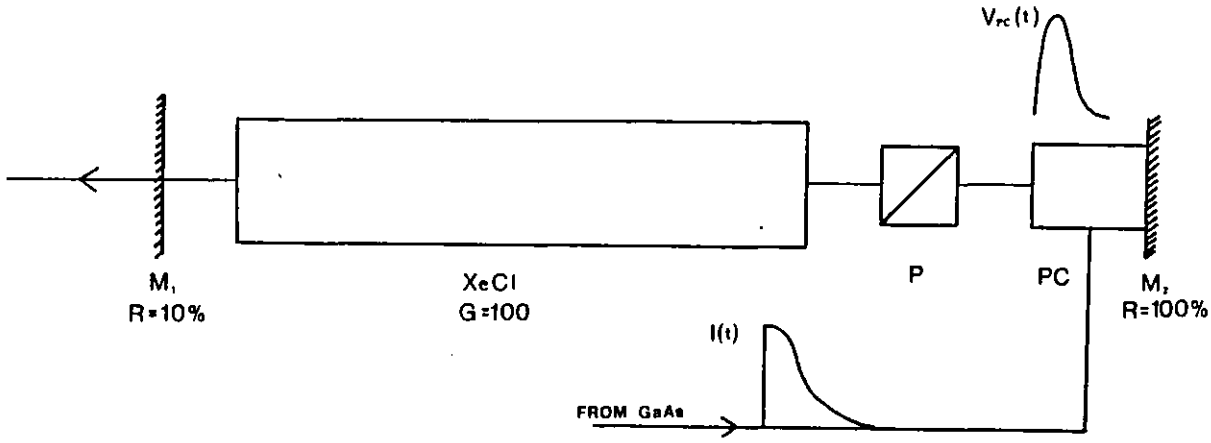

Fig. 8.2. Cavity model used in the computer simulations.

By adding reflections to the voltage pulse applied to the Pockel's cell to account for impedance mismatch, a more realistic situation could be simulated. Also, by delaying the voltage pulse $V_{PC}(t)$ with a set delay time every roundtrip the effect of a cavity mismatch between the dye laser and the XeCl laser was investigated.

8.4 Results

The capacitance of the Pockel's cell used in our experiment was specified to be $\sim$ 5pF and the impedance of the conducting GaAs switch at t = 0 was 1Ω [3, 4]. Thus the computer simulations were made using these values in the calculations of $I_{PC}(t)$ and $V_{PC}(t)$. A plot of $V_{PC}(t)$ against time is shown in Fig. 8.3 together with a plot of $V_{PC}(t)$ with reflections (top). (The amplitude of the first reflection was half the amplitude of the main pulse and arrived at the Pockel's cell 400ps delayed. Reflections of reflections were also taken into account). The duration of the voltage pulse in the first case was $\sim$ 520ps and in the second case $\sim$ 900ps. Reflections trailing 800ps after the main signal gave rise to four almost independent voltage pulses on the

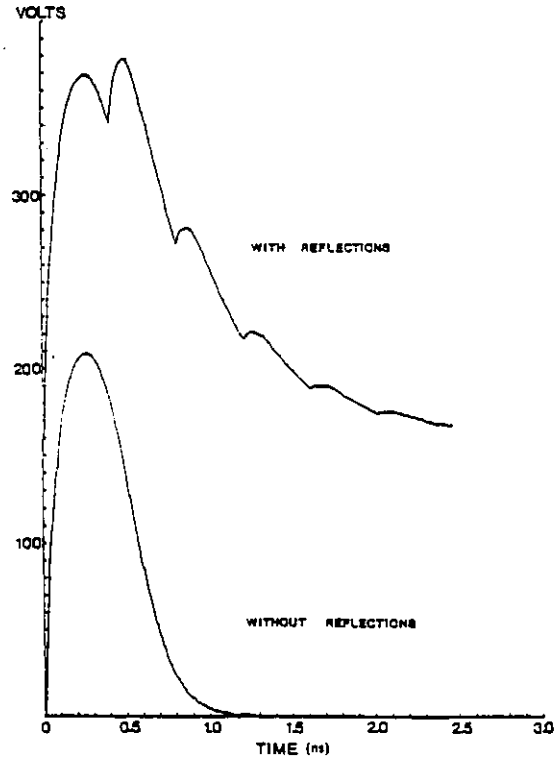

Fig. 8.3

Temporal evolution of the voltage pulse applied across the Pockel's cell (C=5pf and z_o = 1Ω) Lagtime = 400ps(top).

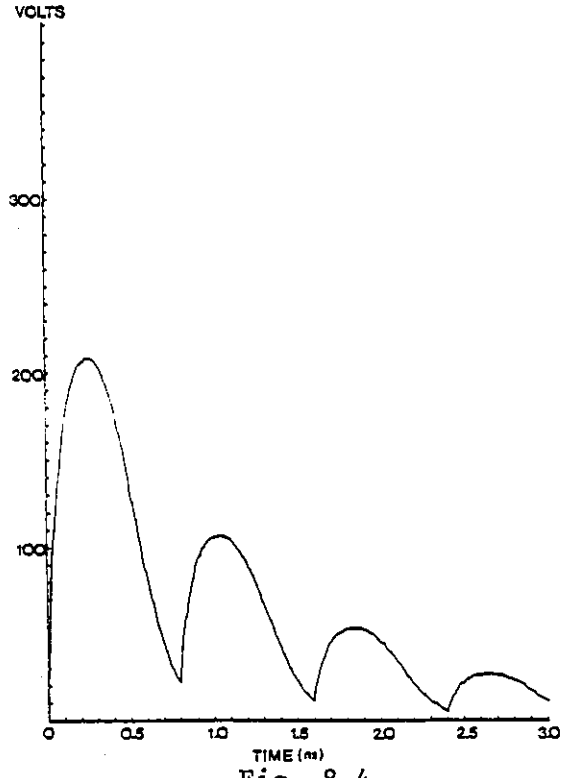

Fig. 8.4

Temporal evolution of the voltage pulse applied across the Pockel's cell (C=5pf and z_o=1Ω, lagtime = 800ps).

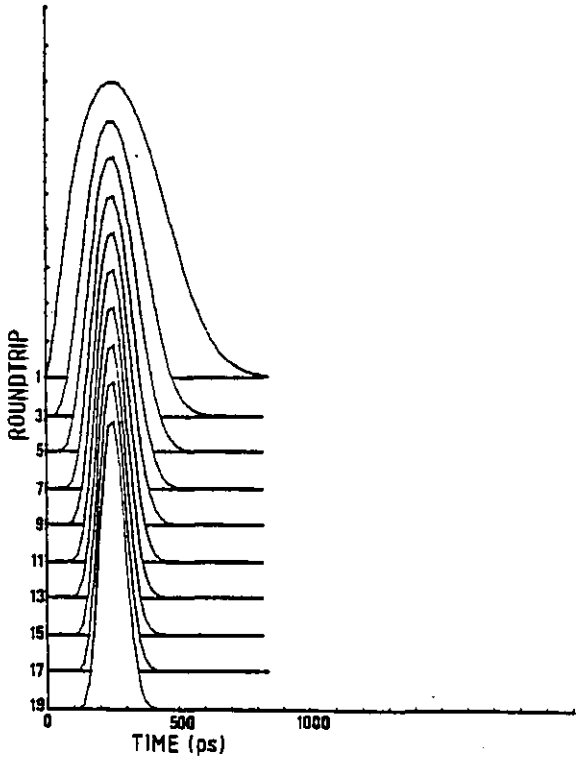

Fig. 8.5

Evolution of light pulses showing pulse compression. (Duration after roundtrip 1:∿400ps, duration after roundtrip 19:∿110ps)

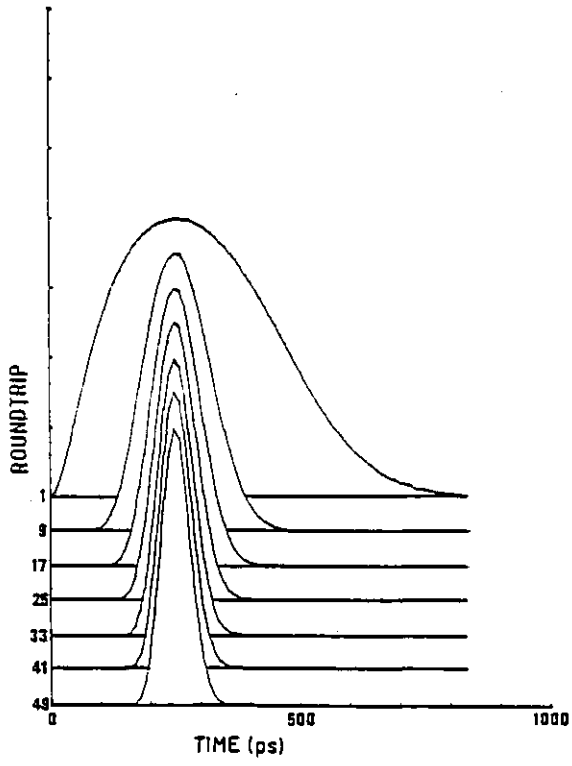

Fig. 8.6

Evolution of light pulses for 49 cavity roundtrips. (Pulse duration after roundtrip 1:∿400ps, pulse duration after roundtrip 49:∿70ps)

Pockel's cell lasting a total of 3ns. Fig. 8.4 illustrates this. The "gate-opening"time of the modulator is thus typically $\sim$ 0.5ns or greater, depending on the reflections and therefore on the quality of the electrical connections of the Pockel's cell. Fig. 8.5 illustrates the evolution of the normalized mode-locked pulses, assuming a voltage signal on the Pockel's cell with no ringing. The pulses are shown after every second roundtrip in the cavity. A total of nineteen roundtrips was assumed for this simulation. With a cavity roundtrip time of $\sim$ 8ns, as in our experiment, the gain would then have to be above threshold for $\sim$ 160ns. To achieve this, e-beam sustained discharge pumping would have to be employed. Fig.8.6 is a computer plot of the pulse evolution for a laser with even longer gain duration (>400ns above threshold). The pulses are shown after every eighth roundtrip. This simulation was made in order to investigate the effect of the modulator on pulses of relatively short duration. The plots show that the temporal compression is more dramatic for the initial pulses. This is expected since the width of the first pulses is of the same order as the width of the modulating signal. After a few passes, however, the duration of the light pulse becomes much shorter than that of the modulating signal, and the latter has less effect on the pulse.

If consecutive pulses are examined, it appears that an approximate expression for the pulse shortening is:

$$\tau_n \sim \tau_1 N^{-\frac{1}{2}} \qquad (8.9)$$

where N is the number of roundtrips and τ_1 is the duration of the first pulse. Thus the pulse compression seems to be inversly proportional to the square root of the number of roundtrips. This is perhaps not surprising, since both the shape of the initial light pulse and the transmission function $\sin^2(\pi V_{PC}/2V_{\lambda/4})$ can be approximated to a gaussian in shape near the peak. In the computer model the transmission function of the Pockel's cell modulator is in fact identical to the

first pulse, since the initial flux is assumed to be constant.

When reflections are taken into account and the voltage signal applied to the Pockel's cell exhibits ringing, the effect on the mode-locking is to cause structured pulse. The computer simulation of the pulse evolution in this case is shown in Figs. 8.7 and 8.8. Fig. 8.7 corresponds to the voltage pulse shown in Fig. 8.3 (top) where the first reflected voltage signal lags the main voltage signal on the Pockel's cell by 400ps. In this case the pulse evolving in the cavity consists

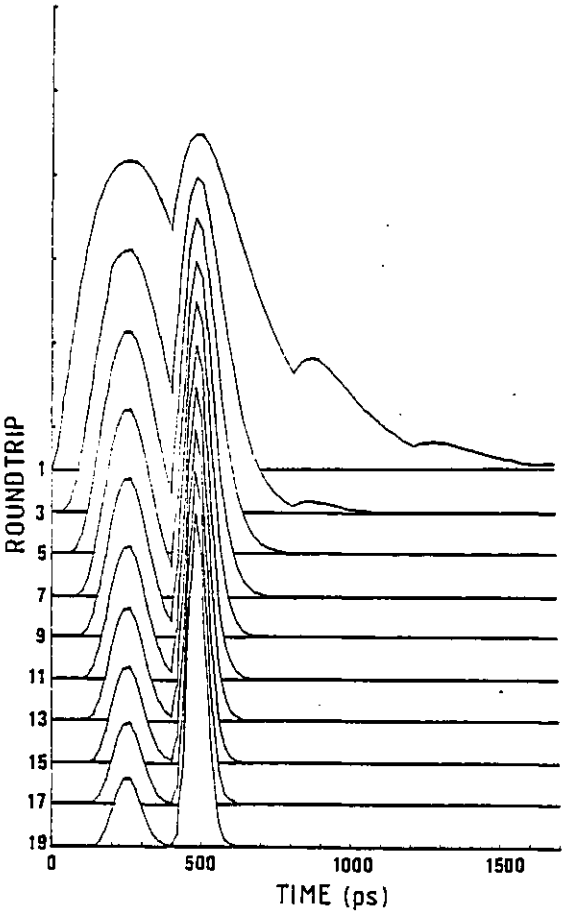

Fig. 8.7
Evolution of light pulses when reflections are taken into account (lagtime:400ps)

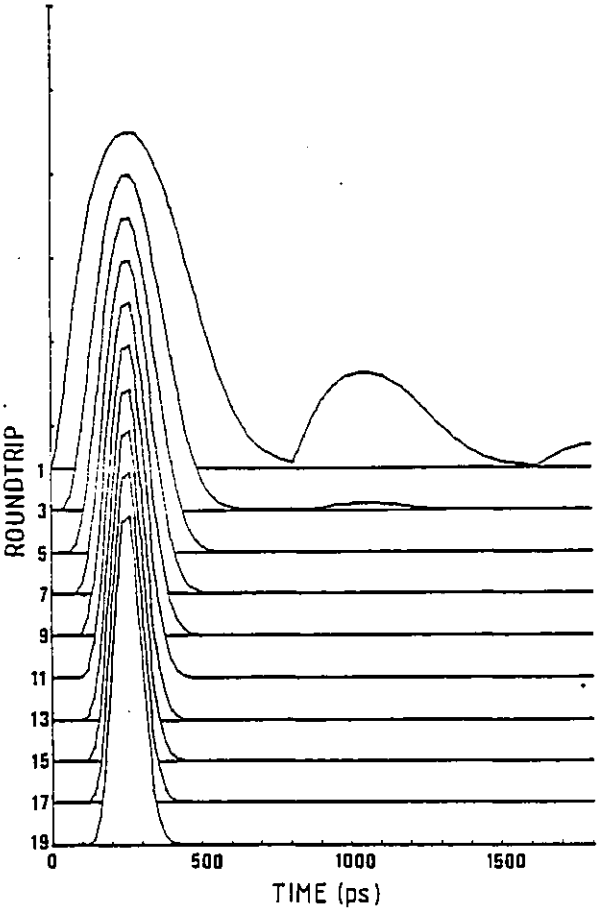

Fig. 8.8
Evolution of light pulses when reflections are taken into account (lagtime:800ps)

of two fairly intense pulses. With each pass through the modulator however, the first of these looses intensity relative to the second. The shape of the initial pulses is very similar to the shape of the voltage signal applied to the Pockel's cell. The strongest pulse tends to dominate after a few roundtrips. The duration of the dominating pulse after 19 passes is in fact shorter than in the case where there was no ringing.

When the first reflection of the voltage signal arrives at the Pockel's cell 800ps behind the main signal the sub-pulse caused by this reflection disappears after very few passes (Fig. 8.8). The main pulse then evolves in much the same way as when no ringing is present. If the amplitude of the reflections were higher, the sub-pulse would last longer as was the case in Fig.8.7.

The plots showing the formation of sub-pulses are in good agreement with the results obtained in the experiment. The lagtime of 400ps for the reflection of the Pockel's cell voltage was in fact chosen since a second peak separated from the main peak of the mode-locked pulse by $\sim$ 400ps was observed on some streak records.

8.5 Further computer simulations

When the initial value for the impedance of the conducting switch was increased from $Z_o = 1\Omega$ to $Z_o = 10\Omega$ (corresponding to reducing the intensity of the dye laser pulses illuminating the semiconductor[3]), the voltage signal on the Pockel's cell changed substantially. The duration of the voltage pulse reduced to $\sim$ 370ps. A plot of $V_{PC}(t)$ in this case (assuming the capacitance of the Pockel's cell to be 5pF) is shown in Fig. 8.9. The corresponding signal with reflections lagging

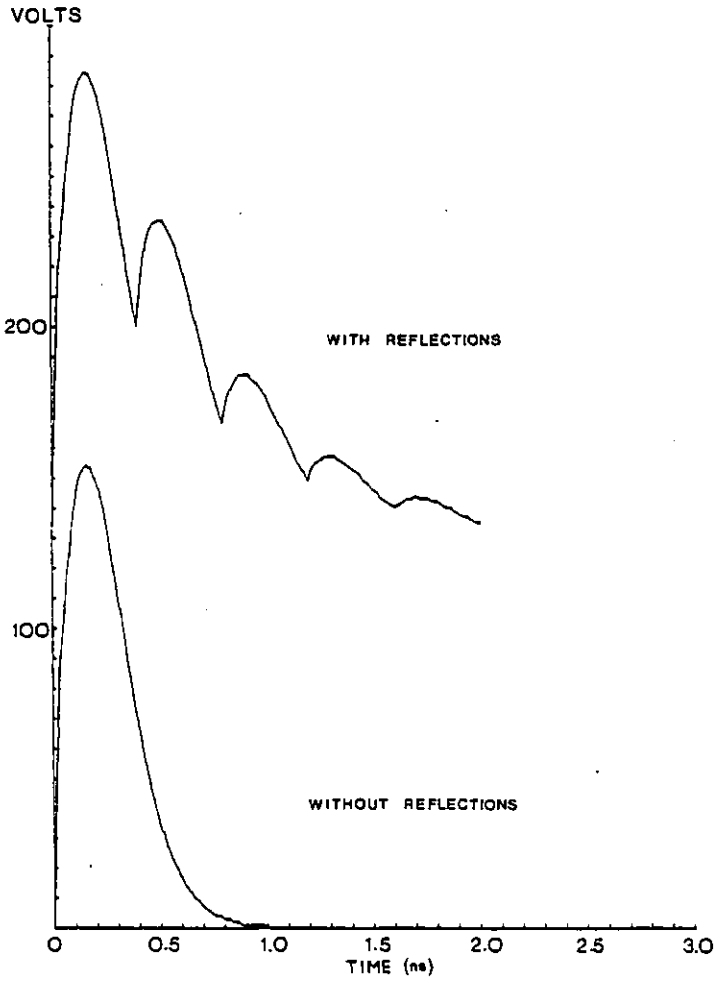

Fig. 8.9. Temporal evolution of voltage applied across the Pockel's cell with z_o=10Ω(C=5pF)

400ps is also shown (top).

The initial and final mode-locked pulse durations were substantially shorter than for the lower value of the impedance and the successive pulse durations approximately obeyed Relation 8.9. The sub-pulse caused by the reflections on the Pockel's cell did in this case disappear after a few roundtrips. Again this was expected, since the amplitude of the reflected signal was low. The duration of the dominant pulse was found to be the same as for no ringing.

The capacitance of the Pockel's cell has a low value and is therefore difficult to measure. To account for inaccuracy in the capacitance specified by the Pockel's cell manufacturers (5pF), the computer program was run with C = 10pF. The duration of the voltage pulse $V_{PC}(t)$ was in this case 570ps compared to 520ps with the lower capacitance. This was found to have little effect on the temporal evolution of the light pulses. Fig. 8.10 shows the evolution of the pulses with an intermediate value of 5Ω for z_o and with C=10pF, taking reflections into account. In this case the second peak is not as intense as in Fig. 8.7 and eventually gets

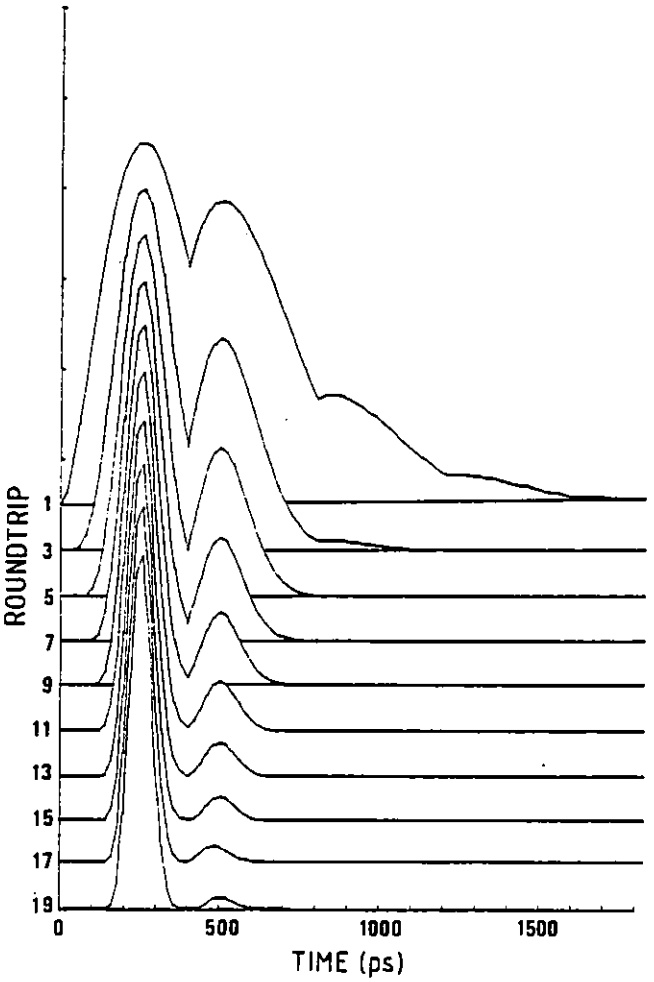

Fig. 8.10

Evolution of light pulses with z_o = 5Ω and C=10pF. (Duration after roundtrip 1: ∿600ps, duration after roundtrip 19: ∿ 80 ps).

suppressed.

The simulations indicate that the important factor in determining the duration of the voltage signal on the Pockel's cell (and hence the duration of the mode-locked pulses), is the current switched by the GaAs device rather than the capacitance of the Pockel's cell. The current depends on the impedance of the conducting switch (Relation 8.1). The impedance depends on the intensity of the pulses illuminating the semiconductor. At high illumination levels the duration of the voltage pulse increases. Lower light intensities yield shorter duration voltage pulses, but also gives rise to a signal of lower amplitude. Therefore the amount of light illuminating the gap should be determined from the compromise between the voltage pulse amplitude and duration.

8.6 Computer simulation for mismatched cavities

By introducing a delay of the voltage applied to the modulator for each roundtrip, a cavity mismatch between the dye laser and the excimer laser was simulated (i.e. a temporal mismatch between the XeCl

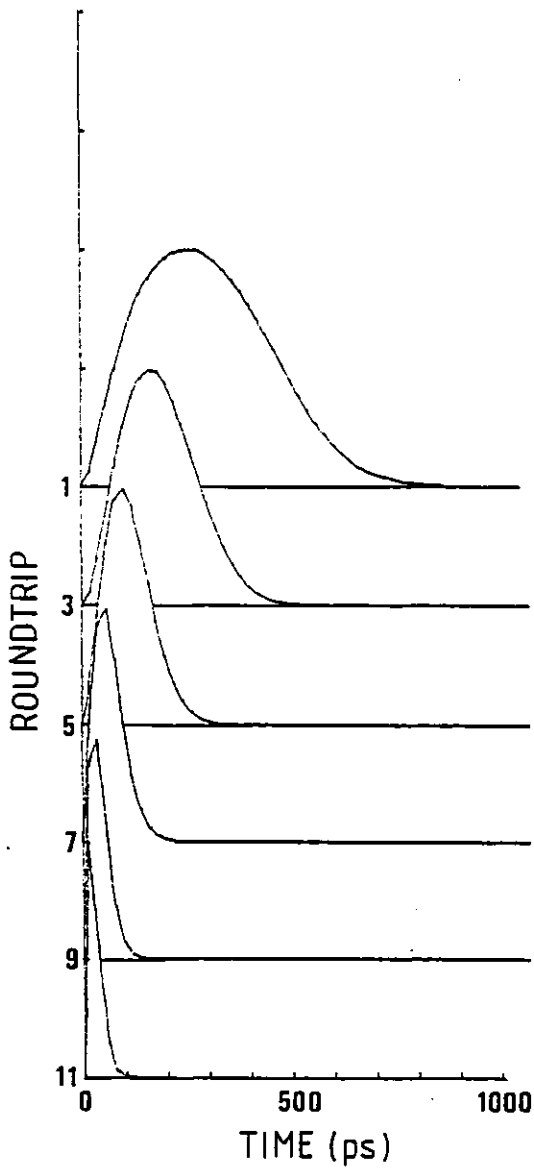

Fig. 8.11
Evolution of light pulses for mismatched cavities. Pulse duration after roundtrip 1: ∿ 400ps, pulse duration after roundtrip 11:∿30ps

cavity roundtrip time and the arrival of the voltage pulse on the Pockel's cell). A mismatch of 100ps corresponding to the situation where the XeCl cavity is 1.5cm longer than the dye laser cavity was introduced. A plot of the pulse evolution is shown in Fig. 8.11, assuming no reflections at the Pockel's cell. The pulse compression is much more dramatic than for the case where the cavities are perfectly matched. This is not surprising since the effect of the mismatch is to delay the arrival of the pulse with respect to the modulating signal thus reducing the "gate opening" time. After 11 roundtrips the pulse misses the "open gate" entirely, and lasing stops. Cavity matching should therefore be accurate since a mismatch causes lasing to cease prematurely.

8.7 Conclusion

Although the theoretical model employed was somewhat limited in that the inductance of the Pockel's cell and saturation effects in the

gain medium were ignored, the simulatations agreed reasonably well with the experimental results described in the previous chapter.

The computer simulations show that the effect of the Pockel's cell modulator alone is not sufficient to yield pulses of ultrashort duration, since the pulses after a few roundtrips become much shorter than the modulating signal. However, generation of bandwidth limited pulses could still be feasible, if other compression mechanisms such as saturable absorption or amplification, were also present.

Finally, the computer plots indicated that apart from compressing the pulses to a steady state duration, the advantage of a large number of roundtrips is to suppress sub-pulses and to cause the intensity profile to assume a more symmetric shape. With e-beam sustained discharge pumping, the actively mode-locked excimer laser should thus provide a train of relatively constant duration, symmetrically shaped picosecond pulses.

References - Chapter 8

1 Dirk J. Kuizenga and A.E. Siegman, IEEE J. Quant. Electron., QE-6, 694 (1970).

2 S.E. Harris and O.P. McDuff, IEEE J. Quant. Electron., QE-1, 245 (1965).

3 W. Margulis, PhD Thesis, University of London (1981)

4 W. Margulis and S. Laval, Submitted to Appl. Phys. Lett., (1981)

GENERAL CONCLUSION

The method of probing gain and absorption with frequency doubled pulses from a mode-locked Rhodamine 6G dye laser proved to be successful in estimating gain and loss coefficients of the XeCl excimer laser. Second harmonic generation, necessary to match the dye laser wavelength with that of the excimer laser, was as expected more efficient with the mode-locked dye laser output than with the unmodulated output. Synchronization of the dye laser with both the electron beam and discharge pumped XeCl laser was not difficult since the dye laser pulse train lasted significantly longer than the gain in the excimer lasers. This also ensured that the XeCl medium was probed both during and after pumping. The amplitudes of the near delta-function shaped probe pulses could readily be measured from the oscilloscope traces (by comparing with reference pulses) thus determining the amount of amplification or absorption in the XeCl medium. An important advantage of employing picosecond probe pulses was the greater accuracy attained since the ultrashort pulses could easily be distinguished from slower electrical noise signals on the oscilloscope traces. The amplitude of the probe signal did therefore not include any components due to noise. The energy density in the ultraviolet pulses from the dye laser was substantially less than the saturation energy density for XeCl, thus ensuring that the measurements were linear. The aid of a computer to analyse the amplification and absorption data and plot the resulting gain and loss curves was advantageous, since the most accurate results were obtained when the average of a large number of data was taken.

Absorption studies performed with the electron beam pumped XeCl laser indicated that vibrational relaxation of the bound ground state

manifold is rapid. This conclusion was reached since within the accuracy of the experiment, the population in the different vibrational levels decayed at the same rate. Furthermore, the lower laser levels did not show any accumulation of population. The ground state lifetime was shorter at higher xenon partial pressures and the rate of dissociation due to xenon was found by experiment to be $k_{Xe} \sim 6.3\ (\pm 1.1) \times 10^{-12} cm^3\ s^{-1}$. When compared with the values reported by other workers, this confirmed that quenching of the XeCl-X-state by Xe is slower than quenching by the halogen donor HCl.

Probing in the afterglow period of both the electron beam and discharge pumped XeCl laser, verified the presence of unidentified transient and stable absorbers. Since such losses could impair efficiency, particularly of long gain duration lasers, further studies should be made to identify the nature of these species. Absorption in discharge pumped lasers is a more serious problem than in electron beam pumped lasers, since the length of the active medium is generally greater in the former. In the XeCl discharge laser the amplitude of the probe pulse was found to decrease by as much as 25% after $\sim$ thirty shots. This implies reduced energy extraction efficiency particularly for high repetition rate systems. Further probing with different wavelengths should reveal the spectral as well as temporal characteristics of the absorbers. Varying the constituent gases and the materials of the laser electrodes and chamber should also aid in identifying the species.

The feasibility of employing the XeCl discharge laser as a high power amplifier for short duration pulses was as expected found to depend on the wavelength of the input pulses. For wavelengths corresponding to the XeCl laser transition, large peak amplification factors of up to 500 in a single pass and 4200 in a double pass yielded

peak energies of ∿ 800μJ in a single picosecond pulse. Significant amplification at wavelengths overlapping other strong XeCl transitions was also observed. The lack of gain on the 3-0 transition was attributed to rapid thermalization of the excited state vibrational manifold. This was consistent with observations made with the electron beam pumped laser. Thus in order to extend the tunability of the XeCl amplifier by increasing the population in higher vibrational levels, the temperature of the laser medium could be elevated. This has been demonstrated with other rare-gas halide lasers.

When the discharge laser was arranged in a regenerative amplifier configuration and the dye laser input pulses were tuned to the main XeCl laser transition, the input pulses were found to deplete the population inversion in the XeCl laser which therefore did not reach threshold for self-oscillation. The excimer laser was then injection mode-locked yielding an output pulse train of high power picosecond pulses. With the use of an electron-optical streak camera, the shortest pulse duration was found to be ∿ 7ps. Peak powers of ∿ 200MW were thus generated in a single picosecond pulse.

Further experiments showed that it was, however, not possible to suppress self-oscillation of the XeCl laser when the wavelength of the input pulses overlapped the relatively strong 1-6 transition originating from a higher vibratinal level. The modulation of the output was in this case incomplete. The results indicated that the vibrational levels in the XeCl-B-state were not cross-coupled on the timescale of the pulse since population from the laser levels was not depleted sufficiently fast. This confirmed that vibrational relaxation within picoseconds is, as expected not feasible at pressures of ∿ 2 atmospheres.

The presence of a second intense pulse trailing the injection

mode-locked pulse by ∿ 500ps in a cavity mismatch situation, suggested that the gain recovers in less than a nanosecond since the first pulse saturates the medium and the second pulse cannot receive significant amplification before the gain is restored. (Pumping on this time-scale is insignificant). A more accurate estimate for the gain recovery time could thus be obtained by varying the delay of the second pulse and investigating the time necessary for the gain to recover sufficiently for the trailing pulse to be amplified. This could be achieved with the aid of an electron-optical streak camera. It would then be possible to determine the rate of vibrational relaxation and thus at what time-scale the spectrum of XeCl is homogeneously broadened.

The effect of gain saturation on the pulse duration was studied in a computer simulation of the injection mode-locking experiment. The simulation of the pulse evolution showed that gain saturation does not necessarily imply pulse shortening. The effect of saturation was found to be strongly dependent on the shape of the input pulses. By obtaining simultaneous streak records of input and output pulses it should be possible to investigate pulse compression due to gain saturation experimentally. Careful investigation of streak records could reveal the pulse shapes and serve to confirm theoretical models based on different input pulse profiles.

Finally, by employing the mode-locked dye laser in conjunction with a semiconductor switching device that in turn activated an intra-cavity Pockel's cell loss modulator, it was possible to generate a 100% modulated train of subnanosecond pulses from the discharge pumped XeCl laser. The success of this active mode-locking technique was due to the good modulation depth and short duration of the signal delivered to the Pockel's cell modulator. Using the electron-optical streak camera, the shortest pulse duration was found to be ∿ 0.4ns. A

theoretical simulation of the active mode-locking process indicated that pulses of shorter duration are possible if more roundtrips were available. The effect of the modulator, however, is diminished as the pulse compresses since the pulse duration becomes substantially shorter than the modulating signal. Thus to generate bandwidth limited pulses, other pulse shortening mechanisms, such as gain saturation or saturable absorption, should be present.

In conclusion, investigation of gain and loss coefficients by the use of probe pulses from a mode-locked dye laser has lead to greater understanding of the relaxation processes in XeCl and of the potential of the XeCl laser as a tunable amplifier.

The large small signal gain coefficients found in both the electron beam and discharge pumped XeCl laser renders these systems suitable for high power pulse amplification. Mode-locking experiments showed that picosecond pulse generation is possible with excimer lasers and theoretical models indicated that for these purposes it is advantageous to employ electron beam sustained discharge pumping yielding longer gain durations and therefore shorter pulses.

The XeCl laser should be a useful source of high power u.v. pulses for purposes ranging from nonlinear optics and photochemistry to separation of isotopes and remote sensing of the upper atmosphere. Generation of extreme vacuum ultraviolet radiation or coherent X-rays by multiphoton processes is a possibility for the future.

APPENDIX 2

PUBLICATIONS

COMPUTER PROGRAM FOR ANALYSIS OF ABSORPTION DATA

```
870  REM
875  REM PROGRAM XeCl
880  OPTION BASE 1
885  DIM Title$[30],Result$[25]
890  SHORT L,To,Tr,Ts,Nd,Gmin,Gmax,St
895  SHORT Inp(35,25),Ip(30,4),Outp(35,25),Op(30,4),T(35,25)
900  SHORT Nodat(25),Nocdat(4),Crat(4),Rat1(30,4),Nodata(60)
905  SHORT Rat(35,25),Mean(60),Ampl(35,25),Alfa(35,25),Sigma(25),Sigma1(25)
910  SHORT Alpha(30,60),Sigma2(60),Low(60),Up(60),Mid(60),C(60)
915  INTEGER Cph,Iph,Ic,Id,Ia,Nophot,Noslots,It,Ti,Ilog
920  BEEP
925  INPUT "TYPE IN DATE",Date$
930  BEEP
935  INPUT "TRANSITION",Transition$
940  Transition$="Trans."&Transition$
945  BEEP
950  INPUT "LASER LENGTH IN cm",L
955  BEEP
960  INPUT "CAVITY ROUNDTRIP TIME",Tr
965  Cph=1                          ! COUNTS No. OF CALIBRATION PHOTOS
970  Iph=1                          ! COUNTS No. OF ORDINARY PHOTOS
975  Nophot=1
980 Start1:INPUT "CAL.RATIO (1) OR CAL.DATA (2)?",Answ
985  ON Answ GOTO Crat,Cdata
990 Crat:BEEP
995  INPUT "TYPE CAL.RATIO, SIGMA AND VARIATION",Crat(Cph),Sigma(Cph),Sigma1(Cph
)
1000 GOTO Start2
1005 Cdata:BEEP
1010 INPUT "TYPE NUMBER OF CAL.DATA",Nocdat(Cph)
1015 Crat(Cph)=0
1020 FOR Ic=1 TO Nocdat(Cph)        ! Ic COUNTS No. OF DATA IN CAL. PHOTO
1025 READ Ip(Ic,Cph),Op(Ic,Cph)
1030 Rat1(Ic,Cph)=Op(Ic,Cph)/Ip(Ic,Cph)
1035 Crat(Cph)=Crat(Cph)+Rat1(Ic,Cph)
1040 NEXT Ic
1045 Crat(Cph)=Crat(Cph)/Nocdat(Cph)
1050 Sigma(Cph)=0
1055 FOR Ic=1 TO Nocdat(Cph)
1060 Sigma(Cph)=Sigma(Cph)+(Rat1(Ic,Cph)-Crat(Cph))^2
1065 NEXT Ic
1070 Sigma(Cph)=SQR(Sigma(Cph)/(Nocdat(Cph)-1))
1075 Sigma1(Cph)=100*Sigma(Cph)/Crat(Cph)
1080 PRINT "Crat=";Crat(Cph);"Sigma=";Sigma(Cph);"Variation=";Sigma1(Cph)
1085 DISP "IF EVERYTHING IS O.K. PRESS CONT !"
1090 PAUSE
1095 Start2:INPUT "DO YOU WANT PRINTED OUTPUT (Y/N)?",A$
1100 IF A$="Y" THEN PRINTER IS 0
1105 IF A$="N" THEN PRINTER IS 16
1110 PRINT Date$,Transition$
1115 BEEP
1120 INPUT "TYPE SHOT No.",Shot$
1125 BEEP
1130 INPUT "TYPE ATTENUATION FACTOR",Nd
1135 BEEP
1140 INPUT "TYPE ZERO TIME",To
1145 BEEP
1150 INPUT "TYPE NUMBER OF DATA",Nodat(Iph)
1155 FOR Id=1 TO Nodat(Iph)
```

```
1160 READ Inp(Id,Iph),Outp(Id,Iph)
1165 T(Id,Iph)=To+(Id-1)*Tr
1170 IF Inp(Id,Iph)=0 THEN 1190
1175 Rat(Id,Iph)=Nd*Outp(Id,Iph)/Inp(Id,Iph)
1180 Ampl(Id,Iph)=Rat(Id,Iph)/Crat(Cph)
1185 Alfa(Id,Iph)=100*LOG(Ampl(Id,Iph))/L
1190 NEXT Id
1195 PRINT
1200 PRINT USING 1205;Shot$,Crat(Cph),Sigma(Cph),Sigma1(Cph)
1205 IMAGE "SHOT No.",3A,5X,"Cal.ratio=",2D.2D,5X,"Sigma=",D.2D,1X,"[",D.2
D,"%]"
1210 PRINT
1215 PRINT "No    INPUT      OUTPUT      AMPL      ALPHA      TIME[ns]"
1220 PRINT "                                       [%/cm]"
1225 FOR Id=1 TO Nodat(Iph)
1230 PRINT USING 1240;Id,Inp(Id,Iph),Outp(Id,Iph),Ampl(Id,Iph),Alfa(Id,Iph),T(Id
,Iph)
1235 NEXT Id
1240 IMAGE 2D,3X,2D.2D,5X,3D.2D,5X,3D.2D,4X,MD.2D,5X,3D.2D
1245 BEEP
1250 INPUT "MORE PHOTOGRAPHS (Y/N)?",B$
1255 IF B$="Y" THEN 1275
1260 BEEP
1265 INPUT "ARE YOU SURE (Y/N)?",C$
1270 IF C$="Y" THEN Start3
1275 Iph=Iph+1
1280 Nophot=Iph
1282 WAIT 2000
1285 BEEP
1290 INPUT "DO YOU WANT TO CHANGE CAL.RATIO (Y/N)?",Crat$
1295 IF Crat$="N" THEN GOTO Start2
1300 Cph=Cph+1
1305 GOTO Start1
1310 Start3:INPUT "DO YOU WANT PRINTED OUTPUT (Y/N)?",D$
1315 IF D$="Y" THEN PRINTER IS 0
1320 IF D$="N" THEN PRINTER IS 16
1325 INPUT "ENTER TIME SLOT",Ts
1330 Ti=1
1335 FOR K=-(30-Ts) TO 250 STEP Ts
1340 It=1
1345 Mean(Ti)=0
1350 FOR Iph=1 TO Nophot
1355 Ia=1
1360 FOR Id=1 TO Nodat(Iph)
1365 IF Inp(Id,Iph)=0 THEN 1420
1370 IF (T(Id,Iph)>=K-Ts) AND (T(Id,Iph)<K) THEN 1380
1375 GOTO 1420
1380 Alpha(It,Ti)=Alfa(Id,Iph)
1385 Mean(Ti)=Mean(Ti)+Alpha(It,Ti)
1390 Low(Ti)=K-Ts
1395 Up(Ti)=K
1400 Mid(Ti)=(Low(Ti)+Up(Ti))*.5
1405 It=It+1
1410 Ia=Ia+1
1415 IF Ia>2 THEN 1425
1420 NEXT Id
1425 NEXT Iph
1430 Nodata(Ti)=It-1
1435 IF Nodata(Ti)=0 THEN 1450
```

```
1440 Mean(Ti)=Mean(Ti)/Nodata(Ti)
1445 Ti=Ti+1
1450 NEXT K
1455 Noslots=Ti-1
1460 FOR Ti=1 TO Noslots
1465 Sigma2(Ti)=0
1470 IF (Nodata(Ti)=0) OR (Nodata(Ti)=1) THEN 1495
1475 FOR It=1 TO Nodata(Ti)
1480 Sigma2(Ti)=Sigma2(Ti)+(Alpha(It,Ti)-Mean(Ti))^2
1485 NEXT It
1490 Sigma2(Ti)=SQR(Sigma2(Ti)/(Nodata(Ti)-1))
1495 NEXT Ti
1500 PRINT
1505 PRINT Date$;Transition$
1510 FOR Ti=1 TO Noslots
1515 PRINT
1520 PRINT USING 1525;Ti,Low(Ti),Up(Ti),Nodata(Ti),Mean(Ti),Sigma2(Ti)
1525 IMAGE "TIME SLOT ",2D,3X,"[",M3D.2D,"-",M3D.2D,"]",3X,"Nodata=",2D,3X,"ME
AN=",M2D.2D,3X,"Sigma=",MD.2D
1530 NEXT Ti
1535 INPUT "DO YOU WANT A PLOT (Y/N)?",E$
1540 IF E$="Y" THEN GOSUB Plot
1545 GCLEAR
1550 EXIT GRAPHICS
1555 INPUT "REPEAT WITH NEW TIME SLOT(Y/N)?",F$
1560 IF F$="Y" THEN Start3
1565 STOP
1570 Plot:Lp$="N"
1575 BEEP
1580 Plot1:INPUT "TYPE LOWER AND UPPER LIMITS AND STEP",Gmin,Gmax,St
1585 PLOTTER IS "GRAPHICS"
1590 GRAPHICS
1595 LINE TYPE 1
1600 FRAME
1605 LDIR 0
1610 LORG 6
1615 MOVE 65,98
1620 IF Lp$="N" THEN Title$="GAIN AS FUNCTION OF TIME"
1625 IF Lp$="Y" THEN Title$="LOG GAIN AS FNCT OF TIME"
1630 LABEL USING "10A,5X,25A,5X,11A";Transition$,Title$,Date$
1635 MOVE 60,4
1640 LABEL USING "K";"TIME[ns]"
1645 LDIR PI/2
1650 MOVE 2,55
1655 IF Lp$="N" THEN LABEL USING "K";"GAIN [%/cm]"
1660 IF Lp$="Y" THEN LABEL USING "K";"LOG GAIN"
1665 LOCATE 12,120,15,92
1670 FRAME
1675 SCALE -40,240,Gmin,Gmax
1680 AXES 10,.05,0,0,2,2
1685 LDIR 0
1690 LORG 8
1695 CSIZE 2.5
1700 FOR I=Gmin TO Gmax STEP St
1705 MOVE -45,I
1710 LABEL USING "MD.2D";I
1715 NEXT I
1720 LDIR PI/2
1725 FOR J=-40 TO 240 STEP 20
1730 MOVE J,Gmin-.02
```

```
1735 LABEL USING "M3D.2D";J
1740 NEXT J
1745 LORG 5
1750 IF Lp$="Y" THEN Logplot1
1755 FOR K=1 TO Noslots
1760 MOVE Mid(K),Mean(K)-Sigma2(K)
1765 DRAW Mid(K),Mean(K)+Sigma2(K)
1770 MOVE Mid(K),Mean(K)
1775 LABEL USING "K";"*"
1780 NEXT K
1785 BEEP
1790 PAUSE
1795 INPUT "DO YOU WANT A HARD COPY (Y/N)?",Hc$
1800 IF Hc$="N" THEN 1820
1805 DUMP GRAPHICS
1810 INPUT "DO YOU WANT TO DUMP GRAPHICS (Y/N)?",Dg$
1815 IF Dg$="Y" THEN 1805
1820 GCLEAR
1825 INPUT "DO YOU WANT A LOG PLOT (Y/N)?",Lp$
1830 IF Lp$="N" THEN 2190
1835 Ilog=1
1840 Logplot:INPUT "ENTER LIMITING TIME SLOTS",Left,Right
1845 IF Ilog=1 THEN Plot1
1850 GRAPHICS
1855 Logplot1:Nosl=Right-Left+1      ! No.OF SLOTS WITHIN INTERVAL
1860 FOR L=Left TO Right
1865 C(L)=LOG(ABS(Mean(L)))
1870 MOVE Mid(L),LOG(ABS(Mean(L)-Sigma2(L)))
1875 DRAW Mid(L),LOG(ABS(Mean(L)+Sigma2(L)))
1880 MOVE Mid(L),C(L)
1885 LABEL USING "K";"*"
1890 NEXT L
1895 BEEP
1900 PAUSE
1905 Pt=0
1910 INPUT "DO YOU WANT TO REMOVE A POINT?",Point$
1915 IF Point$="N" THEN 1975
1920 Pt=Pt+1
1925 INPUT "TYPE No.OF TIME SLOT",Nm(Pt)
1930 PEN -1
1935 GRAPHICS
1940 MOVE Mid(Nm(Pt)),LOG(ABS(Mean(Nm(Pt))-Sigma2(Nm(Pt))))
1945 DRAW Mid(Nm(Pt)),LOG(ABS(Mean(Nm(Pt))+Sigma2(Nm(Pt))))
1950 MOVE Mid(Nm(Pt)),C(Nm(Pt))
1955 LABEL USING "K";"*"
1960 BEEP
1965 PAUSE
1970 GOTO 1910
1975 PEN 1
1980 Midbar=Meanbar=Prod=Sig=0
1985 Pt=1
1990 FOR L=Left TO Right
1995 IF L=Nm(Pt) THEN 2025
2000 Midbar=Midbar+Mid(L)
2005 Meanbar=Meanbar+C(L)
2010 Prod=Prod+Mid(L)*C(L)
2015 Sig=Sig+Mid(L)^2
2020 GOTO 2030
2025 Pt=Pt+1
2030 NEXT L
```

```
2035 Nosl=Nosl-(Pt-1)
2040 Midbar=Midbar/Nosl
2045 Meanbar=Meanbar/Nosl
2050 Prod=Prod/Nosl
2055 Sig=Sig/Nosl-Midbar^2
2060 M(Ilog)=(Prod-Meanbar*Midbar)/Sig
2065 B(Ilog)=Meanbar-M(Ilog)*Midbar
2070 MOVE 0,B(Ilog)
2075 DRAW 240,M(Ilog)*240+B(Ilog)
2080 BEEP
2085 PAUSE
2090 INPUT "NEW LIMITING TIME SLOTS (Y/N)?",T1$
2095 M(Ilog+1)=B(Ilog+1)=0
2100 IF T1$="N" THEN 2115
2105 Ilog=Ilog+1
2110 GOTO Logplot
2115 M=M(1)-M(2)
2120 B=B(1)-B(2)
2125 Result$="Lifetime="&VAL$(DROUND(1/ABS(M),3))&"ns"
2130 MOVE 0,B
2135 DRAW -B/M,0
2140 LDIR 0
2145 MOVE 200,Gmax-.1
2150 LABEL USING "18A";Result$
2155 BEEP
2160 PAUSE
2165 INPUT "DO YOU WANT A HARD COPY (Y/N)?",Hc$
2170 IF Hc$="N" THEN 2190
2175 DUMP GRAPHICS
2180 INPUT "DO YOU WANT TO DUMP GRAPHICS (Y/N)?",Dg$
2185 IF Dg$="Y" THEN 2175
2190 RETURN
2195 END
```

COMPUTER PROGRAM FOR INJECTION MODE-LOCKING MODEL

```
00100 PROGRAM INJLOK(INPUT,OUTPUT,GRACE1,TAPE5=INPUT,TAPE6=GRACE1)
00110 DIMENSION G(120),PZERO(1605),PIN(1605),POUT(1605),GAIN(1605)
00120 SIGMA=7.2
00130 PEAKG=0.075
00140 MISMAT=0
00150 CROSEC=4.5
00160 PMAX=0.
00165 AREA=0.
00170 K=0
00180 T1=0.
00182 LIMSUP=0
00184 LIMINF=0
00190 SIG=3
00200 SIG=SIG*20.
00210 WRITE(6,18)
00220 18 FORMAT(" WHAT IS THE INPUT ENERGY IN MICROJOULES ?")
00230 READ(5,*)ENERGY
00240 L=10
00250 MISM=MISMAT*20
00260 NOSAT=1
00270 SUMJ=0.
00280 DO 1 I=1,110
00290 T=I
00300 1 G(I)=(100./(1.7725*2*SIGMA))*EXP(-((T/3.-18.)/(2*SIGMA))**2)
00310 WRITE(6,30)
00320 30 FORMAT("  T(NS)      GAIN",/)
00330 ANORM=PEAKG/G(55)
00340 DO 20 I=1,110
00350 G(I)=G(I)*ANORM
00370 20 CONTINUE
00380 DO 32 I=1,110,3
00390 K=K+1
00400 32 WRITE(6,33)K,G(I)
00410 33 FORMAT(1X,I4,2X,F9.4)
00420 21 FORMAT(1X,I5,4X,F7.2)
00430 DO 2 J=1,1600
00440 PZERO(J)=4./((EXP((T1-600.)*1.763/SIG)+EXP(-(T1-600.)*1.763/SIG))**2)
00445 AREA=AREA+PZERO(J)
00450 2 T1=T1+0.5
00460 WRITE(6,24)
00470 24 FORMAT(/," NORMALIZED INPUT",/,"  T(.5PS)        N",/)
00480 ANORM=1.56*ENERGY/AREA
00490 DO 19 J=1,1600
00510 PIN(J)=PZERO(J)*ANORM
00530 19 PZERO(J)=PZERO(J)*ANORM
00540 I=0
00542 DO 38 J=1,1600,10
00544 38 WRITE(6,21)J/10,PIN(J)*500.
00550 WRITE(6,11)      SIG/10,3.33*SIGMA,ENERGY,PEAKG,CROSEC,MISMAT
00560 11 FORMAT(/," WIDTH OF INPUT PULSE: ",F3.0," PS FWHM",/,
00570+" WIDTH OF GAUSSIAN: ",F3.0," NS FWHM   ",/," INPUT EN/VOL :",
00580+F7.3," MICROJOULES",/," PEAK GAIN:",F5.3,/," SIGMA:",F5.2," 10**-16",
00590+/," MISMATCH= ",I3," PS")
00600 CROSEC=CROSEC*2.*0.0001
00610 6 I=I+1
00620 N=(I-8)/22
00630 R=N*22+8-I
00640 IF(R.EQ.0)I=I+6
00650 NPASS=I/11
00660 N=I/22
00670 R=N*22-I
```

```
00680 IF(R.EQ.0)WRITE(6,4)NPASS/2
00690 4 FORMAT(////," AFTER ",I2," ROUNDTRIP(S) IN THE LASER THE OUTPUT IS",
00700+//,"   I(.5PS)          N NORM         GAIN",//)
00710 DO 3 J=1,1600
00720 SUMJ=SUMJ+PIN(J)
00730 GAIN(J)=1./(1.-(1.-EXP(-G(I)*L))*(EXP(-CROSEC*NOSAT*SUMJ)))
00740 POUT(J)=PIN(J)*GAIN(J)
00750 IF((PMAX-POUT(J)).LT.0)PMAX=POUT(J)
00760 3 PIN(J)=POUT(J)
00770 ENERGY=SUMJ*0.03/1.56
00780 N=I/22
00790 R=N*22-I
00800 IF(R.NE.0)GO TO 8
00810 DO 35 J=1,1600,10
00815 OUT=POUT(J)*PZERO(1201)/PMAX
00820 35 WRITE(6,7)J/10,OUT*500.,GAIN(J)
00825 7 FORMAT(3X,I5,8X,F7.2,7X,F8.2)
00826 PHALF=PMAX/2.
00827 DO 10 J=1,1599
00832 IF(POUT(J).GT.PHALF)LIMSUP=J
00833 IF(POUT(1600-J).GT.PHALF)LIMINF=1600-J
00834 10 CONTINUE
00835 WIDTH=(LIMSUP-LIMINF)/20.
00850 DO 5 J=1,1600
00855 JMISM=J+MISM*NPASS/2
00860 IF((JMISM-1600).GT.0)JMISM=1600
00865 IF(JMISM.LE.0)JMISM=1
00870 PIN(J)=0.04*POUT(J)
00880 5 CONTINUE
00890 WRITE(6,17)NPASS/2,ENERGY*WIDTH,WIDTH
00900 17 FORMAT(/," ENERGY DENSITY IN THE PULSE AFTER ",I2," ROUNDTRIP(S):",
00910+2X,F8.0," MICROJOULES  ",/," PULSE DURATION:",F4.1," PS FWHM",/)
00920 8 SUMJ=0.
00930 PMAX=0.
00940 IF(I.LT.110)GO TO 6
00950 STOP
00960 END
```

COMPUTER PROGRAM FOR ACTIVE MODE-LOCKING MODEL

```
00100 PROGRAM XECL(INPUT,XECL32,TAPE5=INPUT,TAPE6=XECL32)
00110 DIMENSION VPC(4005),IGAIN(55),POUT(2,4005)
00120 FRACT=0.5
00130 LAGTME=800.
00140 DELTAV=0.
00150 V=0.
00160 DELTAT=1.
00170 VAPPL=700.
00180 Z=1.
00190 TAL=100.
00200 C=5.
00210 TIME=0.
00220 WRITE (6,1) VAPPL,Z,TAL,C,FRACT,LAGTME
00230 1 FORMAT(" VAPPL=",F5.0,"   Z=",F5.1,"   TAL=",F4.0,"   CAPAC=",F3.0,
00240+/," AMPLITUDE OF REFLECTION=",F2.1," COMPARED TO THE PEAK",/,
00250+" AND OCCURING ",I4," PS AFTER THE MAIN VOLTAGE PULSE",/)
00260 WRITE (6,2)
00270 2 FORMAT(" TIME  IOUT  VOLTAGE")
00280 DO 4 I=1,3001
00290 AIOUT=VAPPL/(100.+Z*EXP(TIME/TAL))
00300 V=V+DELTAV
00310 DELTAV=(2.*DELTAT/C)*(AIOUT-V/33.3333)
00320 J=I-1
00330 M=I-LAGTME
00340 VPC(I)=V
00350 IF(I.GT.LAGTME)VPC(I)=VPC(I)+FRACT*VPC(M)
00360 IF(MOD(J,20).EQ.0) WRITE(6,3)TIME,AIOUT,VPC(I)
00370 3 FORMAT(F6.0,F6.3,F6.0)
00380 4 TIME=TIME+DELTAT
00390 IGAIN(1)=1
00441 DO 5 ITIME=1,2001
00442 5 POUT(1,ITIME)=1
00444 IT=0.
00450 DO 7 NPASS=2,20
00452 IGAIN(NPASS)=100
00454 PMAX=0.
00470 DO 6 ITIME=1,2001
00480 M=ITIME+IT
00490   POUT(2,ITIME)=0.1*IGAIN(NPASS)*POUT(1,ITIME)*(SIN
00500+(3.14159*VPC(M)/1300.))**2
00501 IF(PMAX.LT.POUT(2,ITIME))PMAX=POUT(2,ITIME)
00503 6 CONTINUE
00504 R=2./PMAX
00505 DO 11 ITIME=1,2001
00506 11 POUT(1,ITIME)=POUT(2,ITIME)
00520 WRITE (6,8) NPASS
00530 8 FORMAT(//," TIME   PASS",I3)
00550 DO 10 I=1,2001,20
00560 K=I-1
00564 POUT(2,I)=POUT(2,I)*R
00570 WRITE (6,9) K,POUT(2,I)
00580 9 FORMAT(I5,F8.3)
00590 10 CONTINUE
00592 IT=IT+100
00594 7 CONTINUE
00600 STOP
00610 END
```

APPENDIX 1

COMPUTER PROGRAMS

Vibrational Relaxation Studies in Noble Gas Halides

M.H.R. Hutchinson, C.D.P. Levy *and* **G.M. Reksten**
Physics Department, Imperial College of Science and Technology

In this work we investigated the scaling of e-beam diodes used for pumping noble gas halides, and the kinetics of the XeCl ground state in e-beam pumped systems. For high power, large volume applications such as nuclear fusion, e-beams are essential for efficient pumping.

At the top of Fig.1 is shown a conventional co-axial diode. This is limited to powers below about 10 GW, because beyond this the return current flowing axially to earth along the anode creates a magnetic field strong enough to cause beam pinching onto the centre of the anode, leading to foil rupture [1]. We have developed a co-axial diode which is scalable in that pinching effects at high current levels are avoided. The return current geometry has been changed to a radial path out along a conducting sheet inserted through a gap in the anode. This reduces the magnetic field strength B and changes its direction favourably. Electrons in the gap region are deflected towards the anode, if B is high enough.

The diode can be increased in length and power indefinitely, since B reaches a maximum proportional to the current density.

The output from a diode we built using radial return geometry was comparable to that from an axial return diode, e.g. 1 joule in 20 ns from unoptimised KrF, at an e-beam power of 10 GW. Slight pinching was evident using axial return geometry. Increasing the power level would be impossible using axial return geometry, whereas using radial return the efficiency would increase due to increased coupling of electrons in the gap, to the anode.

XeCl lases at 308 nm between two bound states, on the v' - v" transitions 0 - 1 and 0 - 2, where v' is an upper

state vibrational level, v" a ground state level [2]. The ground state has a well depth of about kT, and is thermally unstable. Assuming no population in the upper state, and no dominant background absorption, the population in a v" level is directly proportional to the absorption coefficient on a vibronic transition out of it [3].

Fig.2 shows the experimental arrangement used to probe XeCl. The output from a tunable mode-locked Rhodamine 6G dye laser was frequency doubled, resulting in a picosecond pulse train 400 ns long with pulse separation of 6.2 ns and bandwidth 1 Å, narrow enough to pick out different v' - v" transitions. A Pulserad 110A e-beam generator (35 kA, 500 kV, 30 ns) was synchronised to fire as the picosecond pulse train passed through the XeCl cell. The pulse train was

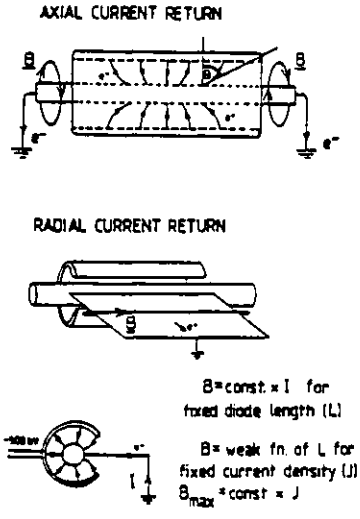

Fig.1

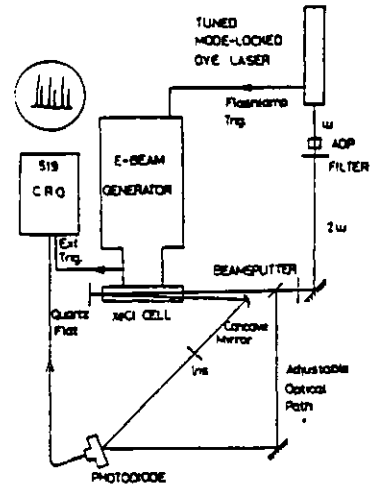

Fig.2

split into two, half going direct to a fast photodiode and the other half making a double pass through the XeCl cell before hitting the same photodiode. A quartz flat back reflector reduced ASE and a spatial filter cut down its detection. The photodiode sees two interleaved pulse trains, and the ratio of their heights at any time relative to a calibration ratio gives the gain or loss in the cell. All optical losses except those due to absorption by the e-beam pumped XeCl gas mixture were made to cancel by taking

calibration shots through the unexcited XeCl cell. Timing accuracy of this system is ± 2 ns, due to jitter in triggering the 519 oscilloscope and uncertainty due to double passing.

Fig.3 shows the results of probing the 1 - 0 transition at 3058.7 Å. Several shots were taken, each probing the cell at 6.2 ns intervals. Each data point represents the average of a 5 ns time slot. Zero time corresponds to the beginning of the e-beam pump pulse. An initial gain region is followed by a gap in the data due to ASE, and then by the decay tail of absorption. Fig.4 shows the same result semi-logarithmically, together with results of 2 - 0 at 3040.8 Å and 2 - 1 at 3043.3 Å. We also probed on 2 - 2 and 0 - 2 transitions. To within experimental accuracy, all v" levels decay with a lifetime of 20 ns (± 3) using a typical laser mixture. Absorption decreased if the Xe concentration was changed from optimum or if the laser was tuned off resonance, implying decay is due to XeCl ground state.

We conclude that vibrational relaxation is fast compared to the decay time of 20 ns, since v" = 0 is populated and all levels have the same lifetime. The observed decay is due to collisional dissociation of the ground state. Vibrational relaxation in the upper state must also be very

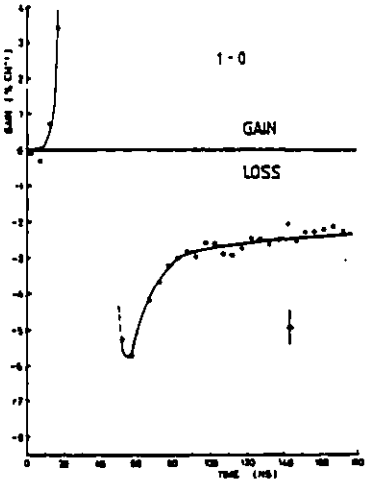

Fig.3

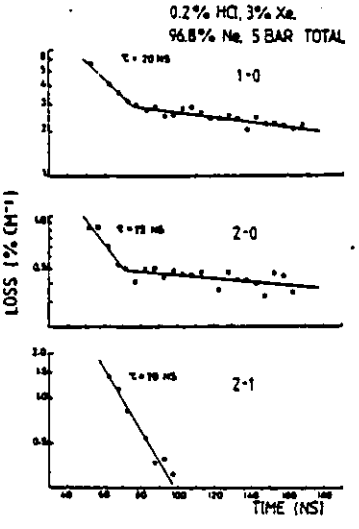

Fig.4

fast, since we observe gain from v' = 0,1 but not v' = 2, implying thermalisation. The slower lifetime of 250 ns is sometimes not visible due to noise. We believe it may be due to slow decay of an equilibrium concentration of XeCl in the ground state, due to chemical scavenging of free Cl atoms by Cl or H atoms.

In conclusion, powerful, efficient XeCl lasers will not be limited by e-beam problems, but it appears that bottlenecking in the ground state may reduce efficiency.

References

[1] L.P. Bradley, High Power Gas Lasers, IOP Conference Series, No. 29 (1975).

[2] J. Tellinghuisen et al., J. Chem. Phys., 64, 2484 (1976).

[3] S.F. Fulghum et al., Appl. Phys. Lett., 33, 926 (1978).

Picosecond injection mode-locking of the XeCl laser

G. Reksten, T. Varghese, and D. J. Bradley
Optics Section, Blackett Laboratory, Imperial College, London SW7 2AZ, England

(Received 24 November 1980; accepted for publication 30 December 1980)

Ultrashort pulse generation has been achieved in a UV-preionized transverse discharge XeCl laser by injection mode-locking using the second harmonic of a passively mode-locked Rh 6G dye laser tuned to the XeCl gain bandwidth. Temporal measurements using a Photochron II streak camera showed pulse durations ~7 ps with single-pulse peak power of ~150 MW.

PACS numbers: 42.55.Hq

Several attempts have been made to mode lock rare-gas–halide lasers. Active mode-locking of the XeF laser[1] and passive mode-locking of the KrF laser[2] have, in each case, produced pulses of ~2-ns durations. Failure to achieve picosecond pulse durations arose because of the short durations (15 ns) of the gain in the discharge-pumped laser systems employed. As a consequence there was not a sufficient number of cavity round trips to produce appreciable pulse narrowing. The spectral bandwidth of the XeCl laser transition is large enough (~0.5 nm[3]) to support pulses of subpicosecond duration. We have employed injection mode locking[4] of this laser to produce, for the first time, picosecond pulses with a rare-gas–halide laser. Pulses of ~7-ps duration and peak powers of ~150 MW are thus obtained.

The experimental arrangement is illustrated in Fig. 1. The second-harmonic pulse train of a passively mode-locked Rh 6G dye laser output[5] was injected into the XeCl laser cavity through an uncoated quartz flat which served as the output coupler. A flat 100% reflectivity mirror completed the laser resonator. Two apertures A_1 and A_2 restricted laser action in the cavity to an area equal to that of the injected beam. The UV-preionised, discharge-pumped XeCl medium was operated under high-gain conditions (maximum small signal gain ~500) and the windows were antireflection coated and tilted to prevent self-oscillation. The gas mixture was typically 6-Torr HCl + 90-Torr Xe + Ne at 2000 Torr total pressure. Without apertures the output energy was ~70 mJ in a 30-ns pulse at 30-kV charging voltage. The dye laser

 0003-6951/81/070513-03$00.50

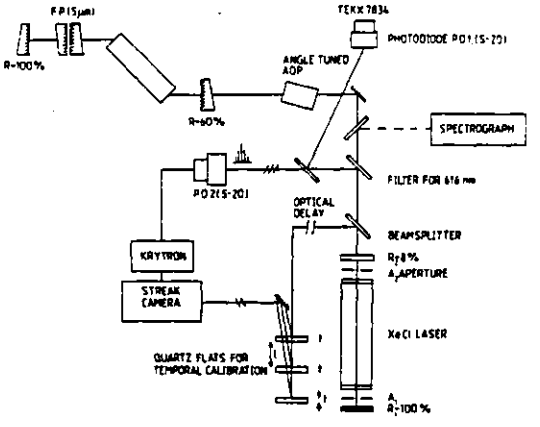

FIG. 1. Experimental arrangement.

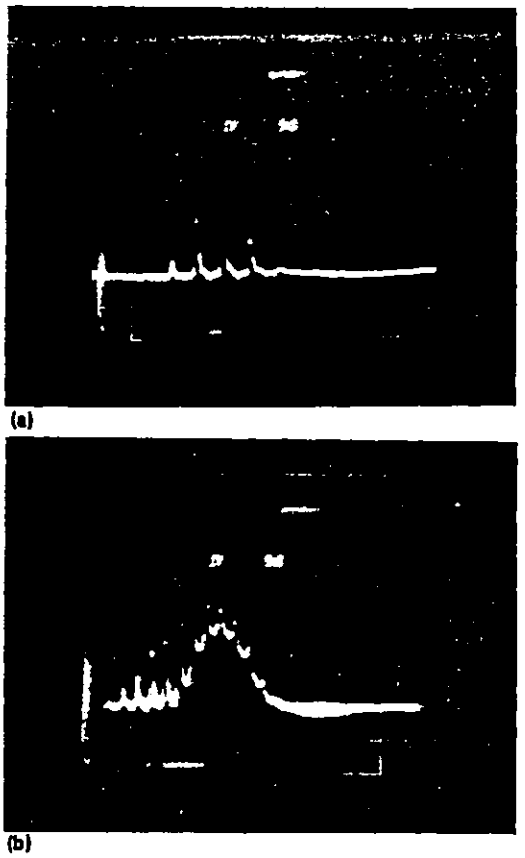

FIG. 2. Oscilloscope trace of injection mode-locked output of XeCl laser. Time scale 5 ns per major division. (b) Oscilloscope trace showing deterioration of mode locking for low-input energy.

second-harmonic pulse train had peak pulse energy ~ 300 nJ giving an energy density $\sim 1\ \mu J\ cm^{-2}$. The pulse separation was ~ 8.3 ns and the train contained ~ 100 pulses. An intracavity 5-μm gap Fabry-Perot étalon permitted spectral tuning of the dye laser to the XeCl transition at 308 nm and the bandwidth of the second-harmonic output was ~ 2.5 Å. The length of the dye laser cavity was ajusted to be either equal to that of the XeCl cavity or half this length. Good mode locking was obtained in both cases showing that the gain recovery time in the XeCl laser is less than 4 ns.

The two lasers were synchronized so that the XeCl laser would fire when the shortest pulses, late in the dye laser pulse train,[5] were injected. Careful adjustments were made so that the pulses followed a path exactly along the axis of the XeCl laser. This alignment was found to be critical for good injection locking to take place. If the two lasers were not well aligned, the modulation of the XeCl output was incomplete, and self-lasing would build up in the XeCl cavity.

The gain duration of the XeCl laser was ~ 40 ns and the output pulse train had five pulses [Fig. 2(b)]. With an input pulse energy density of $1\ \mu J\ cm^{-2}$, the second pass, after reflection from the 100% mirror, showed gain saturation. The XeCl laser was found to lock completely to the injected pulses. The mode-locked pulse train emitted by the XeCl laser had practically zero background energy between the pulses. The peak energy in a single phase was ~ 1 mJ.

The threshold energy requirement for good mode locking was investigated by varying the input pulse energy. If the energy of the injected pulses was low, amplification after a few round trips of the XeCl cavity was not sufficient to deplete the gain enough to prevent the laser reaching threshold at the peak of the discharge gain. In this case, self-lasing competed with the picosecond pulse in the cavity and resulted in incomplete modulation. When the frequency-doubled input pulses from the dye laser were attenuated by a factor of 15; by inserting two glass slides in the beam, background lasing started to appear. Thus, for a discharge laser of the type used in our experiment, input pulse energies of close to 1 $\mu J\ cm^{-2}$ are needed to generate a 100% modulated injection-locked pulse train. Figure 2(b) shows an oscillogram of the XeCl laser output when the injected pulses were attenuated. An intense background was also obtained when the injected laser beam was not correctly aligned along the axis of the XeCl laser. A similar effect was obtained when the dye laser was tuned away from the peak of the discharge laser gain bandwidth.

The XeCl cavity had to be accurately matched to be equal to or double the dye-laser cavity length. Any temporal mismatch between the pulse propagating in the XeCl laser and the injected dye-laser pulses increases with the number of roundtrips. Subpulses could sometimes be resolved on a fast time scale on the oscilloscope by looking at the last pulses in the train where the separation was greatest. In our experiment the cavity lengths were adjusted in this manner by monitoring the pulses on a fast time scale on the oscilloscope. For very accurate adjustment, a streak camera was employed.

The duration of the dye laser and injection-locked pulses were measured with a Photochron II streak camera[6] with an S20 photocathode. The duration of the shortest pulses in the dye laser second-harmonic pulse train was found to be ~ 6 ps. The duration (Fig. 3) of the shortest

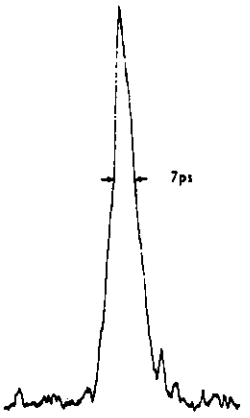

FIG. 3. Streak photograph of injection mode-locked XeCl laser. Streak-camera time resolution ~2 ps.

injection mode-locked XeCl pulses was found to be ~7 ps (FWHM), giving a peak power of ~150 MW for 1 mJ energy. There is very little background energy between the pulses. Since our results show that a typical injection mode-locked pulse was of about the same duration as an injected pulse, it can be concluded that there are no significant pulse-temporal broadening mechanisms in XeCl for pulses as short as 6 ps.

The saturation energy density for XeCl is estimated to be ~700 μJ cm^{-2}.[7] The peak energy density measured for a single pulse in the injection-locked pulse train exceeded this value, thus the pulses could be further shortened by gain saturation, as found with dye lasers[8] if the number of round trips were not limited. With other pumping methods, such as *e*-beam-sustained discharges, which give longer gain duration, bandwidth-limited (~1 ps for XeCl) pulses could be obtained, even if the injected pulses are not as short. The use of bandwidth-limiting elements in the XeCl laser cavity would also help the generation of bandwidth-limiting pulses.[5]

In summary, injection mode locking of XeCl has been achieved by injecting low-power, frequency-doubled picosecond pulses from a conventional flashlamp-pumped Rh 6G dye laser. A 100% modulated pulse train consisting of ultrashort pulses of up to 150 MW peak power was produced by the XeCl laser.

This method of mode locking could be extended to other rare-gas excimer and exciplex lasers, using the third harmonic of the Nd:glass laser to mode-lock the XeF laser, and the fourth harmonic of the Ruby laser for the Xe_2 laser.

The authors thank M. H. R. Hutchinson, W. Sibbett, and J. R. Taylor for the experimental help and useful discussions. We are pleased to acknowledge financial support from the Science Research Council. One of us (T.V.) was supported by the Education Ministry of the Government of India.

[1]C. P. Christensen, L. W. Braverman, W. H. Steiner, and C. Wittig, Appl. Phys. Lett. 29, 424 (1976).
[2]T. Efthimiopoulos, J. Banic, and B. P. Stoicheff, Can. J. Phys. 57, 1437 (1979).
[3]J. Reintjes, Opt. Lett. 5, 342 (1980).
[4]E. I. Moses, J. J. Turner, and C. L. Tang, Appl. Phys. Lett. 28, 258 (1976).
[5]D. J. Bradley, *Topics in Applied Physics*, edited by S. L. Shapiro (Springer, Heidelberg, 1977), pp. 17-81.
[6]D. J. Bradley and W. Sibbett, Appl. Phys. Lett. 27, 382 (1975).
[7]M. Rokni, J. A. Mangano, J. H. Jacob, and J. C. Hsia, IEEE J. Quantum Electron. QE-14, 464 (1978).
[8]G. H. C. New, IEEE J. Quantum Electron. QE-10, 115 (1974).

Active mode locking of a XeCl laser

Grace Reksten, Thomas Varghese, and Walter Margulis
Optics Section, Blackett Laboratory, Imperial College, Prince Consort Road, London SW7 2AZ, England.

(Received 23 February 1981; accepted for publication 24 April 1981)

Active mode locking of a UV preionized transverse discharge XeCl laser has been achieved by modulating the gain using an intracavity Pockel's cell. The output was 100% modulated, and pulses as short as ~310 ps were measured. Generation of shorter pulses by the same method is discussed briefly.

PACS numbers: 42.60.Fc, 42.60.Da, 42.60.Kg

Rare-gas halide lasers have proved to be powerful sources of UV radiation and can be scaled to provide pulses of very high energies. High-power, short-duration pulses are important for many applications, such as nonlinear optics, spectroscopy, and photochemistry,[1,2] and considerable effort has therefore been made to generate picosecond pulses from these systems.

Single-subnanosecond, 308-nm wavelength XeCl laser pulses have been obtained by slicing techniques,[3] and picosecond UV radiation has been generated by amplification of second-harmonic dye laser pulses in XeCl.[4,5] Recently, the generation of ultrashort pulses by injection mode locking was reported.[6] In this case a 100% modulated output train was produced, with individual pulse durations of ~7 ps. This method is, however, somewhat limited by the fact that the injected pulses must have the same wavelength as the particular rare-gas–halide laser. Previous attempts to mode-lock XeF and KrF lasers have been only partially successful in that the output pulses were relatively long ($\lesssim$2 ns) with incomplete modulation.[7,8] These methods failed to produce ultrashort pulses, since the duration of optical gain in conventional discharge and *e*-beam systems is too short for mode locking to build up.

Recently a new mode-locking technique was reported.[9] A flashlamp-pumped dye laser was used to activate a semiconductor switching device. The picosecond voltage pulses thus generated were applied to an intracavity Pockel's cell that actively modulated a coumarin dye laser. In this letter we report the extension of this technique to rare-gas halide lasers. A GaAs switch driven by a flashlamp-pumped Rh6-G dye laser activated an intracavity Pockel's cell in a XeCl laser, and a 100% modulated train of 5–8 pulses was generated by the excimer laser. Individual pulse durations as short as ~310 ps were measured.

The experimental arrangement is shown in Fig. 1. A conventional flashlamp-pumped dye laser was used. The mode-locked output consisted of about 400 pulses of ~5-ps duration. The energy per pulse was ~20 μJ. The cavity length was adjusted to be either equal to the XeCl cavity or half this length.

The excimer laser was a UV preionised discharge system operated at 30-kV charging voltage. The gas mixture used was 12-Torr HCl + 100-Torr Xe + Ne = 1500 Torr. The maximum laser output produced from this system was ~70 mJ. In the configuration used for this experiment, however, the free-lasing output was substantially reduced due to lossy elements in the cavity. Synchronization between the two lasers was not critical, since the duration of the dye laser pulse train was much longer than the duration of the discharge pumping.

The XeCl laser cavity was defined by mirrors M_4 (R = 100%) and M_3 (R = 80%), and the roundtrip time was 8.3 ns. A Glan–Thompson polarizer (P) was inserted between the laser medium and the KDP Pockel's cell (PC), which was placed very close to the output coupler M_3. Apertures (A) of 1 cm diameter were placed at both ends of the cavity to restrict lasing to the area covered by the Pockel's cell.

The modulating arrangement differed slightly from the one described in[9] and was operated as follows: Initially lasing in the XeCl amplifier is inhibited by the application of a dc voltage $V_{\lambda/4}$ (~650 V) to the Pockel's cell. Light reaches mirror M_3 circularly polarized, is reflected back, and after the second pass through the Pockel's cell has its linear polarization restored, but rotated by a total of 90°. It is then rejected by polarizer P, and since no feedback is allowed into the amplifier the laser does not reach threshold. When, however, a short duration voltage pulse is added to the dc voltage $V_{\lambda/4}$, the polarization of light traveling through the Pockel's cell is rotated by a total of more than 90°. A short-duration burst of light which is not linearly polarized is then formed. Its horizontal component is not rejected by the polarizer and is fed back into the amplifying medium allowing the laser to reach threshold. The arrival of this pulse of light at the Pockel's cell after a round trip in the cavity is synchronized with the application of a subsequent short-duration voltage pulse switched by the GaAs device, allowing further amplification and buildup of a mode-locked pulse train. Synchronization

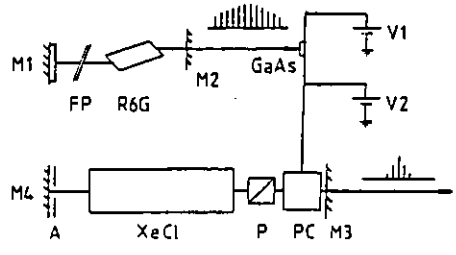

FIG. 1. Experiment arrangement.

 0003-6951/81/140129-03$00.50

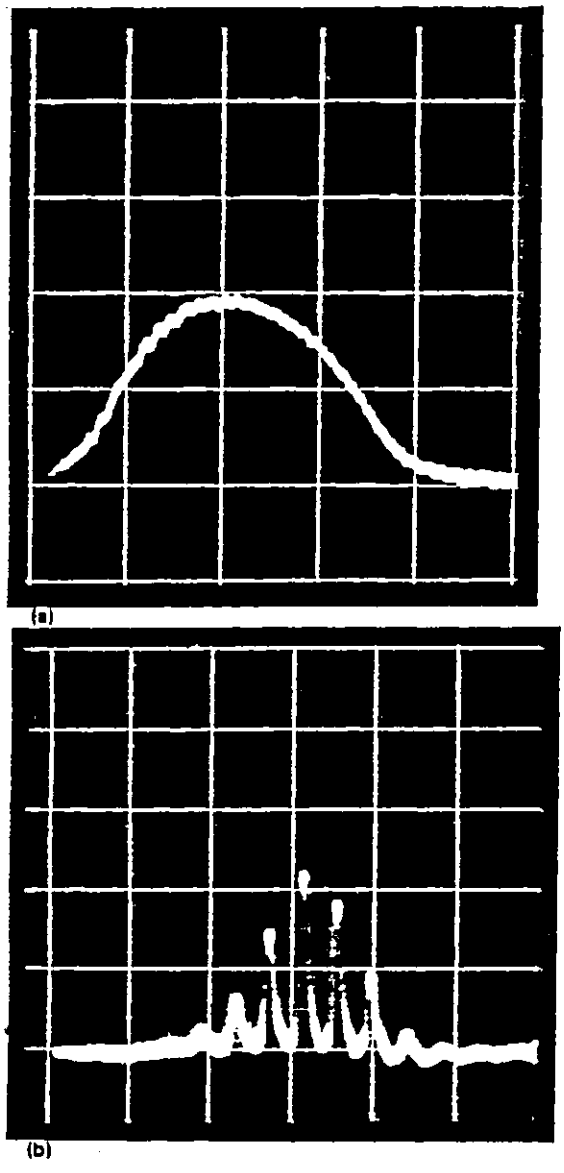

FIG. 2. (a) Oscilloscope trace of unmodulated XeCl laser output. Vertical scale: 2 V/division. Horizontal scale: 10 ns/division. (b) Oscilloscope trace of mode-locked XeCl laser output. Vertical scale: 2 V/division. Horizontal scale: 10 ns/division.

was achieved by adjusting the pulse separation of the dye laser to be equal to or half that of the XeCl cavity round-trip time.

The short-duration voltage pulses used were provided by a semiconductor switching device[10] consisting of a slab of semi-insulating GaAs connected between a dc power supply and the Pockel's cell. Initially the high impedance of the device prevents voltage from appearing across the load. However, when illuminated by a picosecond laser pulse, photoinduced carriers cause the conductivity of the semiconductor to increase by several orders of magnitude. In this way the voltage is effectively transmitted to the Pockel's cell.

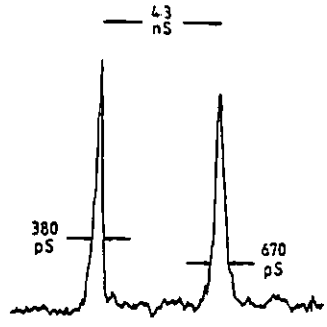

FIG. 3. Microdensitometer trace of streak photograph showing two consecutive output pulses. Streak camera time resolution ~200 ps.

Semi-insulating GaAs was chosen, since it is capable of switching several kilovolts with picosecond rise times.[11] It is also particularly useful for high-repetition-rate applications, since the recombination time of optically excited carriers is only ~100 ps.[12] If the electric field across the slab is limited to $\lesssim 3$ kV/cm, electrons in the conduction band, promoted by the activating light pulse, exhibit a very high mobility ($\sim 7000\ \mathrm{cm^2\ V^{-1}\ s^{-1}}$). In this case even a relatively modest optical energy ($\sim 10\ \mu$J) illuminating the device is sufficient for efficient switching. Also by limiting the voltage applied to the switch, electrical breakdown can be avoided. Typically, pulses of 200-V amplitude were switched by the GaAs device when biased to 700 V. It should be pointed out that voltage pulses appearing across the Pockel's cell exhibited ringing and were somewhat integrated. This was mainly due to impedance mismatch and the finite capacitance of the Pockel's cell (~5 pF). The Pockel's cell used in our experiment has a rise time of ~250 ps.

With no voltage on the Pockel's cell the unmodulated laser output lasted ~25 ns as shown in Fig. 2(a). When voltage pulses of ~200-V amplitude were applied to the Pockel's cell and added to the $V_{\lambda/4}$ dc bias, a 100% modulated train of pulses was generated by the XeCl laser. The train lasted 20–30 ns and the pulse separation was ~4 or 8 ns depending on the dye laser cavity length. An oscillogram of the latter is shown in Fig. 2(b).

The pulse durations were measured with a UV-sensitive Photochron II streak camera.[13] Slow sweep speeds were used (~ 1–4×10^8 cm/s) allowing the observation of series of pulses and the background (if any) between them. Figure 3 is a microdensitometer trace of consecutive pulses showing no background and 100% modulation. In this case the round-trip time of the dye laser cavity was half that of the XeCl laser, as in Fig. 2(b). Therefore the excimer laser was double pulsing, and the streaks shown correspond to pulses that have evolved from different initial bursts of light. The recorded width of the pulse shown on the left is ~380 ps FWHM. When deconvolving the 200-ps time resolution of the camera, as used in our experiment, this corresponds to a real pulse duration of ~310 ps.

The relatively long pulse durations obtained in our experiment could be improved by the use of impedance-matched Pockel's cells of faster rise time. Furthermore,

since pulse narrowing occurs with each pass of the light pulse through the modulator, a large number of round trips is desired, and it would therefore be advantageous to use systems with longer gain durations (such as *e*-beam sustained discharge lasers). Alternatively the introduction of a second Pockel's cell at the other end of the XeCl laser cavity should, for the same reason, shorten the pulses. Synchronized voltage pulses can be applied to each cell by using a single GaAs switch connected to both elements by suitable lengths of cable.

In our experiment the energy density of each UV light pulse was much less than the expected saturation energy density ($\sim 700\,\mu J\,cm^{-2}$).[14] If single-pulse energies were higher, pulse shortening by gain saturation (analogous to the mode-locked dye laser)[15] could become significant. In order to increase the energy available in the picosecond pulses, lower loss elements (PC and P) could be used. In our case the useful area of the beam was restricted by the physical size of the polarizer and the diameter of the Pockel's cell. Also the short-wavelength cutoff of the former ($\sim 0.3\,\mu m$) was close to the wavelength of the XeCl laser. This fact should be considered, if the method is to be extended to shorter-wavelength excimer lasers. Extention to longer-wavelength lasers should be straightforward. Finally, if the energy density is sufficient to saturate a dye in a passive mode-locking arrangement, a hybrid system could be used, also leading to shorter pulses.

In conclusion, we have for the first time demonstrated generation of 100% modulated trains of subnanosecond pulses from an excimer laser by a method that can easily be extended to other excimer systems.

The authors thank Prof. D. J. Bradley, M. H. R. Hutchinson, and J. R. Taylor for the use of facilities at Imperial College and for useful discussions. We are pleased to acknowledge financial support from the Science Research Council. T. Varghese is supported by the Education Ministry of the Government of India, and W. Margulis by a studentship from CNPq of Brazil.

[1] W. K. Bischel, J. Bokor, D. J. Kliger, and C. K. Rhodes, IEEE J. Quantum Electron. QE-15, 380 (1979).
[2] J. Reintjes, IEEE J. Quantum Electron. QE-15, 33D (1979).
[3] T. J. Pacala and J. B. Laudenslager, Appl. Phys. Lett. 37, 366 (1980).
[4] M. Maeda, T. Mizunami, A. Sato, O. Uchino, and Y. Miyazoe, Appl. Phys. Lett. 36, 636 (1980).
[5] G. Reksten, T. Varghese, and D. J. Bradley (unpublished).
[6] G. Reksten, T. Varghese, and D. J. Bradley, Appl. Phys. Lett. 38, 513 (1981).
[7] C. P. Christensen, L. W. Braverman, W. H. Steier, and C. Wittig, Appl. Phys. Lett. 29, 424 (1976).
[8] T. Efthimiopoulos, J. Banic, and B. P. Stoicheff, Can. J. Phys. 57, 1437 (1979).
[9] W. Margulis, W. Sibbett, and J. R. Taylor, Opt. Commun. 35, 153 (1980).
[10] D. H. Auston, Appl. Phys. Lett. 26, 101 (1975).
[11] G. Morou and W. Knox, Appl. Phys. Lett. 35, 492 (1979).
[12] Chi H. Lee, Appl. Phys. Lett. 30, 84 (1977).
[13] D. J. Bradley and W. Sibbett, Appl. Phys. Lett. 27, 382 (1975).
[14] M. Rokni, J. A. Mangano, J. H. Jacob, and J. C. Hsia, IEEE J. Quantum Electron. QE-14, 464 (1978).
[15] G. H. C. New, IEEE J. Quantum Electron. QE-10, 115 (1974).